

DOCTORAL THESIS

A Novel Workflow for Early Design Stages to Ensure Daylight and Summer Thermal Comfort in Buildings

Abel Sepúlveda Luque

TALLINN UNIVERSITY OF TECHNOLOGY
DOCTORAL THESIS
34/2022

A Novel Workflow for Early Design Stages to Ensure Daylight and Summer Thermal Comfort in Buildings

ABEL SEPÚLVEDA LUQUE



TALLINN UNIVERSITY OF TECHNOLOGY

School of Engineering

Department of Civil Engineering and Architecture

This dissertation was accepted for the defence of the degree 20/05/2022

Supervisor:

Dr. Francesco De Luca
School of Engineering
Tallinn University of Technology
Tallinn, Estonia

Co-supervisor:

Prof. Jarek Kurnitski
School of Engineering
Tallinn University of Technology
Tallinn, Estonia

Opponents:

Prof. Michela Turrin
Design Informatics
Delft University of Technology
Delft, the Netherlands

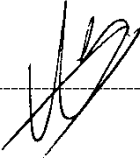
Prof. Francesco Goia
Department of Architecture and Technology
Norwegian University of Science and Technology
Trondheim, Norway

Defence of the thesis: 21/06/2022, Tallinn

Declaration:

Hereby I declare that this doctoral thesis, my original investigation and achievement, submitted for the doctoral degree at Tallinn University of Technology has not been submitted for doctoral or equivalent academic degree.

Abel Sepúlveda Luque



signature



European Union
European Regional
Development Fund



Investing
in your future

Copyright: Abel Sepúlveda Luque, 2022

ISSN 2585-6898 (publication)

ISBN 978-9949-83-855-4 (publication)

ISSN 2585-6901 (PDF)

ISBN 978-9949-83-856-1 (PDF)

Printed by Auratrükk

TALLINNA TEHNIKAÜLIKOOL
DOKTORITÖÖ
34/2022

Uudne töövoog projekteerimise algfaasis, et tagada päevavalgus ja suvine soojusmugavus hoonetes

ABEL SEPÚLVEDA LUQUE



Contents

List of Publications	7
Author's Contribution to the Publications	8
Introduction	9
Abbreviations	13
Symbols	15
1 Background	17
1.1 Solar access in buildings	17
1.2 Daylight provision in buildings	17
1.3 Overheating risk in buildings without mechanical ventilation	18
1.4 Glare protection in buildings	19
1.5 Requirements in Estonian residential and office buildings	19
1.6 Indoor comfort modeling and simulation techniques	20
1.7 Impact of the building envelope on multi-performance fulfillment	22
2 Methods	24
2.1 Development of multi-objective optimization workflow for building massing and envelope design decisions	25
2.1.1 SEs generation with SET	26
2.1.2 Building envelope generation	27
2.1.3 Sun hours and radiation analysis	28
2.1.4 Building performance assessment	28
2.2 Creation of rules of thumb and prediction formulas for room-level design decisions	29
2.2.1 Parametric studies to develop rules of thumb	30
2.2.2 Parametric studies to develop daylight and overheating prediction formulas	33
2.2.3 Climate conditions	35
2.2.4 Assessment criterion for overheating risk	36
2.2.5 Thermal model for overheating simulations	36
2.3 Benchmark of methods for annual glare assessment	39
2.3.1 Test room	39
2.3.2 Daylight calculation methods and Radiance parameters	40
2.3.3 Selection of fenestration systems	41
2.3.4 Optical characterization of complex fenestration systems	42
3 Results and discussion	44
3.1 First phase: defining building orientation, volume, and windows location considering solar access	44
3.2 Second phase: window sizing considering daylight provision and overheating risk	47
3.2.1 Simplified method based on daylight and overheating rules of thumb for window sizing	47
3.2.2 Detailed method based on daylight and overheating prediction formulas for window sizing	55
3.2.3 Example of designing windows properties and dimensions using prediction formulas to balance daylight and overheating protection	64
3.3 Third phase: defining shading optical properties to provide sufficient glare protection according to the EN17037	67

3.3.1 Setting Radiance parameters for illuminance calculations.....	68
3.3.2 Selecting methods and material models for static DGP calculations.....	70
3.3.3 Choice of the fastest method for dynamic glare assessment	74
3.3.4 Sampling strategies to speedup annual glare calculations	78
4 Conclusions	82
4.1 Future work	84
References	87
Abstract.....	97
Lühikokkuvõte.....	99
Appendix	101
Paper I.....	101
Paper II.....	111
Paper III.....	125
Paper IV	143
Curriculum vitae.....	160
Elulookirjeldus.....	163

List of Publications

The thesis is based mainly on data presented in the following peer-reviewed journal and conference publications:

- I Sepúlveda, A., & De Luca, F. (2020, May). A multi-objective optimization workflow based on solar access and solar radiation for the design of building envelopes in cold climates. In *Proceedings of the 11th Annual Symposium on Simulation for Architecture and Urban Design* (pp. 1–8).
- II Sepúlveda, A., De Luca, F., Thalfeldt, M., & Kurnitski, J. (2020). Analyzing the fulfillment of daylight and overheating requirements in residential and office buildings in Estonia. *Building and Environment*, 180, 107036.
- III Sepúlveda, A., De Luca, F., & Kurnitski, J. (2022). Daylight and overheating prediction formulas for building design in a cold climate. *Journal of Building Engineering*, 45, 103532.
- IV Sepúlveda, A., Bueno, B., Wang, T., & Wilson, H. R. (2021). Benchmark of methods for annual glare risk assessment. *Building and Environment*, 201, 108006.

Author's Contribution to the Publications

The author of this thesis developed the original idea of Paper I, modeled the cases study, collected, and analyzed the simulation results as well as the writing of the whole manuscript, and methodology applied to two cases study supported by the supervisor Francesco De Luca.

The author of this thesis structured the concepts and the scope of Paper II, defined the objectives and developed the methodology of the study. He conducted the energy and daylight simulations. He collected and analyzed the simulation results, synthesized the outcomes and wrote the research paper under coauthors' supervision.

The author of the thesis structured the scope, aims, and methodology of Paper III. He obtained all daylight and thermal simulation results and analyzed them. The case study was proposed by his supervisor Francesco De Luca. He wrote the whole paper under coauthors' supervision.

In Paper IV, the author of this thesis developed the methodology of the study. He conducted the daylight and glare simulations. He collected and analyzed the simulation results, synthesized the outcomes, and wrote the research paper under coauthors' supervision.

Introduction

Comfortable, healthy, and energy efficient buildings are key in the future since almost the 80% of the world population would live in urban areas by 2050 (Sanaieian et al., 2014). There are design criteria recommended by building standards and local regulations to ensure these type of buildings in the future. Furthermore, human-centric design has become one of the central criteria in architectural design. Designers have to consider multiple building performances such as indoor comfort and energy efficiency during early design stages as well as during renovation plans.

Typically, a good level of indoor comfort in buildings includes a balance between visual comfort and thermal comfort. On one hand, summer thermal comfort in buildings without active cooling systems could easily be violated by the overheating phenomenon in modern buildings located at high latitudes with large window areas and high thermal insulation levels. Thus, the excess of indoor temperature can lead to overheating phenomenon that causes thermal discomfort, which can have long-term negative effects on building users' performance and health (Beizaee et al., 2013). Overheating in a room could be induced by a critical combination of facade orientation, window construction, level of external obstructions, inefficient natural ventilation strategy, type of shading system, and its control, etc (Simson, 2019). Countries like Estonia, have specific regulations for protection against overheating in building without cooling systems (Estonian Government, 2015).

On the other hand, the European Union recently presented the standard EN 17037:2018 that defines the requirements for visual comfort in buildings (European commission, 2018), which include direct sun exposure, daylight provision, and glare protection. Visual comfort in buildings has a critical impact on occupants' health and mental performance (Duffy and Czeisler, 2009; Lockley, 2009). At the same time, daylight is the most preferred light source by building users (Knoop et al., 2019). The design of excessive large window areas improve the daylight provision but also overheating risk in buildings. Within the Estonian context, the combined fulfilment of daylight and overheating minimum requirements in residential buildings could be challenging (Simson et al., 2017b). However, excess of daylight levels could provoke discomfort glare to buildings users (Quek et al., 2021). Daylight glare could be an issue in educational and office buildings where building users have limitations to correct their viewing direction or sit position to avoid glare discomfort during tasks such as attending to the speaker, read a book, work with the computer, etc (Jakubiec and Reinhart, 2012). This exposure to glare discomfort could lead to headache problems, vision loss and reduction of their performance in daily activities (Pierson et al., 2017).

In parallel, there is the Estonian daylight standard EVS 894:2008/A2:2015 which sets minimum requirements for solar access and daylight provision in new dwellings (Estonian Centre for Standardization, 2015). Both, the Estonian and the European standards are recommended by the Estonian government from 2019. The consequences of the use of one or another standard by designers in terms of design flexibility during early design stages are unknown. Moreover, the simultaneous consideration of different requirements of building performances during early design stages could be confusing for designers because some building performances oppose to each other, for instance: daylight with overheating or daylight/solar access with daylight glare.

The evolution of building performance simulation tools in the field of daylight and thermal dynamic simulations enabled the possibility for architects to consider different

criteria during early design stages (Kharvari, 2020; Solemma LLC, 2016). Nevertheless, there is a lack of integrated methods and studies that help designers to understand the impact of their design decisions at different levels: building (orientation, shape, volume, and interior floor plan), facade (windows location, windows size, and windows construction), and shading level (shadings type, optical/thermal properties of the shadings, and shadings control algorithm) on the building overall performance (solar access, daylight provision, glare protection, overheating risk, etc).

This thesis presents an innovative workflow to help architects to design buildings with adequate levels of solar access, daylight provision and protection against overheating and daylight glare. This proposed workflow consists of three design phases. During the first phase, a multi-objective workflow is recommended to help architects and designers to make decisions to building and facade level to ensure adequate solar access levels according to the Estonian standard. In the second phase, rules of thumb and prediction formulas are used to facade level to ensure a good balance between daylight provision and overheating protection. Finally, in the third phase, an efficient shading system selection is proposed to ensure a certain glare protection level according to the European standard EN17037:2018.

The main objectives of the thesis can be summarized as follows:

- To propose an easy-to-use multi-objective optimization workflow based on solar access to help architects and designers to design building envelope efficiently (Paper I),
- To investigate the effect of different daylight assessment criteria on the combined fulfillment of daylighting and overheating requirements and its implications for the design of residential and office rooms in Estonia (Paper II),
- To develop daylight and overheating prediction formulas that can help architects and designers to conduct efficient window sizing process during early design stages (Paper III),
- To propose efficient assessment methods to assess glare protection during the shading selection process according to the European standard EN17037 (Paper IV).

The following methods were used to achieve the objectives:

- Parametric studies to obtain general rules of thumb and prediction formulas for the combined fulfilment of daylight and overheating requirements,
 - Thermal dynamic simulations using the validated software EnergyPlus (U.S. Department of Energy, 2015),
 - Daylight and glare dynamic calculations using the validated software Radiance (Ward, 1994), DIVA-for-Rhino (Jakubiec and Reinhart, 2011), and HoneyBee (“Honey Bee,” 2020),
 - Original python programs and Grasshopper plug-ins were developed in order to process the results from visual comfort and thermal analyses.

This thesis is based on peer-reviewed journal and conference articles.

In Paper I, a workflow based on multi-objective optimization for the design of the building envelope is proposed. The workflow has the potential to be adopted by designers, being integrated in the Grasshopper plug-in for Rhinoceros that is a widely used design platform. The proposed workflow shows a successful way to deal with complex multi objective design goals during early design stages such as maximization of the building volume, maximization of the solar access and minimization of the mean incident solar radiation.

In Paper II, it is evaluated the reliability of the daylight requirements defined by the Estonian standard based on the mean daylight factor (DF) with respect to the minimum DF requirements defined by the European standard method, EN 17037:2018 and IES LM-83-12, based on the spatial daylight autonomy (sDA) for office and residential buildings. The effect of window airing on overheating and on the combination of overheating and daylighting was also studied. A simulation-based methodology was applied to assess the daylighting and overheating performance in a single-window room considering different parameters. Indoor comfort-based rules of thumb for the design of offices and residential rooms were suggested. The results suggested a synergistic formulation of daylighting and overheating requirements in new building regulations to make the combined fulfillment easier for the designers.

In Paper III, a coupled method based on prediction formulas that can be used to assess daylight provision and overheating risk in buildings is developed. In addition, this method can be used for the design of interior floor plan and window sizing in order to rooms fulfill simultaneously both performances. The considered daylight provision requirements are based on the minimum Daylight Factor (minDF) defined by the European standard EN17037, and the overheating risk requirements are based on the degree-hour (DH) metric adopted by the Estonian regulation. The proposed coupled method has big potential to help architects and designers to achieve the combined daylight provision and overheating risk fulfillment during early design stages. Moreover, authors recommend the proposed coupled method to regulation makers for future building standards and regulations.

In Paper IV, state-of-the-art methods for annual glare analysis and develop strategies are benchmarked to reduce the computational time (CPU time) without compromising the accuracy of glare calculations. The Radiance-based tool *rtrace* and the Radiance-based five-phase method (5pm) are applied to a single room. Sensitivity analyses of Radiance parameters, calculation methods, and Bidirectional Scattering Distribution Function (BSDF) materials to model isotropic fabrics are conducted. The findings of this article can help architects and practitioners to set up parameters and calculation methods for efficient annual glare protection assessment according to the EN 17037 needed during shading selection process.

Novelty and practical outcomes of the thesis:

- The realization of a multi-objective optimization method that uses own developed open source Grasshopper tools for Rhinoceros to create solar envelopes considering different criteria such as building volume, solar access of the building envelope, mean incident solar radiation, quality of the sunlight, and solar access ordinances. These tools are called “Solar Envelope Tools” (SET) and they are available online for free download for designers (Sepúlveda and De Luca, 2022). Prior to the publication of SET, there were no open source tools that could take into account in an integrated form windows from

the surrounding buildings, urban context, different solar ordinances, and different qualitative criteria to filter sun vectors used to generate the solar envelope.

- The Estonian daylight standard has limited reliability in properly predicting the daylight potentials of building interiors. In many cases, it overestimates daylight availability for different orientations. The present thesis will be presented to local authorities and regulatory bodies to increase their awareness about the need to promote a new and more efficient daylight regulation in Estonia. Hence, this research will contribute to the development of a compulsory building daylight regulation;

- The development of a coupled method based on prediction formulas to easily integrate the daylight provision and overheating performance analysis during window sizing design process. This method will be proposed to regulatory bodies and authorities aiming to the synergistic formulation of daylighting and overheating requirements in new building regulations to make it easier for designers to fulfill both requirements;

- New methodology based time step-based ray-tracing method that helps designers to efficiently compare several complex fenestration systems (CFSs) in terms of annual glare protection performance during early design stages of the building design process.

Limitations of the work:

- The work considers specific climate, building properties, and architecture of typical features of existing buildings in Estonia. Despite most of the methods proposed in this thesis focuses on Estonian climate/building regulations, it can be used in similar climates with simple parameter changes;

- The principal focus of thesis were indoor comfort during early design stages;

- This study does not consider future climate conditions in cases studies based mainly of city of Tallinn, Estonia;

- The methods developed in this thesis can be applied on the design of residential and office/educational buildings. Other types of buildings such as hospital or commercial buildings might have different necessities in terms of building performances and space distribution that this thesis does not cover;

- This thesis is mainly based on daylight and thermal simulations from calibrated and recommended set up parameters from own and third published studies.

Abbreviations

3pm	Three-phase method
3pmD	Three-phase method considering direct component of the solar radiation
5pm	Five-phase Method
aBSDF material	Radiance BSDF material with peak extraction
BSDF	Bidirectional Scattering Distribution Function
BSDF material	Radiance material defined with BSDF data set without considering peak extraction
CAD	Computer-aided design
Cd1	Condition that is fulfilled if minDF1 is higher than a target value minDF1t
Cd2	Condition that is fulfilled if minDF2 is higher than a target value minDF2t
cds	Direct sun coefficient simulation
CFS	Complex Fenestration System
C _i	Multi-objective criterion i
CIE	Commission Internationale de l'Eclairage
Context	Surrounding building
CPU time	Computational time
D	Daylight matrix
DA	Daylight Autonomy
DC	Two-phase method
D _D	Daylight matrix considering null number of ambient bounces (-ab 0)
DeadAngle	Dead angle input
DF	Daylight factor
Dfb	Warm humid continental climate
DF _{mean}	Daylight criterion based on mean Daylight Factor
DF _{min}	Daylight criterion based on minimum Daylight Factor
DGP	Daylight Glare Probability
DGPs	Simplified Daylight Glare Probability
DH	Temperature excess in Degree-Hours
DH _{max}	Maximum Temperature excess in Degree-Hours
eDGPs	Enhanced Simplified Daylight Glare Probability
HVAC	Heating, ventilation, and air conditioning
IDA-ICE	IDA Indoor Climate and Energy
maxDH _{EST}	Maximum Temperature excess in Degree-Hours according to Estonian regulations
maxWFR	Maximum Window-to-Floor Ratio
maxWWR	Maximum Window-to-Wall Ratio
MinAltitude	Minimum altitude input
minDF	Minimum Daylight Factor

minDF1	Minimum DF value for the first half of the reference plane closer to the window
minDF1t	Target value for minDF1
minDF2	Minimum DF value for at least the 95% of the entire the reference plane
minDF2t	Target value for minDF2
minDF _c	Target minDF1 for European country C
minWFR	Minimum Window-to-Floor Ratio
minWWR	Minimum Window-to-Wall Ratio
mISR	Mean incident solar radiation (W/m ²)
mISR'	Relative mean incident solar radiation (W/m ²)
MV	Infiltration and mechanical ventilation
N, NE, E, SE, S, SW, W, NW	North, North-East, East, South-East, South, South-West, West, North-West.
NV	Windows airing technique
NZEB	Nearly Energy Zero Buildings
OW	Solar access maximization
OI	Solar incident radiation maximization
RMSE	Root Mean Square Error
S	Sky Vector
SA	Solar Access
S _b	Sky Vector considering the exclusive contribution of the sun
sDA	Spatial Daylight Autonomy
SD _n	Sum of daily daytime sun time steps each n days during the first semimanual period
SE	Solar Envelope
SET	Solar Envelope Tools
SolEnvGen	"Solar Envelope Generator" Grasshopper component
SunPathGen	"Sun Path Generator" Grasshopper component
SunVectGen	Sun Vectors Generator
SunVectSel	Sun vectors sorted and selected input
SV _n	Sum of daily visible sun time steps each n days during the first semimanual period
TRY	Test Reference Year
T	Transmission matrix
UDI	Useful Daylight Index
VectorsType	Vectors Type
V _b	View matrix considering the exclusive contribution of the sun (-ab 1)
V	View matrix
WWR	Window-to-Wall Ratio
WFR	Window-to-floor ratio

Symbols

α	Weight factor for the maximization of building volume (-)
ab	Number of ambient bounces
ad	Number of ambient divisions
β	Weight factor for the maximization of solar access (-)
γ	Weight factor for minimization of solar radiation (-)
E_v	Vertical illuminance at eye level
fDGpT	Annual glare metric or percentage of occupied hours with Daylight Glare Probability higher than a threshold DGpT
g or g-value	Solar factor (-)
$g_{max,i}$	Maximum g-value to not overheat a certain room i (-)
h	Number of time steps considered in a dynamic glare assessment (hours)
H	The number of time steps when using the 5 phase-method (hours)
h_{max}	The maximum number of time steps when using rtrace (hours)
L_s	Luminance distribution (cd)
MF	Number of Reinhart sky-patch subdivisions
q_{50}	Air leakage rate of building envelope at 50 Pa pressure difference, $m^3/(h \cdot m^2)$
ω_s	Solid angle subtended by the sources (sr)
P	Position Index
ρ_{ndif}	Normal-diffuse visible reflectance
rd	Room depth (m)
rdif	Diffuse reflectance (-)
rw	Room width (m)
t_0	CPU time required by the arithmetic combination of the results from the phases 3pm, 3pmD, and cds
τ_{3pm}	CPU time required by the 3-phase method
τ_{3pmD}	CPU time required by the direct 3-phase method
τ_{5pm}	CPU time required by the 5-phase method
t_c	CPU time required by the sky and octree generation and the commands <i>rtrace</i> and command <i>evalglare</i>
t_{cds}	CPU time required to create the octree and sun coefficient matrix C_{cds}
τ_{cds}	CPU time required by the cds phase
t_{dcD}	CPU time required for the multiplication of the matrices V_D , T, D_D , and S_D
td	Diffuse transmittance (-)
t_{dc}	CPU time required for the multiplication of the matrices V, T, D, and S
t_{dcs}	CPU time required for the multiplication of the matrixes C_{cds} and S_{cds}
T_{dc}	Sum of CPU time required by sky vectors generation of the phases: 3pm, 3pmD, and cds

$\tau_{dir\ dir}$	Direct-direct visible transmittance
$\tau_{dir\ dif}$	Direct-diffuse visible transmittance
$\tau_{dir\ h}$	Direct-hemispherical visible transmittance
t_M	CPU time required to create the view and daylight matrices
T_M	Sum of CPU time required by the octree generation in the phases: 3pm, 3pmD, and cds
τ_m	CPU time required by arithmetic operations of all results from phases 3pm, 3pmD, and cds
t_{MD}	CPU time required to create the octree required by the direct 3-phase method
t_{MF}	CPU time required to create the suns and material map generation
t_s	Specular transmittance (-)
t_s	CPU time required to create a sky vector
T_s	Sum of CPU time required by sky vectors generation of the phases: 3pm, 3pmD, and cds
t_{sD}	CPU time required to create a sky vector (S_D) with the exclusive contribution of the sun
t_{sF}	CPU time required to create a sky vector (S_{cds}) with only the contribution of the sun and selected Reinhart sky subdivisions (MF)
τ_{ndif}	Normal-diffuse visible transmittance
τ_{nh}	Normal-hemispherical visible transmittance
τ_{nn}	Normal-normal visible transmittance or openness factor
T_h	Mean air hourly temperature (°C)
T_{vis}	Visible transmittance (%)
U-value	Thermal transmittance ($W/m^2 \cdot K$)
V_r	Volume ratio (-)
V_r'	Relative volume ratio (-)
W_r	Windows ratio (-)
W_r'	Relative windows ratio (-)

1 Background

1.1 Solar access in buildings

Solar access (SA) has been considered as design criterion by architects since ancient times. Apart from being crucial for the development of the urban fabric, one of the main aspects of the visual comfort in buildings is the exposure to sunlight or SA (European commission, 2018). SA is related to the direct component of daylight, which has been proved beneficial for well-being of building users (Lockley, 2009; Samuels, 1990). New buildings influence the SA levels of the urban environment and vice versa. Most of countries have standards and/or regulations to ensure the SA rights of building occupants. These minimum SA minimum requirements are normally expressed in terms of the number of hours per day during a specific analysis period (continuous or discrete) when the sun is visible from the window of a determined building (De Luca and Dogan, 2019; Estonian Centre for Standardization, 2015; European commission, 2018).

SA regulations influence building density and maximum buildable volume. In practice, architects use the so-called solar envelope (SE) method in early design stages. The SE method is a method introduced by Knowles to calculate maximum volume new buildings cannot exceed to guarantee required SA of the surrounding buildings (Knowles, 1980). There are two main approaches to calculate the SE: additive algorithm based on the calculation of the maximum height to each grid point of the plot and subtractive algorithm based on the removal of grid volumes from the theoretical buildable block. The first one is the most used for SE generation due to its simplicity (Capeluto and Shaviv, 2001; Sanaieian et al., 2014) and the second one, although it has been proved time-consuming, is useful as building massing technique (De Luca, 2017a).

There is no specification in terms of quality of the sunlight; hence, this allows flexibility to generate SEs even for the same regulation and urban environment (De Luca et al., 2018a). Thus, the consideration of other aspects for the SE generation such as the urban context (De Luca and Voll, 2017) or climate conditions (Capeluto and Plotnikov, 2017) can influence the shape of the SE. In recent years, the additive algorithm has been implemented in several tools like LadyBug tools (Sadeghipour Roudsari, 2012) and DIVA4Rhino (Solemnia LLC, 2016), both Grasshopper plug-ins for Rhinoceros software. Nevertheless, these tools do not calculate urban context-dependent SEs.

Different pattern layouts can influence total floor area and SA performance of the building masses located in urban areas (De Luca, 2017b). Optimal building clusters for direct solar access in urban environments in Estonia, including type of interior/exterior floor plan layout, and buildable floor area were investigated (De Luca et al., 2018b). Indeed, the optimization of building clusters can give detailed information about the building envelope design but typically, a unique SE per urban environment was considered, which can limit the flexibility during the building massing stage.

1.2 Daylight provision in buildings

According to the European standard EN17037, daylight provision is one of the main aspects of visual comfort in buildings, and it is defined as the “level of illuminance achieved across a fraction of a reference place for a fraction of daylight hours within a space”(European commission, 2018). The presence of moderate levels of daylight in indoor spaces improve the physiological and psychological wellbeing of people (Liu et al., 2017; Samuels, 1990). Moreover, characteristics of daylight such as intensity and color benefit

the circadian cycle in humans (Duffy and Czeisler, 2009). In fact, daylight is the most preferred source of light by building occupants (Knoop et al., 2019). In addition, daylight is recommended as a design criterion during early design stages since well daylit indoor spaces have been proved economically highly valuable by building owners (Turan et al., 2020).

In practice, there are several metrics that can be used to assess daylight provision. On one hand, the widely used static daylight metric Daylight Factor (DF) is quantified as the ratio between indoor and external horizontal illuminance under overcast conditions (BSI, 2008). On the other hand, dynamic daylight metrics consider the dynamic performance of daylight in buildings regarding occupants' behavior and surrounding climate conditions (Reinhart et al., 2006). For instance, the daylight autonomy (DA) metric, which generally is more applicable than DF, quantifies the percentage of occupied hours when horizontal illuminance in a specific point of the reference plane is above a defined threshold (Bian and Ma, 2017). The useful daylight autonomy (UDI) uses a range of illuminances instead of a single threshold, it was proved more informative metric for daylight assessment than DA (Nabil and Mardaljevic, 2006). Unlike DA and UDI metrics, which contains only temporal information about the daylight provision, the spatial daylight autonomy (sDA) metric contains also spatial information, since it is defined as the percentage of the reference plane with horizontal illuminance above a defined threshold during at least a specific fraction of time, whether daytime (European commission, 2018) or occupied hours (Illuminating Engineering Society and The Daylight Metric Committee, 2013).

Despite the existence of consolidated daylight assessment methods, not every European country has defined yet a concept of adequate daylight and a suitable daylight metric (Sokol and Martyniuk-Peczek, 2016). The adoption of new standards such as the EN17037:2018 by European countries could be challenging for practitioners because new daylight assessment criteria would influence their daily design practice.

1.3 Overheating risk in buildings without mechanical ventilation

Thermal discomfort caused by the overheating phenomenon, produced by the excess of indoor temperature, can have negative effects on building users' satisfaction and health on the long-term (Beizaee et al., 2013; Liu et al., 2017; Santamouris and Kolokotsa, 2015). The severity of the seasonal overheating risk in dwellings is influenced by the urban surroundings, local architecture, occupant behavior, and climate. Future climate conditions affected by the global warming effect will aggravate overheating risk in buildings. Moreover, the urban heat island effect combined with the global warming effect will aggravate overheating risk in buildings (Yannas and Rodríguez-Álvarez, 2020). Specifically, residential buildings are prone to have overheating risk problems due to the lack of cooling or efficient natural/mechanical ventilation strategies (Fosas et al., 2018; Hamdy and Jan Hensen, 2015; Lomas and Porritt, 2017; Simson, 2019). The assessment of overheating risk in residential buildings has been widely investigated in temperate climates (Gupta and Gregg, 2018; Maivel et al., 2015; Morey et al., 2020; Mourkos et al., 2020; Voll et al., 2016a). A study on thermal comfort in 1134 English dwellings demonstrated that the renovation plans should include practical measures against overheating risk in residential buildings (Beizaee et al., 2013).

Estonia has specific overheating requirements that must be met if there is no mechanical space cooling system in new/renovated buildings. Overheating requirements in Estonia are based on the metric degree-hour (DH) ($^{\circ}\text{C}\cdot\text{h}$), which represents the accumulation of

the hourly indoor temperature excess (related to a temperature set point) during a specific period of warm season (June 1–August 31). The use of simulation-based methodology is recommended to assess summer thermal comfort in Estonian residential buildings (Hamburg and Kalamees, 2019).

1.4 Glare protection in buildings

Although daylighting in indoor spaces is beneficial for human health, the excess light can be disturbing for the human eye. Thus, glare is defined in the EN1037 as the “condition of vision in which there is discomfort or a reduction in the ability to see details or objects, caused by an unsuitable distribution or range of luminance, or by extreme contrasts” (European commission, 2018). Glare protection plays a critical role in the achievement of a good level of visual comfort in types of building where the occupants have limited flexibility to adapt their viewing direction to avoid visual discomfort, such as office or educational buildings. Glare protection is difficult to assess since it depends on many factors (Osterhaus, 2005). Relevant factors are the luminance and size of the glare source, adaption level of the human eye, contrast effect, saturation effect, view direction, and attractiveness of the view through the window (Pierson et al., 2017). Survey techniques in combination with simulation-based methods have been widely used to predict glare in indoor spaces (Mangkuto et al., 2017; Shafavi et al., 2020; Wienold and Christoffersen, 2006; Yamin Garretón et al., 2018).

There are two main effects to quantify glare in practice. The saturation effect is related to the brightness of the field of view. The contrast effect is influenced by the luminance distribution of the scene. Glare metrics that consider exclusively the saturation effect, outperformed contrast-driven glare metrics in bright-light scenarios. However, contrast-driven glare metrics outperform saturation-driven glare metrics in low-light scenarios (Quek et al., 2021). Glare metrics that consider both effects are known as hybrid glare metrics. The most robust glare metric nowadays is a hybrid metric called Daylight Glare Probability (DGP) (Wienold et al., 2019). The DGP formula has two terms, the first one is proportional to the vertical illuminance at eye level (E_v) and represents the saturation effect. The second term quantifies the contrast effect of the scene, which is related to the luminance of the glare sources L_s (cd/m^2), the solid angle ω_s subtended by the sources (sr), Guth’s position index (P), and E_v (Eq. (1)) (Wienold and Christoffersen, 2006).

$$DGP = 5.87 \cdot 10^{-5} E_v + 9.18 \cdot 10^{-2} \log \left(1 + \sum_i \frac{L_{s,i}^2 \cdot \omega_{s,i}}{E_v^{1.87} P_i^2} \right) + 0.16 \quad (1)$$

For DGP values lower or equal to 0.35, daylight glare is considered imperceptible. DGP values higher than 0.35 and lower than 0.40 are associated with perceptible but mostly not disturbing glare. When DGP values are higher than 0.40 and lower than 0.45, glare is perceptible and often disturbing. Finally, DGP values higher than 0.45 are associated with disturbing daylighting glare.

1.5 Requirements in Estonian residential and office buildings

Currently in Estonia, there are two valid daylight standards: the Estonian standard EVS 894:2008/A2:2015 “Daylight in Dwellings and Offices” (Estonian Centre for Standardization, 2015) and the European standard EN 17037 “Daylight in buildings” (European commission, 2018).

The Estonian standard includes recommendations for minimum requirements of solar access for new residential buildings and mean DF-based daylight requirements for residential and office buildings. According to the Estonian standard, each apartment of a new residential building should receive at least 2.5 hours of direct sun daily from March 21 until August 21. This SA requirement specifies the quantity but not the quality of the direct sun that received each apartment. Moreover, the Estonian standard's daylight assessment criterion is based on mean DF values.

The European standard daylight assessment criteria can be fulfilled by using two criteria: minimum DF and sDA metrics. Previous studies showed disagreements between dynamic and static daylight metrics in Estonian educational buildings (De Luca et al., 2019a). Thus, it is important to understand how the European standard affects the design of the building envelope and refurbishment plans. No extensive studies have been conducted to evaluate its impact on the construction practice of residential and office buildings.

Glare protection classes defined in the EN 17037 are based on previous studies with fabrics and the DGP metric (Wienold et al., 2017). According to EN 17037, the annual percentage of discomfort glare hours (fDGp) should be lower than 5% for a shading device to protect against glare. Glare hours are considered as the occupied hours with an associated DGP above a threshold DGp: 0.35, 0.40, and 0.45 for high, medium, and minimum level of glare protection, respectively (European commission, 2018). The calculation methods to conduct glare risk assessments are usually time-consuming and require a certain level of expertise by architects and designers.

Estonia has specific overheating requirements that must be met if there is no mechanical space cooling system in a new or a renovated building. Overheating requirements in Estonia are based on the metric degree-hour (DH) (°C·h), which represents the accumulation of the hourly indoor temperature excess (related to a temperature set point) during a specific period of warm season (June 1–August 31). The maximum DH is 150 °C h and 100 °C h for residential and non-residential buildings, respectively. The temperature set point is 27 °C and 25 °C for residential and non-residential buildings, respectively (Estonian Government, 2018, 2015).

1.6 Indoor comfort modeling and simulation techniques

Modeling and simulation techniques are crucial as design tools for architects and designer during early design stages and renovation plans. The prediction of both thermal and daylight levels in indoor spaces represents the basis of the human-centric architectural design practice nowadays. By using approaches based on simulations, architects and designers are able to conduct thermal and daylight annual assessment in more viable way in terms of time and economical resources than via field experimental measurements.

For thermal simulations, several validated softwares such as EnergyPlus (U.S. Department of Energy, 2015) and IDA-ICE (Kropf and Zweifel, 2002) are widely used by practitioners. Different approaches can be considered in practice to model a building, for overheating calculations, it has been proved a reliable approach to use single-zone approach (Simson et al., 2017a). Moreover, the consideration of constant thermal properties of the window glazing is a more conservative approach to assess overheating than using angle-dependant thermal properties (Thalfeldt et al., 2016).

The development of the open-source software Radiance based on the ray-tracing technique allowed reliable climate-based daylight modelling (CBDM) in buildings (Ward, 1994). The use of CBDM is key for reliable assessment of daylight provision in buildings (Kong et al., 2018; Mardaljevic, 1999). Along the last decade, several friendly-use applications such DAYSIM (Reinhart and Pierre-Felix, 2009), LadyBug/HoneyBee (“Honey Bee,” 2020; Sadeghipour Roudsari, 2012), DIVA-for-Rhino (Solemma LLC, 2016), and Fener (Bueno et al., 2015) were created in order to increase availability of Radiance-based simulations in the building design community.

A suitable modeling of glazing units in combination with external/internal shading systems known as complex fenestration systems (CFSs) is crucial to obtain reliable daylight/glare predictions (Thanachareonkit and Scartezzini, 2010; Tzempelikos and Chan, 2016). The optical properties of the CFSs are calculated from bidirectional scattering distribution function (BSDF) datasets, which represent the angular distribution of light scattered by the CFS. BSDF datasets can be obtained via measurement using a photogoniometer (Apian-Bennewitz, 2010; Stover, 2012; Ward, 2014) or via simulation using ray-tracing or analytical techniques (McNeil, 2015; McNeil et al., 2013). As an example of ray-tracing techniques, the Radiance genBSDF program was used to generate BSDF datasets of CFS such as venetian blinds (Uribe et al., 2019) and complex three-dimensional textiles (Mainini et al., 2019; Sepúlveda, 2018). Thus, the use of BSDF data sets to represent the angular-dependent behavior of the CFS is critical to not underestimate daylight glare risk (Inanici and Hashemloo, 2017a). Even when modeling of opaque materials, small changes in diffuse reflectance of opaque surfaces of the interior (Brembilla et al., 2018; De Luca et al., 2019b; Kharvari, 2020) or exterior (Bugeat et al., 2020) scene have significant effects in lighting levels of indoor spaces.

The Radiance *rtrace* method has been used mainly for static glare/daylight analysis because of its reliability and high computational requirements (CPU time) (Jones and Reinhart, 2017). However, matrix-based methods can recycle information from the whole scene: view, daylight, and sky matrix. The most widely used matrix-based methods are the 2-phase (DC), 3-phase (3pm), and 5-phase method (5pm). Glare calculations implies more time-consuming simulations than daylight calculations, since the calculation of the DGP metric consist on three steps: the calculation of E_v , the rendering of a scene (.hdr file) as seen from an observer for which glare is to be evaluated, and the calculation of the DGP as shown in Eq. (1). Speedup strategies such as the use of *rtrace* with null ambient bounces (-ab 0) to generate the luminance maps in combination with vertical illuminance calculations were used to approximate (called enhanced simplified DGP (eDGPs)) the DGP (Wienold et al., 2017). The DC and 3pm are reliable for annual daylighting calculations with static and switchable CFSs, respectively (Subramaniam, 2017). The 5pm applies the indirect contribution from the sky from the 3pm and the direct component of the sun from an accurate DC simulation using a more accurate discretized sky model (Reinhart subdivisions) (McNeil, 2013). Indeed, the 5pm and *rtrace* methods were proven to be more reliable than the 3-phase method for DGP calculations (Lee et al., 2018a, 2018b). Abravesh et al. proposed another method for annual glare assessments based on the eDGPs where E_v is calculated using the 3pm (Abravesh et al., 2019).

Although, previous investigations compared CBDM techniques and proposed ranges for simulation parameters to ensure the accuracy of daylight assessments (Ward, 1994; Wienold et al., 2019, 2017). For annual glare assessment, many factors can influence the choice of the best calculation method: the type of CFS and its model material, parameters

for renderings, parameters for illuminance calculations, number of time steps, number of scenes (different viewpoints, viewing directions, surface materials, etc.), and number of CFSs. In practice, there is a lack of consideration of trade-off criteria for annual glare assessment. Suitable knowledge of these factors could help software developers to implement optimized models for glare risk assessment.

1.7 Impact of the building envelope on multi-performance fulfillment

In practice, architects and designers have to make design decisions during early design stages and renovation plans. Typical design decisions are at building level (e.g. building orientation/volume and interior floor plan), facade level (e.g. windows location/size and walls/windows constructions), room level (shading system, shading/ventilation control). Inadequate design decisions could lead to poor performance buildings. Thus, performance-driven design criteria are necessary to ensure a good balance between visual and thermal comfort in buildings nowadays.

Daylight has a significant positive influence on the energy efficiency of buildings (Alva et al., 2020; Chi et al., 2017; Kuhn et al., 2001; Ponmalar and Ramesh, 2014). Daylight and solar heat gains in winter can reduce the energy consumption when a suitable shading control is considered (Grynning et al., 2014). Previous investigations emphasize the need to design synergistically glazed areas and shading to provide adequate daylight in building interiors and reduce energy consumption for lighting (Gago et al., 2015; Haase and Grynning, 2017) and for heating and cooling (Kim et al., 2017; Yu and Su, 2015). External shading is an efficient solution to reduce glare risk for building occupants (Al-Obaidi et al., 2017), and has the advantage of not relying on occupant operation; occupants often leave the operable internal shade closed and also use it when is not needed, causing an avoidable electric light energy consumption (O'Brien et al., 2013). Moreover, excessive direct sun exposure can lead to high levels of daylight provision and solar gains, increasing the indoor temperature and consequently overheating risk.

In cold climates, overheating is considered a limiting function of the daylight provision, since buildings with high thermal resistance are common to save heating energy in winter, and facades with high window-to-wall ratios (WWRs) are designed to increase the daylight provision (Thalfeldt et al., 2013). However, these measures can generate thermal discomfort during the warm season. Previous studies propose rules of thumb to help architects and designers to choose optimal design strategies and renovation plans to achieve a combined fulfillment of daylight and overheating requirements (De Luca et al., 2019b; Simson, 2019; Vanhoutteghem et al., 2015). Window shading elements can reduce the overheating of residential premises depending on facade orientation and distance of surrounding buildings, especially at northern latitudes; thus, a careful envelope design is recommended (Voll et al., 2016b). A suitable use of complex fenestration systems (glazing combined with shading systems) could balance visual comfort and energy efficiency in different climates (Bueno and Sepúlveda, 2019; Hoffmann et al., 2016; Uribe et al., 2019). Among dynamic shading systems, interior shading is a popular low-cost alternative for existing buildings, since they are easy to install, but they are less effective in terms of the thermal protection they provide (Balaras et al., 2002). Within Danish context, it has been proved difficult the achievement of a good balance between daylight provision, energy consumption, and overheating risk: low g-values and high light transmittance values were recommended for south-oriented rooms and high g-values for north-facing windows to reduce the heating demand (Vanhoutteghem et al., 2015).

A vast number of investigations focused on the optimization of different building performances, used optimization Grasshopper plug-ins within the software Rhinoceros 3D (Mangkuto et al., 2016; Rabani et al., 2021; Toutou et al., 2018; Zhu et al., 2020). Additionally, recent investigations included machine learning technique to speedup multi-objective optimization of architectural spaces (Chegari et al., 2021; Ekici et al., 2021; Geyer and Singaravel, 2018; Zhu et al., 2020). However, despite of the accuracy to predict building performances, these approaches might not be attractive as design tools by non-experienced architects and designers because they required steep learning-curve and are not intuitive due to the “black box” nature typical of machine learning multi-objective optimization approaches (Wang et al., 2021). Several methods to predict daylight provision based on prediction formulas (Lee et al., 2019; Reinhart and Lo Verso, 2010), graphical tools (Cammarano et al., 2015; Pellegrino et al., 2017), and rules-of-thumbs (Loche et al., 2021; Simson, 2019) have been proposed since two decades ago. Nevertheless, there is a lack of prediction methods, which are easy to use by not simulation or optimization experts, for the combined assessment of daylight provision and overheating risk. Furthermore, there is an urge necessity to propose integrated methods to help architects during early stages of the design process. In fact, by using easy-to-use integrated methods like the proposed in this thesis, architects and designers could achieve better building designs in much less time than with single performance-based approach because the later one does not consider the conflict between different building performances such as daylight-overheating or solar access-building volume, etc.

2 Methods

In this section, the methodology followed to achieve each of the main objectives of this thesis is explained. Overall, three easy-to-use simulation-based methods are developed to be applied to different levels during early design stages: building level, facade level, and room level (Figure 1). Thus, the structure of this section is the following:

- Section 2.1 (Paper I): the multi-objective optimization workflow for building massing, which is the first phase of the innovative workflow proposed in this thesis, is presented step by step together with the case study;
- Section 2.2: the parametric models used to generate rules of thumb (section 2.2.1, Paper II) and prediction formulas (section 2.2.2, Paper III) for facade level design decisions, which constitute the second phase of the innovative workflow proposed in this thesis, are presented in detail. The case study for the application of the prediction formulas is explained in section 2.2.2.1. In addition, thermal model for overheating simulations (section 2.2.5), climate conditions (section 2.2.3), and overheating risk criterion (section 2.2.4) are described;
- Section 2.3 (Paper IV): the test room (section 2.3.1), daylight calculation methods and Radiance parameters (section 2.3.2), selected fenestration systems (2.3.3), and their optical characterization (section 2.3.4) are explained in detail. All these methodological decisions are the basis of the different analyses (section 3.3) that support the efficient assessment methods for glare protection according to the EN 17037. These glare assessment methods constitute the third phase of the innovative workflow proposed in this thesis.

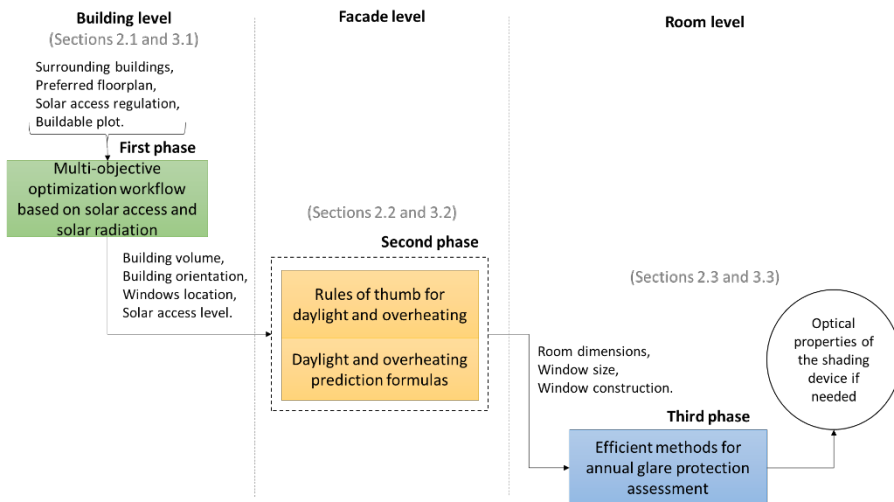


Figure 1. General structure of this thesis and phases of the proposed innovative workflow.

2.1 Development of multi-objective optimization workflow for building massing and envelope design decisions

The first phase of the proposed method is a multi-objective optimization workflow based on SA and solar radiation of the design of building envelopes in context where SA is critical, as in cold climates (Paper I). The aim of this case study is to analyze how SEs based on different criteria influence the building envelope design for a preferred floor plan and different objectives. The possible objectives are: (1) maximization of total floor area, (2) maximization of SA performance of the new building envelope; and (3) minimization of incident solar radiation in the warm season of the facade area that fulfill the minimum sun hours according to the SA ordinance.

Specifically, the minimum SA requirements for new residential buildings in Estonia can be considered from the Estonian standard (Estonian Centre for Standardization, 2015) and from the EN17037 (European commission, 2018). According to the first one, at least one room per each apartment should have a minimum number of direct sun hours of 2.5 from April 22 until August 22 while the new building should not block more than 50% of the SA of the surrounding residential buildings. According to the EN17037, at least one habitable room per each apartment should have a minimum number of direct daily sun hours between February 1 and March 21, which depends on the level of solar access the designer would choose: 1.5 h, 3 h, or 4 h for minimum, medium, and high level of recommendation for exposure to sunlight, respectively. In this work, only the Estonian standard was considered because it provides more flexibility in the design of new residential buildings in Estonia than considering the EN17037 (De Luca and Sepúlveda, 2021).

The outputs of this workflow are the optimal method to generate the SE with the novel Grasshopper plug-in Solar Envelope Tools (SET), the number of floor plan divisions, orientation/size of the building, and zone of the facade that fulfills the SA requirements for a given multi-objective criterion. Implicitly, this workflow also provides flexibility in the creation of the interior floor plan of the building. This workflow has four main phases (Figure 2): SEs generation using SET, building envelope generation (using in-built Grasshopper components and Python functions), solar analysis of the building envelope using SET and the assessment of the building performance based on multi-objective criteria.

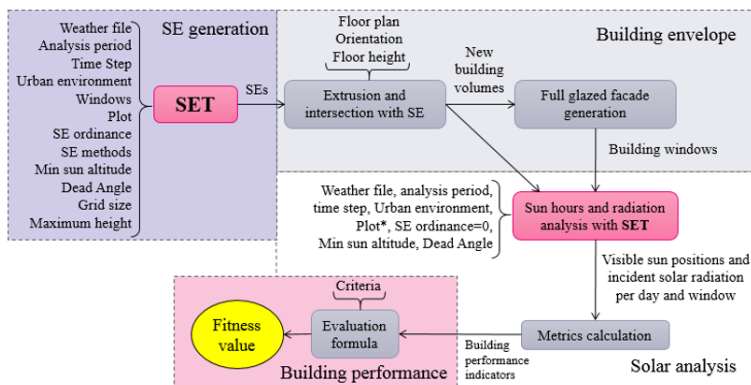


Figure 2. Workflow for the building performance assessment.

In order to study how SEs generated by different criteria influence the building envelope design and use this information to optimize the performance of the new building, the workflow shown in Figure 2 is defined. This workflow has four main phases: SEs generation using SET, building envelope generation (using in-built Grasshopper components and Python functions), solar analysis of the building envelope using SET and the assessment of the building performance based on multi-objective criteria.

2.1.1 SEs generation with SET

The first step in the SE generation using SET is to extract climate information about the location of the case study (latitude, longitude, UTC and hourly direct normal solar radiation for the annual period) using the component “Location Data Reader”. After this, it is necessary to calculate the sun vectors of the analysis period using the component “Analysis Period” (SunVectGen). Using SunVectGen, the designer can introduce a specific time step and multiple analysis periods. When the selected time step is different than 1 (hourly), SunVectGen uses a linear interpolation to calculate the direct normal solar radiation in each time step.

The main feature of SET is the possibility to filter and select sun vectors that fulfill different conditions. The filtering process consists of identifying the sun vectors of the analysis period that are not blocked by the surrounding buildings (Context) and fulfill the minimum defined solar altitude (MinAltitude) and dead angle (DeadAngle). This filtering process is run for every existing window introduced as input. Once the filtered sun vectors are identified, a sorting and selection process can be performed taking into account the specific SA ordinances at hand and sorting methods. The SA ordinance of each case study determines the SA minimum requirements for the new building. The sorting methods that can be selected through the input SunVectSel, allows taking into account different sun light quality criteria (Table 1). Consequently, the sorted and selected sun vectors can be used to generate the SE using the component “Solar Envelope Generator” (SolEnvGen) which gives as output: (1) the points of the final SE; (2) the SE points for each window. Additionally, the sun vectors filtered and selected for each window can be visualized using the component “Sun Path Generator” (SunPathGen).

Table 1. Available sorting methods in SunVectSel component.

Sorting method (VectorsType)	Description
1	Larger solar altitude first.
2	Larger solar incident radiation first.
3	Sun vectors out the plot with large solar altitude first, then vectors through the plot with large solar altitude first.
4	Sun vectors out the plot with large solar altitude first, then vectors through the plot with larger incident solar radiation first.
5	Sun vectors out the plot with large solar altitude first, then vectors through the plot close to the corners of the plot first.

The workflow has been tested on one urban area located in Tallinn, Estonia (Figure 3). A plot 90 x 90 m in size is considered to build a new residential building. The SA rights according to the Estonian standard are described in section 2.2. The choice of a suitable time step is essential for the accuracy of the generated SE and the required computational time (De Luca and Dogan, 2019). Thus, a time step of 2 (one sun vector per 30 minutes) is used for the case study. The minimum angle between a sun ray and the building facade (window dead angle) is set to 10° (Darula et al., 2015). The minimum sun altitude is set to 12° (European commission, 2018). The distance between grid points on the buildable plot is set to 9 min order to achieve a good balance between SE accuracy and computational time cost (De Luca et al., 2018b). Moreover, the maximum buildable height was set to 30 m.

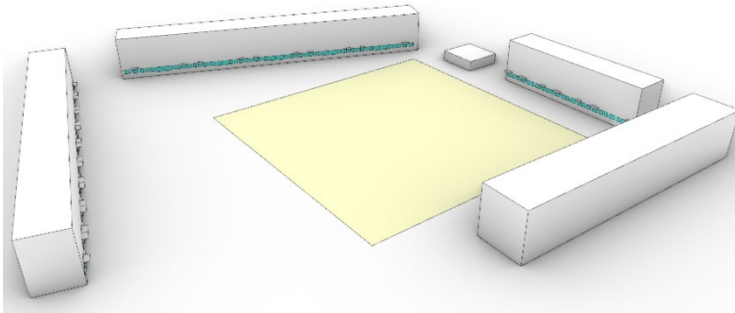


Figure 3. Virtual urban environment for Tallinn case study.

2.1.2 Building envelope generation

Once the different SEs have been created, the new building volumes can be generated extruding a selected floor plan. Thus, the following step is to generate optimal windows for the new building facades. Nowadays, facades with high window to wall ratios (WWRs) are a common solution at northern latitudes due to the lack of sun hours during the winter and the importance of the view to the outside. The component used to select the sun vectors requires windows as simple surface geometry, which are used for sun hours and radiation analyses. The distance between window centroids was set to 3 m. The floor plan considered for the main cases study is a linear floor plan typology defined by ASHRAE (Dogan et al., 2015) with different number of divisions: 3, 4, and 5 (Figure 4). Moreover, different orientations (from south to south-west every 45 degrees counterclockwise) are chosen in order to study its effect on the building performance.

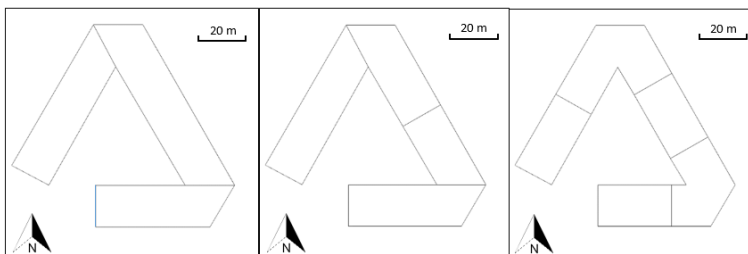


Figure 4. Different number of floor plan divisions (south oriented): 3, 4, and 5 (from left to right).

2.1.3 Sun hours and radiation analysis

The third phase consists of sun light hours and incident solar radiation analysis of the new building. The objective of this part of the proposed workflow (Figure 2) is to study how the urban environment affects the SA and solar radiation received by the new building. In this analysis, surroundings and new building must be provided as input in *SunVectSel* component as urban context. Windows created in the previous phase are also used. To use *SunVectSel* for this sun hours and radiation analysis is necessary to define an auxiliary plot different from the plot used for the main cases study defined in the first phase of the workflow since it is not necessary to generate any *SE* in this step. However, the rest of the settings (dead angle, minimum solar altitude, weather files, time steps, etc.) are the same of those defined in section 2.2.1.

The outputs of this phase are the building performance indicators calculated in relation to the visible sun positions and the incident solar radiation for each time step and window. These performance indicators are:

- Volume ratio (V_r) (-) as the relation between the total volume of the new building and the volume of the SE,
- Window ratio (W_r) (-) as the relation between the number of windows of the new building that fulfill the SA requirements and the total number of windows,
- Mean incident solar radiation ($mISR$) (W/m^2) as the mean (for the analysis periods defined in section 2.1) incident solar radiation received by the windows of the new building that fulfill the SA requirements.

Thus, knowing V_r , W_r , and $mISR$ for the new building several aspects can be determined: (1) how its volume is fitting the SE volume; (2) which ratio of the total facade area is fulfilling the SA requirements, and (3) the level of solar radiation exposure of the facade.

2.1.4 Building performance assessment

In this last phase of the workflow, the building performance indicators are used to calculate the objective variables, which are the variables of the proposed objective linear function F (2) that represent the building performance. Thus, it is possible to compare building designs through the value F (fitness value). The objectives of the evaluation formula (2) are: maximization of Vr' (OV) (3); maximization of Wr' (OW) (4); minimization of $mISR$ (OI) (5). The values of these objective variables are between 0 to 1 (6) and they represent the level of fulfillment of the building i within a set of n possible new buildings (1, 2, ..., i , ..., n).

$$F(Vr'_i, Wr'_i, mISR'_i) = \alpha Vr'_i + \beta Wr'_i + \gamma mISR'_i \quad (2)$$

$$Vr'_i = \frac{Vr_i}{\max(Vr_i)} \quad (3)$$

$$Wr'_i = \frac{Wr_i}{\max(Wr_i)} \quad (4)$$

$$mISR'_i = 1 - \frac{mISR_i}{\max(mISR_i)} \quad (5)$$

$$\alpha + \beta + \gamma = 1 \quad (6)$$

The coefficients α , β , and γ are the weight factors whose values depends on the chosen criteria. For the case study, different criteria were taken into account to evaluate the fitness value of each building design (Table 2). The fitness value is always between 0 and 1. Value 1 is associated to an ideal building performance, and that would mean that the new building fulfills all the objectives previously mentioned at the same time.

In summary, the workflow is applied to one case study (Tallinn case), five sorting methods (Table 1), one floor plan typology with three number of divisions (3, 4, and 5), and eight different orientations (from South to North-West every 45°). Moreover, these 120 cases are evaluated according to eleven multi-objective criteria (Table 2) in order to evaluate which criteria offers the best trade-off building performance.

Table 2. Coefficients of the objective function for different criteria. OV = Volume maximization, OW = Solar access maximization, and OI = Solar incident radiation minimization.

	OV(α)	OW(β)	OI(γ)
C1	1	0	0
C2	0	1	0
C3	0	0	1
C4	0.5	0.5	0
C5	0.5	0	0.5
C6	0	0.5	0.5
C7	0.3	0.3	0.3
C8	0.7	0.3	0
C9	0.3	0.7	0
C10	0	0.7	0.3
C11	0	0.3	0.7

2.2 Creation of rules of thumb and prediction formulas for room-level design decisions

In this section, the parametric models used to generate rules of thumb (section 2.2.1) and prediction formulas (section 2.2.2) for room-level design decisions, which constitute the second phase of the innovative workflow proposed in this thesis, are presented in detail. The case study for the application of the prediction formulas is explained in section 2.2.2.1. In addition, thermal model for overheating simulations (2.2.5), climate conditions (2.2.3), and overheating risk criterion (2.2.4) are described.

2.2.1 Parametric studies to develop rules of thumb

The aim of this case study is to achieve the following objective: to investigate the effect of different daylight assessment criteria on the combined fulfillment of daylighting and overheating requirements and its implications for the design of residential and office rooms in Estonia (Paper II). A simulation-based methodology with the single-zone approach was used for the assessment of daylighting and overheating. The first part of this methodology was to generate the room variations from the room parameters. The second step was to run the daylight simulations (DIVA for Rhino) using different assessment criteria, sDA, DF_{mean} , and DF_{min} , for residential and office rooms. The validated software Energy Plus was used for overheating simulations. Once the calculations were completed, different daylight criteria were compared. The effect of the window airing on overheating levels was analyzed, and the combined fulfillment of daylight and overheating was analyzed relative to the room parameters.

A parametric model of a generic residential/office room was created in Grasshopper environment that runs within the Rhinoceros 3D computer-aided design (CAD) application. The model generated two geometrical models (one for daylight and another for thermal indoor climate simulations) using different room parameters (Figure 5). The building typology used is a common typology in Tallinn (TUT nZEB Research Group, 2017). The building has five floors and a total height of 17 m, with the ground floor occupied by commercial facilities and four regular floors with 2.8 m floor-to-ceiling distance. The test room is located in the middle of the second and third floors to obtain an average obstruction by the surrounding buildings. The surrounding buildings are modeled as a continuous facade of the same height of the test building (17 m) and located at 45 m from the center of the test room toward four cardinal directions with a typical high-density city center setting and a sparse new development setting in Tallinn.

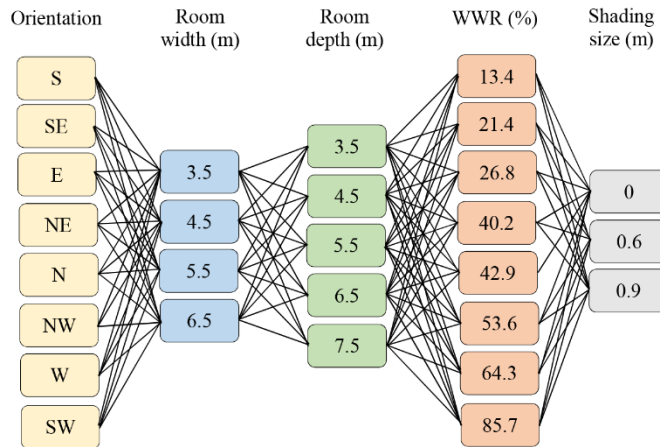


Figure 5. Diagram of room parameter combinations.

The room size parameters and number of orientations were selected to obtain a representative sample of typical residential living rooms and office rooms in Estonia. The small 3.5 m × 3.5 m rooms represent a single-employee office of approximately 12 m². Intermediate rooms represent living rooms and medium-size offices with an area of 20–40 m². The larger rooms with a size of 6.5 m × 7.5 m represent large offices of ~50 m².

The window sizes used in this study represent typical floor and regular sill (0.9 m from the floor) windows used in residential and office buildings in Estonia (TUT nZEB Research Group, 2017). The window height can be 1.5 m or 2.4 m while the distance from the upper frame to the slab level is 0.37 m. The maximum width for a single glazed area is 1.5 m. WWRs values were calculated considering a frame width of 5 cm for each window (without dividers).

The different shading systems considered in the model are illustrated in Figure 6. Thus, no shading system was considered for rooms facing north (N) because direct sunlight is not relevant for that orientation. However, for south (S), southeast (SE), and southwest (SW) orientations, fixed horizontal shading was used. Apart from horizontal shading, fixed vertical shadings were used in the east (E), northeast (NE), northwest (NW), and west (W) orientations. The reason for the different layout of shading devices for south, southeast, and southwest (horizontal) orientations and all the others (vertical and horizontal) is that horizontal shadings perform well for southerly orientations, and vertical shadings perform well for easterly and westerly orientations due to the low sun angle. In this study, the horizontal shadings for southerly orientations were extended on the side to increase protection from direct sunlight and also when the sun is not perpendicular to the façade; the vertical shadings for easterly and westerly orientations were added the horizontal overhang to increase protection, creating a “crate” system that is also recommended in the literature (DeKay and Brown, 2001; Haglund, 2010). The selected sizes for the shading device depths of 0.6 m and 0.9 m correspond to the recommended optimal sizes of shading in relation to window height (maximum 0.4 h, where h is the height of the window) (TUT nZEB Research Group, 2017). The source of the fixed shading device is the facade plane.

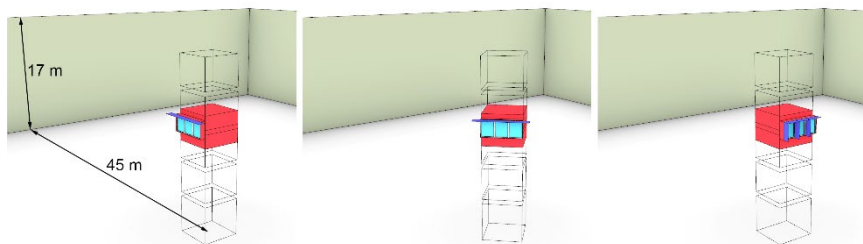


Figure 6. Modeled 3.5 m × 3.5 m rooms S, SE, and E oriented for the daylight analysis (shading size of 0.6 m).

The Radiance parameters used for the sDA and DF simulations were chosen following the recommendation made by Reinhart (Illuminating Engineering Society and The Daylight Metric Committee, 2013). The minimum DA illuminance threshold was defined according to the requirements of the Estonian standard EVS 894:2008/A2:2015, which are 300 lux and 500 lux for residential and office rooms, respectively. The weather data for sDA simulations were obtained from the Tallinn-Harku meteorological station for the year 2014 (described in section 2.4). The occupancy schedule used for climate-based daylight assessment in office rooms is from 08:00 to 18:00 during weekdays as required by the method LM-83-12 (Illuminating Engineering Society and The Daylight Metric Committee, 2013). For residential rooms, an “always occupied” schedule was used because residential buildings are assumed to be occupied all day throughout the week. CIE overcast sky conditions were considered for DF calculations by DIVA (DAYSIM).

The daylight analysis grid is located at 0.8 m height from the floor and the spacing between the grid points is 0.5 m (Illuminating Engineering Society and The Daylight Metric Committee, 2013). DIVA is a Grasshopper plug-in for Rhinoceros that uses the validated software DAYSIM (Radiance-based software) for daylight calculations (Jakubiec and Reinhart, 2011; Reinhart and Pierre-Felix, 2009; Reinhart and Herkel, 2000). Specifically, DIVA components “daylight factor” and “annual daylight” were used to assess the daylight intensity according to the criteria of interest presented in section 2.2.

In parametric analysis, three different daylight assessment criteria were considered (DF_{mean} , DF_{min} , and sDA). The DF_{mean} criterion requires a minimum mean DF of 1.5% and 2.0% for residential and office rooms, respectively. IES LM-83-12 defines a minimum sDA of 55% (for a DA threshold of 300 lux for all types of buildings). Thus, at least 55% of the area is lit with at least 300 lux in 50% of the occupied hours. For office rooms, a DA threshold of 500 lux was considered instead of 300 lux, as recommended by the European lighting standard EN12464-1 (European Committee for Standardization, 2011). For both, residential and office test rooms, interior finishing materials had standard diffuse reflectance values, commonly used for daylight simulations when real building material data are not available (De Luca et al., 2018a; Dogan and Park, 2019; Reinhart, 2018). The reflectance of the opaque surfaces in the model is shown in Table 3. Moreover, triple glazed windows with 18 mm gap (CalumenLive, 2021) were considered because of their reliability in terms of cost and energy performance within the Estonian context (Pikas et al., 2015; Thalfeldt et al., 2017, 2013).

Table 3. Reflectance values for opaque surfaces recommended by the European standard EN17037 for daylight simulations (European commission, 2018).

Surface	Reflectance (-)
Interior walls	0.5
Floor	0.2
Ceiling	0.7
External floor	0.2
External facade	0.3

The Grasshopper plug-in ArchSIM (Dogan, 2014) was used to define the model for thermal calculations at residential rooms described in section 2.7. The .idf file generated by ArchSIM was edited and set up all the desired parameters such as the number of warming days, frame width, or boundary conditions of each surface. The edited the .idf file was used as input to the validated software Energy Plus version 8.4 (U.S. Department of Energy, 2015). After simulations, a DH metric value was calculated for each room combination using the hourly mean air temperature (T_h) during the warm season (section 2.3).

2.2.2 Parametric studies to develop daylight and overheating prediction formulas

The aim of this case study is to achieve the following objective: to develop prediction formulas that help architects and practitioners to estimate overheating risk levels and daylight provision for different climate conditions and regulations (Paper III). A simulation-based methodology with the single-zone approach was used for the assessment of daylighting and overheating in residential buildings. The only differences between this parametric model and the one described in section 2.8.2 are the following:

- Surrounding buildings were considered at a distance of 17 m from the floor level of the test room, using a continuous facade and varied height to model different mean obstruction angles (θ_s) from 0° to 35.0° (Figure 7);

- The visible transmittance of the glazing system was varied from 45% to 80% and the g-values, which are associated to different glazing systems commonly considered within the Estonian context (Simson et al., 2017b; Thalfeldt et al., 2013), were varied from 0.24 to 0.61 (with U-values from 0.21 to 1.4 $W/m^2 \cdot K$) (Figure 7).

- No shading system was considered in the parametric model because one of the main principles of the coupled method to be used during early stage design is to maximize daylight provision and quantify the potential overheating risk while minimizing design costs related to unnecessary shading system.

- Only minDF-based daylight assessment criterion (section 2.2) was considered in this case study and DH-based overheating assessment criterion (section 2.3);

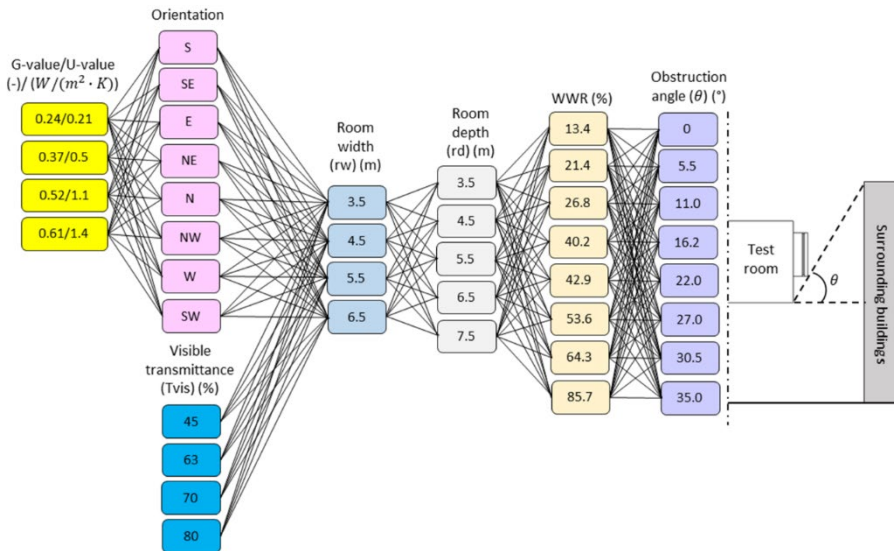


Figure 7. Diagram of room parameter combinations and representation of the obstruction angle ϑ for a generic room. Window-to-wall ratio=WWR. An obstruction angle is considered null ($\vartheta = 0^\circ$) when the roof of the surrounding building/external obstruction is at the same level or below the floor level of the test room. The total number of room combinations is 5120 and 40960 for daylight and thermal simulations, respectively.

The European standard EN 17037:2018 proposed two methods for the daylight assessment. For this parametric analysis, only the minDF-based criterion (DF_{\min}) was considered. Thus, the fulfillment of minimum daylight provision according to the static method defined by the EN 17037 consists in the simultaneous fulfillment of two conditions. The first condition (Cd1) is fulfilled if the minimum DF value for the first half of the reference plane closer to the window (minDF1) is higher than a target value (minDF1t), which depends on each EU country (1.5%–2.8%) (e.g. minDF1 \geq 2.2% for Estonia, minDF1 \geq 1.8% for Spain, etc.). The second condition (Cd2) is fulfilled when the minimum DF value for at least the 95% of the entire the reference plane (minDF2t) should be higher than a target value, which depends on each EU country (0.5%–0.9%) (e.g. minDF2 \geq 0.7% for Estonia, minDF2 \geq 0.6% for Spain, etc.) (Figure 8).

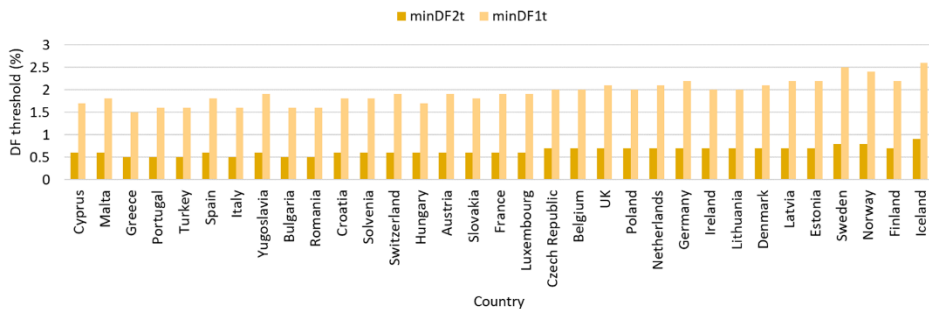


Figure 8. Minimum thresholds for different European countries defined by the European standard EN 17037 for target DF for the first half of the reference plane closer to the window (minDF1) and minimum target DF for at least the 95% of the reference plane (minDF2).

The coupled method based on the developed prediction formulas were combined in order to choose design decisions that help to achieve a good balance between daylight provision and overheating risk protection in a new residential building in Estonia. These design decisions consist of the selection of window's size and thermal properties for each designed bedroom and kitchen-living rooms. On one hand, a good level of daylight provision is achieved when the minimum requirement according to the minDF-based method defined by the European standard EN 17037 is fulfilled. On the other hand, the maximum overheating risk level is based on the DH-metric, which has the potential to be adopted by EU countries as overheating metric in the future. It was considered the design of a multi-store building located in a middle-density urban area of Tallinn, Estonia (Latitude: 59.39°, Longitude: 24.67°) (Figure 9). The building has a length of 82 m and a width of 17 m. The number of floors is 10 floors where the first floor is habilitated for commercial, building access, and parking uses. There are 12 apartments of 94.5 m² (13.5 m width x 7 m depth) per floor and the floor height is 3 m where 2.8 m is the room height. Each apartment has one 4 x 6 m bedroom and one 6 x 6 m open kitchen-living room. The mean obstruction angles are between 0° (higher floors) and 20° (lower floors).

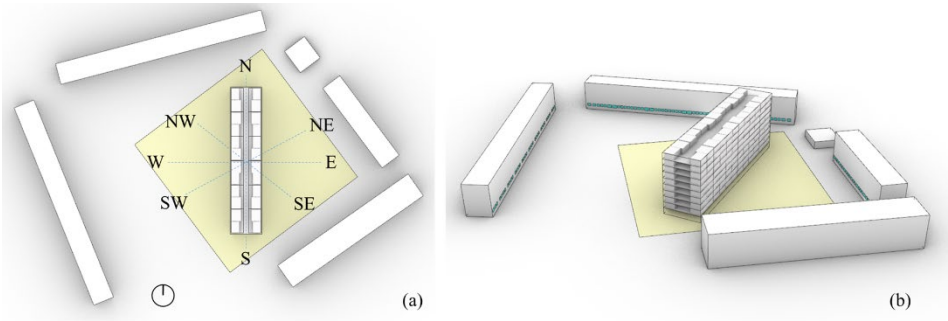


Figure 9. Top view (a) and perspective view (b) of the building (E-W) and surrounding environment used in the case study in Tallinn, Estonia.

2.2.3 Climate conditions

The room combinations from both parametric models analyzed in this thesis are within the Estonian context, specifically the capital of Estonia: Tallinn (Latitude: 59.4370° N, Longitude: 24.7536° E), which is located at the north coast of the country. Tallinn has a warm humid continental climate (Dfb) according to Köppen-Geiger classification (CLIMATE-DATA.ORG, 2021). The average annual temperature is +6.4°C and the average temperature during the warm season is +16.2°C (Estonian Weather Service, 2021a). The wettest months are July and August (average precipitation of 82–85 mm), while the driest months are from March to May with an average precipitation of 35–37 mm (Estonian Weather Service, 2021b). The average number of sun hours is 1922.7 during the year, where December is the darkest month with 20.7 sun hours and July is the most sunlit month with 312.1 sun hours (Estonian Weather Service, 2021c).

For the thermal calculations conducted in this thesis, climate conditions related to the year 2014 were considered (Figure 10) for thermal and daylight dynamic calculations. The warm season of the year 2014 reached higher outdoor temperatures than the typical climate of the Estonian region (TRY). The TRY is built from selected monthly weather data from 1970–2000. Therefore, TRY temperature profile is smoother than 2014 temperature profile (Figure 10a).

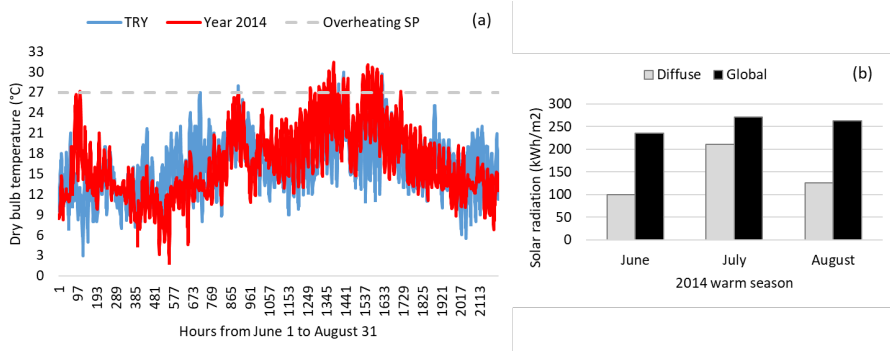


Figure 10. Dry bulb temperature (a) and solar radiation profiles (b) for different weather data sets. SP = set point.

2.2.4 Assessment criterion for overheating risk

Estonia has specific overheating requirements that must be met if there is no mechanical space cooling system in a new or a renovated building. Window airing is not permitted in overheating simulations of non-residential buildings. Installation of openable windows is not regulated by these requirements. In this thesis, overheating risk in residential buildings with natural ventilation (window airing technique) is analyzed. Overheating requirements in Estonia are based on the metric degree-hour (DH) ($^{\circ}\text{C}\cdot\text{h}$) (Eq. (7)), which represents the accumulation of the hourly indoor mean air temperature (T_h) excess (related to a temperature set point of $27\text{ }^{\circ}\text{C}$) during a specific period of the warm season (June 1–August 31). The use of simulation-based methodology is recommended to assess summer thermal comfort in Estonian residential buildings (Hamburg and Kalamees, 2019). Thus, the expression to calculate the DH metric from simulated T_h values of a residential room during the warm season is the following:

$$DH = \sum_{h=1}^N (T_h - 27) (^{\circ}\text{C} \cdot \text{h}) \quad (7)$$

Where N is the number of occupied hours (from June 1 to August 31). According to the Estonian regulations, DH threshold must not exceed $150\text{ }^{\circ}\text{C}\cdot\text{h}$ ($\text{maxDH}_{\text{EST}}$) in residential buildings (Estonian Government, 2012).

2.2.5 Thermal model for overheating simulations

The validated software Energy Plus was used for thermal indoor energy simulations required by cases studies explained in sections 2.8.2, 2.8.4, and 2.8.5 (U.S. Department of Energy, 2015). The hourly mean air temperature (T_h) was the variable of interest to assess the overheating risk in terms of the DH metric (section 2.3). Construction materials for the walls, slab, and floor are shown in Table 4. Slab floor and interior walls consist of 250 mm layer of concrete. The external wall is composed of three layers of concrete and expanded polystyrene, with a thermal transmittance of $0.128\text{ W}/(\text{m}^2\text{K})$. Moreover, triple glazed windows with 18 mm gap (CalumenLive, 2021) was considered for section 3.2.1 because of their reliability in terms of cost and energy performance within the Estonian context (Pikas et al., 2015; Thalfeldt et al., 2017, 2013). Windows were modeled using a simplified model, which has been proved to be more conservative than the detailed model for overheating risk calculations (Thalfeldt et al., 2016). Window simplified model is based on constant properties: solar/visible transmittance, U-value, and internal/external emissivity values. These optical and thermal properties were not included as independent variables of the parametric model (section 3.2.2), mainly because architects and designers are used to follow recommendations about cost-optimal window constructions for different climate contexts (Saadatian et al., 2021b, 2021a; Simko and Moore, 2021).

Slab floor and interior walls were considered as adiabatic surfaces (Abel Sepúlveda et al., 2020). However, it was considered heat transfer through the exterior wall and solar exposure. Required usage profiles for internal gains in residential buildings by Estonian regulations can be seen in Figure 11. For a multi-apartment building, the number of square meters per person is 28.3 (Estonian Government, 2015) and the mean level of activity is 1.2 MET (Table 5).

The consideration of infiltration is mandatory by Estonian regulations. The infiltration air flow rate (q_i) is calculated using Eq. (8):

$$qi = \frac{q_{50}}{3.6x} A \quad (8)$$

Where A is the area of the building envelope in m², q₅₀ is the average air leakage rate of the building envelope determined by means of an air leakage test at a pressure difference of 50 Pa, which characterizes the air tightness of the building envelope, was set to 3 m³/(h·m²) according to the same regulation, and x is the building factor set to 20 since the typical building in Tallinn has four stories (Estonian Government, 2015).

Table 4. Thermal and optical properties of the building envelope.

Element	Construction	Thermal transmittance (W/(m ² K))	g value (-)	Visual /Solar Transmittance (-)	Exterior/Interior emissivity (-)
External wall	Concrete 150 mm Expanded Polystyrene 280 mm Concrete 50 mm	0.128	-	-	0.9/0.9
Floor slabs, Internal Walls	Concrete 250 mm	3.59	-	-	0.9/0.9
Window frame	Aluminium 50 mm	0.5	-	-	0.9/0.9
Window (CalumenLive, 2021) (sections 3.2.1.2 and 3.2.1.3)	Triple glazing	0.5	0.37	0.63/0.27	0.9/0.9
Window constructions (section 3.2.2)	Variable	[0.21, 0.5, 1.1, 1.4]	[0.24, 0.37, 0.52, 0.61]	[56, 63, 56, 78]	0.9/0.9

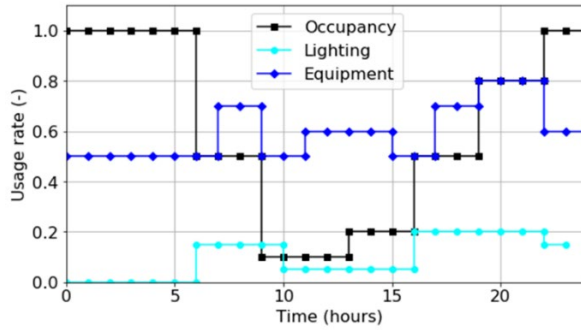


Figure 11. Usage profiles of occupancy, lighting, and equipment for residential buildings in Estonia (Estonian Government, 2015).

Table 5. Internal gain parameters for Estonian residential buildings.

People density	0.0353 p/m ²
Metabolic Rate	1.2 MET
Equipment power density	3 W/m ²
Lighting power density	8 W/m ²
Dimming Control	OFF
Target Illuminance	300 lux

HVAC settings used in the thermal model are displayed in Table 6. Mechanical ventilation was also considered: minimum fresh air of 14.15 L/s per person and minimum fresh air of 0.5 L/s per area (m²). Airing position of the window was set to 10% as defined by Simson et al. (Simson et al., 2017a). With a set point of 25 °C and an openable area of 10% for the window, low heating energy is needed during the warm season due to the occasional low exterior temperatures in Tallinn. The heating system must be switched ON with a set point of 21 °C for residential buildings (Table 5).

Table 6. HVAC settings for residential buildings in Estonia.

Heating system (SP)	ON (21 °C)
Cooling system (SP)	OFF (-)
Window airing (SP)	ON (25 °C)
Mechanical ventilation	Always ON
Minimum Fresh Air per Person	14.15 (L/s/p)
Minimum Fresh Air Area	0.5 (L/s/m ²)
Heat recovery temperature efficiency	80%

2.3 Benchmark of methods for annual glare assessment

In this section, the test room (section 2.3.1), daylight calculation methods and Radiance parameters (section 2.3.2), selected fenestration systems (2.3.3), and their optical characterization (section 2.3.4) are explained in detail (Paper IV). All these methodological decisions are the basis of the different analyses (Table 7) (section 3.3) that support the efficient assessment methods for glare protection according to the EN7037. These glare assessment methods constitute the third phase of the innovative workflow proposed in this thesis.

Table 7. Summary of all the analyses conducted for the development of efficient glare assessment methods. Sec. = section, DCM = daylight calculation method, $r\Delta$ = relative deviation, Glaz = solar-control double glazing unit, TSs = time steps, and $a\Delta$ =absolute deviation. The time steps are for February 5, Freiburg, Germany. VA = Viewing angle refers to the angle between viewing direction and window plane.

Sec.	TSs	VA	CFSs	Radiance material	DCM	Metrics	Output
3.3.1	11:00	-	T100, T5, T3, T1	BRTDfunc	3pm 5pm <i>rtrace</i>	$r\Delta E_v$ (%)	Optimal Radiance parameters
3.3.2	11:00 16:00	45°	T5, T3, T1	BRTDfunc, t45a, t45, t39a, t39, t38a, t38, t37a, t37, Klemsa	3pm 5pm <i>rtrace</i>	DGP (-) E_v (lux)	Suitable material representations
3.3.3	Annual	0°	T1/T3/T5	BRTDfunc	5pm <i>rtrace</i>	CPU time	Fastest daylight calculation method
3.3.4	Annual	45°	Glaz +T1 Glaz +T3 Glaz +T5	Klemsa	5pm <i>rtrace</i>	CPU time (h) $a\Delta fDGp_t$ (%)	Optimal time step sampling strategy

2.3.1 Test room

This part of the study considers a south-oriented test room with two different viewing directions, parallel to the window plane and 45° towards the window (Figure 12). Glare protection criterion was considered according to EN 17037: the annual percentage of discomfort glare hours (fDGpT) should be lower than 5% for a shading device to protect against glare. Glare hours are considered as the occupied hours with an associated DGP above a threshold DGpT: 0.35, 0.40, and 0.45 for high, medium, and minimum level of glare protection, respectively (European comission, 2018). All the opaque surfaces were modeled with the Plastic material primitive in Radiance with reflectance values

recommended by the European standard EN17037 (Table 3). The room is located in Freiburg, Germany (latitude: 48 °N). The day of study for the static analyses is February 5 because of the low solar altitude, which is critical for daylight glare. No exterior obstacle is considered in this case study. It was assumed clear sky conditions for all the simulations (CIE clear sky with the presence of the sun) as is recommended by the EN 17037 for the verification of the glare protection capabilities of shadings for a critical situation (European comission, 2018). In fact, typical weather files might hide a glare risk if, for a particular situation with a critical sun position, the weather file indicates a cloudy sky. Therefore, clear skies should be considered in the simulation for annual glare analyses. This represents a worst-case scenario which is suitable for choosing a glare protection device.

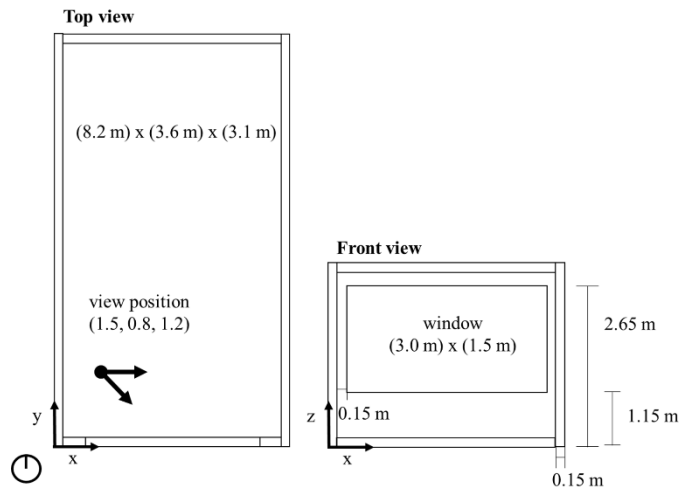


Figure 12. Geometrical information for the south-oriented office room, occupant's position and viewing directions.

2.3.2 Daylight calculation methods and Radiance parameters

It was used the Radiance software v5.4.a for illuminance calculations and renderings ("Radiance 5.4a (2020-09-06)," n.d.). Specifically, the chosen daylight methods were the classic ray-tracing-based daylight method *rtrace* (Ward, n.d.) and matrix-based methods 3pm and 5pm (Lee et al., 2018a). A BSDF Klems data set in .xml format (transmission matrix) is required in 3pm and 3pmD simulations while CFS in cds phase and *rtrace* method can be modeled with different Radiance materials explained in sections 2.2 and 2.3. One of the difficulties in applying these methods is the selection of Radiance parameters for the simulation. It was studied the sensitivity of ambient bounces (ab parameter) and ambient divisions (ad parameter) when using the daylight methods *rtrace* and 3pm (Ward, n.d.). In addition, it was analyzed the sensitivity to the ad parameter and the number of Reinhart sky-patch subdivisions (MF parameter) in 5pm calculations (Inanici and Hashemloo, 2017b). The parameters ab and ad determine the accuracy of the calculation for indirect light from the sky. The MF parameter is related to the accuracy of the sun positions and sky modelling in the direct sun coefficient calculation (cds) within the 5pm simulation. Additional Radiance parameters used for the calculations in this investigation can be seen in Table 8. These Radiance parameters are

recommended in several Radiance tutorials (McNeil, 2014, 2013) and previous investigations (Brembilla et al., 2019; Reinhart and Herkel, 2000). It was used 25 cores of a Linux machine cluster of 56 CPUs to run all the simulations (Processor Intel(R) Xeon(R) CPU E5-2697 v3 @ 2.60GHz).

Table 8. Radiance parameters used for glare simulations by rtrace and 5pm. cds refer to the direct coefficient sun simulation. 3pmD refers to 3pm simulation of the 5pm considering only the direct component of the solar radiation.

Radiance parameters	
	Sky generation: +s (CIE clear sky) -m 1 (MF=1)
3pm	Daylight matrix: -n 25 -c 1500 -ab 4 -ad 1024 -lw 9.76e-4
	View matrix: -n 25 -c 10 -ab 10 -ad 65536 -lw 1.53e-5 -pj 0.7 -x 900 -y 900
	Sky generation: +s (CIE clear sky) -m 1 (MF=1) -d (direct component of the sun)
3pmD	Daylight matrix: -n 25 -c 1500 -ab 0 -ad 1024 -lw 9.76e-4
	View matrix: -n 25 -c 10 -ab 1 -ad 65536 -lw 1.53e-5 -pj 0.7 -x 900 -y 900
5pm	Sky generation: MF=3 (1297 sky subdivisions) (Subramaniam, 2017)
	Daylight coefficient matrix: -n 25 -ab 1 -ad 1024 -pj 0.7 -dc 1 -dt 0 -dj 0 -x 900 -y 900 MF=3
rtrace	-n 25 -lw 1/ad -aa 0.1 -as 1000 -x 900 -y 900
	(The selection of -ad and -ab parameters is justified in section 3.3)

2.3.3 Selection of fenestration systems

In this case study, synthetic fabrics with different optical properties were considered. This allows us to parametrize important characteristic of shading devices such as the specular/diffuse split and the cut-off angle (minimum incident angle for which a CFS completely blocks specular transmission), which are used in the EN 17037 for classification. Fabrics are in general anisotropic depending on the weaving direction. However, for the purposes of this analysis, fabrics are modeled with the Radiance primitive BRTDfunc as being isotropic (due to random or uniform microgeometry (Ward et al., 2021)) with a main view-through component. The BRTDfunc material considers separate specular and diffuse components and a cut-off angle. This approach is a modified version of the analytical Roos model for fabrics defined by Wienold et al. (Wienold et al., 2017). BSDF of these synthetic fabrics are then generated for the analysis.

The accuracy of the simulations with different BSDF representations is assessed as compared with the simulation results using the original material definition (i.e., the BRTDfunc model is considered the “gold standard” in this particular study). One set of fabrics are considered, Table 9 shows the main optical properties for three synthetic fabrics (normal-normal transmittances: 5%, 3%, and 1%) and a representation of a window hollow (no glazing nor shading) named T100 (100% transmission). The cut-off angle of fabrics T5, T3, and T1 was set to 70°. The diffuse reflectance was set to 60% related to a light grey colored fabric.

Table 9. Optical properties for BRTDfunc model for 4 synthetic fabrics (modeled by Roos parameters $p = 4.0$, $q = 2.9$ (Karlsson and Roos, 2000)). τ_{nn} is the normal-normal transmittance, τ_{ndif} is the normal-diffuse transmittance, and ρ_{ndif} is the normal-diffuse reflectance.

Name	τ_{nn} (-)	τ_{ndif} (-)	ρ_{ndif} (-)	Cut-off angle (°)
T100	1.0	0	0	90
T5	0.05	0.15	0.60	70
T3	0.03	0.15	0.60	70
T1	0.01	0.15	0.60	70

2.3.4 Optical characterization of complex fenestration systems

For the optical characterization of fabrics considered for glare calculations (case study explained in section 2.8.6), BSDF data sets were generated using direct functional sampling (Ward, 2013; Ward et al., 2021), as an alternative to the virtual goniophotometer approach (McNeil, 2015; McNeil et al., 2013) and implemented in the Radiance genBSDF program. Direct functional sampling consists of applying the mathematical function that represents the optical behaviour of the material (e.g., the BRTDfunc), sampling rays for each incident and outgoing projected solid angle as required by the BSDF format (e.g. tensor tree generation 7 or Klems). By default, complete sampling consists of 1024 rays per solid angle. However, an adaptive sampling mechanism is in place to reduce the sampling time. Tensor-tree BSDFs were generated using the bsdf2ttree program, where the incident and scattered ray pairs are sampled over each solid angle depending on the tensor-tree resolution. A subtended apex angle of 0.533° (the solid angle of the solar disk) is assumed for direct-direct transmission. Rays scattered beyond this solid angle are allocated to the direct-diffuse transmission. Figure 13 shows that, with an adaptive sampling algorithm, increasing the resolution of the tensor tree decreases the RMSE of direct-hemispherical transmissivity between the BSDF and the analytical function.

The following angular resolutions were analyzed: Klems basis, t37, t38, and t39. Although only isotropic materials are considered in this study, an anisotropic tensor-tree t45 was included in the comparison. For a generic tensor tree -t3/-t4 k, k refers to generation of 22k directions per hemisphere (Lee et al., 2018a). BSDF datasets were modeled with BSDF and aBSDF materials in Radiance. The aBSDF material definition includes a peak extraction algorithm, which separates the transmission peaks, associated with the view-through component of the transmission, from the rest of the BSDF dataset (Ward et al., 2021). Proxy geometry of fabrics were not considered because the storage of their tiny geometry leads to very large computational consuming simulations. Therefore, these material definitions were assigned directly to a polygon surface that represents the window.

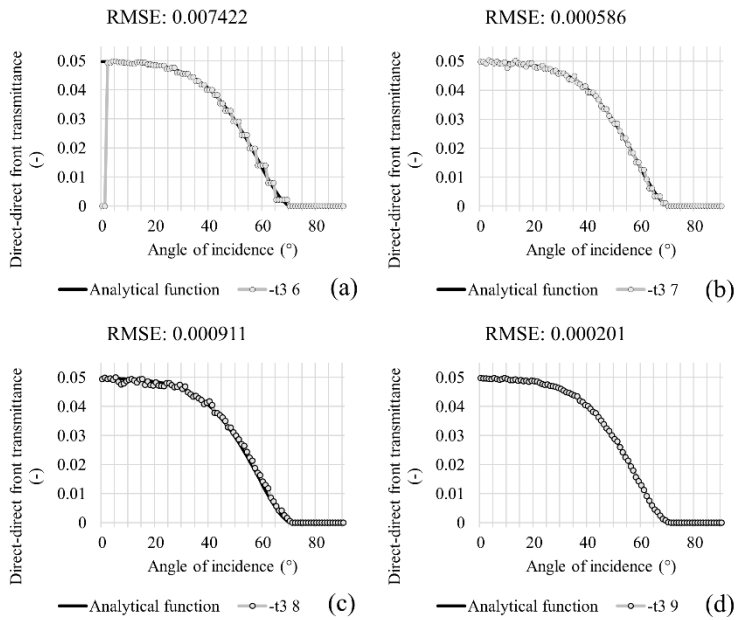


Figure 13. Direct-direct transmittance depending on the angle of incidence for four different isotropic tensor-tree BxDF generated with the Radiance program bsdft2tree. The angular resolution (x) of the isotropic tensor-tree ($-t3\ x$) BxDFs are 6 (a), 7 (b), 8 (c), and 9 (d).

3 Results and discussion

In this section, all the results are presented, analyzed, and discussed. The structure of this section is the following:

- Section 3.1 (Paper I): an example of use of the first phase of the innovative workflow proposed in this thesis is presented. In other words, the building orientation, volume, and windows location are defined by the multi-objective optimization workflow for building envelope presented in section 2.1 that is used for the case study presented in section 2.1.1;

- Section 3.2: Firstly, the rules of thumb for the fulfillment of daylight provision for different assessment criteria (section 3.2.1.1), overheating for different ventilation strategies (section 3.2.1.2), and combined fulfillment of daylight and overheating (section 3.2.1.3) are explained (Paper II). Secondly, the prediction formulas are developed for daylight provision (section 3.2.2.1) and overheating risk (section 3.2.2.2) (Paper III). In addition, an example of use of both prediction formulas is presented and validated in section 3.2.3 (Paper III). The use of either rules of thumb or prediction formulas to help architects and designer to make decision to room-level (e.g. room sizing, window sizing, etc.) constitute the second phase of the innovative workflow proposed in this thesis;

- Section 3.3 (Paper IV): convenient sensitivity analyses to support the recommendation of efficient glare assessment methods, which constitute the third phase of the innovative workflow proposed in this thesis, are developed in this section. As mentioned, for a suitable assessment of DGP-based glare protection metric, it is necessary to calculate properly vertical illuminance and luminance of the field of view. Thus, recommended Radiance parameter for static illuminance simulations are presented and justified in section 3.3.1. Comparison analysis of daylight calculation methods and material models for static glare calculation is presented in section 2.3.2. A criterion to choose daylight calculation method for dynamic glare calculations depending on the required computational time is developed and validated in section 3.3.3. Finally, an evaluation of different sampling strategies for annual glare assessment in terms of computational time and accuracy is presented in section 3.3.

3.1 First phase: defining building orientation, volume, and windows location considering solar access

The values of the objective variables for different criteria (Table 2) used in case study explained in section 2.8.2 can be seen in Figure 14. In these case, five different group of criteria give 5 different optimal solutions:

- The first optimal solution is generated by the 100% volume-weighted criterion (C1),
- The second optimal solution is a 100% SA-based criterion (C2),
- The third optimal solution is generated by a group of criteria based on different trade-off considerations (C3, C5, C7, and C11),

- The fourth optimal solution is generated by a group of criteria based on different trade-off between volume and SA (C4, C8, and C9),
- The fifth optimal solution is generated by a group of criteria based on different trade-off between SA and $mISR$ (C6 and C10).

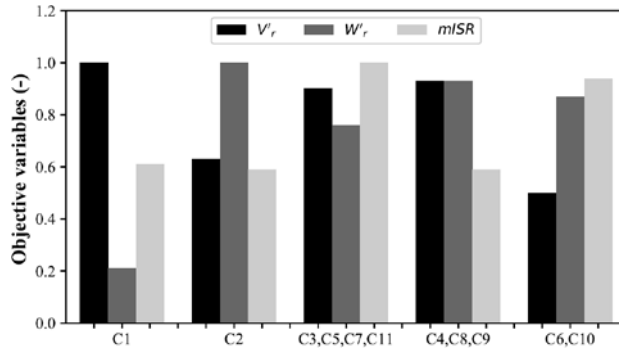


Figure 14. Objective variables values for different criteria in case study explained in section 2.8.2.

The design parameters and the performance indicators for each optimal solution are shown in Table 9. In general, SM 2 and 4 are not recommended for any criteria. The maximization of the building volume ($V_r = 0.24$) is possible by orienting west a floor plan with 5 divisions and considering SM 5 to generate the SE (Figure 15a). Nevertheless, the combination of the SM 1 or 3 with 3 divisions of the floor plan and NW orientation, achieve a low volume fitting with the SE volume $V_r = 0.18$ but high performance in terms of SA ($W_r = 0.87$) and $mISR$ (190.14 W/m^2) (Figure 15e). Moreover, the south orientation combined with a low number of divisions of the floor plan (3 and 4) are associated to high W_r (between 0.84 and 0.97) when SM 1 is considered (Figure 15b and 15d). The only difference between the fifth and the third optimal solution is the number of divisions of the floor plan (4 and 3, respectively). This increment from 4 to 3 divisions of the floor plan generates a self-shadowing phenomenon: the 3% of the whole facade pass to do not fulfill the SA requirement because V_r increases a 5% (Figure 15c and 15e).

Table 9. Design parameters and performance indicators using different criteria (Table 2) for Tallinn case (section 2.8.2).

Criteria	nFPd	Ori.	SM	Vr	Wr	mISR
C1	5	W	5	0.24	0.66	197.39
C2	3	S	1,3	0.19	0.92	197.7
C3,C11,C5,C7	4	NW	1,3	0.23	0.84	188.78
C4,C8,C9	4	S	1	0.23	0.89	197.89
C6,C10	3	NW	1,3	0.18	0.87	190.14

Finally, the third (Figure 14c) and fourth solutions show good trade-off performance. Nevertheless, since the deviations in terms of $mISR$ are around 10 W/m^2 , the fourth optimal solution is the best one (Figure 14d): south-oriented building whose floor plan is divided by 4 sections (SM 1 used for the SE generation) achieve a V_r of 0.23 and the 89% of the facade is fulfilling the SA requirements with a mean incident solar radiation of almost 198 W/m^2 .

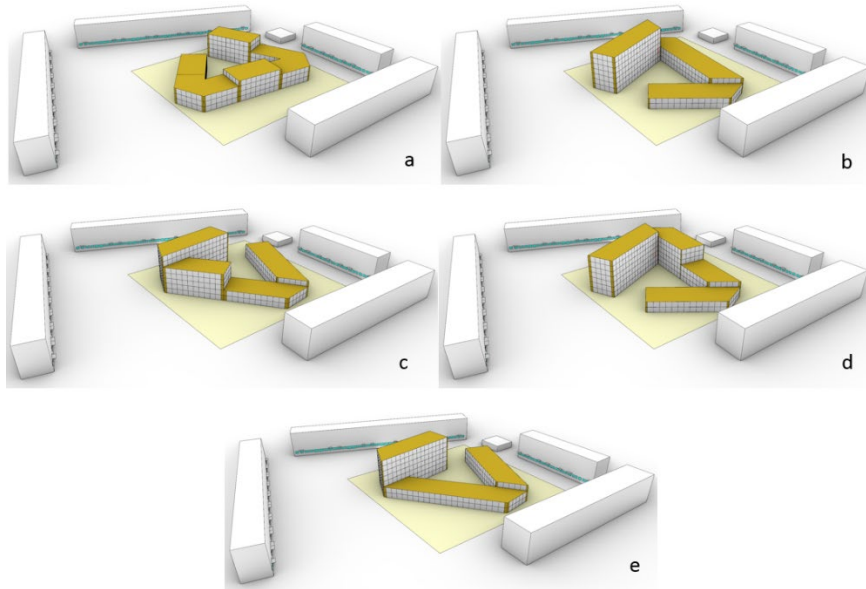


Figure 15. Optimal combinations in Tallinn case.

As seen in this section 3.1, different SEs might fulfill the same SA requirements for a case study. This fact provides flexibility in the early design stages of the architectural design process. In general, considering a large number of possible floor plan divisions, the volumes of the new building can fit better the SE volume. Moreover, the consideration of sorting methods based on larger solar altitudes and sun vectors outside the plot achieve larger SE volume than those based on incident solar radiation. The maximum relative difference in terms of SE volume is almost 50%. Indeed, this difference can be due to the length of the analysis period.

A suitable choice of the design parameters is critical to optimize the new building envelope. If the preferred criteria to design the new residential building is the volume ratio and the SA of the facades, the use of criteria based on trade-off criteria between volume and SA for Tallinn are suitable ones. The optimized building envelope for the case study is shown in Figure 16. The optimal number of floor plan divisions are four and the total floor area is 11617 m^2 . South-oriented floor plan allows good performance between volume and SA of the new buildings (Figure 16): volume ratio higher than 20% and ratio of the facade that fulfill the SA requirements of 89%. This workflow is specially suitable when the SA regulations are strict. First decisions as building orientation, windows location, building footprint, and buildable volumes characterize the solar access of the existing and new buildings. Other requirements related to daylight provision, overheating, energy consumption or glare protection could be fulfilled with a suitable design of interior layout and facade.

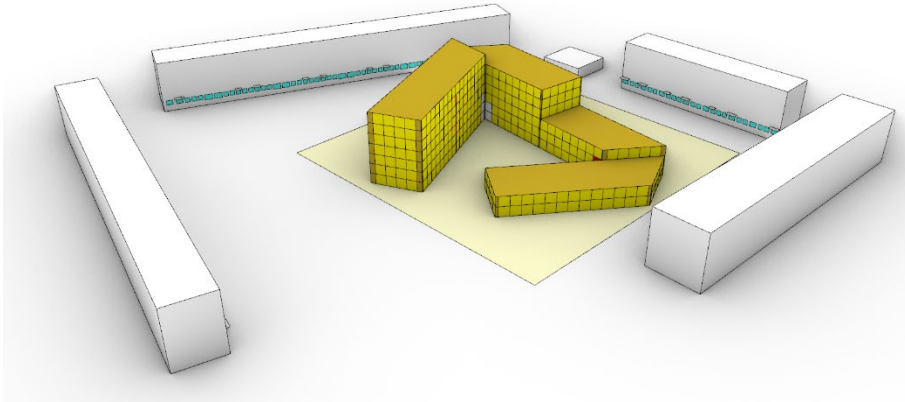


Figure 16. Optimized building envelopes for Tallinn case. Windows in yellow fulfill the SA requirements and the red window has the maximum mean incident solar radiation.

3.2 Second phase: window sizing considering daylight provision and overheating risk

Once the building orientation, volume, location of the windows are defined by the architect or designer by applying the first phase (section 3.1) of the innovative workflow proposed in this thesis, the use of either rules of thumb or prediction formulas to help architects and designer to make decision to room-level (e.g. room sizing, window sizing, etc.) constitute the second phase of the novel workflow proposed in this thesis. Therefore, this section is split into two sections:

- In section 3.2.1 (Paper II), the rules of thumb for the fulfillment of daylight provision for different assessment criteria (section 3.2.1.1), overheating for different ventilation strategies (section 3.2.1.2) and combined fulfillment of daylight and overheating (section 3.2.1.3) are explained.

- In section 3.2.2 (Paper III), the prediction formulas are developed for daylight provision (section 3.2.2.1) and overheating risk (section 3.2.2.2). In addition, an example of use of both prediction formulas is presented and validated in section 3.2.3. Simplified method based on rules of thumb for window sizing

3.2.1 Simplified method based on daylight and overheating rules of thumb for window sizing

3.2.1.1 Rules of thumb for daylight provision at residential and office rooms

According to the results (Figure 17), all the tested room variations that fulfilled the minimum DF of 2.2% for the first half of the reference plane closer to the window also fulfilled the minimum DF of 0.7% for at least 95% of the reference plane. Hence, the minimum DF of 2.2% for the first half of the grid is taken as the critical requirement that ensures the fulfillment of the European standard EN 17037:2018. The percentage of the simulated rooms (3520 combinations) associated with different daylight fulfillment cases is displayed in Figure 17. There is no room that reaches sDA higher than 55% and a

mean DF lower than 1.5 or 2.0 for residential or office use, respectively. In 29% and 32% of the residential and office cases, respectively, the Estonian DF requirement is met, but not the sDA. Nevertheless, there is a 70% agreement between sDA and DF_{mean} for both types of buildings. For residential rooms, the agreement between DF_{mean} and DF_{min} is 58%. There is no room that reaches a minimum DF higher than 2.2% and a mean DF lower than 1.5 or 2.0% for residential or office rooms, respectively. For office rooms, the agreement between DF_{mean} and DF_{min} is approximately 70%, likely due to the stricter DF_{mean} requirement for office use (2.0%) than for residential rooms (1.5%).

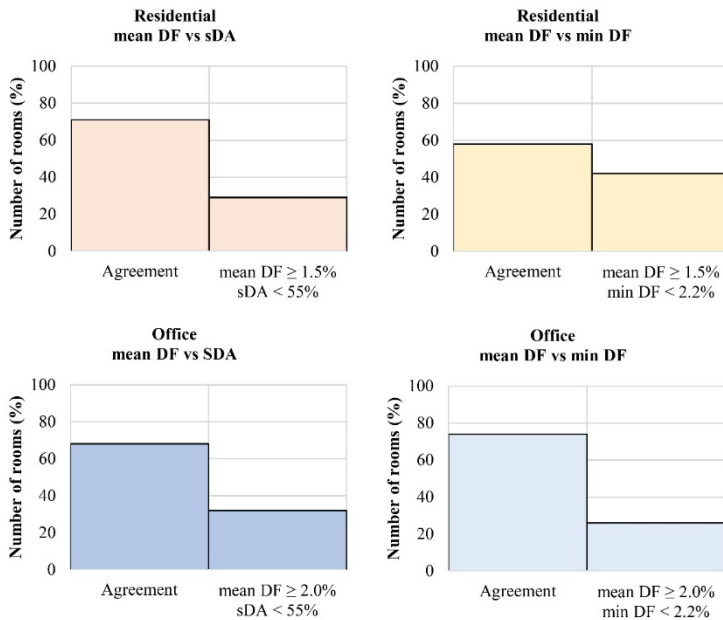


Figure 17. Agreement analysis between different the daylight criteria used (section 2.2).

The minimum WWR (minWWR) to fulfill the daylight requirement for different criteria (DF_{mean} , DF_{min} , and sDA) and office room parameters are presented in Table 10. The IES LM-83-12 is one of the most conservative testing criteria. The NE, NW, and W-oriented office rooms with depths of at least 3.5 m do not fulfill $sDA \geq 55\%$ when shading is used. However, the maximum recommended room depth is 5.5 m when no shading is used (minWWR of 0.86 for S orientation). For shading sizes of 0.6 m or 0.9 m installed in the S- and SE-oriented rooms, the maximum recommended room depth is 4.5 m (minWWR of 0.86). As expected, the shading size is related to the increase in minWWR required for any room combination.

Table 10. Minimum WWR to fulfill the daylight requirements (for DF_{mean} , DF_{min} , and sDA) defined in section 2.2.1 for office rooms.

		Office room depth (m)		3.5	4.5	5.5	6.5	7.5	
Shading size (m)	0 m	DF_{mean}	S,SE,E,NE,N,NW,W,SW	0.27	0.27	0.4	0.4	0.4	
		DF_{min}	S,SE,E,NE,N,NW,W,SW	0.4	0.4	0.86	-	-	
		sDA	S	0.4	0.4	0.86	-	-	
			SE,E,SW	0.4	0.54	-	-	-	
			NE,W	0.4	0.86	-	-	-	
	N, NW	0.54	-	-	-	-			
	0.6 m	DF_{mean}	S,SE,SW	0.4	0.4	0.54	0.54	0.86	
			E,NW,W	0.4	0.54	0.86	-	-	
			NE	0.4	0.54	0.86	0.86	-	
		DF_{min}	S	0.4	0.54	-	-	-	
			SE,SW	0.4	0.86	-	-	-	
			E,NE,NW,W	0.54	-	-	-	-	
		sDA	S,SE	0.4	0.86	-	-	-	
			E	0.86	-	-	-	-	
			NE,NW,W	-	-	-	-	-	
			SW	0.54	0.86	-	-	-	
		0.9 m	DF_{mean}	S,SE,SW	0.4	0.54	0.86	0.86	-
				E,NE,NW,W	0.54	0.86	-	-	-
			DF_{min}	S,SE,SW	0.54	0.86	-	-	-
	E,NE,NW,W			0.86	-	-	-	-	
	sDA		S,SE	0.54	0.86	-	-	-	
E,NE,NW,W			-	-	-	-	-		
SW			0.54	-	-	-	-		

As shown in Table 11, the fulfillment in terms of different daylight requirements in residential rooms is less restrictive than in office rooms: the maximum depth of the office rooms is equal to or less than that of the residential rooms for sDA/DF_{mean} criteria, when the room orientation or shading size is considered, because of the stricter daylight requirements for office rooms.

Table 11. Minimum WWR to fulfill the daylight requirements (for criteria DF_{mean} , DF_{min} and sDA) defined in section 2.2.1 for residential rooms.

Residential room depth (m)			3.5	4.5	5.5	6.5	7.5	
Shading size (m)	0 m	DF_{mean}	S,SE,E,NE,N,NW,W,SW	0.27	0.27	0.27	0.4	0.4
		DF_{min}	S,SE,E,NE,N,NW,W,SW	0.4	0.4	0.86	-	-
		sDA	S,W	0.27	0.4	0.4	0.86	-
			E,SE,NW,SW	0.27	0.4	0.54	0.86	-
			NE	0.4	0.4	0.54	-	-
	N	0.4	0.4	0.86	-	-		
	0.6 m	DF_{mean}	S,SE,SW	0.27	0.4	0.4	0.4	0.54
			E,NE,NW,W	0.4	0.4	0.4	0.54	0.86
		DF_{min}	S	0.4	0.54	-	-	-
			SE,SW	0.4	0.86	-	-	-
			E,NE,NW,W	0.54	-	-	-	-
		sDA	S	0.4	0.4	0.86	-	-
			SE	0.4	0.4	0.64	-	-
			E,W	0.4	0.54	0.86	-	-
			NE,NW	0.4	0.86	-	-	-
			SW	0.4	0.4	0.54	-	-
	0.9 m	DF_{mean}	S,SE,SW	0.4	0.4	0.4	0.54	0.86
			E	0.4	0.54	0.64	0.86	-
			NE,NW,W	0.4	0.4	0.64	0.86	-
		DF_{min}	S,SE,SW	0.54	0.86	-	-	-
			E,NE,NW,W	0.86	-	-	-	-
sDA		S,SE,SW	0.4	0.54	0.86	-	-	
		E	0.54	0.86	-	-	-	
		NE,NW	0.54	-	-	-	-	
		W	0.4	0.86	-	-	-	

Considering the IES LM-83-12 method for living rooms, the following results are obtained:

- Without shading, the maximum recommended room depth is 5.5 m with minimum WWRs varying from 0.40 to 0.86 depending on the orientation.
- With a shading size of 0.6 m, the maximum recommended room depth is 4.5 m for NE and NW orientations but 5.5 m for the other orientations (minWWR from 0.54 to 0.86).
- With a shading size of 0.9 m, the maximum recommended room depth depends also on the orientation: 3.5 m for NE, NW (minWWR = 0.54); 4.5 m for E and W (minWWR = 0.86), and 5.5 m for S, SE and SW (minWWR = 0.86).

When DF_{mean} criterion is considered, the maximum room depth is 7.5 m when no shading is used. However, the maximum depth is 5.5 m for rooms without shading when DF_{min} is considered. For DF_{min} criterion, the maximum recommended depths are 3.5 m (E, NE, NW, and W), 4.5 m (S, SE, and SW) when the shading size is 0.6 m (minWWR between 0.40 and 0.86), and 0.9 m (W, E, NE, NW orientations with minWWR = 0.64). Finally, the maximum room depth does not significantly change when DF_{mean} criterion is considered: 7.5 m for shading size ≤ 0.6 m (minWWR between 0.40 and 0.86) and 6.5 m for E, NE, NW, W-oriented living rooms with shading size of 0.9 m (minWWR = 0.86).

In summary, approximately 30% of the simulated residential and office rooms fulfill DF_{mean} but not the sDA criterion. As shown by previous investigation, the criterion based on sDA is more conservative than the Estonian DF-based criterion for educational buildings (De Luca et al., 2019a). DF_{min} and sDA can be considered equivalent criteria to assess the daylight provision for the most combinations while DF_{mean} criterion can be used for a less conservative room design. The results showed that a suitable combination of shading size and room depth depending on the room orientation considering climate-based daylight assessment criteria is key during the early design stages of building design. The increment of the shading size allows the design of rooms with higher WWR but lower depth, and vice versa, to ensure the fulfillment of the daylight requirements. In general, considering the same room dimension, orientation, and shading size, higher WWRs can be chosen for residential than for office rooms due to the stricter daylight requirements for any daylight criteria. These results are valid for glazing systems whose visual transmittance is approximately 63%. In addition, the presented rules of thumb are based on the facade level, which can be used for each window-side room of multi-apartment buildings located in new urban areas in Estonia. Nevertheless, further daylight assessment should be conducted considering high-density urban areas.

3.2.1.2 Rules of thumb for protection against overheating risk in residential buildings

The percentage of the residential rooms with and without window airing that fulfill the overheating requirement is shown in Figure 18. The first ventilation case (MV) is based on infiltration and mechanical ventilation. The second ventilation case (NV) is based on infiltration, mechanical ventilation, and window airing. Logically, all the rooms that fulfill the DH requirement when mechanical ventilation is used are not overheated when window airing is added. On average, 40.7% of the S, E, W, SE, SW-oriented rooms are overheated using any ventilation type. However, less than 10% of the N, NE and NW-oriented rooms are unconditionally overheated. The average percentage of rooms that fulfill the DH requirement for any ventilation case depends strongly on the orientation: 46% for N, NE, NW; 20% for S, E, and 11% for W, SE, and SW. Finally, 47% of the rooms achieve a DH lower than 150 °C·h when window airing is included.

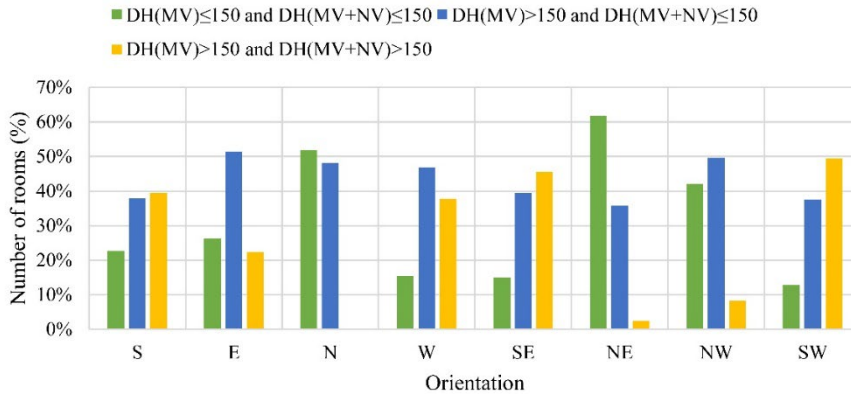


Figure 18. Percentage of the residential rooms per orientation related to all the overheating fulfillment cases for different ventilation strategies: MV = Infiltration and mechanical ventilation, NV = Window airing technique.

As known, one of the limiting function of the daylight provision in residential rooms is the overheating risk that depends strongly on the level of direct solar exposure through the windows during the warm season (Simson et al., 2017a). The results of this study showed that the effect of ventilation on the overheating fulfillment depends strongly on the room orientation. Thus, in at least 25% (and up to 51%) of S, E, W, SE, SW-oriented room combinations, fulfillment of the overheating requirement does not depend on the ventilation system. Thus, only a maximum of 10% of N, NE, NW-oriented room combinations are overheated even when window airing is added to the mechanical ventilation system. Nevertheless, at least 39% of the combination rooms become “not overheated” when window airing is added to the mechanical ventilation system. These results might be conservative for retrofit decisions because a simplified model (Thalfeldt et al., 2016) was used to characterize the optical and thermal performance of the windows, which are more suitable for early design stages of the building design. In general, the use of fixed shading increases the glazed areas without increasing the risk of overheating in residential rooms. There are other actions on WWR and g-value (Voll et al., 2016b) that can improve the protection against overheating depending on the orientation of the room and ventilation strategy used (De Luca et al., 2018a).

The critical WWR*g-value (defined by Simson et al. (Simson et al., 2017a) as a relevant design parameter when overheating is considered for mechanically ventilated rooms) is shown for different orientations and shading sizes in Figure 19. For N, NE, and NW orientations, maximum WWR*g-value is between 0.05 (without shading) and 0.15 (NE). Since no shading was considered for N-oriented rooms, maximum WWR*g-value was set manually as a conservative estimate to the same limit as in the case without shading (0.08). Maximum WWR*g-value is 0.05 for the other orientations (for shading sizes of 0.6–0.9 m). The most restrictive orientations for mechanically ventilated rooms are W, SE, and SW. No W-oriented-room fulfills the DH requirements when only infiltration and mechanical ventilation are considered. Nevertheless, if a shading size of 0.9 m is used in SE and SW-oriented rooms, maximum WWR*g-value is 0.05.

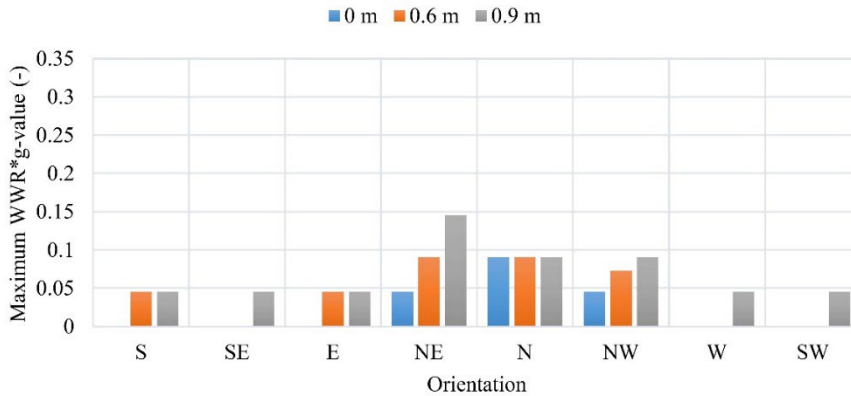


Figure 19. Maximum WWR*g-value to avoid overheating according to the Estonian regulations for different orientations and shading sizes considering infiltration and mechanical ventilation.

The critical WWR*g-value for mechanically and naturally ventilated rooms is shown for different orientations and shading sizes in Figure 20. For N, NE, and NW orientations, maximum WWR*g-value is from 0.10 (without shading) to 0.32; whereas it is between 0.05 and 0.21 for the other orientations. The most restrictive orientations for mechanically and naturally ventilated rooms are W, SE, and SW whose maximum WWR*g-values are between 0.05 and 0.16. Apart from E and S orientations, the use of shading has the highest impact on SW and SE orientations when natural ventilation is added: maximum WWR*g-value ranges from 0.05 without shading to 0.15 with a shading size of 0.9 m.

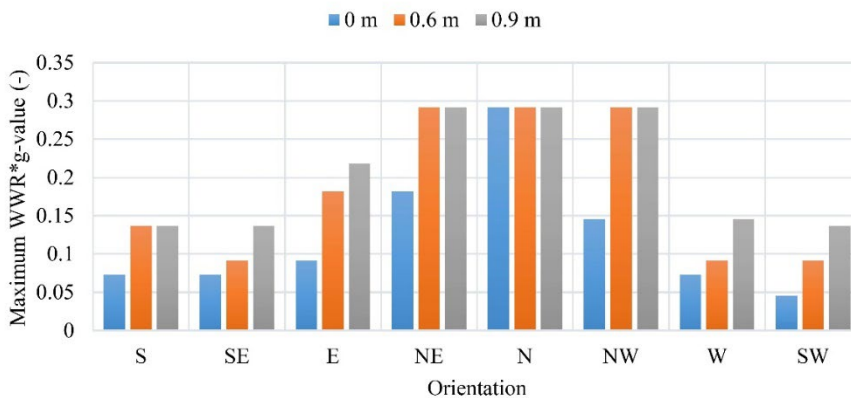


Figure 20. Maximum WWR*g-value to avoid overheating according to the Estonian regulations for different orientations and shading sizes considering infiltration, mechanical ventilation, and window airing.

According to these results, the use of windows with lower g-values for the most problematic facade orientations is recommended; i.e., S, SE, E, W, and SW as a previous study on nZEB Danish single-family houses suggested (Vanhouthehem et al., 2015). The presented results can vary depending on the set point considered for the window airing strategy and openable area ratio. In this study, a set point of 25 °C (previous research

used 27 °C (Thalfeldt et al., 2016)) was used for the window airing control with a 10% of openable area. A new methodology based on the multi-zone approach using different set points for window airing would help to understand how the overheating levels in residential rooms change.

3.2.1.3 Rules of thumb for the combined fulfilment between daylight and overheating prevention requirements in residential buildings

The level of combined fulfillment depending on the room dimension, orientation, and shading size is shown in Figure 21. On the one hand, N orientations allow a higher flexibility for the design of residential rooms. On the other hand, most of the S, SE, W, and SW-oriented rooms cannot meet both requirements when no shading is used. Most room combinations can fulfill the DF_{mean} criterion. Nevertheless, for high (6.5 m) or low (3.5–4.5 m) room depths and no shading, the combined fulfillment is compromised because of poor daylight or high overheating levels, respectively. The increment of the shading size allows the combined fulfillment of rooms with depths ≤ 5.5 m and different orientations such as S, SE, E, W, and SW.

w	d	Shading size (m)																							
		0								0.6								0.9							
		S	SE	E	NE	N	NW	W	SW	S	SE	E	NE	N	NW	W	SW	S	SE	E	NE	N	NW	W	SW
3.5	3.5	0	0	2	3	3	3	0	0	3	3	3	3	-	3	2	1	3	3	2	3	-	3	2	2
	4.5	1	1	1	3	3	3	1	0	3	2	2	2	-	2	2	2	2	2	2	1	-	1	1	2
	5.5	1	1	1	3	3	2	1	1	1	1	1	1	-	1	1	1	1	1	1	1	-	1	1	1
	6.5	0	0	1	1	1	1	0	0	1	1	1	1	-	1	1	1	1	1	1	1	-	1	1	1
	7.5	1	1	1	1	1	1	1	0	1	1	1	1	-	1	0	1	0	0	0	0	-	0	0	0
4.5	3.5	1	1	2	3	3	3	1	1	3	1	3	3	-	3	2	1	3	2	2	2	-	3	2	2
	4.5	1	0	1	3	3	3	0	0	2	2	2	2	-	3	1	1	2	2	2	1	-	2	1	2
	5.5	1	1	1	3	3	3	1	1	2	1	1	1	-	1	1	1	1	1	1	1	-	1	0	1
	6.5	1	1	1	2	1	1	1	1	1	1	1	1	-	1	1	1	1	1	1	1	-	1	0	1
	7.5	0	0	1	1	1	1	0	0	1	1	1	1	-	1	0	1	1	1	0	0	-	0	0	1
5.5	3.5	1	1	2	3	3	3	1	0	2	2	2	3	-	3	1	2	3	2	2	3	-	3	2	2
	4.5	0	0	1	3	3	3	0	0	2	1	2	3	-	3	1	1	2	2	2	2	-	2	2	2
	5.5	1	0	1	3	3	2	1	0	2	1	1	2	-	2	1	1	2	2	1	1	-	1	1	2
	6.5	1	1	1	3	3	2	1	1	1	1	1	1	-	1	1	1	1	1	1	1	-	1	0	1
	7.5	1	1	1	1	1	1	1	1	1	1	1	1	-	1	1	1	1	1	1	1	-	1	0	1
6.5	3.5	1	0	1	3	3	2	1	0	1	2	2	3	-	3	1	2	3	2	2	3	-	3	2	2
	4.5	0	0	1	3	3	2	0	0	2	1	2	3	-	3	1	1	2	2	2	2	-	2	1	2
	5.5	0	0	1	3	3	2	0	0	1	1	1	2	-	2	1	0	2	2	1	1	-	1	1	1
	6.5	1	1	1	1	1	1	1	1	1	1	1	1	-	1	0	1	1	1	1	1	-	1	0	1
	7.5	1	1	1	2	1	1	1	1	1	1	1	1	-	1	1	1	1	1	0	1	-	1	0	1

Figure 21. Level of the combined fulfillment depending on the daylight criteria considered (3 = always, 0 = never, 1 = DF_{mean} is fulfilled, 2 = pair of criteria are fulfilled and white cells with “-” = not simulated) for different room (MV+NV) configurations where: w = room width (m) and d = room depth (m).

When window airing is added, most of the NE, N, and NW-oriented residential rooms with room depths lower than 5.5 m are considered good room designs because they fulfill both daylighting and overheating requirements for any daylight criteria considered. Nevertheless, as discovered in a previous research, in deep S-oriented rooms, either summer indoor comfort or daylight provision is compromised with the use of shading (Vanhoutteghem et al., 2015). Moreover, the combined fulfillment in most of the SE, W, and SW-oriented rooms with depths ≥ 6.5 m and fixed shading depends on the daylight criteria (DF_{mean} , DF_{min} , and sDA). The use of fixed shading allows the combined fulfillment in S-oriented rooms but decreases the maximum depth for N orientations. This result highlights the importance of a careful envelope design to achieve combined fulfillment

for any daylight assessment criterion. The use of switchable shading devices combined with window airing strategies can improve the flexibility of the building design in early design stages. However, its investment costs may be higher than fixed shading.

3.2.2 Detailed method based on daylight and overheating prediction formulas for window sizing

3.2.2.1 Prediction of daylight provision

The aim of this section is to propose a formula for the estimation of the daylight provision of side-lit rooms (Paper III). This prediction formula could help designers and practitioners not only to fulfill the minDF-based daylight requirements but also to understand the impact of the design parameters such as visible transmittance of the glazing system (T_{vis}), room depth (rd), room width (rw), and WWR on daylight provision.

The percentage of all the room combinations of the parametric model for different fulfillment conditions between Cd1 and Cd2 can be seen in Figure 22. According to the results, there is no room combination that fulfills Cd2 and not Cd1 for any T_{vis} considered between 45% and 80%. Thus, for the parametric model based on side-lit rooms, Cd1 represent a more restrictive requirement than Cd2. From this point of the paper, the prediction of daylight provision is focused on the estimation of minDF1 (for Cd1) instead of minDF2 (for Cd2). The calculation of minDF1 speed up twice daylight simulations because only the half of the grid points is needed. From this point of the manuscript, the variable minDF1 is referred as minDF.

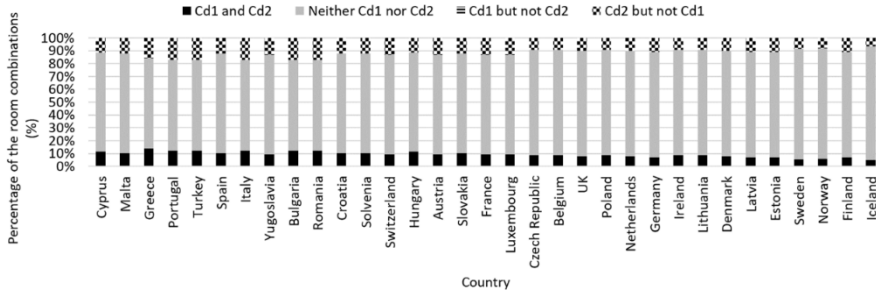


Figure 22. Percentage of the rooms combinations of the parametric model that fulfills different combinations of conditions defined by the European standard EN 17037 (Cd1 and Cd2) for $T_{vis} = 80\%$. The first condition (Cd1) is fulfilled if minDF1 is higher than a target value (Figure 8). The second condition (Cd2) is fulfilled when minDF2 is higher than a target value (Figure 8).

In general, minDF related to any room combination could depend on the design parameters such as T_{vis} , θ , WWR, rw , and rd . Thus, the general prediction formula can be written as follows:

$$\text{minDF}(T_{vis}, \theta, WWR, rw, rd) = f(T_{vis}, \theta, WWR, rw, rd) \quad (8)$$

Eq. (8) might be expressed as the product of one polynomial function ($p1(T_{vis})$) and the minDF related to $T_{vis} = 45\%$ for each room combination:

$$\text{minDF} = p1(T_{vis}) \cdot \text{minDF}(45, \theta, WWR, rw, rd) \quad (9)$$

The linear correlation between minDF and minDF45 for each Tvis value is higher than 0.996 in terms of R² (Figure 23a). Moreover, the dependency of the slopes from linear fitting functions (dotted lines from Figure 23a) with Tvis values is strongly linear (R² = 1) (Figure 23b). Therefore, Eq. (9) can be rewritten as follows:

$$\text{minDF} = (a \cdot Tvis + b) \cdot \text{minDF}(45, \theta, WWR, rw, rd) \quad (10)$$

$$\text{minDF} = (0.0264275 \cdot Tvis - 0.19129264) \cdot \text{minDF}(45, \theta, WWR, rw, rd) \quad (11)$$

Where a and b are the fitting coefficients related to the dotted line shown in Figure 23b. According to Figure 23c, the agreement between simulated and predicted minDF values is 0.997 and 0.060 in terms of R² and RMSE, respectively.

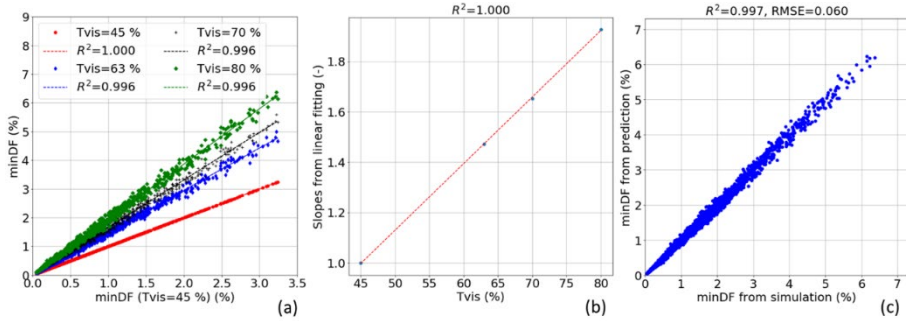


Figure 23. Linear dependency between minimum daylight factor of the half of the reference plane closest to the window (minDF) for different Tvis values and minDF for Tvis = 45% (a). Linear dependency between the slopes from linear fitting functions (a) and different Tvis values and minDF for Tvis = 45% (b). Agreement between minDF from simulations and prediction formula (Eq. (9)) (c).

Eq. (8) might be expressed as the product of two polynomial functions ((a · Tvis – b) and p2(θ)) and the minDF related to Tvis = 45% and θ = 0° for each room combination:

$$\text{minDF} = (a \cdot Tvis + b) \cdot p2(\theta) \cdot \text{minDF}(45, 0, WWR, rw, rd) \quad (12)$$

The linear correlation between minDF and minDF for Tvis = 45% and θ = 0° for each θ value is higher than 0.960 in terms of R² (Figure 24a). Moreover, the dependency of the slopes from linear fitting functions (dotted lines from Figure 24a) with Tvis values is strongly linear (R² = 0.968) (Figure 24b). Therefore, Eq. (10) can be rewritten as follows:

$$\text{minDF} = (a \cdot Tvis + b) \cdot (c \cdot \theta + d) \cdot \text{minDF}(45, 0, WWR, rw, rd) \quad (13)$$

$$\text{minDF} = (a \cdot Tvis + b) \cdot (-0.0208 \cdot \theta + 1.0772) \cdot \text{minDF}(45, 0, WWR, rw, rd) \quad (14)$$

Where c and d are the fitting coefficients related to the dotted lines shown in Figure 24b. According to Figure 24c, the agreement between simulated and predicted minDF values is 0.914 and 0.379 in terms of R² and RMSE, respectively.

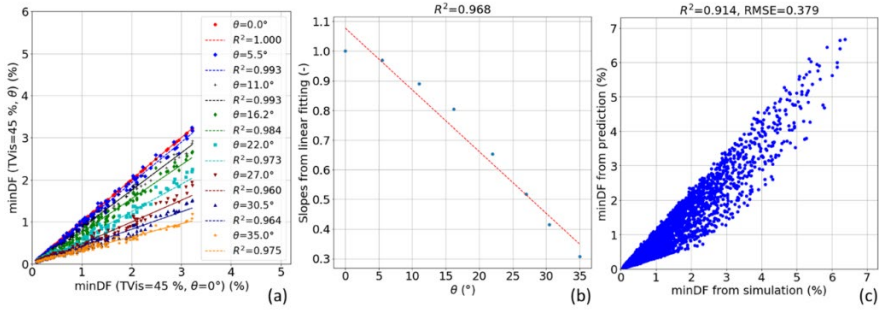


Figure 24. Linear dependency between minimum daylight factor of the half of the reference plane closest to the window (*minDF*) for different θ values and *minDF* for $T_{vis} = 45\%$ and $\theta = 0^\circ$ (a). Linear dependency between the slopes from linear fitting functions (a) and different T_{vis} values and *minDF* for $T_{vis} = 45\%$ (b). Agreement between simulated and predicted *minDF* values (Eq. (14)) (c).

In addition, the combination of design parameters WWR, r_w , and r_d can be expressed as the window-to-floor ratio (WFR):

$$WFR = \frac{\text{Window area}}{\text{Floor area}} = \frac{WWR \cdot \text{External facade area}}{\text{Floor area}} = \frac{WWR \cdot r_h \cdot r_w}{r_w \cdot r_d} = \frac{WWR \cdot r_h}{r_d} \quad (15)$$

Where r_h is the room height. Thus, Eq. (13) can be written as follows:

$$\text{minDF} = (a \cdot T_{vis} + b) \cdot (c \cdot \theta + d) \cdot \text{minDF}(45,0,WFR) \quad (16)$$

The linear correlation between *minDF* and WFR for $T_{vis} = 45\%$ and $\theta = 0^\circ$ is 0.902 in terms of R^2 (Figure 25a). Therefore, Eq. (12) can be rewritten as follows:

$$\text{minDF} = (a \cdot T_{vis} + b) \cdot (c \cdot \theta + d) \cdot (e \cdot WFR + f) \quad (17)$$

$$\text{minDF} = (a \cdot T_{vis} + b) \cdot (c \cdot \theta + d) \cdot (0.0532 \cdot WFR - 0.2637) \quad (18)$$

Where e and f are the fitting coefficients related to the dotted lines displayed in Figure 25a. According to Figure 25b, the agreement between simulated and predicted *minDF* values is 0.910 and 0.310 in terms of R^2 and RMSE, respectively.

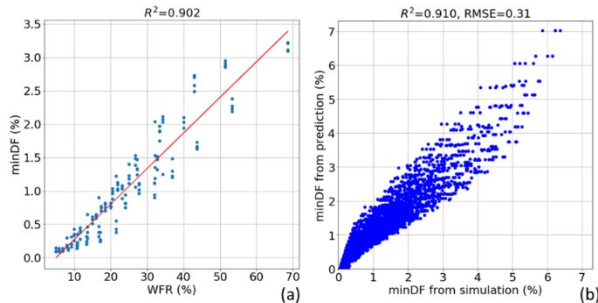


Figure 25. Linear dependency between minimum daylight factor of the half of the reference plane closest to the window (*minDF*) for and window-to-floor ratio (WFR) (for $T_{vis} = 45\%$ and $\theta = 0^\circ$) (a). Agreement between simulated and predicted *minDF* values (Eq. (18)) (b).

The minDF relative deviation in terms of (Root mean square error (RMSE)/minDF1t or target minDF) for different European countries can be seen in Figure 26. Although the RMSE/minDF1t tends to be higher in countries with lower target minDFs (e.g. Cyprus: 1.7%, Malta: 1.8%, Greece: 1.5%, Portugal: 1.6%, etc.) than countries with higher daylight requirements such as Denmark (2.1%), Estonia (2.2%), Norway (2.4%), Sweden (2.5%), or Iceland (2.8%). The relative RMSE for any European country is up to 0.21.

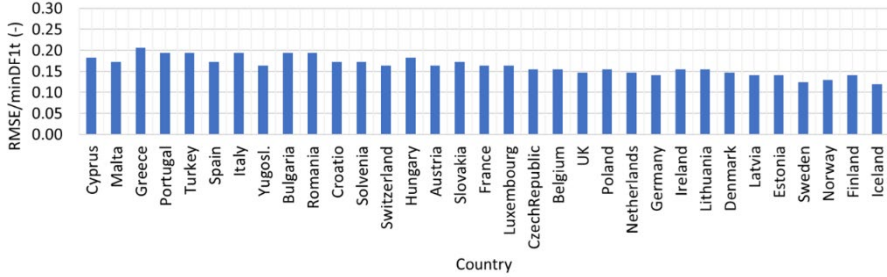


Figure 26. Relative deviation (Root mean square error/minDF1t) of the prediction of minDF with respect to simulated minDF values (5120 room combinations) for linear polynomial fitting strategy. RMSE is 0.31 (Figure 25b) and the target minDF value (minDF1t) depends on each EU country according to the European standard EN 17037 (1.5%–2.8%).

As explained, a, b, c, d, e, and f are the fitting coefficients, whose values depend on the reflectance values of the interior/exterior scene and room typology. Meaning that each combination of reflectance values and room typology, a calibration of the minDF formula is needed. Each new calibration would require at least 6 minDF simulations. The calibration would have three steps, as shown in this section 3.4.1. Despite the substantial computational time savings (6 instead of 5120 minDF simulations), the accuracy of the prediction formula could be compromised. A minDF relative deviation of 0.21 could be acceptable when the number of minDF simulations is very large and the computational speed is a primary aspect within the design process. The proposed minDF prediction formula Eq. (18) can be used for parametric analyses that consider the following design parameter ranges: $T_{vis} = 45\text{--}80\%$, $\theta = 0\text{--}35^\circ$, $rw = 3.5\text{--}6.5$ m, $rd = 3.5\text{--}7.5$ m, and $WWR=13.4\text{--}85.7\%$. Outside these ranges because the accuracy of the prediction formula might vary. By using the minDF prediction formula (Eq. (18)), the designer can assess calculate the minimum WWR for each room i ($minWWR_i$) that ensures a minDF1t: considering Eq. (15), Eq. (17) can be rewritten as follows:

$$minWWR_i = \left(\frac{rd_i}{e \cdot rh_i} \right) \cdot \left(\frac{minDF_C}{(a \cdot T_{vis} + b) \cdot (c \cdot \theta_i + d)} - f \right) \quad (19)$$

Where the minDF_C is the target minDF for European country C (e.g. minDF_C = 2.2% for Estonia) according to the European standard EN17037. For instance, for $T_{vis} = 63\%$, $\theta_i = 15.8^\circ$, and minDF_C = 2.2% (Estonian context), the minWWR values calculated with Eq. (19) for different room depths (3.5, 4.5, 5.5, 6.5, and 7.5 m) are the following: 53.0%, 68.1%, 83.3%, 98.4%, and 113.6%. Since WWR values above 90% are not technically viable in practice, the maximum room depth is 5.5 m (with minWWR = 83.3%) to ensure minDF = 2.2% according to the predicted values, which agrees with the rule of

thumb proposed in previous investigation within the Estonian context: maximum room depth of 5.5 m with a minWWR of 86% (De Luca et al., 2018a). An example of use of the minWWR formula (Eq. (19)) to a case study is presented in section 3.7.

3.2.2.2 Prediction of overheating risk

The aim of this section is to propose a formula for the estimation of the overheating risk of side-lit rooms in terms of the DH metric. The DH prediction formula could be used by architects and designers to facilitate and speed up assessment of the potential overheating risk of a determined room design or for room/window sizing during early design stages, without the need of complex and time-consuming simulations. Among 5120 simulated room combinations for each orientation, the critical orientations are the south orientations as can be seen in Figure 27. In the first part of this analysis, S orientation was considered since its mean DH value is the highest, leading to high relative deviations in terms of RMSE/ maxDH_{EST} (with maxDH_{EST} = 150 °C·h).

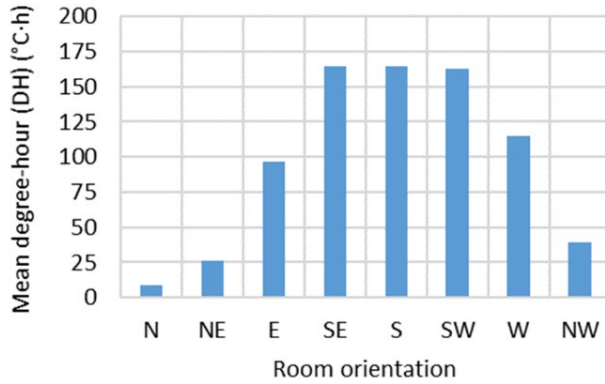


Figure 27. Mean DH value (among 5120 room combinations) for different room orientations.

In general, DH related to any room combination with a certain orientation (Ori) (e.g. Ori = S) could depend on the design parameters such as g (g -value), θ , and WFR. Thus, the general prediction formula can be written as follows:

$$DH_{Ori} = f(g, \theta, WFR) \quad (20)$$

According to Figure 28, $DH_{Ori}(g, \theta, WFR)$ can be expressed linearly with $DH_{Ori}(g_0, \theta, WFR)$ with $g_0=0.24$ (-) for each room combination:

$$DH_{Ori}(g, \theta, WFR) = A(g) \cdot DH_{Ori}(g_0, \theta, WFR) + B(g) \quad (21)$$

The linear correlation between $DH_{Ori}(g, \theta, WFR)$ and $DH_{Ori}(g_0, \theta, WFR)$ for each g -value is higher than 0.844 in terms of R^2 (Figure 28a). Moreover, the dependency of the slopes from linear fitting functions (dotted lines from Figure 28a) with g -values is strongly linear ($R^2 = 0.969-0.977$) (Figure 28c and 28d). Therefore, Eq. (21) can be rewritten as follows:

$$DH_{Ori}(g, \theta, WFR) = A(g) \cdot DH_{Ori}(g_0, \theta, WFR) + B(g) \quad (22)$$

$$DH_{Ori}(g, \theta, WFR) = (a_1g + a_2) \cdot DH_{Ori}(g_0, \theta, WFR) + (b_1g + b_2) \quad (23)$$

$$DH_{Ori}(g, \theta, WFR) = (1.4 \cdot g + 0.7) \cdot DH_{Ori}(g_0, \theta, WFR) + (341.1 \cdot g - 86.0) \quad (24)$$

Where $A(g)$ and $B(g)$ are the fitting coefficients related to the dotted lines displayed in Figure 28a. According to Figure 28b (Eq. (24)), the agreement between simulated and predicted DH_s values is 0.924 and 0.215 in terms of R^2 and RMSE/DHmax, respectively.

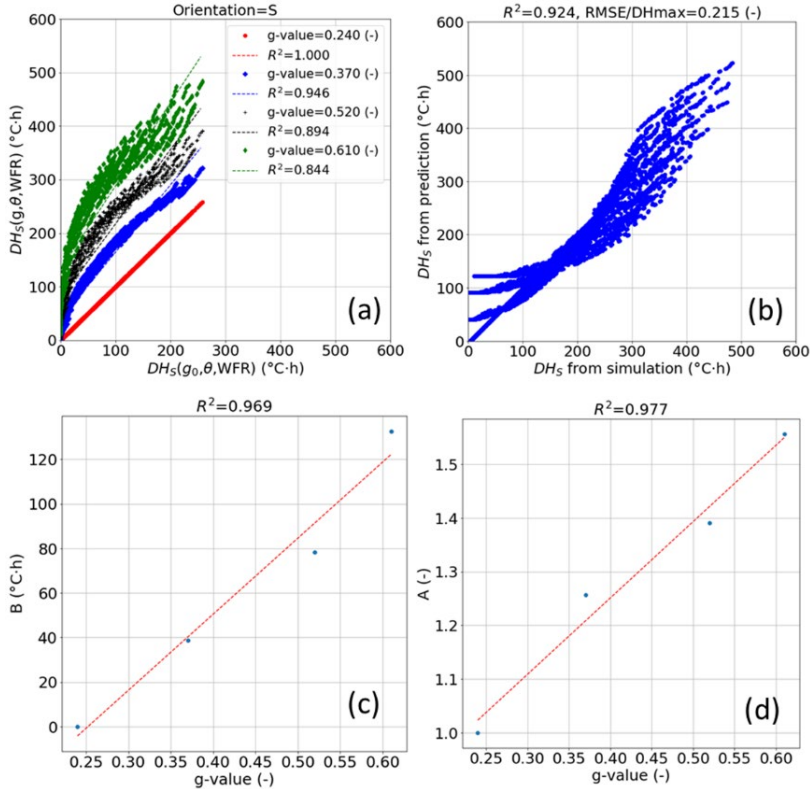


Figure 28. Linear dependency between degree-hours (DH) for south oriented rooms for different g -values (g) ($DH_s(g, \theta, WFR)$) and DH_s for $g_0 = 0.24$ (-) ($DH_s(g_0, \theta, WFR)$) (a). Linear dependency between A(c) and B(d) coefficients and different g -values. Agreement between $DH_s(g, \theta, WFR)$ from simulations and prediction formula (b) (Eq. (24)).

At the same time, $DH_{Ori}(g_0, \theta, WFR)$ can be correlated linearly with $DH_{Ori}(g_0, \theta_0, WFR)$ with $\theta_0=0^\circ$ for each room combination:

$$DH_{Ori}(g_0, \theta, WFR) = C(\theta) \cdot DH_{Ori}(g_0, \theta_0, WFR) + D(\theta) \quad (25)$$

The linear correlation between $DH_{Ori}(g_0, \theta, WFR)$ and $DH_{Ori}(g_0, \theta_0, WFR)$ for each θ value is higher than 0.972 in terms of R^2 (Figure 29a). Moreover, the dependency of the slopes from linear fitting functions (dotted lines from Figure 28a) with θ is strongly linear ($R^2 = 0.922$ – 0.961) (Figure 29b). Therefore, Eq. (25) can be rewritten as follows:

$$DH_{Ori}(g_0, \theta, WFR) = C(\theta) \cdot DH_{Ori}(g_0, \theta_0, WFR) + D(\theta) \quad (26)$$

$$DH_{Ori}(g_0, \theta, WFR) = (c_1\theta + c_2) \cdot DH_{Ori}(g_0, \theta_0, WFR) + (d_1\theta + d_2) \quad (27)$$

$$DH_{Ori}(g_0, \theta, WFR) = (-0.006 \cdot \theta + 1) \cdot DH_{Ori}(g_0, \theta_0, WFR) + (-0.384 \cdot \theta - 0.4) \quad (28)$$

Where $C(\theta)$ and $D(\theta)$ are the fitting coefficients associated to the dotted lines shown in Figure 29a. Thus, Eq. (22) can be expressed as follows:

$$DH_{Ori}(g, \theta, WFR) = A(g) \cdot (C(\theta) \cdot DH_{Ori}(g_0, \theta_0, WFR) + D(\theta)) + B(g) \quad (29)$$

According to Figure 29b (predicted values calculated with Eq. (28)), the agreement between simulated and predicted DH_s values is 0.945 and 0.183 in terms of R² and RMSE/DHmax, respectively.

Finally, $DH_{Ori}(g_0, \theta_0, WFR)$ can be expressed as a parabolic function with WFR as independent variable for each room combination according to Figure 30a (Eq. (29) and Eq. (31)). The dependency is strongly parabolic (R² = 0.984) (Figure 30a):

$$DH_{Ori}(g_0, \theta_0, WFR) = e_1 \cdot WFR^2 + e_2 \cdot WFR + e_3 \quad (30)$$

$$DH_{Ori}(g_0, \theta_0, WFR) = -0.058 \cdot WFR^2 + 8.771 \cdot WFR - 6.817 \quad (31)$$

Moreover, Eq. (29) can be rewritten as follows:

$$DH_{Ori}(g, \theta, WFR) = A(g) \cdot [C(\theta) \cdot (e_1 \cdot WFR^2 + e_2 \cdot WFR + e_3) + D(\theta)] + B(g) \quad (32)$$

Where e_1 , e_2 , and e_3 are the fitting coefficients associated to lines displayed in Figure 30a. According to Figure 30b (predicted values calculated with Eq. (32)), the agreement between simulated and predicted DH_s values is 0.952 and 0.172 in terms of R² and RMSE/DHmax, respectively. For the rest of room orientations, the RMSE/DHmax is below 0.20 (Table 12).

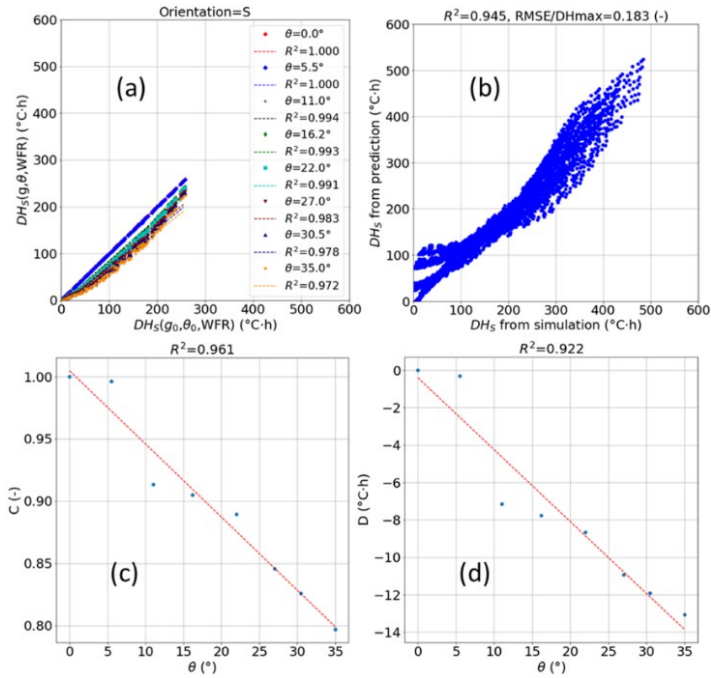


Figure 29. Linear dependency between degree-hours (DH) for south oriented rooms for different g -values (g) ($DH_S(g_0, \theta, WFR)$) and ($DH_S(g_0, \theta_0, WFR)$) (a). $g_0 = 0.24$ (-) and $\theta_0 = 0^\circ$. Linear dependency between C (c) and D (d) coefficients and different θ values. Agreement between $DH_S(g, \theta, WFR)$ from simulations and prediction formula (b) (Eq. (29)).

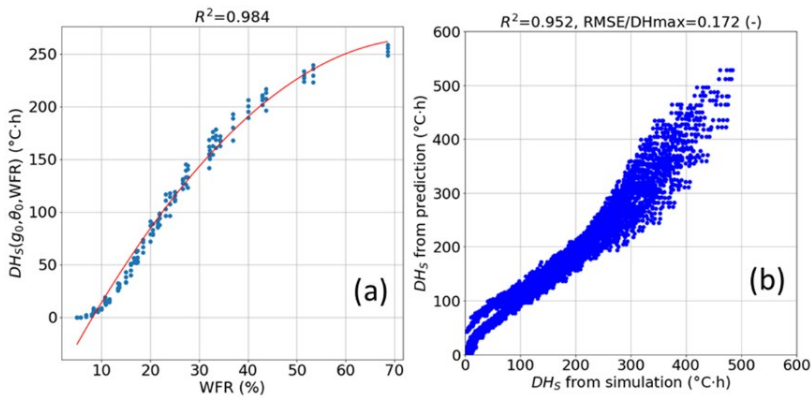


Figure 30. Linear dependency between degree-hours (DH) for south oriented rooms ($DH_S(g_0, \theta_0, WFR)$) and window-to-floor ratio (WFR) (a). $g_0 = 0.24$ (-) and $\theta_0 = 0^\circ$. Agreement between $DH_S(g_0, \theta, WFR)$ from simulations and prediction formula (b) (Eq. (31)).

As explained in this section 3.2, the 11 fitting coefficients ($a_1, a_2, b_1, b_3, c_1, c_2, d_1, d_2, e_1, e_2,$ and e_3) for the DH prediction formula (Eq. (32)) depend mainly on the room orientation (Table 6), room typology, natural ventilation control, HVAC settings, and opaque constructions materials. Meaning that each combination of natural ventilation control, room typology, HVAC settings, and opaque constructions materials, a calibration of the DH formula is needed. Each new calibration would require at least 11 minDF

simulations. The calibration would have three steps, as shown in this section 3.2. Despite the substantial computational time savings (11 instead of 5120 DH simulations for each orientation), the accuracy of the prediction formula could be compromised. A DH relative deviation of 0.20 could be acceptable when the number of DH simulations is very large and the computational speed is the main design criterion. The proposed minDF prediction formula Eq. (18) can be used for parametric analyses that consider the following design parameter ranges: g-value = 0.27–0.61 (-), $\theta = 0$ –35°, rw = 3.5–6.5 m, rd = 3.5–7.5 m, and WWR = 13.4–85.7%. An example of use of the DH formula (Eq. (32)) for window sizing is presented in section 3.7.

Table 12. Fitting coefficients and relative deviation in terms of DH RMSE/maxDH (-) for different room orientations and fitting strategy explained in this section 3.2 (Eq. (32)). RMSE = Root Mean Square Error and maxDH = 150 °C·h according to the Estonian regulation.

	N	NE	E	SE	S	SW	W	NW
a1	9.632	5.943	2.928	2.003	1.422	1.771	2.666	4.409
a2	-1.255	-0.308	0.361	0.548	0.682	0.598	0.394	0.000
b1	35.214	90.872	239.231	347.875	341.146	309.132	208.895	86.555
b2	-9.763	-24.273	-61.272	-87.680	-86.024	-77.670	-53.236	-22.904
c1	-0.027	-0.031	-0.025	-0.012	-0.006	-0.014	-0.027	-0.031
c2	0.811	0.978	1.083	1.046	1.005	1.060	1.067	0.928
d1	0.003	0.007	-0.207	-0.525	-0.384	-0.624	-0.236	0.051
d2	-0.222	-0.821	-1.967	0.215	-0.411	-0.441	-5.783	-2.907
e1	0.021	0.032	-0.018	-0.060	-0.058	-0.074	-0.062	0.004
e2	-0.684	-0.381	5.115	8.792	8.771	10.086	8.930	2.792
e3	4.659	-1.021	-46.563	-65.734	-68.171	-70.123	-61.321	-27.913
RMSE/maxDH (-)	0.088	0.159	0.195	0.183	0.172	0.179	0.190	0.156

Moreover, the consideration of a maxDH lower than 150 °C·h by local regulations would lower the accuracy of the DH prediction formula and higher polynomial fitting order might be needed to maintain an acceptable relative deviation. For a different climate, not only maxDH (defined by local regulations) would be different, but also the warm season considered typical HVAC settings, ventilation strategies, and envelope optical/thermal properties. Theoretically, all these aspects could influence on the accuracy of the prediction of the DH metric.

According to minDF (Eq. (18)) and DH (Eq. (32)) prediction formulas, for g-value = 0.37, Tvis = 63%, and $\theta_i = 15.8^\circ$, the maximum room depth to fulfill both requirements is 5.5 m (Table 13). This is only possible for N, NE, and NW room orientations according to the predictions. This fact is supported also by rules of thumb for side-lit rooms without shading recommended in a previous investigation within the Estonian context (Abel Sepúlveda et al., 2020).

Table 13. Predicted degree-hours (DH) (Eq. (32)) and minDF (Eq. (18)) values for room combinations that fulfil $\text{minDF} \geq 2.2\%$ and $\text{DH} \leq 150 \text{ }^\circ\text{C}\cdot\text{h}$. The visible transmittance of the glazing (T_{vis}) is 63% and the g -value 0.37. The mean obstruction angle (θ) is 15.8° .

Room orientation	rd (m)	WWR (%)	DH ($^\circ\text{C}\cdot\text{h}$)	minDF (%)
NE	3.5	53.6	44.9	2.228
		64.3	65.1	2.731
		85.7	118.1	3.737
	4.5	85.7	70.1	2.842
	5.5	85.7	46.5	2.272
N	3.5	53.6	14.5	2.228
		64.3	24	2.731
		85.7	50.9	3.737
	4.5	85.7	26.5	2.842
	5.5	85.7	15.3	2.272
NW	3.5	53.6	76.5	2.228
		64.3	95.8	2.731
		85.7	135.4	3.737
	4.5	85.7	100	2.842
	5.5	85.7	78.2	2.272

3.2.3 Example of designing windows properties and dimensions using prediction formulas to balance daylight and overheating protection

For a certain room i , when $\text{minWFR} = \text{maxWFR}$ (equivalent to $\text{minWWR} = \text{maxWWR}$) there is an unique combination of g -value and T_{vis} values that ensure the combined fulfillment between daylight provision and overheating protection. For a certain T_{vis} value and room i , there is a maximum g -value ($g_{\text{max},i}$) (Eq. (33)) from the combination of Eq. (18) and Eq. (32)).

$$g_{\text{max},i} = \frac{\text{maxDH} - a_2 \cdot [(c_1 \cdot \theta_i + c_2) \cdot (e_1 \cdot \text{WFR}^2 + e_2 \cdot \text{WFR} + e_3) + (d_1 \cdot \theta_i + d_2)] - b_2}{a_1 \cdot [(c_1 \cdot \theta_i + c_2) \cdot (e_1 \cdot \text{WFR}^2 + e_2 \cdot \text{WFR} + e_3) + (d_1 \cdot \theta_i + d_2)] + b_1} \quad (33)$$

If the window have a g -value lower or equal to $g_{\text{max},i}$, the room i will not be overheated ($\text{DH} < \text{maxDH}$). On the contrary, if the g -value is higher than $g_{\text{max},i}$, there room i will be overheated. For a T_{vis} range from 50% to 80%, the g_{max} values for each room i can be seen in Figure 31. For SE oriented rooms, the g_{max} value is much lower than for NW oriented rooms, this is because SE oriented rooms are more prone to overheating and therefore windows with low g -value are needed (Simson et al., 2017a). In addition, for rooms with NW orientation, depending on the T_{vis} considered the g_{max} values goes from 0.4 to 0.7 for T_{vis} values from 50% to 80%, respectively. In fact, for a

certain room i when T_{vis} increases, $minWWR$ decreases because there is no need for larger window sizes if the glazing system is more transparent. Thus, this leads to a decrease of $maxWWR$ (considering during the design: $minWWR = maxWWR$), which allows a selection of a higher g -value. In summary, Figure 31 shows that highly transparent glazing systems with low g -values are preferred design solutions to achieve a good-balance between daylight provision and overheating protection.

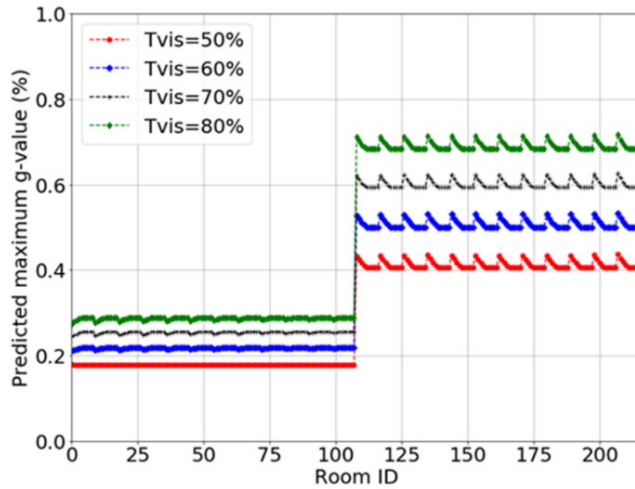


Figure 31. Maximum g -value (g_{max}) for each room residential building located in Tallinn, Estonia ($T_{vis} = 50\text{--}80\%$) to achieve a good balance between daylight provision and overheating protection ($minWFR=maxWFR$) (Eq. (33)). Room ID range 1–108 and 109–215 refers to SE and NW oriented rooms, respectively.

Specifically, the selection of windows constructions with T_{vis} of 80% and g -value of 0.27 could achieve both performances in SE oriented rooms. For NW oriented room, a T_{vis} of 60% and g -value of 0.5 could achieve both performances. The $minWWR$ for each room is shown in Fig 16. The $minWWR$ values are between 40–60% and 52–72% for SE and NW oriented rooms, respectively. Thus, these $minWWR$ differences for each room orientation are due to slight variations of room depth (rd_i) and obstruction level (θ_i). In summary, from these two analyses (Figure 31 and 32), the window construction could be selected depending on the room orientation (T_{vis} and g -values) and window size. Apart from the selection of the window's g -value and T_{vis} , it is also possible to consider as design solution such different room depths (Sayın and Çelebi, 2020) or orientation/typology of the building floor plan (Sepúlveda and De Luca, 2020). However, the presented prediction formulas cannot be used in parametric analyses regarding the set point for the window airing operation (Simson, 2019) or nighttime ventilation (Voll et al., 2016b) since these design parameters were not considered as independent variables.

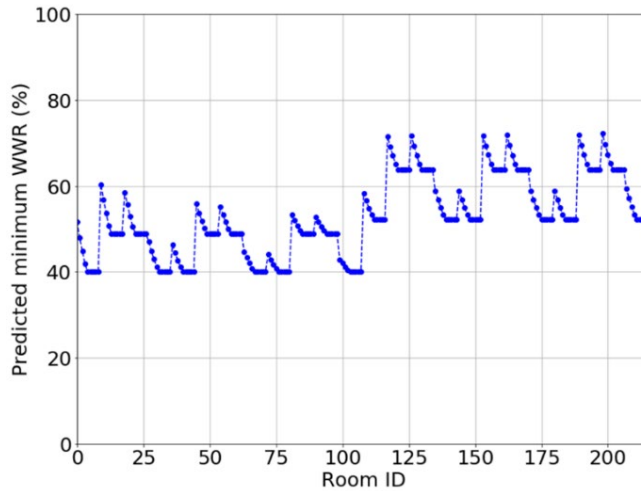


Figure 32. Minimum window-to-wall ratio (*minWWR*) for each room of the residential building located in Tallinn, Estonia ($T_{vis} = 80\%$ for SE rooms and $T_{vis} = 60\%$ for NW rooms) to reach sufficient daylight provision according to the EN 17037 (Eq. (18)). Room ID range 1–108 and 109–215 refers to SE and NW oriented rooms, respectively.

According to the case study, the prediction accuracy in terms of relative RMSE is 0.130 and 0.199 for *minDF* and *DH* values, respectively (Figure 33). For SE rooms, the deviations are lower than for NW rooms because of the lower *g*-value selected (0.27 against 0.50). In fact, the fitting accuracy decreases with the *g*-value, as can be seen in Figure 33b. Moreover, *DH* deviations are higher than initially calculated (0.156 from Table 13) because the case study only contains SE/NW oriented rooms (216 combinations), while for the calculation of 0.156 a wide range of room configurations was used (5120 combinations).

A relative RMSE of 0.20 might not be acceptable for pure assessment purposes in existing buildings. Thus, the use of the coupled method might be justified during early design stages, when the number of simulations is very large and the accuracy is not the main priority. However, the coupled method is opposite to a “black box” approach, which is typical of machine learning-based multi-objective optimization approaches. Although the prediction of daylight and thermal performances can be very accurate ($R^2 \sim 0.99$) but the training of the prediction models require much large datasets for each variable (~ 100) (Wang et al., 2021). The coupled method can be represented graphically, which can be attractive for architects and designers, since these type of user-friendly 2D methods are key to process and communicate to the designer (Kleindienst and Andersen, 2012).

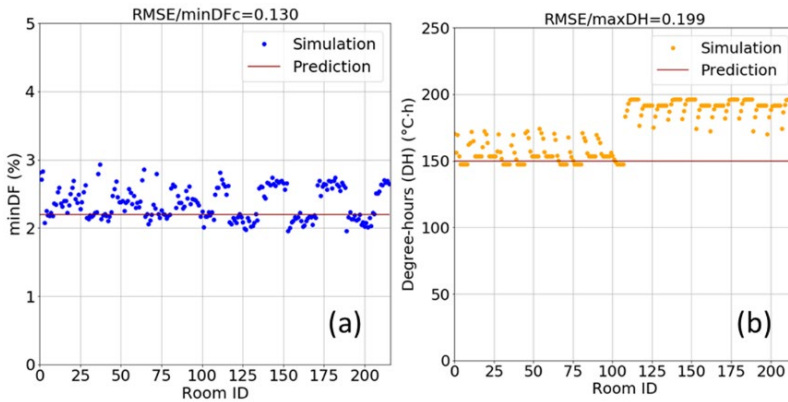


Figure 33. Comparison between simulated and predicted minDF (a) and DH (b) values for each room. Room ID range 1–108 and 109–215 refers to SE ($T_{vis} = 80\%$ and $g\text{-value} = 0.27$) and NW ($T_{vis} = 60\%$ and $g\text{-value} = 0.5$) oriented rooms, respectively. The minDF and DH values were calculated for rooms with minWWR obtained with Eq. (18) and Eq.(32), respectively. RMSE = Root mean square error, minDFc = 2.2%, and maxDH = 150°C·h.

Firstly, the main advantage of using the prediction formulas is the minimization of the time-consuming design iterations to achieve the combined fulfillment of daylight and overheating performances in new buildings. Secondly, by using the graphical coupled method, designers and architects can understand the impact of their design decisions on the combined fulfillment of daylight and overheating requirements without conducting simulations. Therefore, the proposed method based on Eq. (18) and Eq. (32), can help architects and designers to make fast performance-driven decisions regarding window sizing process during early design stages.

3.3 Third phase: defining shading optical properties to provide sufficient glare protection according to the EN17037

Once building and facade level decisions are made the architect/designer by conducting the first and second phase of the innovative workflow proposed in this thesis, the shading selection (interior roller shade) could be conducted efficiently by applying the third phase of the workflow. The third phase is based on the selection of certain daylight model decisions in order to speedup annual glare simulations without compromising accuracy (Paper IV). In this section, all the necessary sensitivity analyses to support the recommendation of efficient glare assessment methods, which constitute the third phase of the innovative workflow proposed in this thesis, are developed in this section. As mentioned, for a suitable assessment of DGP-based glare protection metric, it is necessary to calculate properly vertical illuminance and luminance distribution of the field of view. Therefore, this section is split into four sections: recommended Radiance parameter for static illuminance simulations are presented and justified in section 3.3.1, comparison analysis of daylight calculation methods and material models for static glare calculation is presented in section 2.3.2, a criterion to choose daylight calculation method for dynamic glare calculations depending on the required computational time is developed and validated in section 3.3.3, and an evaluation of different sampling strategies for annual glare assessment in terms of computational time and accuracy is developed in section 3.3.4.

3.3.1 Setting Radiance parameters for illuminance calculations

This static analysis aims to investigate the influence of Radiance parameters and the openness factor (fabrics T100, T5, T3, and T1) on vertical illuminance at eye level calculated by different methods (3pm, 5pm, and *rtrace*). The analyzed time instant for this sensitivity analysis is 11:00 on February 5. At this time, the solar disk is in the field of view. It was assumed an acceptable relative deviation in terms of vertical illuminance of 15%. In Figure 34, the vertical illuminance at eye level calculated with the 3-phase method for different ad and ab parameters is shown. The minimum values of the ad and ab parameters to have an acceptable vertical illuminance are 5000 and 3, respectively.

The vertical illuminance at eye level calculated with the 5pm for different Radiance parameters can be seen in Figure 35. The Radiance parameters chosen for this sensitivity analysis are ad and MF in the direct sun coefficient simulation (cde). The ab and ad parameters for the 3-phase method were set to 10 and 65536, respectively (McNeil, 2013) to minimize the uncertainty from 3pm and 3pmD calculations. The minimum values of ad and MF parameters for the cde phase in order to have acceptable vertical illuminance calculated by the 5pm are 500 and 3, respectively.

Figure 36 shows the vertical illuminance at eye level calculated with the *rtrace* method for different ad and ab parameters. The minimum values of ad and ab parameters to have acceptable vertical illuminance are ad 500 and ab 4, respectively. Previous investigation regarding complex 3D textiles used an ab parameter of 5 for the time-point DGP calculations (Mainini et al., 2019). In summary, the ad parameter does not have significant influence on illuminance calculations when an analytical BRTDfunc model is applied to characterize the optical behaviour of fabrics. However, the ab and MF parameters have relevant influence on the results, with 3 and 4 being the minimum recommended ab parameters when using the 3pm and *rtrace* method, respectively. The minimum MF parameter for 5pm simulations is 3.

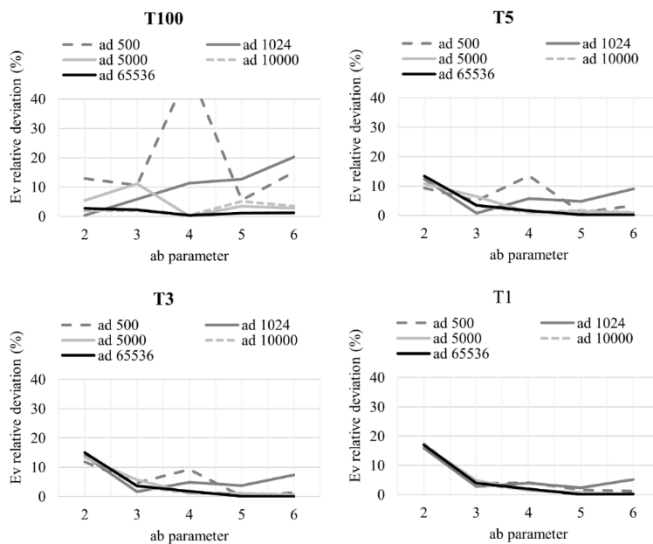


Figure 34. Relative deviation (with respect to the consecutive previous ab value: 2 relative to 1, 3 relative to 2, etc.) of vertical illuminance at eye level (Ev) calculated with the 3-phase method (11:00 February 5) for different ad, ab parameters, and fabrics T100 (upper left), T5 (upper right), T3 (bottom left), and T1 (bottom right).

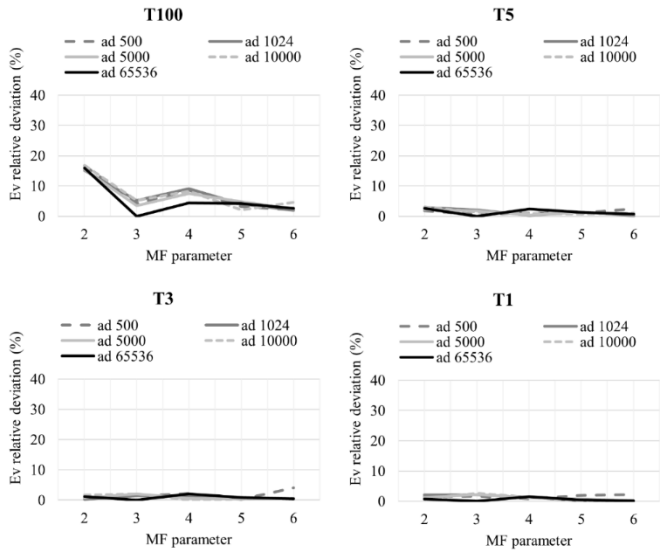


Figure 35. Relative deviation (with respect to the consecutive previous *ab* value: 2 relative to 1, 3 relative to 2, etc.) of vertical illuminance at eye level (*Ev*) calculated with the 5-phase method (11:00 February 5) for different *ad*, *ab* parameters, and fabrics T100 (upper left), T5 (upper right), T3 (bottom left), and T1 (bottom right).

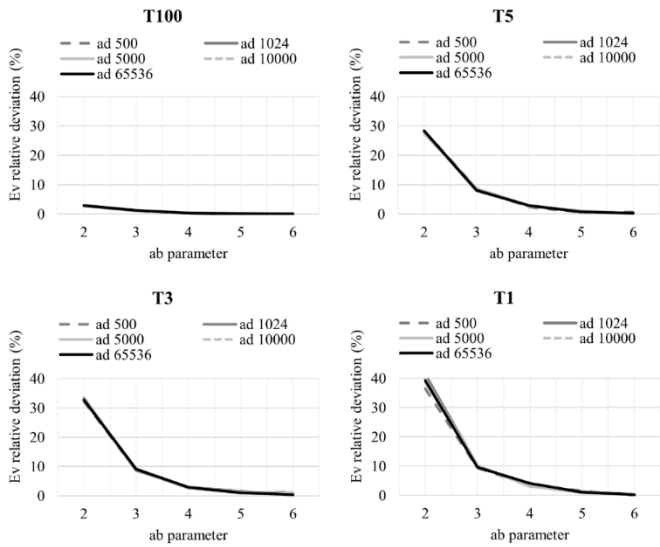


Figure 36. Relative deviation (with respect to the consecutive previous *ab* value: 2 relative to 1, 3 relative to 2, etc.) of vertical illuminance at eye level (*Ev*) calculated with the *rtrace* method (11:00 February 5) for different *ad*, *ab* parameters, and fabrics T100 (upper left), T5 (upper right), T3 (bottom left), and T1 (bottom right).

3.3.2 Selecting methods and material models for static DGP calculations

The aim of this static analysis is to study the influence of different Radiance materials, angular resolutions to represent the BSDF data, and daylight calculation methods on vertical illuminance, DGP, and luminance maps. Two time steps were considered: February 5 at 11:00, when the solar disk is in the field of view, and 16:00, when the solar disk is not in the field of view (but a bright patch from direct solar transmission onto the east-oriented wall is present). In this study, one viewing direction is selected: 45° towards the window. This analysis focused on three isotropic fabrics: T5, T3, and T1 (section 2.3.3), which were modeled using different Radiance materials (BRTDfunc, BSDF, and aBSDF) and angular resolutions (Klems basis and tensor tree). Four BSDF datasets were generated considering tensor tree formalisms (resolutions -t3 7, -t3 8, -t3 9, and -t4 5 by using the BSDF2tree method (section 2.3.4). Two Radiance materials were used: aBSDF (with peak extraction algorithm) and BSDF (without peak extraction) materials. An additional BSDF dataset using the Klems angular description (145x145 patches) was generated and modeled with aBSDF material (with peak extraction). Radiance parameters for the simulations are indicated in Table 8. Here, the ambient bounces and ambient divisions were set to $ab = 4$ and $ad = 500$, respectively, according to Figure 36. However, this ad value leads to an underestimation of the illuminance when tensor-tree BSDF formats without peak extraction are used with *rtrace*. In order to get acceptable results in this case, the ad parameter has to be increased to $ad = 1e6$ (Ward et al., 2021). This leads to 51 times more CPU time when using tensor-tree BSDF formats without peak extraction in the DGP calculation. On the other hand, it was demonstrated that the results of the 5pm do not improve in a conclusive fashion when either the ad or the MF parameters are increased. The luminance maps for fabrics T5, T3, and T1 are displayed in Figure 37. In general, the *rtrace* and 5pm methods show good agreement in terms of vertical illuminance, DGP values, and luminance distributions.

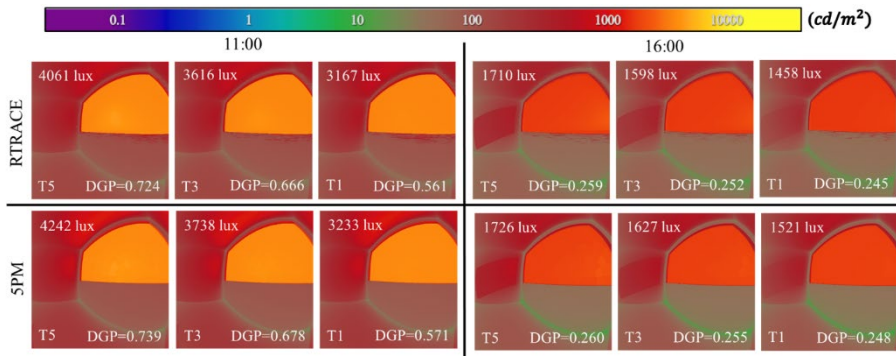


Figure 37. Luminance maps, vertical illuminances, and DGP at 11:00 (first three columns) and at 16:00 (last three columns) on February 5, in Freiburg, Germany, generated by the 5pm (upper row) and *rtrace* (bottom row) methods when using isotropic fabrics with different openness factor (5%, 3%, and 1%) defined with an analytical BRTDfunc model.

The results of the comparison are shown in Figure 38 and Figure 39. The comparison is very different, depending on whether the solar disk is in the field of view or not. If the solar disk is not within the field of view, all analyzed cases predict a similar DGP, which ranges between 0.24 and 0.26. The difference in vertical illuminance calculated by the different methods ranges between 200 lux and 400 lux. The lowest value of vertical

illuminance is obtained with the 3pm, which scatters the light into large solid angles (Klems patches), sometimes leading to discrepancies for point-in-space calculations. It is, however, known that the 3pm calculates the average illuminance over a plane reliably and is therefore suitable for daylighting calculations.

For the time step in which the solar disk is in the field of view, the discrepancies among the different methods are significant. The reference values for the comparison are those calculated by directly applying the BRTDfunc material in the ray-tracing calculation, because this material is the one used to generate the BSDF. The material definitions and BSDF resolutions that get closer to the reference value are t45a and Klemsa, both applying the peak extraction algorithm. A tensor-tree format without peak extraction must have a resolution of exponent 9 (2^9) to reach a DGP value within ± 0.05 of the one calculated for the reference case (by using $ad = 1e6$). The peak extraction algorithm combined with the tensor-tree format does not improve the comparison.

It can be concluded that the choice of the optical representation of the fenestration has a critical impact on the DGP calculation. As reported in the literature (Lee et al., 2018a, 2018b), the 3pm is not suitable for DGP calculations when the solar disk is in the field of view. However, due to its simplicity and low computational requirements, the Klems BSDF with peak extraction (aBSDF Radiance material) might offer an efficient representation of anisotropic fabrics with a main view-through component for glare calculations.

11:00 (sun visible)

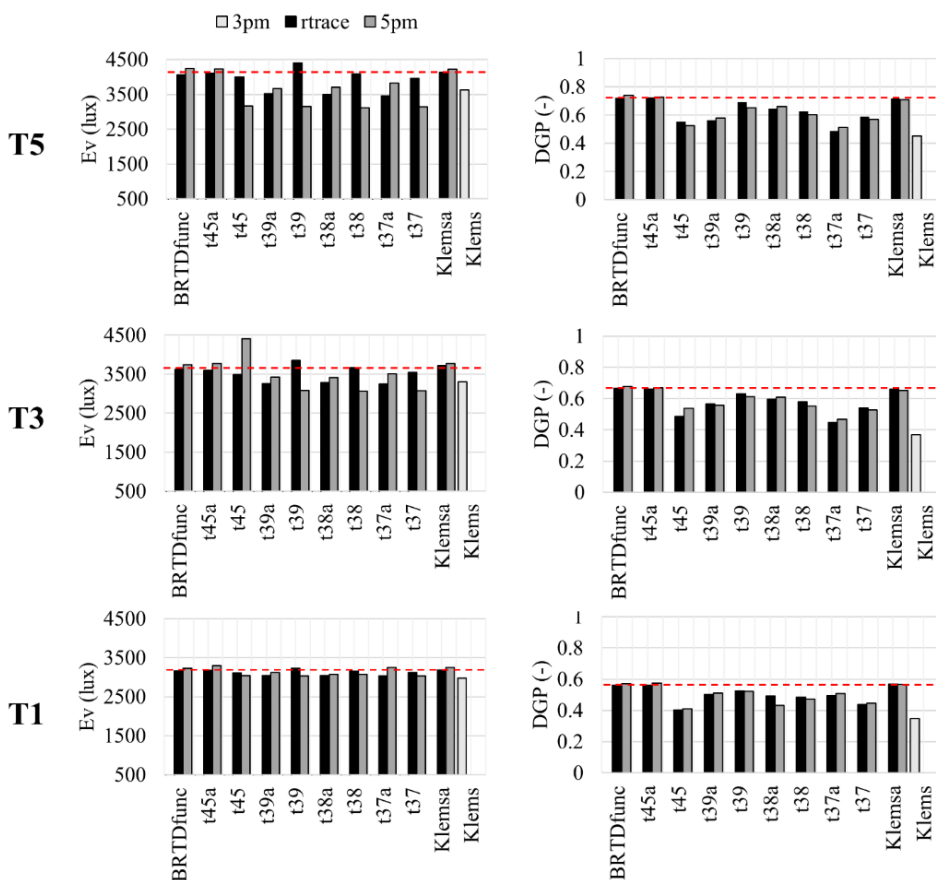


Figure 38. Vertical illuminance at eye level (left column) and DGP values (right column) at 11:00 (February 5) for different daylight methods, Radiance materials, and fabrics (T5 (first row), T3 (second row), and T1 (third row)). The suffix a refers to the Radiance material aBSDF. The number of ambient divisions (ad parameter) is 1024, 500, and 1e6 for 5pm, rtrace (BRTDfunc and aBSDF material), and rtrace (BSDF material). Discontinuous line refers to the reference value (BRTDfunc material).

16:00 (sun not visible)

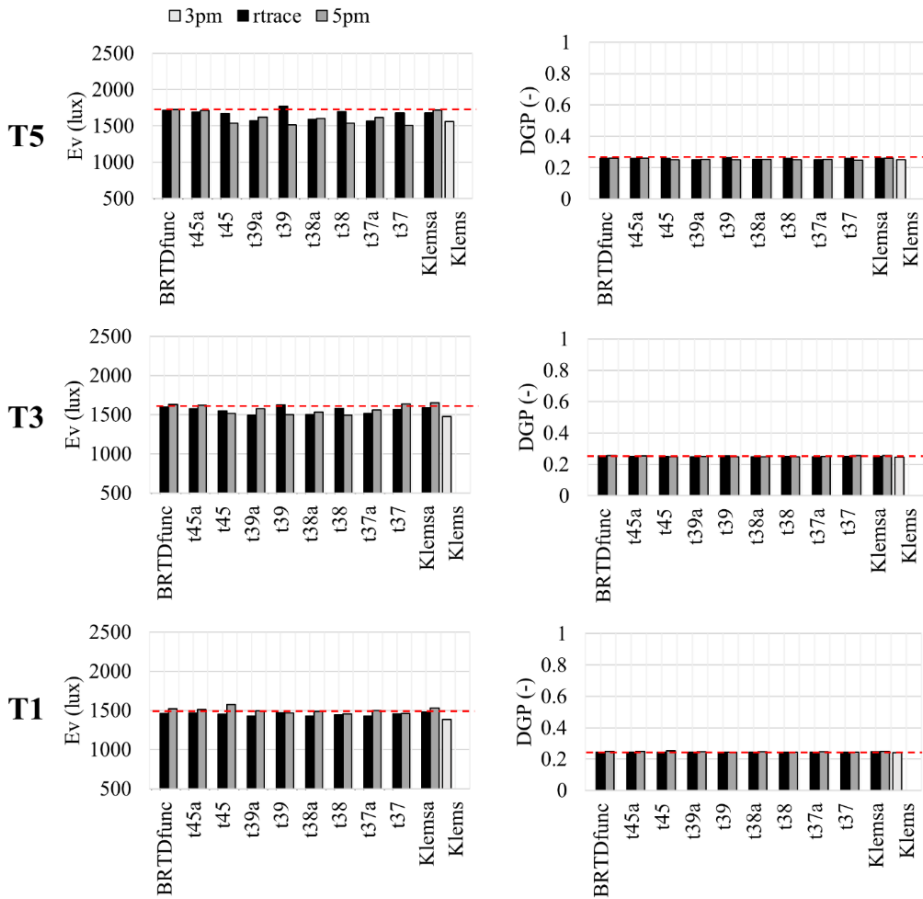


Figure 39. Vertical illuminance at eye level (left column) and DGP values (right column) at 16:00 (February 5) for different daylight methods, Radiance materials, and fabrics (T5 (first row), T3 (second row), and T1 (third row)). The suffix a refers to the Radiance material aBSDF. The number of ambient divisions (ad parameter) is 1024, 500, and 1e6 for 5pm, rtrace (BRTDfunc and aBSDF material), and rtrace (BSDF material). Discontinuous line refers to the reference value (BRTDfunc material).

3.3.3 Choice of the fastest method for dynamic glare assessment

For annual simulations, the number of time steps, scenes and CFSs affect the CPU time, which can be decisive in determining the most suitable daylight calculation method. Typically, the number of time steps in annual glare simulations is referred to daytime hours (4380). The number of different scenes depends on the number of view positions and directions to assess glare risk as well as the different geometrical models (geometrical variations of the 3D model that represent the interior/exterior scenes). As mentioned in section 1.6, the 5pm reuses information referring to the scene. Nevertheless, a direct simulation based on the DC (phase cds) must be conducted for every window state, which may compromise the use of the 5pm when the number of different facade states or scenes is large. Moreover, the *rtrace* method does not reuse information for the scene or the sky, being slower than the 5pm for annual DGP calculations without a sampling strategy. Annual glare analyses with different Radiance parameters and sampling strategies could justify the use of one or the other method.

The first objective of this section is to define the CPU time required by any annual glare assessment when using the *rtrace* and 5pm methods. This time analysis is based on formulas that represent the coding structure of the required Radiance commands to run the *rtrace* method and 5pm simulations (Subramaniam, 2017). The second objective is to propose a criterion based on CPU time for the selection of the daylight method depending on the annual glare analysis of interest. The independent variables that define any annual glare analysis are the number of scenes (n), number of time steps (h), and the number of CFSs considered (c). Thus, the CPU time required by the 3pm can be expressed as follows:

$$\tau_{3pm} = t_s h + n(t_M + t_{dc} h c) \quad (34)$$

Where:

t_s = CPU time required to create a sky vector (S) (the same for illuminance calculations and rendering generation),

t_M = CPU time required to create the view (V) and daylight (D) matrices (for illuminance calculations and rendering generation),

t_{dc} = CPU time required for the multiplication of the matrices V, T, D, and S (for illuminance calculations and rendering generation).

The CPU time required by the 5pm for the direct 3pm (3pmD) is the following:

$$\tau_{3pmD} = t_{sD} h + n(t_{MD} + t_{dcD} h c) \quad (35)$$

Where:

t_{sD} = CPU time required to create a sky vector (S_D) with the exclusive contribution of the sun (the same for illuminance calculations and rendering generation),

t_{MD} = CPU time required to create the octree (black plastic material), view with $ab = 1$ (V_D), and daylight with $ab=0$ (D_D) matrices (for illuminance calculations and rendering generation),

t_{dcD} = CPU time required for the multiplication of the matrices V_D , T, D_D , and S_D (for illuminance calculations and rendering generation),

The CPU time required by the cds phase of the 5pm is the following:

$$\tau_{cds} = t_{sF} h + n(t_{MF} + t_{cds} c + t_{dcF} h c) \quad (36)$$

Where:

t_{sF} = CPU time required to create a sky vector ($S_{c_{ds}}$) with only the contribution of the sun and selected Reinhart sky subdivisions (MF) (the same for illuminance calculations and rendering generation),

t_{MF} = CPU time required to create the suns (the same for illuminance calculations and rendering generation) and material map generation (for rendering),

$t_{c_{ds}}$ = CPU time required to create the octree (black plastic material) and sun coefficient matrix $C_{c_{ds}}$ (for illuminance calculations and rendering generation),

$t_{d_{cs}}$ = CPU time required for the multiplication of the matrixes $C_{c_{ds}}$ and $S_{c_{ds}}$ (for illuminance calculations and rendering generation).

The computational time required by arithmetic operations of all results from the previous phases (3pm, 3pmD, and cds) can be expressed as:

$$\tau_m = t_0nhc \quad (37)$$

Where:

t_0 = CPU time required by the arithmetic combination of the results from the phases 3pm, 3pmD, and cds (for illuminance calculations and rendering generation).

Finally, the CPU time required by the 5pm is the sum of all the previously defined CPU times:

$$\tau_{5pm} = \tau_{3pm} + \tau_{3pmD} + \tau_{c_{ds}} + \tau_m \quad (38)$$

In addition, the CPU time required by the *rtrace* method is the following:

$$\tau_{rtrace} = t_cnhc \quad (39)$$

Where:

t_c = CPU time required by the sky and octree generation (common for illuminance calculations and rendering) and the commands *rtrace* (for illuminance calculations and rendering generation) and command *evalglare* (for DGP calculations).

Combining equations (38) and (39), it can be expressed mathematically whether the *rtrace* method is faster than the 5pm for the same generic daylight glare analysis:

$$\tau_{rtrace} \leq \tau_{5pm} \quad (40)$$

$$t_cnhc \leq \tau_{3pm} + \tau_{3pmD} + \tau_{c_{ds}} + \tau_m \quad (41)$$

$$t_cnhc \leq T_s h + T_M n + T_{dc}nhc + t_{c_{ds}}nc \quad (42)$$

In order to speed up the glare calculations, it was proposed to analyse fewer time steps when using *rtrace* than when using the 5pm. Furthermore, equation (42) can be rewritten as follows:

$$t_cnhc \leq T_s H + T_M n + T_{dc}nHc + t_{c_{ds}}nc \quad (43)$$

where h and H are the time steps for *rtrace* and for the 5pm, respectively. The maximum number of time steps when using *rtrace* (Eq. (44)) (h_{max}) depends on time parameters (t_c, T_s, T_M, T_{dc} , and $t_{c_{ds}}$), the number of scenes (n), number of CFSs (c), and the number of time steps considered when using the 5pm (H).

$$h_{max} = \frac{(T_M + t_{c ds} c) n + (T_s + T_{dc} n c) H}{t_c n c} \quad (44)$$

For an initial annual glare evaluation (considering clear sky conditions), only one window state is considered ($c = 1$) and the most problematic viewpoint/direction is analyzed ($n = 1$). This initial annual glare assessment is key to identify time steps with a risk of daylight glare. In practice, these time steps could be analyzed when comparing different shading devices that could provide a desired degree of glare protection. Thus, h_{max} can be expressed as follows:

$$h_{max} = \frac{(T_M + t_{c ds})}{t_c} + \frac{(T_s + T_{dc})}{t_c} H \quad (45)$$

The value of the time parameters depends on the Radiance parameters and the machine used to run the glare simulations. It was used 25 cores of a Linux machine cluster of 56 CPUs to run all the simulations (Processor Intel(R) Xeon(R) CPU E5-2697 v3 @ 2.60GHz). The Radiance parameters used for each phase of the 5pm are shown in Table 8. In practice, at least an initial static calculation using *rtrace* and 5pm is necessary in order to calculate all the time parameters that can be seen in Table 14.

Table 14. Values of all time parameters for *rtrace* and 5pm calculations when using $n=25$ (Eq. (45)).

	Parameter	Value (seconds)
	t_s	0.1
3pm	t_M	8453.2
	t_{dc}	6.0
	t_{sD}	0.05
3pmD	t_{MD}	520.2
	t_{dcD}	5.5
	t_{sF}	0.1
5pm	t_{MF}	1.0
	$t_{c ds}$	22125
c ds	t_{dcF}	3.0
	Arith. comb	t_0
rtrace ab=[1, 2, 3, 4, 5]	t_c	[7.0, 32.4, 60, 72.6, 77.6]

The graphical representation of Eq. (45) can be seen in Figure 40. The fastest method to assess glare risk in terms of DGP, depending on the combination of h and H , can be determined from Figure 40. Thus, the 5pm is faster than the *rtrace* method for all the points above the line which represents h_{max} . By contrast, for all the combinations of h

and H below the line, the *rtrace* method is faster than the 5pm for the annual glare analysis of interest.

A typical annual simulation of 4380 time steps with 5pm delivers results 7 times faster than the *rtrace* method with ab 5 (from Eq. (38) and (39)). On the other hand, a single-hour 5pm simulation (without precalculated matrices) requires the same CPU time as 174 hours simulated with the *rtrace* method. For ab 2, the feasible range of h_{max} is between 522 and 2097 hours when a single scene and CFS are considered. Nevertheless, the range of h_{max} is between 174 and 699 hours for ab 5. Thus, there is high potential to speed up annual glare simulations by selecting adequate sampling strategies. A simple criterion based on CPU time was defined for the selection of the fastest method to be used in annual glare assessments. In addition, the proposed expressions Eq. (34), Eq. (38), and Eq. (39) can be used as prediction formulas to approximate CPU time required by daylight calculation methods such as 3pm, 5pm, and *rtrace*, respectively.

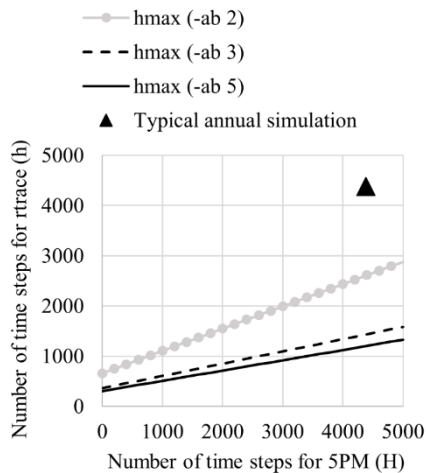


Figure 40. Maximum number of time steps to run with *rtrace* method depending on the number of time steps chosen to run the 5pm (for one scene and one window state).

In cases in which many annual simulations are required, it might be advisable to calculate in advance the computational cost of alternative sampling strategies. The formulation presented in section 3.2, in particular Eq. (38) and Eq. (39), can be used for this purpose. The computational cost of the SV5 sampling strategy (DGP calculated for the daily visible sun hours once every 5 days) is calculated by the 5pm and *rtrace* methods for the T1 fabric and a viewing direction 45° towards the window (Table 15). The required CPU time by the 5pm to solve for 168 hours/year is 9.8 hours against 3.6 hours when using *rtrace* (-ab 4). The predicted CPU time shows good agreement with actual CPU times. For the calculation of 168 DGP values, one window state, and one scene, the *rtrace* method with ab 4 is faster than the 5pm according to Figure 41. The graph also shows, on one hand that *rtrace* method than the 5pm for a SD7 sampling strategy (298 DGP values). On the other hand, the 5pm is faster than *rtrace* for a SD1 sampling strategy (2190 DGP values).

Table 15. CPU times for different daylight methods, fabric T1, viewing direction 45° towards to the window, and sampling strategy SV5 (168 hours/year).

	5pm	rtrace (-ab 4)
Predicted	9.6	3.4
CPU time (h)		
Real	9.8	3.6
CPU time (h)		

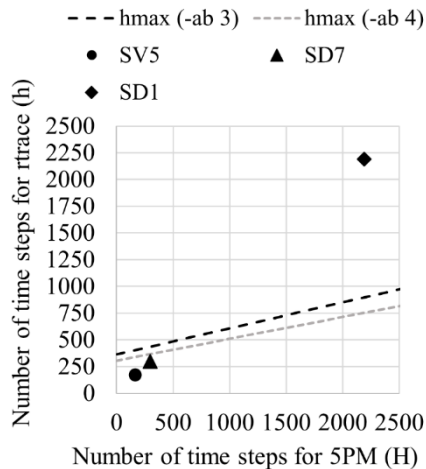


Figure 41. Maximum number of time steps to run with the rtrace method depending on the number of time steps chosen to run using the 5pm for different sampling strategies (for one scene and one window state). SDK and SVK are sampling strategies based on selected daytime and “sun visible” hours each K days of the semi-annual period, respectively.

3.3.4 Sampling strategies to speedup annual glare calculations

The aim of this analysis is to propose efficient sampling strategies for annual glare assessment under clear sky conditions. The annual glare protection was quantified with the annual glare metric fDGpT defined by the European standard EN 17037 (maximum fDGpT = 5%). In this case, the CFS was defined as a combination of a solar-control double glazing unit (DGUSC) “ipascal neutral 50/27” ($\tau_{nh} = 49\%$) (INTERPANE Glasgesellschaft mbH, 2018) and an isotropic fabric T1 as the interior shading system. Fabrics T1, T3, and T5 were selected to cover a range of fabrics with openness factor between 1% and 5% for accuracy comparisons. However, only T1 was analyzed in terms of CPU time since time parameters are similar in both cases (Table 14). The chosen viewing direction of the room occupant is 45° towards the window plane (critical scenario). As demonstrated in section 3.3.4, it is necessary to define the number of time steps of the simulation in order to establish the most computationally efficient method to run an annual glare assessment. The analyzed sampling strategies are shown in Table 16. Since only sunny skies should be considered in the glare evaluation, the simulation of only half of the year (from winter to summer solstice) already provides all sun positions in the sky and reduces

the computational time by half. Another sampling strategy consists of simulating only the time steps where the solar disk is in the field of view (“visible” sun hours). Thus, the number of hours of “visible” sun hours depends strongly on the scene elements such as viewing position/direction, window size, room orientation, etc. This strategy assumes that no diffuse and/or specular reflection of the sun on any surface of the scene or the shading device will cause glare when this is not in the field of view, which is a reasonable assumption in many cases.

The maximum number of time steps is associated with the sampling strategy SD1 (2190) daylighting hours for a half-year simulation), which is the sampling strategy proposed by the EN 17037 standard for clear skies. The required CPU time is 21.3 h (Eq. 38) and 66.9 h (Eq. (39)) when using the 5pm and the *rtrace* method ($ab = 4$), respectively. Therefore, the 5pm was chosen to run the annual glare analyses using the different sampling strategies defined in Table 16. The Radiance parameters used in the simulations can be seen in Table 8. In addition, an aBSDF Radiance material with Klems angular resolution and peak extraction was used to model the CFS for the direct sun coefficient calculation (phase cds).

Table 16. Sampling strategies and their associated number of time steps. SDn/SVn represents the sum of daily daytime/visible sun time steps each n days during the first semimanual period.

(Sampling strategy) Number of time steps		December 21- June 21	
		Daytime	Visible sun
Day steps	1	(SD1) 2190	(SV1) 820
	3	(SD3) 703	(SV3) 276
	5	(SD5) 420	(SV5) 168
	7	(SD7) 298	(SV7) 119
	9	(SD9) 227	(SV9) 94
	11	(SD11) 180	(SV11) 77

The time steps considered by each sampling strategy can be seen in Figure 42. In this analysis, the frequency of DGP calculation (day steps) was varied from 1 (daily) to 11 (once every 11 days). The first step is to compare the required computational time for each sampling strategy (Figure 43). The CPU time can vary from 21 hours to approximately 9 hours depending on the sampling strategy used. For a day step of 1, the consideration of visible sun (SV1) instead of daytime hours decreases the CPU time by 35% compared to strategy SD1.

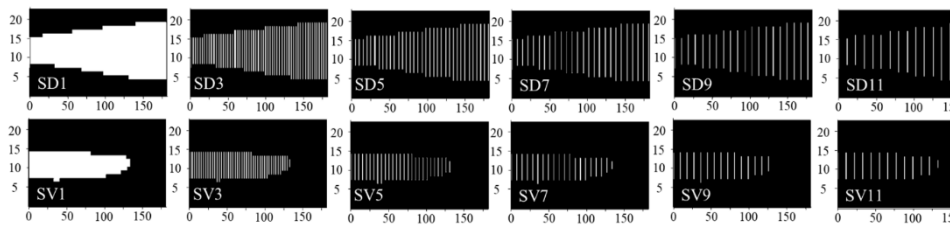


Figure 42. Time steps considered by each sampling strategy. The horizontal axis represents the days of the first half of the year and the vertical axis represents the hours per day. SDn (upper row)/SVn (bottom row) represents the sum of daily daytime/visible sun time steps each n days during the first semimanual period.

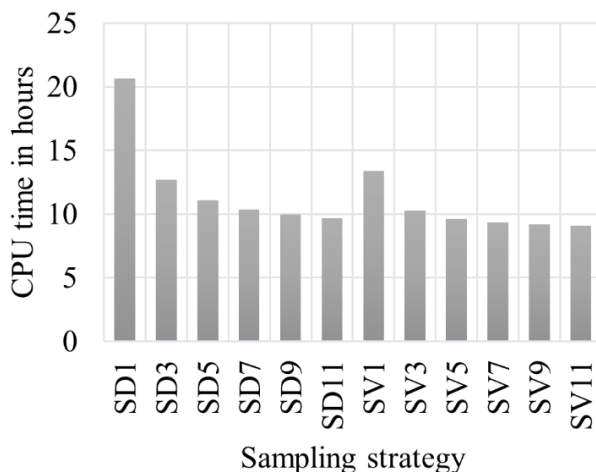


Figure 43. Required CPU time for the 5pm depending on the sampling strategy.

Once analyzed the sampling strategies in terms of CPU time, it is necessary to compare these sampling strategies in terms of accuracy. Sampling strategy SD1 was set as the reference sampling strategy because it has the maximum number of time steps within the sampling strategies presented. Figure 44 shows the absolute deviation of the fDGpT value for each sampling strategy from that for strategy SD1 when using T1, T3, and T5. Sampling strategies based on daytime hours (SD1, SD3, SD5, SD7, SD9, and SD11) can produce a maximum absolute fDGpT deviation up to 1.2%, 2.4%, and 2.5%, when using T1, T3, and T5, respectively. Consideration of only the “sun visible” hours (SV1, SV3, SV5, SV7, SV9, and SV11) leads to a maximum absolute fDGpT deviation up to 1.7%, 3%, and 3.5%, when using T1, T3, and T5, respectively.

A good trade-off between accuracy and CPU time depends on the shading device and the number of hours of visible sun for a certain view position and direction. From the cases analyzed, a sampling strategy SD7 can be safely applied assuming an absolute f0.45 (fDGpT with DGpT = 0.45) deviation of less than 1% (CPU reduction of 57% by using with the *rtrace* method (-ab 4) with respect SD1 with the 5pm). If a f0.45 deviation of 2% was acceptable, e.g. for comparing design alternatives, a sampling strategy SV5 would be appropriate (CPU time reduction of 76%). There are also other approaches to reduce the

simulation time of annual glare simulations based on GPU technology (Jones, 2019) or the novel Raytraverse method (Wasilewski et al., 2021) which should be further investigated.

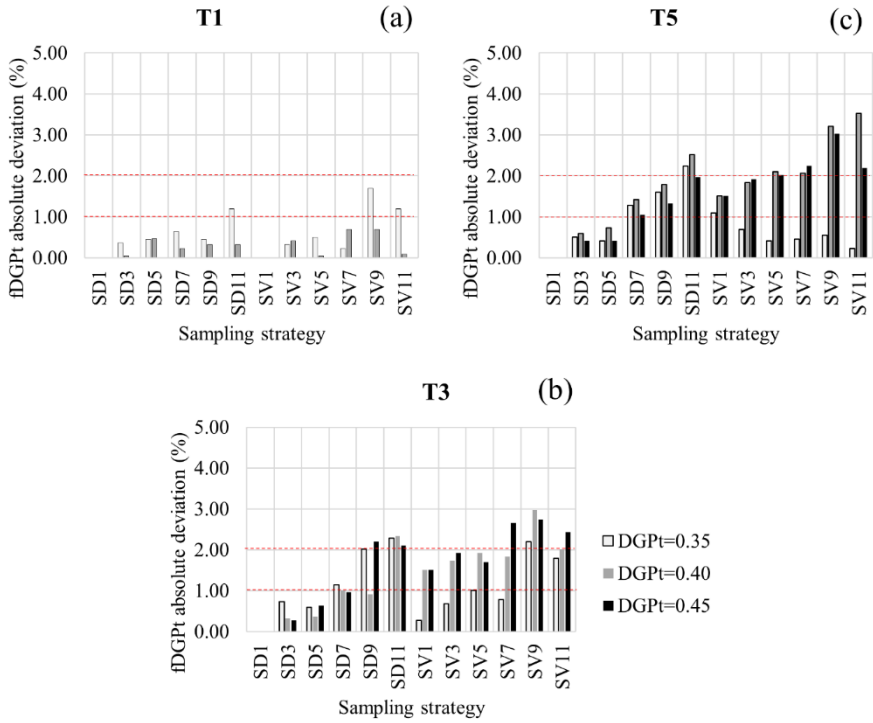


Figure 44. Absolute deviations in terms of the annual glare metric defined by EN17037 (fDGpT) for different sampling strategies and isotropic fabrics: T1 (a), T3 (b), and T5 (c). The sampling strategy SD1 (daytime hours each day during the semi-annual period) was set as the benchmark for the deviation calculation.

4 Conclusions

This thesis presents an innovative workflow to help architects to design buildings with adequate levels of solar access, daylight provision, and protection against overheating and daylight glare. This proposed workflow consists of three design phases. During the first phase, the proposed multi-objective workflow is recommended to help architects and designers to make decisions to building level to ensure adequate solar access levels according to the Estonian standard. In the second phase, rules of thumb and prediction formulas are used to facade level to ensure a good balance between daylight provision and overheating protection. Finally, in the third phase, efficient shading system selection is recommended to ensure a certain glare protection level according to the European standard EN17037:2018.

The first objective of this thesis is to propose an easy-to-use multi-objective optimization workflow based on solar access to help architects and designers to design buildings orientation, massing, and envelope efficiently. The second objective is to propose rules of thumb obtained from analyzing the effect of different daylight assessment criteria on the combined fulfillment of daylighting and overheating protection requirements and its implications for the design of residential and office rooms in Estonia. The third objective is to develop daylight and overheating prediction formulas that can help architects and designers to efficiently select window type during early design stages. The fourth objective of this thesis is to propose efficient assessment methods to assess glare protection defined by the European standard EN17037.

The main research outcomes are as follows:

1. Regarding the window sizing process, within the context of the European standard EN17037, the fulfillment of a target minimum DF of the half of the reference plane closer to the window side (minDF) in side-lit rectangular rooms implies the fulfillment of a target minimum DF in at least 95% of the reference plane (Paper II);
2. The definition of a prediction formula based on polynomial fitting for the estimation of minDF based on visible transmittance of the glazing, room depth, window-to-wall ratio (WWR), and obstruction angle parameters is viable in terms of computation time with a relative accuracy of 0.21 for any European country. Moreover, the definition of an overheating risk prediction formula based on polynomial fitting for the estimation of the Degree-hour (DH) metric, which is used by the Estonian regulation, based on g-value, window-to-floor ratio (WFR), and obstruction angle parameters is viable in terms of computation time with a relative accuracy of 0.21 for the design of residential buildings within the Estonian context (Paper III);
3. Regarding shading selection process, for the particular case of fabrics with a view-through specular component without light-redirecting effects, the combination of a low-resolution BSDF, such as the Klems format, and a peak extraction algorithm, such as the one offered by Radiance's aBSDF material, provide a suitable representation for glare analysis using the 5pm or rtrace methods. Furthermore, for fabrics in which rotational invariance can be

assumed, a representation based on the Radiance BRTDfunc material can be useful, because it only requires the normal-normal transmittance, the normal-diffuse transmittance and the cut-off angle of the fabric (Paper IV).

The potential applications of the results for architects and designers are as follows:

1. We recommend the use of the multi-objective optimization method presented in this thesis in the early design stages of residential buildings in cold climates. How to exploit the SA requirements to optimize the building performance using different multi-objective criteria is investigated. This workflow is especially suitable when the SA regulations are strict, such as the Estonian context. First decisions as building orientation, windows location, building footprint, and buildable volumes are critical, since they characterize the solar access of the existing and new buildings. Other requirements related to daylight provision, overheating, energy consumption, or glare protection could be fulfilled with a suitable design of interior layout and façade (Paper I);
2. The proposed coupled method based on minDF and DH prediction formulas has big potential to help designers to consider a performance-driven criterion based on daylight provision and overheating risk requirements during early design stages design. Thus, they could create interior floor and window sizing plans efficiently. Combining the prediction formulas, the window's size and properties (g-value and visible transmittance) that ensure the combined fulfillment of minDF-based and DH-based requirements can be calculated and represented graphically. By using this design approach, designers can save considerable time required by daylight and energy simulations because there is no need to conduct time-consuming iterative design processes based on simulations to design well daylit and not overheated buildings (Paper III);
3. When evaluating glare protection of different shading device, a suitable sampling strategy for annual glare risk assessments can make a time step-based ray-tracing method (the *rtrace* method in this paper) more computationally efficient than the alternative five-phase method. For cases in which no diffuse and/or specular reflections of the sun from any surface of the scene or the shading device will cause glare when this is not in the field of view, a sampling strategy that takes into account only the hours when the solar disk is in the field of view can reduce the computational time considerably. This strategy can be combined with semi-annual evaluations (for clear skies) and a suitable sampling strategy (e.g. one day per week) to further reduce the computational time. The sensitivity analysis of Radiance parameters for the *rtrace* method presented in the study can help to optimize the computational cost of simulations. Thus, by using this methodology, designers could efficiently compare several CFSs in terms of annual glare protection performance during early design stages of the building design process (Paper IV).

The main potential applications of the results for regulation makers are as follows:

1. The Estonian daylight standard EVS 894:2008/A2:2015 has limited reliability in properly predicting the daylight potentials of building interiors. In many cases, it overestimates daylight availability for different orientations. Therefore, it is necessary to increase the awareness about the need to promote a new and more efficient daylight regulation in Estonia. This will be done considering the new European standard EN 17037 also analyzed in this study, since there is a strong disagreement between the Estonian standard and the European Standard EN 17037 in assessing the daylight for residential and office buildings. This aspect should be considered in the development of the guidelines for the new daylight regulation, establishing minDF-based requirements proposed in the EN 17037. Hence, this research will contribute to the development of the compulsory building daylight regulation (Paper II);
2. Evidence strengthens the findings of the existing literature about the conflicting requirements of overheating in building regulations and the Estonian daylight standard. Considering the new European standard, the requirements will not change significantly. However, if the daylight regulation incorporates the results of the dynamic daylight analysis presented in this thesis, the conflicts will increase because larger glazed areas will be necessary to fulfill the daylight requirement. Nevertheless, several cases that fulfill both requirements will increase when passive measures such as window airing or fixed shading are adopted. This suggests, firstly, the synergistic formulation of daylighting and overheating protection requirements in new building regulations to make it easier for designers to fulfill both daylight and overheating protection requirements. Secondly, this suggests the promotion of the use of building design features such as efficient materials and passive measures to reduce overheating while ensuring appropriate daylight levels (Paper II);
3. The author recommends to regulation makers the consideration of the coupled method based on prediction formulas proposed in this thesis. European countries might adopt DH-based overheating protection requirements with climate-dependent thresholds as benchmark to assess overheating risk in buildings. Furthermore, the achievement of the combined fulfillment between DF-based daylight provision requirements according to the European standard EN17037 and DH-based overheating protection requirements in buildings would be much simpler and affordable (At least, no daylight simulations are needed during the design process within the European framework, thanks to the work in this thesis) during the early design stages (Paper III);

4.1 Future work

Regarding the multi-objective optimization method in the early design stages of the design of residential buildings in cold climates part of the first phase of the workflow, different criteria are considered and the entire possible building envelope are evaluated and the maximum fitness value searched. This brute-force approach could not be affordable in terms of computational time when the number of design alternatives are very large (e.g. more than 200). Future work is to apply optimization algorithms such as

genetic algorithm in large optimization design cases. Additionally, this method will be implemented in a Grasshopper tool for Rhinoceros to help architects and designers to choose between possible building design strategies.

For the development of the rules of thumb part of the second phase (simplified method) of the workflow, the effect of different daylight assessment criteria on the combined fulfillment of daylighting and overheating requirements and its implications for the design of residential and office rooms in Estonia, are recommended for a specific cost-optimal (within the Estonian context) triple glazed system ($T_{vis} = 0.63$, g -value = 0.37) and fixed shading type. In addition, the control algorithm for the window airing system was based on a basic set point (25 °C) between the heating set point (21 °C) and the overheating limit (27 °C) (defined in the Estonian regulation), with the window airing position of 10%. The rules of thumb used in this study might have lacked some special cases in terms of combined fulfillment that deserve further study from an architectural point of view. Furthermore, different assumptions in terms of window airing control and complex fenestration systems (glazing and shading system) have different impacts on daylight provision and risk of overheating. Therefore, future research should conduct sensitivity analyses for different window airing controls, glazing systems, and switchable shading devices. Another future path could be the development of prediction models to estimate the daylight provision and risk of overheating in Estonian buildings. Finally, this study can help architects, designers, and engineers understand the good practices not only in early design stages of the design of the buildings but also in the retrofitting stage to achieve satisfactory levels of indoor comfort in buildings.

The coupled method based on prediction formulas, which is part of the detailed method used in the second phase of the workflow, was applied to a single case study located in a cold climate. Moreover, an accuracy of 0.21 for minDF and DH predictions might not be acceptable for some design criteria. It was studied side-lit room typology specific to Estonia. Thus, the viability of the proposed coupled method based on prediction formulas should be further quantified for different climates, construction materials, and room typologies (e.g. rooms with multiple orientations). The accuracy of DH predictions was quantified for a specific combination of HVAC settings recommended for the Estonian context by local regulations and previous investigations. Settings such as the natural ventilation strategy (e.g. openable area and temperature set point), infiltration rates, construction materials, or occupancy profiles are influenced in practice by specific local regulations of each European country. Therefore, further investigations should study the validity of approaches based on DH prediction formula in different climate and regulation contexts. Finally, this coupled method will be implemented as an interactive tool such as a Grasshopper plug-in for Rhinoceros 3D that could be used not only by architects and designers as a design tool but also for educational purposes. This interactive tool could be included in a general framework to optimize the design of residential buildings within the Estonian context.

Regarding efficient annual glare assessment based on the selection of optimal Radiance parameters, in practice, this decision depends on the trade-off between illuminance/DGP accuracy and CPU time. A lower ab parameter can be very valuable in early design stages of the building design process when glare risk in multiple indoor spaces with several fabrics must be assessed. Moreover, for daylight glare assessment considering building occupants positions different from those closer to the window, optimal ab parameters might vary from those recommended in this thesis and therefore, must be further studied. There are also other approaches apart from annual glare

assessment methods based on the selection of optimal Radiance parameters, daylight calculation methods, CFS modelling techniques, and sampling strategies to reduce the simulation time of annual glare simulations based GPU technology (Jones, 2019) or the novel Raytraverse method (Wasilewski et al., 2021) which should be further investigated.

References

- Abravesh, M., Bueno, B., Heidari, S., Kuhn, T.E., 2019. A method to evaluate glare risk from operable fenestration systems throughout a year. *Build. Environ.* <https://doi.org/10.1016/j.buildenv.2019.106213>
- Al-Obaidi, K.M., Ismail, M.A., Munaaim, M.A.C., Abdul Rahman, A.M., 2017. Designing an integrated daylighting system for deep-plan spaces in Malaysian low-rise buildings. *Sol. Energy*. <https://doi.org/10.1016/j.solener.2017.04.001>
- Alva, M., Vlachokostas, A., Madamopoulos, N., 2020. Experimental demonstration and performance evaluation of a complex fenestration system for daylighting and thermal harvesting. *Sol. Energy*. <https://doi.org/10.1016/j.solener.2020.01.012>
- Apian-Bennewitz, P., 2010. New scanning gonio-photometer for extended BRDF measurements, in: *Reflection, Scattering, and Diffraction from Surfaces II*. <https://doi.org/10.1117/12.860889>
- Balaras, C.A., Drousa, K., Argiriou, A.A., Wittchen, K., 2002. Assessment of energy and natural resources conservation in office buildings using TOBUS. *Energy Build.* 34. [https://doi.org/10.1016/S0378-7788\(01\)00107-4](https://doi.org/10.1016/S0378-7788(01)00107-4)
- Beizaee, A., Lomas, K.J., Firth, S.K., 2013. National survey of summertime temperatures and overheating risk in English homes. *Build. Environ.* <https://doi.org/10.1016/j.buildenv.2013.03.011>
- Bian, Y., Ma, Y., 2017. Analysis of daylight metrics of side-lit room in Canton, south China: A comparison between daylight autonomy and daylight factor. *Energy Build.* <https://doi.org/10.1016/j.enbuild.2016.12.059>
- Brembilla, E., Chi, D.A., Hopfe, C.J., Mardaljevic, J., 2019. Evaluation of climate-based daylighting techniques for complex fenestration and shading systems. *Energy Build.* <https://doi.org/10.1016/j.enbuild.2019.109454>
- Brembilla, E., Hopfe, C.J., Mardaljevic, J., 2018. Influence of input reflectance values on climate-based daylight metrics using sensitivity analysis. *J. Build. Perform. Simul.* 11. <https://doi.org/10.1080/19401493.2017.1364786>
- BSI, 2008. BS 8206-2: Lighting for buildings. Code of practice for daylighting, British Standards Institute.
- Bueno, B., Sepúlveda, A., 2019. A Specific Building Simulation Tool for the Design and Evaluation of Innovative Fenestration Systems and their Control, in: *International Building Performance Simulation Association -IBPSA-: Building Simulation 2019. 16th Conference of IBPSA. Proceedings : Rome, Italy, 2-4 September 2019.*
- Bueno, B., Wienold, J., Katsifaraki, A., Kuhn, T.E., 2015. Fener: A Radiance-based modelling approach to assess the thermal and daylighting performance of complex fenestration systems in office spaces. *Energy Build.* <https://doi.org/10.1016/j.enbuild.2015.02.038>
- Bugeat, A., Beckers, B., Fernández, E., 2020. Improving the daylighting performance of residential light wells by reflecting and redirecting approaches. *Sol. Energy* 207. <https://doi.org/10.1016/j.solener.2020.07.099>
- CalumenLive, 2021. SGG CLIMATOP 6 (18 ARGON 90) 4 (18 ARGON 90) 4 COOL-LITE SKN 174 F2 PLANITHERM XN F5 [WWW Document]. URL <https://calumenlive.com/find-glazing> (accessed 6.14.19).
- Cammarano, S., Pellegrino, A., Lo Verso, V.R.M., Aghemo, C., 2015. Assessment of daylight in rooms with different architectural features. *Build. Res. Inf.* 43. <https://doi.org/10.1080/09613218.2014.922359>

- Capeluto, I.G., Plotnikov, B., 2017. A method for the generation of climate-based, context-dependent parametric solar envelopes. *Archit. Sci. Rev.* 60. <https://doi.org/10.1080/00038628.2017.1331334>
- Capeluto, I.G., Shaviv, E., 2001. Modeling the Design of Urban Fabric With Solar Rights Considerations. *Sol. Energy* 70.
- Chegari, B., Tabaa, M., Simeu, E., Moutaouakkil, F., Medromi, H., 2021. Multi-objective optimization of building energy performance and indoor thermal comfort by combining artificial neural networks and metaheuristic algorithms. *Energy Build.* 239. <https://doi.org/10.1016/j.enbuild.2021.110839>
- Chi, D.A., Moreno, D., Navarro, J., 2017. Design optimisation of perforated solar façades in order to balance daylighting with thermal performance. *Build. Environ.* <https://doi.org/10.1016/j.buildenv.2017.09.007>
- CLIMATE-DATA.ORG, 2021. Climate: Estonia.
- Darula, S., Christoffersen, J., Malikova, M., 2015. Sunlight and insolation of building interiors., in: *Energy Procedia*. <https://doi.org/10.1016/j.egypro.2015.11.266>
- De Luca, F., 2017a. Solar form finding. Subtractive Solar Envelope and Integrated Solar Collection Computational Method for High-Rise Buildings in Urban Environments, in: *Disciplines and Disruption - Proceedings Catalog of the 37th Annual Conference of the Association for Computer Aided Design in Architecture (ACADIA)*.
- De Luca, F., 2017b. From Envelope to Layout. Buildings Massing and Layout Generation for Solar Access in Urban Environments, in: *Sharing Computational Knowledge! ShoCK! Proceedings of the 35th International Conference on Education and Research in Computer Aided Architectural Design in Europe (ECAADe) Vol. 2*.
- De Luca, F., Dogan, T., 2019. A novel solar envelope method based on solar ordinances for urban planning. *Build. Simul.* 12. <https://doi.org/10.1007/s12273-019-0561-1>
- De Luca, F., Dogan, T., Kurnitski, J., 2018a. Methodology for determining fenestration ranges for daylight and energy efficiency in Estonia, in: *Simulation Series*. <https://doi.org/10.22360/simaud.2018.simaud.007>
- De Luca, F., Kiil, M., Simson, R., Kurnitski, J., Murula, R., 2019a. Evaluating Daylight Factor Standard through Climate Based Daylight Simulations and Overheating Regulations in Estonia, in: *Proceedings of Building Simulation 2019: 16th Conference of International Building Performance Simulation Association*.
- De Luca, F., Kiil, M., Simson, R., Kurnitski, J., Murula, R., 2019b. Evaluating Daylight Factor Standard through Climate Based Daylight Simulations and Overheating Regulations in Estonia, in: *Proceedings of Building Simulation 2019: 16th Conference of International Building Performance Simulation Association*.
- De Luca, F., Nejur, A., Dogan, T., 2018b. Facade-Floor-Cluster-Methodology for Determining Optimal Building Clusters for Solar Access and Floor Plan Layout in Urban Environments, in: *Conference: 36th ECAADe Conference - Computing for a Better TomorrowAt: Faculty of Civil Engineering, Architecture and Environmental Engineering, Lodz University of Technology, Volume: 2, 585-594*.
- De Luca, F., Sepúlveda, A., 2021. Analyzing daylight and solar access performance in urban environments in Estonia, in: *Proceedings of Building Simulation 2021: 17th Conference of IBPSA: 17th IBPSA International Conference and Exhibition (BS2021)*.
- De Luca, F., Voll, H., 2017. Computational method for variable objectives and context aware solar envelopes generation, in: *Simulation Series*. <https://doi.org/10.22360/simaud.2017.simaud.037>

- Dekay, M., Brown, G.Z., 2001. SUN, WIND & LIGHT: Architectural Design Strategies, Society of Building Science Educators.
- Dogan, T., 2014. Archsim energy modelling software [WWW Document].
- Dogan, T., Park, Y.C., 2019. A critical review of daylighting metrics for residential architecture and a new metric for cold and temperate climates. *Light. Res. Technol.* <https://doi.org/10.1177/1477153518755561>
- Dogan, T., Saratsis, E., Reinhart, C., 2015. The optimization potential of floor-plan typologies in early design energy modeling, in: 14th International Conference of IBPSA - Building Simulation 2015, BS 2015, Conference Proceedings.
- Duffy, J.F., Czeisler, C.A., 2009. Effect of Light on Human Circadian Physiology. *Sleep Med. Clin.* <https://doi.org/10.1016/j.jsmc.2009.01.004>
- Ekici, B., Kazanasmaz, Z.T., Turrin, M., Taşgetiren, M.F., Sariyildiz, I.S., 2021. Multi-zone optimisation of high-rise buildings using artificial intelligence for sustainable metropolises. Part 1: Background, methodology, setup, and machine learning results. *Sol. Energy* 224. <https://doi.org/10.1016/j.solener.2021.05.083>
- Estonian Centre for Standardization, 2015. EVS 894:2008+A2:2015: Daylight in Dwellings and Offices.
- Estonian Government, 2018. Estonian Government Ordinance No 63. Ordinance No 63. (11.12.2018) Hoone energiatõhususe miimumnõuded. (Minimum requirements for energy performance of buildings). *Riigi Teataja*, I, 13.12.2018, 14.
- Estonian Government, 2015. Ordinance N° 58. Methodology for calculating the energy performance of buildings. RTI,09.06.2015, 21.
- Estonian Government, 2012. Minimum requirements for energy performance. Annex 68, RT I, 24.01.2014, 3.
- Estonian Weather Service, 2021a. Climate normals: Temperature.
- Estonian Weather Service, 2021b. Climate normals: Precipitation.
- Estonian Weather Service, 2021c. Climate normals: Sunshine.
- European commission, 2018. BS EN 17037:2018: Daylight in buildings.
- European Committee for Standardization, 2011. Standard EN12464-1:2011 Light and lighting— Lighting of work places—Part 1: Indoor work places.
- Fosas, D., Coley, D.A., Natarajan, S., Herrera, M., Fosas de Pando, M., Ramallo-Gonzalez, A., 2018. Mitigation versus adaptation: Does insulating dwellings increase overheating risk? *Build. Environ.* 143. <https://doi.org/10.1016/j.buildenv.2018.07.033>
- Gago, E.J., Muneer, T., Knez, M., Köster, H., 2015. Natural light controls and guides in buildings. Energy saving for electrical lighting, reduction of cooling load. *Renew. Sustain. Energy Rev.* <https://doi.org/10.1016/j.rser.2014.08.002>
- Geyer, P., Singaravel, S., 2018. Component-based machine learning for performance prediction in building design. *Appl. Energy* 228. <https://doi.org/10.1016/j.apenergy.2018.07.011>
- Grynning, S., Time, B., Matusiak, B., 2014. Solar shading control strategies in cold climates - Heating, cooling demand and daylight availability in office spaces. *Sol. Energy.* <https://doi.org/10.1016/j.solener.2014.06.007>
- Gupta, R., Gregg, M., 2018. Assessing energy use and overheating risk in net zero energy dwellings in UK. *Energy Build.* 158. <https://doi.org/10.1016/j.enbuild.2017.10.061>
- Haase, M., Grynning, S., 2017. Optimized facade design - Energy efficiency, comfort and daylight in early design phase, in: *Energy Procedia.* <https://doi.org/10.1016/j.egypro.2017.09.666>

- Haglund, K., 2010. Window selection methodologies and optimization in highperformance commercial buildings. BEST2 Conf. Portl.
- Hamburg, A., Kalamees, T., 2019. How well are energy performance objectives being achieved in renovated apartment buildings in Estonia? *Energy Build.* <https://doi.org/10.1016/j.enbuild.2019.07.006>
- Hamdy, M., Jan Hensen, L.M., 2015. Ranking of dwelling types in terms of overheating risk and sensitivity to climate change, in: 14th International Conference of IBPSA - Building Simulation 2015, BS 2015, Conference Proceedings.
- Hoffmann, S., Lee, E.S., McNeil, A., Fernandes, L., Vidanovic, D., Thanachareonkit, A., 2016. Balancing daylight, glare, and energy-efficiency goals: An evaluation of exterior coplanar shading systems using complex fenestration modeling tools. *Energy Build.* <https://doi.org/10.1016/j.enbuild.2015.12.009>
- Honey Bee, 2020.
- Illuminating Engineering Society, The Daylight Metric Committee, 2013. LM-83-12 Approved Metric: IES Spatial Daylight Autonomy (sDA) and Annual Sunlight Exposure (ASE), Illuminating Engineering Society of North America (IESNA).
- Inanici, M., Hashemloo, A., 2017a. An investigation of the daylighting simulation techniques and sky modeling practices for occupant centric evaluations. *Build. Environ.* 113. <https://doi.org/10.1016/j.buildenv.2016.09.022>
- Inanici, M., Hashemloo, A., 2017b. An investigation of the daylighting simulation techniques and sky modeling practices for occupant centric evaluations. *Build. Environ.* <https://doi.org/10.1016/j.buildenv.2016.09.022>
- INTERPANE Glasgesellschaft mbH, 2018. PERFORMANCE DATA FOR LOW E AND SOLAR CONTROL GLASS.
- Jakubiec, J.A., Reinhart, C.F., 2012. The 'adaptive zone'-A concept for assessing discomfort glare throughout daylight spaces. *Light. Res. Technol.* <https://doi.org/10.1177/1477153511420097>
- Jakubiec, J.A., Reinhart, C.F., 2011. DIVA 2.0: Integrating daylight and thermal simulations using rhinoceros 3D, DAYSIM and EnergyPlus, in: Proceedings of Building Simulation 2011: 12th Conference of International Building Performance Simulation Association.
- Jones, N., 2019. Better, Faster, Stronger Super-Fast Glare Analysis and Real-Time Visualization.
- Jones, N.L., Reinhart, C.F., 2017. Speedup Potential of Climate-Based Daylight Modelling on GPUs, in: Conference: Building Simulation 2017: 15th International Conference of the International Building Performance Simulation Association. San Francisco, pp. 975–984.
- Karlsson, J., Roos, A., 2000. Modelling the angular behaviour of the total solar energy transmittance of windows. *Sol. energy* 69. [https://doi.org/10.1016/S0038-092X\(00\)00083-9](https://doi.org/10.1016/S0038-092X(00)00083-9)
- Kharvari, F., 2020. An empirical validation of daylighting tools: Assessing radiance parameters and simulation settings in Ladybug and Honeybee against field measurements. *Sol. Energy* 207. <https://doi.org/10.1016/j.solener.2020.07.054>
- Kim, S.H., Shin, K.J., Kim, H.J., Cho, Y.H., 2017. A Study on the Effectiveness of the Horizontal Shading Device Installation for Passive Control of Buildings in South Korea. *Int. J. Polym. Sci.* <https://doi.org/10.1155/2017/3025092>
- Kleindienst, S., Andersen, M., 2012. Comprehensive annual daylight design through a goal-based approach. *Build. Res. Inf.* 40. <https://doi.org/10.1080/09613218.2012.641301>

- Knoop, M., Stefani, O., Bueno, B., Matusiak, B., Hobday, R., Wirz-Justice, A., Martiny, K., Kantermann, T., Aarts, M.P.J., Zemmouri, N., Appelt, S., Norton, B., 2019. Daylight: What makes the difference? *Light. Res. Technol.* <https://doi.org/10.1177/1477153519869758>
- Knowles, R., 1980. The Solar Envelope. *Sol. Law Report*. 1.
- Kong, Z., Utzinger, D.M., Humann, C., 2018. Evaluation of a hybrid photo-radiometer sky model compared with the Perez sky model. *Energy Build.* 178. <https://doi.org/10.1016/j.enbuild.2018.08.022>
- Kropf, S., Zweifel, G., 2002. Validation of the Building Simulation Program IDA-ICE According to CEN 13791 "Thermal Performance of Buildings - Calculation of Internal Temperatures of a Room in Summer Without Mechanical Cooling - General Criteria and Validation Procedures." Luzern.
- Kuhn, T.E., Bühler, C., Platzer, W.J., 2001. Evaluation of overheating protection with sun-shading systems. *Sol. Energy.* [https://doi.org/10.1016/S0038-092X\(01\)00017-2](https://doi.org/10.1016/S0038-092X(01)00017-2)
- Lee, E.S., Geisler-Moroder, D., Ward, G., 2018a. Modeling the direct sun component in buildings using matrix algebraic approaches: Methods and validation. *Sol. Energy.* <https://doi.org/10.1016/j.solener.2017.12.029>
- Lee, E.S., Geisler-Moroder, D., Ward, G., 2018b. Validation of the Five-Phase Method for Simulating Complex Fenestration Systems with Radiance against Field Measurements.
- Lee, J., Boubekri, M., Liang, F., 2019. Impact of building design parameters on daylighting metrics using an analysis, prediction, and optimization approach based on statistical learning technique. *Sustain.* 11. <https://doi.org/10.3390/su11051474>
- Liu, C., Kershaw, T., Fosas, D., Ramallo Gonzalez, A.P., Natarajan, S., Coley, D.A., 2017. High resolution mapping of overheating and mortality risk. *Build. Environ.* <https://doi.org/10.1016/j.buildenv.2017.05.028>
- Loche, I., Bleil de Souza, C., Spaeth, A.B., Neves, L.O., 2021. Decision-making pathways to daylight efficiency for office buildings with balconies in the tropics. *J. Build. Eng.* 43. <https://doi.org/10.1016/j.jobe.2021.102596>
- Lockley, S.W., 2009. Circadian Rhythms: Influence of Light in Humans, in: *Encyclopedia of Neuroscience.* <https://doi.org/10.1016/B978-008045046-9.01619-3>
- Lomas, K.J., Porritt, S.M., 2017. Overheating in buildings: lessons from research. *Build. Res. Inf.* <https://doi.org/10.1080/09613218.2017.1256136>
- Mainini, A.G., Zani, A., De Michele, G., Speroni, A., Poli, T., Zinzi, M., Gasparella, A., 2019. Daylighting performance of three-dimensional textiles. *Energy Build.* <https://doi.org/10.1016/j.enbuild.2019.02.036>
- Maivel, M., Kurnitski, J., Kalamees, T., 2015. Field survey of overheating problems in Estonian apartment buildings. *Archit. Sci. Rev.* <https://doi.org/10.1080/00038628.2014.970610>
- Mangkuto, R.A., Kurnia, K.A., Azizah, D.N., Atmodipoero, R.T., Soelami, F.X.N., 2017. Determination of discomfort glare criteria for daylit space in Indonesia. *Sol. Energy.* <https://doi.org/10.1016/j.solener.2017.04.010>
- Mangkuto, R.A., Rohmah, M., Asri, A.D., 2016. Design optimisation for window size, orientation, and wall reflectance with regard to various daylight metrics and lighting energy demand: A case study of buildings in the tropics. *Appl. Energy.* <https://doi.org/10.1016/j.apenergy.2015.11.046>
- Mardaljevic, J., 1999. Sky Models for Lighting Simulation, in: *Daylight Simulation: Validation, Sky Models and Daylight Coefficients.*

- McNeil, A., 2015. genBSDF Tutorial.
- McNeil, A., 2014. BSDFs, Matrices and Phases.
- McNeil, A., 2013. The 5--phase method.
- McNeil, A., Jonsson, C.J., Appelfeld, D., Ward, G., Lee, E.S., 2013. A validation of a ray-tracing tool used to generate bi-directional scattering distribution functions for complex fenestration systems. *Sol. Energy*. <https://doi.org/10.1016/j.solener.2013.09.032>
- Morey, J., Beizaee, A., Wright, A., 2020. An investigation into overheating in social housing dwellings in central England. *Build. Environ.* 176. <https://doi.org/10.1016/j.buildenv.2020.106814>
- Mourkos, K., Hopfe, C.J., McLeod, R.S., Goodier, C., Swainson, M., 2020. The impact of accurately modelling corridor thermodynamics in the overheating risk assessment of multi-residential dwellings. *Energy Build.* 224. <https://doi.org/10.1016/j.enbuild.2020.110302>
- Nabil, A., Mardaljevic, J., 2006. Useful daylight illuminances: A replacement for daylight factors. *Energy Build.* <https://doi.org/10.1016/j.enbuild.2006.03.013>
- O'Brien, W., Kapsis, K., Athienitis, A.K., 2013. Manually-operated window shade patterns in office buildings: A critical review. *Build. Environ.* <https://doi.org/10.1016/j.buildenv.2012.10.003>
- Osterhaus, W.K.E., 2005. Discomfort glare assessment and prevention for daylight applications in office environments, in: *Solar Energy*. <https://doi.org/10.1016/j.solener.2004.11.011>
- Pellegrino, A., Cammarano, S., Lo Verso, V.R.M., Corrado, V., 2017. Impact of daylighting on total energy use in offices of varying architectural features in Italy: Results from a parametric study. *Build. Environ.* 113. <https://doi.org/10.1016/j.buildenv.2016.09.012>
- Pierson, C., Wienold, J., Bodart, M., 2017. Discomfort glare perception in daylighting: Influencing factors, in: *Energy Procedia*. <https://doi.org/10.1016/j.egypro.2017.07.332>
- Pikas, E., Thalfeldt, M., Kurnitski, J., Liias, R., 2015. Extra cost analyses of two apartment buildings for achieving nearly zero and low energy buildings. *Energy*. <https://doi.org/10.1016/j.energy.2015.03.026>
- Ponmalar, V., Ramesh, B., 2014. Energy efficient building design and estimation of energy savings from daylighting in Chennai. *Energy Eng. J. Assoc. Energy Eng.* <https://doi.org/10.1080/01998595.2014.10846858>
- Quek, G., Wienold, J., Sarey Khanie, M., Erell, E., Kaftan, E., Tzempelikos, A., Konstantzos, I., Christoffersen, J., Kuhn, T., Andersen, M., 2021. Comparing performance of discomfort glare metrics in high and low adaptation levels. *Build. Environ.* 206. <https://doi.org/https://doi.org/10.1016/j.buildenv.2021.108335>
- Rabani, M., Bayera Madessa, H., Nord, N., 2021. Achieving zero-energy building performance with thermal and visual comfort enhancement through optimization of fenestration, envelope, shading device, and energy supply system. *Sustain. Energy Technol. Assessments* 44. <https://doi.org/10.1016/j.seta.2021.101020>
- Radiance 5.4a (2020-09-06), n.d.
- Reinhart, C., Pierre-Felix, B., 2009. Experimental validation of autodesk® 3ds max® design 2009 and daysim 3.0. *LEUKOS - J. Illum. Eng. Soc. North Am.* <https://doi.org/10.1582/LEUKOS.2009.06.01001>

- Reinhart, C.F., 2018. Daylighting Handbook II. Daylight Simulations. Dynamic Facades. Building Technology Press, Cambridge, MA.
- Reinhart, C.F., Herkel, S., 2000. The Simulation of annual daylight illuminance distributions-a state-of-the-art comparison of six RADIANCE-based methods. Energy Build. [https://doi.org/10.1016/S0378-7788\(00\)00042-6](https://doi.org/10.1016/S0378-7788(00)00042-6)
- Reinhart, C.F., Lo Verso, V.R.M., 2010. A rules of thumb-based design sequence for diffuse daylight. Light. Res. Technol. 42. <https://doi.org/10.1177/1477153509104765>
- Reinhart, C.F., Mardaljevic, J., Rogers, Z., 2006. Dynamic daylight performance metrics for sustainable building design. LEUKOS - J. Illum. Eng. Soc. North Am. <https://doi.org/10.1582/LEUKOS.2006.03.01.001>
- Saadatian, S., Freire, F., Simões, N., 2021a. Embodied impacts of window systems: A comparative assessment of framing and glazing alternatives. J. Build. Eng. 35. <https://doi.org/10.1016/j.jobbe.2020.102042>
- Saadatian, S., Simões, N., Freire, F., 2021b. Integrated environmental, energy and cost life-cycle analysis of windows: Optimal selection of components. Build. Environ. 188. <https://doi.org/10.1016/j.buildenv.2020.107516>
- Sadeghipour Roudsari, M., 2012. Ladybug Tools.
- Samuels, R., 1990. Solar efficient architecture and quality of life: the role of daylight and sunlight in ecological and psychological well-being. Energy Environ. 1990s. Proc. 1st World Renew. Energy Congr. Environ. 1990s. Proc. 1st World Renew. Energy Congr.
- Sanaieian, H., Tenpierik, M., Linden, K. Van Den, Mehdizadeh Seraj, F., Mofidi Shemrani, S.M., 2014. Review of the impact of urban block form on thermal performance, solar access and ventilation. Renew. Sustain. Energy Rev. <https://doi.org/10.1016/j.rser.2014.06.007>
- Santamouris, M., Kolokotsa, D., 2015. On the impact of urban overheating and extreme climatic conditions on housing, energy, comfort and environmental quality of vulnerable population in Europe. Energy Build. 98. <https://doi.org/10.1016/j.enbuild.2014.08.050>
- Sayın, S., Çelebi, G., 2020. A practical approach to performance-based building design in architectural project. Build. Res. Inf. 48. <https://doi.org/10.1080/09613218.2019.1669008>
- Sepúlveda, A., 2018. Validation of a geometrical model in RADIANCE for the design of textile shading devices.
- Sepúlveda, A., De Luca, F., 2022. Solar Envelope Tools (SET).
- Sepúlveda, A., De Luca, F., 2020. A Multi-Objective Optimization Workflow based on Solar Access and Solar Radiation for the Design of Building Envelopes in Cold Climates, in: Symposium on Simulation for Architecture and Urban DesignAt: TU Wien, Vienna (Online).
- Sepúlveda, A., De Luca, F., Thalfeldt, M., Kurnitski, J., 2020. Analyzing the fulfillment of daylight and overheating requirements in residential and office buildings in Estonia. Build. Environ. 180. <https://doi.org/10.1016/j.buildenv.2020.107036>
- Sepúlveda, A., De Luca, F., Thalfeldt, M., Kurnitski, J., 2020. Analyzing the fulfillment of daylight and overheating requirements in residential and office buildings in Estonia. Build. Environ. 180. <https://doi.org/10.1016/j.buildenv.2020.107036>
- Shafavi, N.S., Tahsildoost, M., Zomorodian, Z.S., 2020. Investigation of illuminance-based metrics in predicting occupants' visual comfort (case study: Architecture design studios). Sol. Energy. <https://doi.org/10.1016/j.solener.2019.12.051>

- Simko, T., Moore, T., 2021. Optimal window designs for Australian houses. *Energy Build.* 250. <https://doi.org/10.1016/j.enbuild.2021.111300>
- Simson, R., 2019. Overheating prevention and daylight in buildings without mechanical cooling. Tallinn University of Technology. <https://doi.org/https://doi.org/10.23658/taltech.54/2019>
- Simson, R., Kurnitski, J., Kuusk, K., 2017a. Experimental validation of simulation and measurement-based overheating assessment approaches for residential buildings. *Archit. Sci. Rev.* <https://doi.org/10.1080/00038628.2017.1300130>
- Simson, R., Kurnitski, J., Maivel, M., 2017b. Summer thermal comfort: compliance assessment and overheating prevention in new apartment buildings in Estonia. *J. Build. Perform. Simul.* <https://doi.org/10.1080/19401493.2016.1248488>
- Sokol, N., Martyniuk-Peczek, J., 2016. The Review of the Selected Challenges for an Incorporation of Daylight Assessment Methods into Urban Planning in Poland, in: *Procedia Engineering.* <https://doi.org/10.1016/j.proeng.2016.08.814>
- Solemma LLC, 2016. DIVA [WWW Document]. URL www.solemma.net (accessed 3.15.19).
- Stover, J.C., 2012. Optical scattering: Measurement and analysis: Third edition, *Optical Scattering: Measurement and Analysis: Third Edition.* <https://doi.org/10.1117/3.975276>
- Subramaniam, S., 2017. Daylighting Simulations with Radiance using Matrix-based Methods.
- Thalfeldt, M., Kurnitski, J., Voll, H., 2016. Detailed and simplified window model and opening effects on optimal window size and heating need. *Energy Build.* <https://doi.org/10.1016/j.enbuild.2016.06.002>
- Thalfeldt, M., Pikas, E., Kurnitski, J., Voll, H., 2017. Window model and 5 year price data sensitivity to cost-effective façade solutions for office buildings in Estonia. *Energy.* <https://doi.org/10.1016/j.energy.2017.06.160>
- Thalfeldt, M., Pikas, E., Kurnitski, J., Voll, H., 2013. Facade design principles for nearly zero energy buildings in a cold climate. *Energy Build.* <https://doi.org/10.1016/j.enbuild.2013.08.027>
- Thanachareonkit, A., Scartezzini, J.L., 2010. Modelling Complex Fenestration Systems using physical and virtual models. *Sol. Energy* 84, 563–586. <https://doi.org/https://doi.org/10.1016/j.solener.2009.09.009>
- Toutou, A., Fikry, M., Mohamed, W., 2018. The parametric based optimization framework daylighting and energy performance in residential buildings in hot arid zone. *Alexandria Eng. J.* 57. <https://doi.org/10.1016/j.aej.2018.04.006>
- Turan, I., Chegut, A., Fink, D., Reinhart, C., 2020. The value of daylight in office spaces. *Build. Environ.* <https://doi.org/10.1016/j.buildenv.2019.106503>
- TUT nZEB Research Group, 2017. LIGINULLENERGIA ELUHOONED RIDA- JA KORTERELAMUD. Tallinn, Estonia.
- Tzempelikos, A., Chan, Y.C., 2016. Estimating detailed optical properties of window shades from basic available data and modeling implications on daylighting and visual comfort. *Energy Build.* 126. <https://doi.org/10.1016/j.enbuild.2016.05.038>
- U.S. Department of Energy, 2015. EnergyPlus Testing with HVAC Equipment Performance Tests CE100 to CE200 from ANSI/ASHRAE Standard 140-2011. Washington, D.C.
- Uribe, D., Vera, S., Bustamante, W., McNeil, A., Flamant, G., 2019. Impact of different control strategies of perforated curved louvers on the visual comfort and energy consumption of office buildings in different climates. *Sol. Energy.* <https://doi.org/10.1016/j.solener.2019.07.027>

- Vanhoutteghem, L., Skarning, G.C.J., Hviid, C.A., Svendsen, S., 2015. Impact of façade window design on energy, daylighting and thermal comfort in nearly zero-energy houses. *Energy Build.* <https://doi.org/10.1016/j.enbuild.2015.05.018>
- Voll, H., De luca, F., Pavlovas, V., 2016a. Analysis of the insolation criteria for nearly-zero energy buildings in Estonia. *Sci. Technol. Built Environ.* <https://doi.org/10.1080/23744731.2016.1195657>
- Voll, H., Thalfeldt, M., De Luca, F., Kurnitski, J., Olesk, T., 2016b. Urban planning principles of nearly zero-energy residential buildings in Estonia. *Manag. Environ. Qual. An Int. J.* <https://doi.org/10.1108/MEQ-05-2015-0101>
- Wang, S., Yi, Y.K., Liu, N., 2021. Multi-objective optimization (MOO) for high-rise residential buildings' layout centered on daylight, visual, and outdoor thermal metrics in China. *Build. Environ.* 205. <https://doi.org/10.1016/j.buildenv.2021.108263>
- Ward, G., 2014. Reducing anisotropic BSDF measurement to common practice, in: *Eurographics Workshop on Material Appearance Modeling.*
- Ward, G., 2013. *bsdf2tree.*
- Ward, G.J., 1994. The RADIANCE lighting simulation and rendering system, in: *Proceedings of the 21st Annual Conference on Computer Graphics and Interactive Techniques, SIGGRAPH 1994.* <https://doi.org/10.1145/192161.192286>
- Ward, G.J., n.d. *RTRACE.*
- Ward, G.J., Wang, T., Geisler-Moroder, D., Lee, E.S., Grobe, L.O., Wienold, J., Jonsson, J.C., 2021. Modeling specular transmission of complex fenestration systems with data-driven BSDFs. *Build. Environ.* <https://doi.org/https://doi.org/10.1016/j.buildenv.2021.107774>
- Wasilewski, S., Grobe, L.O., Schregle, R., Wienold, J., Andersen, M., 2021. Raytraverse: Navigating the Lightfield to Enhance Climate-Based Daylight Modeling.
- Wienold, J., Christoffersen, J., 2006. Evaluation methods and development of a new glare prediction model for daylight environments with the use of CCD cameras. *Energy Build.* <https://doi.org/10.1016/j.enbuild.2006.03.017>
- Wienold, J., Iwata, T., Sarey Khanie, M., Erell, E., Kaftan, E., Rodriguez, R.G., Yamin Garretón, J.A., Tzempelikos, T., Konstantzos, I., Christoffersen, J., Kuhn, T.E., Pierson, C., Andersen, M., 2019. Cross-validation and robustness of daylight glare metrics. *Light. Res. Technol.* <https://doi.org/10.1177/1477153519826003>
- Wienold, J., Tilmann E., K., Christoffersen, J., Andersen, M., 2017. Annual glare evaluation for fabrics. *PLEA 2017 Edinburgh Des. to Thrive.*
- Yamin Garretón, J.A., Colombo, E.M., Pattini, A.E., 2018. A global evaluation of discomfort glare metrics in real office spaces with presence of direct sunlight. *Energy Build.* <https://doi.org/10.1016/j.enbuild.2018.01.024>
- Yannas, S., Rodríguez-Álvarez, J., 2020. Domestic overheating in a temperate climate: Feedback from London Residential Schemes. *Sustain. Cities Soc.* 59. <https://doi.org/10.1016/j.scs.2020.102189>
- Yu, X., Su, Y., 2015. Daylight availability assessment and its potential energy saving estimation -A literature review. *Renew. Sustain. Energy Rev.* <https://doi.org/10.1016/j.rser.2015.07.142>
- Zhu, L., Wang, B., Sun, Y., 2020. Multi-objective optimization for energy consumption, daylighting and thermal comfort performance of rural tourism buildings in north China. *Build. Environ.* 176. <https://doi.org/10.1016/j.buildenv.2020.106841>

Acknowledgements

Firstly, I want to thank my supervisor Dr. Francesco De Luca for all these years of guidance and support. We share the same vision to solve modern and future architectural problems. Thus, he gave me freedom enough to research and relevant feedback when I needed. In addition, I feel very lucky by the support that Prof. Jarek Kurnitski and Prof. Kimmo Sakari Lylykangas gave me during this long journey in Tallinn University of Technology. Thank you very much, it is a pleasure to be working with you both.

Also, I have to thank to my colleagues from the NZEB group: Tuule, Helena, Karl, Meril, Paul, Raimo, Martin Kiil, Martin Thalfeldt, Jaanus, as well as colleagues from the Architecture and Urban Studies group: Nasim, Sara, Dominik, and Hanna. Thanks for the administrative support I received from Ene, Aive, Triinu-Liis, and Kärt. Moreover, I want to express my sincere gratitude to Bruno Bueno for encouraging me to start this PhD journey and his further support through scientific collaborations with Fraunhofer ISE.

This research was partially supported by the Estonian Centre of Excellence in Zero Energy and Resource Efficient Smart Buildings and Districts, ZEBE (grant No. 2014-2020.4.01.15-0016), the programme Mobilitas Pluss (Grant No – 2014-2020.4.01.16-0024, MOBTP88), and Dora Plus PhD student short/long mobility plans funded by the European Regional Development Fund, by the Estonian Research Council (grant No. PSG409) and by the European Commission through the H2020 project Finest Twins (grant No. 856602). This research was partially supported by a Fraunhofer ICON Grant.

Of course, to my family for their invaluable support during not only this long and hard process but my entire lifetime. I love you all. Specially, this thesis is for my mother for her capacity of loving, listening, and be patience 24/7. In addition, I could not be able to do this thesis without enjoying awesome vacations with my friends, you made this also possible, thank you all: Ale, Yago, Mamadu, Olia, Anita, Alfredo, Pomares, etc.

Finally, to Elena for becoming one of the most important persons in my life, thanks for listening and supporting me every single day during all these years, despite being separated thousands of miles away and months between reunions. This thesis is like the prologue of our bright future, I love you so much.

Abel Sepúlveda Luque

May, 2022

Abstract

A novel workflow for early design stages to ensure daylight and summer thermal comfort in buildings

Human-centric design has become one of the central criteria in architectural design. Indoor comfort in buildings has a critical impact on occupants' health and cognitive performance. Designers have to consider multiple building performances such as indoor comfort during early design stages of design process. The achievement of a good level of indoor comfort in buildings typically includes a balance between visual comfort and protection against overheating, which can be challenging for architects and designers. There is a lack of integrated methods and studies that help designers to understand the impact of their design decisions during early design stages at different levels: building (orientation, shape, volume, and interior floor plan), facade (windows location, windows size, and windows construction), and shading level (shadings type, and optical/thermal properties of the shadings) on building overall performance consisted partially on solar access, daylight provision, glare protection, and overheating risk. This thesis presents a general workflow to help architects to design buildings with adequate levels of solar access, daylight provision according to the two standards in force in Estonia and low overheating risk according to Estonian regulations. In addition, this thesis presents methods to speed up the early design stages design process of office buildings with adequate levels of solar access, daylight provision, and glare protection according to the European standard EN17037:2018.

A single-room simulation-based methodology was applied to assess the daylighting and overheating performance in side-lit rooms within the Estonian context. In the first part of this thesis, the aim is to investigate the effect of different daylight assessment criteria on the combined fulfillment of daylighting and overheating requirements and its implications for the design of residential and office rooms in Estonia (Paper II). Moreover, it was developed daylight and overheating prediction formulas that can help architects and designers to conduct efficient window sizing process during early design stages (Paper III). Finally, glare calculation methods in terms of accuracy and computational time were benchmarked (Paper IV). In the second part of this thesis, the methods developed from the first part of the thesis were applied to cases studies. In first place, it was used a proposed easy-to-use multi-objective optimization workflow to help architects and designers to design building envelope efficiently in Tallinn, Estonia (Paper I). The second step consists of using daylight and overheating prediction formulas to select window's size and properties to achieve a good balance between daylight provision and overheating risk protection in a new residential building (Paper III). In third place, it was used efficient assessment methods based on sampling strategies and optimized modeling decisions such as the selection of Radiance parameters or optical model of complex fenestration systems to assess glare protection according to the European standard EN17037 (Paper IV).

Within the current situation in Estonia, the results show that 30% of the combinations fulfill the mean DF requirement but not the sDA requirement. Moreover, there is an agreement between the Estonian standard EVS 894:2008/A2:2015 and European standard EN 17037:2018 for only 54% of room combinations. The addition of window airing increases the maximum window-to-wall ratio by 50% in residential rooms. Regarding the definition of the building envelope, multi-objective criteria based on

volume and solar access achieve the best trade-off solutions with volume ratios higher than 20% and ratio of the windows that fulfill the solar access requirements higher than 57%. Regarding the window sizing process using the minDF and DH-based prediction formulas, the minimum window-to-wall ratio (minWWR) to fulfill minDF-based requirements and maximum g-value to fulfill at the same time DH-based requirements for any room design can be calculated or represented graphically. The prediction accuracy in terms of relative RMSE is up to 0.20 for minDF and DH values (Paper III). For efficient annual glare assessment, based on semi-annual and five days per week simulations for visible sun positions; sampling strategies can decrease the CPU time for annual glare simulations up to 86% when considering clear sky conditions. The most suitable method for DGP simulations depends strongly on the Radiance parameters and the chosen sampling strategy (Paper IV).

The results suggest a synergistic formulation of daylighting and overheating requirements in new building regulations to make the combined fulfillment easier for the designers (Paper II). By using these methods, designers can minimize the number of design iterations during early design stages, as well as the required computational time required by daylight and energy simulations (Paper I and II). The proposed coupled method based on minDF and DH prediction formulas has big potential to help architects and designers to achieve the combined fulfillment between daylight provision and overheating protection during early design stages within the Estonian context. A suitable sampling strategy for annual glare risk assessments can make a time step-based ray-tracing method more computationally efficient than the alternative matrix-based methods (Paper IV). For cases in which no diffuse and/or specular reflections of the sun from any surface of the scene or the shading device will cause glare when this is not in the field of view, a sampling strategy that takes into account only the hours when the solar disk is in the field of view can reduce the computational time considerably. This strategy can be combined with semi-annual evaluations (for clear skies) and a suitable sampling strategy (e.g. one day per week) to further reduce the computational time. The sensitivity analysis of Radiance parameters for the rtrace method presented in the study can help to optimize the computational cost of simulations. Thus, by using this methodology, designers could efficiently compare several complex fenestration systems in terms of annual glare protection performance during early design stages of the building design process.

Lühikokkuvõte

Uudne töövoog projekteerimise algaasis, et tagada päevavalgus ja soojusmugavus hoonetes

Inimkesksest disainist on saanud arhitektuurse disaini üks keskseid kriteeriume. Sisemugavusel hoonetes on kriitiline mõju elanike tervisele ja kognitiivsele jõudlusele. Disainerid peavad projekteerimisprotsessi varases projekteerimisetapis arvestama mitmete hoone jõudlusega, näiteks siseruumide mugavusega. Hoonete siseruumide mugavuse hea taseme saavutamine hõlmab tavaliselt tasakaalu visuaalse mugavuse ja ülekuumenemise eest kaitsmise vahel, mis võib olla arhitektidele ja disaineritele keeruline. Puuduvad integreeritud meetodid ja uuringud, mis aitaksid disaineritel mõista oma projekteerimisotsuste mõju projekteerimise algaasis erinevatel tasanditel: hoone (suund, kuju, maht ja sisemine korruseplaan), fassaad (akende asukoht, akende suurus, ja akende ehitus) ning varjutuse tase (varjundite tüüp ja varjundite optilised/soojusomadused) hoone üldises toimimises koosnes osaliselt päikesevalguse juurdepääsust, päevavalguse tagamisest, pimestamise kaitsest ja ülekuumenemiskiskist. Käesolevas lõputöös esitatakse üldine töövoog, mis aitab arhitektidel projekteerida hooned, millel on piisav päikese ligipääsu tase, päevavalguse tagamine vastavalt kahele Eestis kehtivale standardile ja madal ülekuumenemisoht vastavalt Eesti eeskirjadele. Lisaks tutvustatakse käesolevas lõputöös meetodeid, kuidas kiirendada projekteerimisprotsessi varajastes etappides büroohonete projekteerimisprotsessi, kus on piisav päikesevalguse, päevavalguse tagamise ja pimestamise kaitse vastavalt Euroopa standardile EN17037:2018.

Külglalgustusega ruumide päevavalguse ja ülekuumenemise näitajate hindamiseks Eesti kontekstis kasutati ühetoalist simulatsioonipõhist meetodikat. Käesoleva lõputöö esimeses osas on eesmärgiks uurida erinevate päevavalguse hindamiskriteeriumide mõju päevavalguse ja ülekuumenemise nõuete kombineeritud täitmisele ning selle mõjusid Eesti elu- ja büroorumide projekteerimisele (töö II). Lisaks töötati välja päevavalguse ja ülekuumenemise ennustusvalemid, mis aitavad arhitektidel ja disaineritel korraldada tõhusat akna suuruse määramise protsessi varases projekteerimisetapis (Paber III). Lõpuks võrreldi pimestamise arvutamise meetodeid täpsuse ja arvutusaja osas (IV paber). Käesoleva lõputöö teises osas rakendati juhtumiuuringutes lõputöö esimesest osast välja töötatud meetodeid. Esiteks kasutati välja pakutud hõlpsasti kasutatavat mitme eesmärgi optimeerimise töövoogu, et aidata arhitektidel ja projekteerijatel tõhusalt kavandada hoone välispiirdeid Tallinnas (Paber I). Teine samm seisneb päevavalguse ja ülekuumenemise ennustusvalemite kasutamises akna suuruse ja omaduste valimiseks, et saavutada hea tasakaal päevavalguse tagamise ja ülekuumenemisohu kaitse vahel uues elamus (Paber III). Kolmandaks kasutati tõhusaid hindamismeetodeid, mis põhinesid valimivõtustrateegiatel ja optimeeritud modelleerimisotsustel, nagu näiteks Radiance parameetrite või komplekssete kattesüsteemide optilise mudeli valimine, et hinnata pimestamise kaitset vastavalt Euroopa standardile EN17037 (Paber IV).

Eesti praeguses olukorras näitavad tulemused, et 30% kombinatsioonidest täidab keskmise DF nõuet, kuid mitte sDA nõuet. Pealegi on Eesti standardi EVS 894:2008/A2:2015 ja Euroopa standardi EN 17037:2018 vahel kokkulepe vaid 54% ruumikombinatsioonide kohta. Aknatuulutuse lisamine suurendab eluruumides maksimaalset akna ja seina suhet 50%. Hoone välispiirete defineerimisel saavutavad

mahul ja päikese juurdepääsul põhinevad mitmeeesmärgilised kriteeriumid parimad kompromisslahendused, mille mahusuhted on suuremad kui 20% ja päikese juurdepääsu nõuetele vastavate akende osakaal üle 57%. Seoses akna suuruse määramise protsessiga, kasutades minDF- ja DH-põhiseid ennustusvalemeid, minimaalne akna ja seina suhe (minWWR), et täita minDF-põhiseid nõudeid ja maksimaalne g-väärtus, et täita samaaegselt DH-põhiseid nõudeid mis tahes ruumi jaoks. disaini saab arvutada või graafiliselt esitada. Suhtelise RMSE ennustustäpsus on minDF ja DH väärtuste puhul kuni 0,20 (Paber III). Tõhusaks iga-aastaseks pimestamise hindamiseks, mis põhineb poolaasta ja viis päeva nädalas toimuvatel simulatsioonidel nähtavate päikesepositsioonide jaoks; diskreetimisstrateegiad võivad selge taeva tingimusi arvestades vähendada iga-aastaste pimestamise simulatsioonide protsessori aega kuni 86%. DGP simulatsioonide jaoks sobivaim meetod sõltub tugevalt kiirguse parameetritest ja valitud proovivõtustrateegiast (IV artikkel).

Tulemused viitavad päevalalguse ja ülekuumenemise nõuete sünergilisele sõnastusele uutes ehituseeskirjades, et muuta projekteerijate jaoks kombineeritud täitmine lihtsamaks (Paber II). Neid meetodeid kasutades saavad disainerid minimeerida projekteerimise iteratsioonide arvu varajastes projekteerimisetappides ning päevalalguse ja energiasimulatsioonide jaoks vajalikku arvutusaega (Paber I ja II). Kavandataval minDF ja DH ennustusvalemiteel põhineval sidemeetodil on Eesti kontekstis suur potentsiaal aidata arhitektidel ja disaineritel saavutada päevalalguse tagamise ja ülekuumenemiskaitse kombineeritud täitmine projekteerimise varases etapis. Iga-aastaseks pimestamisrisi hindamiseks sobiv proovivõtustrateegia võib muuta ajasammupõhise kiirjälgimise meetodi arvutuslikult tõhusamaks kui alternatiivsed maatriksipõhised meetodid (IV artikkel). Juhtudel, kui päikese hajutatud ja/või peegeldav peegeldus stseeni üheltki pinnalt või varjatusseadmest ei põhjusta pimestamist, kui see ei ole vaateväljas, proovivõtustrateegia, mis võtab arvesse ainult tunde, mil päike vaateväljas olev ketas võib arvutusaega märkimisväärselt vähendada. Seda strateegiat saab kombineerida poolaasta hindamiste (selge taeva puhul) ja sobiva proovivõtustrateegiaga (nt üks päev nädalas), et arvutusaega veelgi vähendada. Uuringus esitatud rtrace meetodi Radiance parameetrite tundlikkuse analüüs võib aidata optimeerida simulatsioonide arvutuskulusid. Seega saavad disainerid seda meetodikat kasutades tõhusalt võrrelda mitut keerulist kattesüsteemi iga-aastase pimestamiskaitse toimivuse osas hoone projekteerimisprotsessi varases projekteerimisetapis.

Appendix

Paper I

Sepúlveda, A., & De Luca, F. (2020, May). A multi-objective optimization workflow based on solar access and solar radiation for the design of building envelopes in cold climates. In Proceedings of the 11th Annual Symposium on Simulation for Architecture and Urban Design (pp. 1–8).

A Multi-Objective Optimization Workflow based on Solar Access and Solar Radiation for the Design of Building Envelopes in Cold Climates

Abel Sepúlveda and Francesco De Luca

Tallinn University of Technology

Tallinn, Estonia

{absepu, francesco.deluca}@taltech.ee

ABSTRACT

This paper proposes a workflow based on multi-objective optimization for the design of the building envelope. The design variables of the workflow are the sorting method of sun vectors to calculate the solar envelope, the building orientation and the number of floor plan divisions. The objectives are the maximization of the building volume, the maximization of the ratio of the windows that fulfill the solar access requirement and the minimization of the mean incident solar radiation through the windows to reduce the risk of overheating during the warm season. The workflow has the potential to be adopted by designers being integrated in the Grasshopper plug-in for Rhinoceros that is a widely used design platform. The proposed workflow shows a successful way to deal with complex multi objective design goals. Multi-objective criteria based on volume and solar access achieve the best trade-off solutions with volume ratios higher than 20% and ratio of the windows that fulfill the solar access requirements higher than 57%.

Author Keywords

Solar envelope; environmental analysis; building envelope; urban planning; building design; solar access; optimization

1 INTRODUCTION

Cities currently account for over 70% of global carbon emissions and up to 40% of the total world energy consumption. By 2030, the 80% of the world population will live in cities [16]. These high levels of pollution have irreversible repercussions on the climate change due to the global warming effect. The main cause of the high carbon emissions is the dependency of energy production on fossil fuels. Project Horizon 2020 created by the European Union proposes energy efficiency requirements for the nearly zero energy buildings (nZEB). Additionally, it is well known that indoor comfort in buildings is a key factor for human well-being [15]. In terms of indoor comfort, it is not only important the thermal but the visual comfort. The visual comfort includes view out, glare protection, daylight provision and solar access (SA) in buildings [11].

SA is one of the first criterion that architects might must consider in the early stages of the building design. SA

regulations influence building density and maximum buildable volume. The solar envelope (SE) is a method introduced by Knowles to calculate maximum volume new buildings cannot exceed to guarantee required solar access on neighboring facades [13]. The shape and the size of new building envelope have crucial influence on energy performance and indoor comfort levels. It is not only important how the new building will influence the urban environment but the other way around. The solar collection envelope (SCE) is the minimum height of each considered point of the buildable zone that fulfills the SA regulation [2] [9]. Most of the SA regulations specify the minimum quantity of sun hours per apartment during a specific period [6] [12]. There is no specification in terms of quality of the sunlight; hence, this allows flexibility to generate SEs even for the same regulation and urban environment.

Essentially, two different approaches exist to calculate the SE: calculating the maximum height to each grid point of the plot (additive algorithm) or deleting grid volumes from the theoretical buildable block (subtractive algorithm). Subtractive algorithms have been proved to be high time-consuming [21] but useful to use as building massing technique [5]. On the other hand, the additive algorithm defined by Knowles [16] and firstly implemented by Capeluto [2] is the most used for the SE generation due to its simplicity. In recent years, this additive algorithm is implemented in several tools like LadyBug [14] and DIVA4Rhino [20], both Grasshopper plug-ins for Rhinoceros software. Nevertheless, these tools do not calculate urban context-dependent SEs. Indeed, the urban context has been taken into account by De Luca [8] and Capeluto in different SE generation methods [1].

Recently, a novel method based on solar ordinances for urban planning has been developed. The method uses multiple criteria to generate the SE for different SA regulations [6]. The lack of existence of tools that could take into account the urban environment and different solar ordinances to generate the SE, motivated researchers to develop an open-source plug-in for Grasshopper called "Solar Envelope Tools" (SET) [18] based on the previous method mentioned [6]. Another previous research showed

how different pattern layouts influence in terms of total floor area and SA performance of the building masses located in urban areas in Tallinn [4]. However, the performance of the building masses generated from each pattern layout differ from the building envelope performance. Moreover, De Luca, Nejur and Dogan proposed a method for the assessment of optimal building clusters for direct solar access in urban environments in Estonia, preferred type of floor plan layout (interior and exterior) and buildable floor area [7]. In fact, the method for the optimization of building clusters gives detailed information about the building envelope design. Nevertheless, in both mentioned investigations, a unique SE per urban environment was considered. These facts reduce the flexibility of the architectural design process at building envelope level and interior floor layout. Indeed, there is a lack of research about potentialities of different SEs per urban environment for the building envelope design.

The aim of this research is to study how SEs based on different criteria influence the building envelope design for a preferred floor plan and different objectives. The possible objectives are: (1) maximization of total floor area, (2) maximization of SA performance of the new building envelope; and (3) minimization of incident solar radiation in the warm season of the façade area that fulfill the minimum sun hours according to the SA ordinance. Two urban areas, one in Tallinn and another in Warsaw are considered as cases study. The outputs of this workflow are the optimal method to generate the SE with SET, the number of floor plan divisions, orientation/size of the building and zone of the façade that fulfills the SA requirements for a given multi-objective criteria. Implicitly, this workflow also provides flexibility in the creation of the interior floor plan of the building.

2 METHODOLOGY

In order to study how SEs generated by different criteria influence the building envelope design and use this information to optimize the performance of the new building, the workflow shown in Figure 1 is defined. This workflow has 4 main phases: SEs generation using SET, building envelope generation (using in-built Grasshopper components and Python functions), solar analysis of the building envelope using SET and the assessment of the building performance based on multi-objective criteria.

2.1 SEs generation with SET

The first step in the SE generation using SET is to extract climate information about the location of the case study (latitude, longitude, UTC and hourly direct normal solar radiation for the annual period) using the component “Location Data Reader”. After this, it is necessary to calculate the sun vectors of the analysis period using the component “Analysis Period” (SunVectGen). Using SunVectGen, we can introduce a specific time step and multiple analysis periods. When the selected time step is different than 1 (hourly), SunVectGen uses a linear

interpolation to calculate the direct normal solar radiation in each time step.

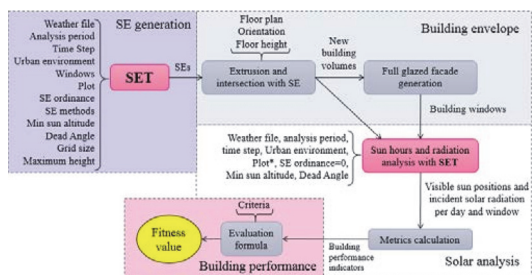


Figure 1. Workflow for the building performance assessment.

The main feature of SET is the possibility to filter and select sun vectors that fulfill different conditions. The filtering process consists of identifying the sun vectors of the analysis period that are not blocked by the surrounding buildings (Context) and fulfill the minimum defined solar altitude (MinAltitude) and dead angle (DeadAngle). This filtering process is run for every existing window introduced as input. Once the filtered sun vectors are identified, a sorting and selection process can be performed taking into account the specific SA ordinances at hand and sorting methods. The SA ordinance of each case study determines the SA minimum requirements for the new building. The sorting methods that can be selected through the input SunVectSel, allows taking into account different sun light quality criteria (Table 1). Consequently, the sorted and selected sun vectors can be used to generate the SE using the component “Solar Envelope Generator” (SolEnvGen) which gives as output: (1) the points of the final SE; (2) the SE points for each window. Additionally, the sun vectors filtered and selected for each window can be visualized using the component “Sun Path Generator” (SunPathGen).

VectorType	Description
1	Larger solar altitude first
2	Larger solar incident radiation first
3	Sun vectors out the plot with large solar altitude first, then vectors through the plot with large solar altitude first
4	Sun vectors out the plot with large solar altitude first and then vectors through the plot with larger incident solar radiation first
5	Sun vectors out the plot with large solar altitude first and then vectors through the plot close to the corners of the plot first.

Table 1. Available sorting methods in SunVectSel.

The workflow has been tested on two existing urban areas: one located in Tallinn, Estonia (59°23'52.6"N 24°41'04.6"E)

(Figure 2) and another in Warsaw, Poland (52°16'42.6"N 20°55'14.5"E) (Figure 3). An identical plot 90x90 m in size is considered to build a new residential building in both locations. According to the Estonian Standard for daylight in dwellings, a new building cannot decrease SA of existing apartments more than 50% of actual sun light hours, and the new apartments must have at least 2.5 hours per day of direct sun light in at least one room. Both requirements need to be fulfilled every day of the period from 22th April to 22th August [12]. The SA requirements in Poland are similar for existing and new residential buildings: each apartment must have at least 3 hours of direct sun light on 21th March and 21th September between 07:00 to 17:00 [17].



Figure 2. Real (up) and virtual (down) urban environment for Tallinn case study [19].

The choice of a suitable time step is essential for the accuracy of the generated SE and the required computational time [6]. Thus, a time step of 2 and 30 are used for Tallinn and Warsaw, respectively. The minimum angle between a sun ray and the building facade (window dead angle) is set to 10 degrees for both urban areas [3]. The minimum sun altitude is set to 12 and 10 degrees for Tallinn and Warsaw, respectively [11]. All the available sorting methods are taken into account for both urban areas. The distance between grid points on the buildable plot is set to 9 meters in order to achieve a good balance between SE accuracy and computational time cost [7]. Finally, the maximum buildable height was set 30 and 50 meters for Tallinn and Warsaw, respectively.

2.2 Building envelope generation

Once the different SEs have been created, the new building volumes can be generated extruding a selected floor plan.

The following step is to generate optimal windows for the new building facades. Nowadays, facades with high window to wall ratios (WWRs) are a common solution at northern latitudes due to the lack of sun hours during the winter and the importance of the view to the outside. The component used to select the sun vectors requires windows as simple surface geometry, which are used for sun hours and radiation analysis. The distance between window centroids is set to 3 m. The floor plan considered for the main cases study is a linear floor plan typology defined by ASHRAE [10] with different number of divisions (3, 4 and 5 divisions) (Figure 4). Moreover, different orientations (from south to southwest every 45 degrees counterclockwise) are chosen in order to study its effect on the building performance.

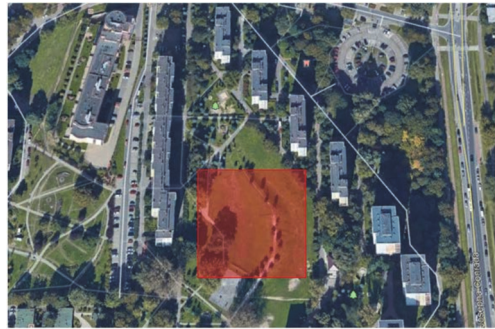


Figure 3. Real (up) and virtual (down) urban environment for Warsaw case study [19].

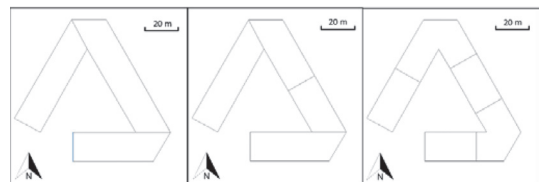


Figure 4. Different number of floor plan divisions (south oriented): 3, 4 and 5 (from left to right).

2.3 Sun hours and radiation analysis

The third phase consists of sun light hours and incident solar radiation analysis of the new building. The objective of this part of the proposed workflow (Figure 1) is to study how the urban environment affects the SA and solar radiation received by the new building. In this analysis, surroundings and new building must be provided as input in SunVectSel

component as urban context. Windows created in the previous phase are also used. To use SunVectSel for this sun hours and radiation analysis is necessary to define an auxiliary plot different from the plot used for the main cases study defined in the first phase of the workflow since we are not interested in to generate any SE in this step. However, the rest of the settings (dead angle, minimum solar altitude, weather files, time steps, etc.) are the same of those defined in the first phase of the workflow.

The outputs of this phase are the building performance indicators calculated in relation to the visible sun positions and the incident solar radiation for each time step and window. These performance indicators are:

- Volume ratio (V_r) (-) as the relation between the total volume of the new building and the volume of the SE,
- Window ratio (W_r) (-) as the relation between the number of windows of the new building that fulfill the SA requirements and the total number of windows,
- Mean incident solar radiation ($mISR$) (W/m^2) as the mean (for the analysis periods defined in section 2.1) incident solar radiation received by the windows of the new building that fulfill the SA requirements.

Thus, knowing V_r , W_r and $mISR$ for the new building we can study how its volume is fitting the SE volume, which ratio of the total facade area is fulfilling the SA requirements and the level of solar radiation exposure of the facade.

2.4 Building performance assessment

In this last phase of the workflow, the building performance indicators are used to calculate the objective variables, which are the variables of the proposed objective linear function F (1) that represent the building performance. Thus, it is possible to compare building designs through the value F (fitness value). The objectives of the evaluation formula (1) are: maximization of V_r' (OV) (2); maximization of W_r' (OW) (3); minimization of $mISR$ (OI) (4). The values of these objective variables are between 0 to 1 (5) and they represent the level of fulfillment of the building i within a set of n possible new buildings (1, 2, ..., i , ..., n).

$$F(Vr'_i, Wr'_i, mISR'_i) = \alpha Vr'_i + \beta Wr'_i + \gamma mISR'_i \quad (1)$$

$$Vr'_i = Vr_i / \max(Vr_i) \quad (2)$$

$$Wr'_i = Wr_i / \max(Wr_i) \quad (3)$$

$$mISR'_i = 1 - mISR_i / \max(mISR_i) \quad (4)$$

$$\alpha + \beta + \gamma = 1 \quad (5)$$

The coefficients α , β and γ are the weight factors whose values depends on the chosen criteria. For the main case studies, different criteria were taken into account to evaluate the fitness value of each building design (Table 2). The fitness value is always between 0 and 1. Value 1 is associated to an ideal building performance and that would

mean that the new building fulfill all the objectives previously mentioned at the same time.

	OV(α)	OW(β)	OI(γ)
C1	1	0	0
C2	0	1	0
C3	0	0	1
C4	0.5	0.5	0
C5	0.5	0	0.5
C6	0	0.5	0.5
C7	0.3	0.3	0.3
C8	0.7	0.3	0
C9	0.3	0.7	0
C10	0	0.7	0.3
C11	0	0.3	0.7

Table 2. Coefficients of the objective function for different criteria. OV=Volume maximization; OW=Solar access maximization; OI=Solar incident radiation minimization.

The workflow is applied to two case studies (Warsaw and Tallinn), different sorting methods (Table 2.1), one floor plan typology with different number of divisions (3, 4 and 5) and 8 different orientations (from South to North-West every 45 degrees). Moreover, these 240 cases are evaluated according to 11 different multi-objective criteria (Table 2.4) in order to evaluate which criteria offers the best trade-off building performance in each case study.

3 RESULTS

In this section, the dependency between the design parameters (sorting method (SM), number of floor plan divisions, orientation and multi-objective criteria) and the building performance indicators (V_r , W_r and $mISR$) are analyzed.

3.1 SE volumes

The volumes of the SEs after considering different SMs can be seen in Figure 5. In general, SMs 1, 3 and 5 allow larger SE volumes than SMs 2 or 4. This fact was expected because the sorting methods 1, 3 and 5 are based on the selection of sun vectors with larger solar altitude and/or whose projection are outside the plot. On the other hand, SMs 2 and 4 take into account sun vectors with high incident solar radiation which normally have lower sun altitude for the surrounding façade facing east and west, limiting the SE volume.

In Warsaw case, the SE volume is between 136770 m^3 and 120793 m^3 . In Tallinn case, the maximum SE volume is 153975 m^3 (SM 3) and the minimum is 78510 m^3 (SM 4). Furthermore, the SE volume is more sensitive to the SMs used in Tallinn than in Warsaw case. This is due to the combined effect of different aspects as surrounding urban environment, plot orientation, latitude, solar radiation,

analysis period, time step, dead angle and minimum solar altitude (Figure 6).

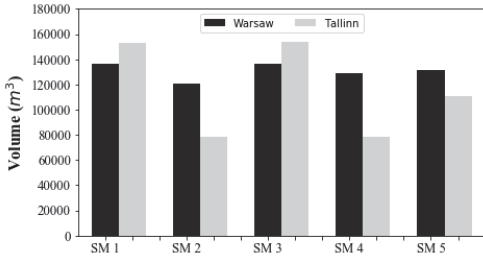


Figure 5. Volume of the SEs using different sorting methods for the cases study.

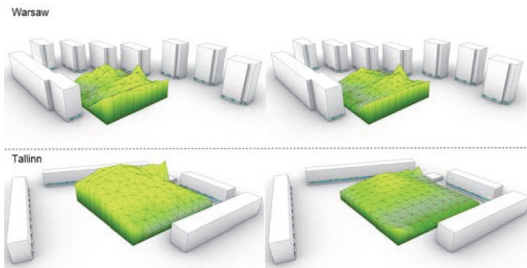


Figure 6. Examples of the generated SEs for both cases study using SM 1 (left) and SM 2 (right).

3.2 Warsaw case

The values of the objective variables for different criteria used in Warsaw case are shown in Figure 7. Different groups of criteria gives the same optimal solution. The first optimal solution is generated by volume-weighted (C1, C5 and C8) and trade-off (C7) criteria. The second optimal solution is obtained regarding SA and *mISR*-based criteria (C2, C3, C6, C9, C10 and C11). The third optimal solution is generated by the criterion C4 that is based on 50% V_r and 50% W_r . In addition, the mean incident solar radiation is minimal in these three solutions ($mISR'=1.0$). The first solution has maximum volume and the second one has maximum SA. Moreover, the third solution is a trade-off between both objectives.

The design parameters and the performance indicators for each optimal solution can be seen in Table 3. South-West is an optimal orientation in Warsaw case (Figure 8). The first and the third solutions have 5 number of floor plan sections while the second one has only 4 divisions. SM 2 is not recommended for any criteria. The consideration of SMs 1, 3 and 5 allow the maximization of SA ($W_r=0.63$) when the floor plan has 4 divisions (Figure 8b). However, if the number of divisions is increased to 5, the use of SM 5 allow the maximization of the volume ($V_r=0.21$) (Figure 8a). Indeed, the use of SM 3 and 5 divisions for the floor plan allow a good trade-off between volume ($V_r=0.2$) and SA ($W_r=0.58$) (Figure 8c). The mean incident solar radiation

for all the solutions is around 100 W/m^2 . Furthermore, the best trade-off solution can be either the first or the third one since there is no much difference in absolute terms for the volume and SA indicators (V_r and W_r).

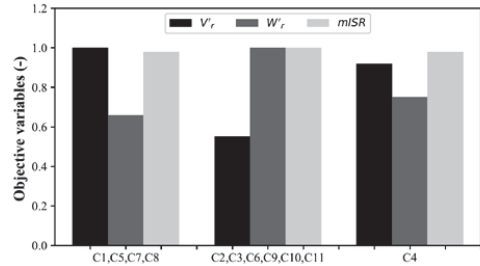


Figure 7. Objective variables values for different criteria in Warsaw case.

Criteria	nFPd	Ori.	SM	V_r	W_r	<i>mISR</i>
C1,C5,C7,C8	5	SW	5	0.21	0.57	100.58
C2,C3,C6,C9, C10,C11	4	SW	1,3,5	0.17	0.63	100.03
C4	5	SW	4	0.20	0.58	100.71

Table 3. Design parameters and performance indicators using different criteria for Warsaw case.

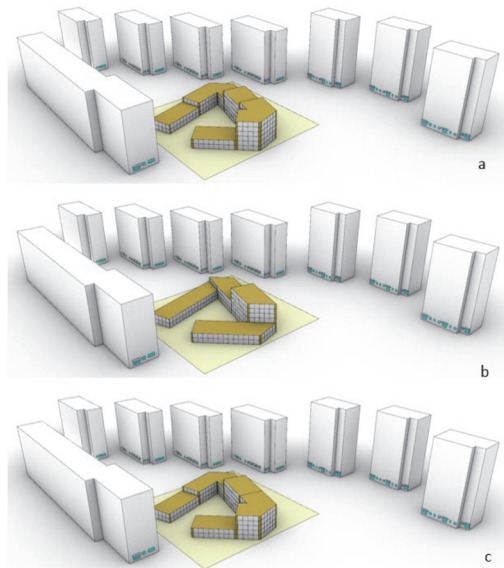


Figure 8. Optimal combinations in Warsaw case.

3.3 Tallinn case

The values of the objective variables for different criteria used in Tallinn case can be seen in Figure 9. In these case, five different group of criteria give 5 different optimal solutions:

- The first optimal solution is generated by the 100% volume-weighted criterion (C1),
- The second optimal solution is a 100% SA-based criterion (C2),
- The third optimal solution is generated by a group of criteria based on different trade-off considerations (C3, C5, C7, C11),
- The fourth optimal solution is generated by a group of criteria based on different trade-off between volume and SA (C4, C8, C9),
- The fifth optimal solution is generated by a group of criteria based on different trade-off between SA and $mISR$ (C6, C10).

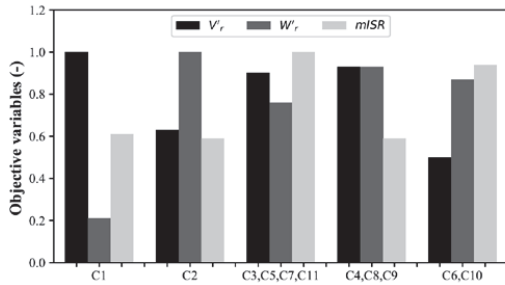


Figure 9. Objective variables values for different criteria in Tallinn case.

The design parameters and the performance indicators for each optimal solution are shown in Table 4. In general, SM 2 and 4 are not recommended for any criteria. The maximization of the building volume ($V_r=0.24$) is possible by orienting west a floor plan with 5 divisions and considering SM 5 to generate the SE (Figure 10a). Nevertheless, the combination of the SM 1 or 3 with 3 divisions of the floor plan and NW orientation, achieve a low volume fitting with the SE volume $V_r=0.18$) but high performance in terms of SA ($W_r=0.87$) and $mISR$ (190.14 W/m^2) (Figure 10e). Moreover, the south orientation combined with a low number of divisions of the floor plan (3 and 4) are associated to high W_r (between 0.84 and 0.97) when SM 1 is considered (Figure 10b 12d). The only difference between the fifth and the third optimal solution is the number of divisions of the floor plan (4 and 3, respectively). This increment from 4 to 3 divisions of the floor plan generates a self-shadowing phenomenon: the 3% of the whole facade pass to do not fulfill the SA requirement because V_r increases a 5% (Figure 10c 12e).

Finally, the third (Figure 9c) and fourth solutions show good trade-off performance. Nevertheless, since the deviations in

terms of $mISR$ are around 10 W/m^2 , the fourth optimal solution is the best one (Figure 9d): south-oriented building whose floor plan is divided by 4 sections (SM 1 used for the SE generation) achieve a V_r of 0.23 and the 89% of the facade is fulfilling the SA requirements with a mean incident solar radiation of almost 198 W/m^2 .

Criteria	nFPd	Ori.	SM	V_r	W_r	$mISR$
C1	5	W	5	0.24	0.66	197.39
C2	3	S	1,3	0.19	0.92	197.7
C3,C11,C5,C7	4	NW	1,3	0.23	0.84	188.78
C4,C8,C9	4	S	1	0.23	0.89	197.89
C6,C10	3	NW	1,3	0.18	0.87	190.14

Table 4. Design parameters and performance indicators using different criteria for Tallinn case.

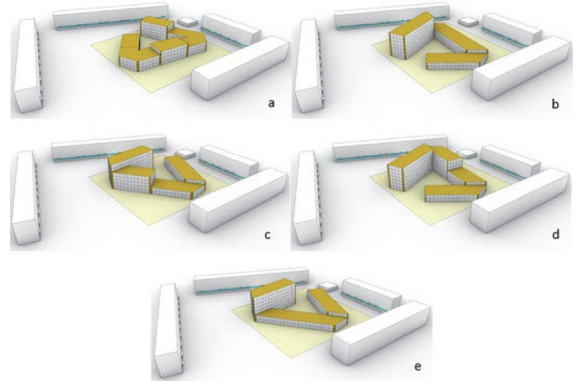


Figure 10. Optimal combinations in Tallinn case.

4 CONCLUSION

Solar access is one of the key criteria for visual comfort that can also affect the thermal comfort and energy efficiency in buildings. There are different ordinances that define the minimum SA requirements for new and existing residential buildings. These requirements are related to the quantity not the quality of direct sun light. Different SEs might fulfill the same SA requirements for a case study. This fact provide flexibility in the early stages of the architectural design process. Previous research just only focused on one SE per urban area.

The aim of this paper is to study the potentiality of different SEs in building envelope design in cold climates. The methodology consists of a workflow based on multi-

objective optimization. The objectives used are: maximizing the volume of the building, maximizing the ratio of the facade that fulfills the SA requirements and minimizing the solar radiation received by a portion of the facade. Thus, this workflow is used to design a new residential building in two locations with different SA ordinances: Warsaw (Poland) and Tallinn (Estonia). The same buildable plot and floor plan typology are used for both case studies. Moreover, the design parameters used are: the number of floor plan divisions, the orientation of the new building, the sorting method of sun vectors for SE generation and multi-objective criteria. Case study consolidates an insightful comparison of various optimization criteria.

In general, considering a large number of possible floor plan divisions, the volumes of the new building can fit better SE volume. Moreover, the consideration of sorting methods based on larger solar altitudes and sun vectors outside the plot achieve larger SE volume than those based on incident solar radiation. Moreover, the maximum relative difference in terms of SE volume is almost 50% and 12%, for Tallinn and Warsaw case, respectively. Indeed, this difference can be due to the length of the analysis periods.

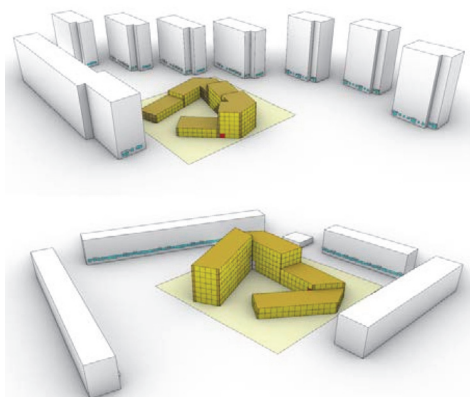


Figure 11. Optimized building envelopes for Tallinn (down) and Warsaw (up) cases. Windows in yellow fulfill the SA requirements and the red window has the maximum mean incident solar radiation.

A suitable choice of the design parameters is critical to optimize the new building envelope. If the preferred criteria to design the new residential building is the volume ratio and the SA of the facades, the use of criteria based on volume-weight for Warsaw and trade-off criteria between volume and SA for Tallinn are suitable ones. The optimized building envelopes for both case studies is shown in Figure 11. The optimal number of floor plan divisions are five and four for Warsaw and Tallinn cases, respectively. The total floor area is 8930 m² and 11617 m² in Warsaw and Tallinn, respectively. South-west (Warsaw) and south (Tallinn) orientations allow good performance between volume and

SA of the new buildings (Figure 11): volume ratio higher than 20% and ratio of the facade that fulfill the SA requirements of 57% and 89%, for Warsaw and Tallinn, respectively.

This research presents a useful workflow to be used in the early stages of the design of residential buildings in cold climates. How to take advantage of the SA requirements to optimize the building performance using different multi-objective criteria is investigated. This workflow is especially suitable when the SA regulations are strict. First decisions as building orientation, windows location, building footprint and buildable volumes characterize the solar access of the existing and new buildings. Other requirements related to daylight provision, overheating, energy consumption or glare protection could be fulfilled with a suitable design of interior layout and façade. In this paper, different criteria are considered and all the possible building envelope are evaluated and the maximum fitness value searched. Future work is to apply this workflow in a larger optimization system (to evaluate different floor plan typologies) based on genetic algorithm (GA). Additionally, this method will be implemented in a Grasshopper tool for Rhinoceros to help architects and designers to choose between possible building design strategies.

ACKNOWLEDGMENTS

The research has been supported by the Estonian Centre of Excellence in Zero Energy and Resource Efficient Smart Buildings and Districts, ZEBE, grant 2014-2020.4.01.15-0016 funded by the European Regional Development Fund, and the European Commission H2020 grant Finest Twins n. 856602.

REFERENCES

1. Capeluto, I. G., and Plotnikov, B. A method for the generation of climate-based, context-dependent parametric solar envelopes. *Architectural Science Review* 60, 5 (2017), 395–407.
2. Capeluto, I. G., and Shaviv, E. Modeling the design of urban fabric with solar rights considerations. Israel: Faculty of Architecture and Town Planning Technion-Israel Institute of Technology Haifa. Recuperado de http://www.ibpsa.org/proceedings/BS1999/BS99_C-22.pdf (1997).
3. Darula, S., Christoffersen, J., and Malikova, M. Sunlight and insolation of building interiors. *Energy Procedia* 78 (2015), 1245–1250.
4. De Luca, F. From envelope to layout-buildings massing and layout generation for solar access in urban environments. *Proceedings of Sharing Computational Knowledge! ShoCK! 35th International Conference on Education and research in Computer Aided Architectural Design in Europe, eCAADe Vol. 2* (2017), 431–440.
5. De Luca, F. Solar form finding: Subtractive solar envelope and integrated solar collection computational method for high-rise buildings in urban environments.

- Proceedings of Disciplines and Disruption - 37th Annual Conference of the Association for Computer Aided Design in Architecture, ACADIA 2017, Cambridge (MA), United States (2017), 212–221.
6. De Luca, F., and Dogan, T. A novel solar envelope method based on solar ordinances for urban planning. *Building Simulation: An International Journal* 12, 5 (2019), 817–834.
 7. De Luca, F., Nejur, A., and Dogan, T. Facade-floor-cluster-methodology for determining optimal building clusters for solar access and floor plan layout in urban environments. *Proceedings of Computing for a better tomorrow. 36th International Conference on Education and research in Computer Aided Architectural Design in Europe, eCAADe, Lodz, Poland Vol. 2 (2018)*, 585–594.
 8. De Luca, F., and Voll, H. Computational method for variable objectives and context aware solar envelopes generation. *8th Annual Symposium on Simulation for Architecture and Urban Design, SimAUD 2017, Toronto, Canada Vol. 11 (2017)*, 281–288.
 9. De Luca, F., and Voll, H. Solar collection multi-isosurface method - computational design advanced method for the prediction of direct solar access in urban environments. *Communications in Computer and Information Science, 17th International Conference on Computer-Aided Architectural Design, CAAD Futures 2017, Istanbul, Turkey 7 (2017)*, 170–187.
 10. Dogan, T., Saratsis, E., and Reinhart, C. The optimization potential of floor-plan typologies in early design energy modeling. *Proceedings of BS2015: 14th Conference of International Building Performance Simulation Association, Hyderabad, India, International Building Performance Simulation Association (IBPSA) (2015)*.
 11. European commission, EN 17037:2018 Daylight in buildings. <https://velcdn.azureedge.net/~media/marketin g/ee/professional/28mai2019%20seminar/veluxen17037 tallinn28052019.pdf>
 12. Daylight in Dwellings and Offices. 894:2008/A2:2015. <https://www.evs.ee/products/evs-894-2008+a2-2015>.
 13. Knowles, R. L. Sun rhythm form. Cambridge, MA, USA: MIT Press. (1981).
 14. Ladybug Tools 2019. <https://www.ladybug.tools/ladybug.html>.
 15. Samuels, R. Solar efficient architecture and quality of life: The role of sunlight in ecological and psychological well-being. In *Proceedings of the 1st World Renewable Energy Congress: Energy and the environment*, Pergamon Press Oxford, UK (1990), 2653–2659.
 16. Sanaieian, H., Tenpierik, M., van den Linden, K., Seraj, F. M., and Shemrani, S. M. M. Review of the impact of urban block form on thermal performance, solar access and ventilation. *Renewable and Sustainable Energy Reviews* 38 (2014), 551–560.
 17. Sokol, N., and Martyniuk-Peczek, J. The review of the selected challenges for an incorporation of daylight assessment methods into urban planning in poland. *Procedia engineering* 161 (2016), 2191–2197.
 18. Solar toolbox 2019. <https://www.food4rhino.com/app/solar-toolbox>.
 19. Google Earth Pro. 2019. <https://www.google.com/intl/es/earth/versions/#earthpro>
 20. Solemma LLC. DIVA. 2019. <https://www.solemma.com/Diva.html>.
 21. Stasinopoulos, T. N. A survey of solar envelope properties using solid modelling. *Journal of Green Building* 13, 1 (2018), 3–30.

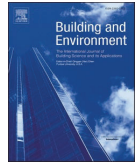
Paper II

Sepúlveda, A., De Luca, F., Thalfeldt, M., & Kurnitski, J. (2020). Analyzing the fulfillment of daylight and overheating requirements in residential and office buildings in Estonia. *Building and Environment*, 180, 107036.



Contents lists available at ScienceDirect

Building and Environment

journal homepage: <http://www.elsevier.com/locate/buildenv>

Analyzing the fulfillment of daylight and overheating requirements in residential and office buildings in Estonia

Abel Sepúlveda^{*}, Francesco De Luca, Martin Thalfeldt, Jarek Kurnitski

Tallinn University of Technology, Department of Civil Engineering and Architecture, Ehitajate tee 5, Tallinn, 19086, Estonia

ARTICLE INFO

Keywords:

Daylighting
Overheating
Window airing
Building performance
Cold climate
Window

ABSTRACT

Daylight and thermal comfort in cold climates have been proved crucial for the well-being of the building occupants. In this study, the reliability of the daylight requirements defined by the Estonian standard based on the mean daylight factor (DF) was evaluated with respect to the minimum DF requirements defined by the European standard method, EN 17037:2018 and IES LM-83-12, based on the spatial daylight autonomy (sDA) for office and residential buildings. The effect of window airing on overheating and also on the combination of overheating and daylighting was studied. Indoor comfort-based rules of thumb for the design of offices and residential rooms were suggested. A simulation-based methodology was applied to assess the daylighting and overheating performance in a single-window room considering different parameters. The results show that 30% of the combinations fulfill the mean DF requirement but not the sDA requirement. Moreover, there is an agreement between the Estonian standard EVS 894:2008/A2:2015 and European standard EN 17037:2018 for only 54% of room combinations. The addition of window airing increases the maximum window-to-wall ratio by 50% in residential rooms. The results suggest a synergistic formulation of daylighting and overheating requirements in new building regulations to make the combined fulfillment easier for the designers.

1. Introduction

The design of the building envelope is crucial in the early stages of construction as well as in the retrofit solutions. The building envelope has a key impact on energy efficiency and indoor comfort (visual and thermal). One of the objectives of the European program Horizon 2020 is to improve the energy efficiency in buildings. The Energy Performance of Buildings Directive 2010/31/EU (EPBD) aims to encourage the member states to define specific requirements for new buildings (starting from 2021) to become nearly zero-energy buildings (nZEBs) [1].

Visual comfort has beneficial effects on the well-being of building residents [2]. The European Union recently presented the standard EN 17037:2018 that defines the requirements for visual comfort in buildings [3], which include the daylight provision [4]. Over the past 25 years, the influence of light on the human well-being has been investigated [5]. The characteristics of daylight that make it essential for human well-being include its intensity and color support for the circadian cycle in humans [6]. Not all the holistic positive effects of daylight can be reproduced artificially; thus, daylighted rooms are preferred to those with electric lighting [7]. There are several methods to evaluate the

daylight intensity in buildings. One of the mostly used assessment methods due to its simplicity is the daylight factor (DF). DF was created in the United Kingdom for daylight assessment under overcast conditions [8]. After 2006, some researchers have started investigating the dynamic performance of daylight in buildings considering its occupants' behavior and the surrounding climate during the year [9]. In some cases, daylight autonomy (DA) is more applicable than DF [10]. The useful daylight illuminance was proved to be a more informative and intuitive metric for daylight assessment than DA [11]. The spatial daylight autonomy (sDA) was approved by the Illuminating Engineering Society as the daylight metric (IES LM-83-12) [12]. The sDA contains spatial and temporal information about the daylight provision. Hence, annual climate-based simulations are required to calculate this metric. Daylight access (direct and diffuse) is highly valued by tenants according to a recent study in the U.S. where tenants pay 5–6% more for spaces with high daylight provision; hence, daylight should be considered in project financing [13]. Nevertheless, not every European country has yet defined a concept of adequate daylight and a suitable daylight metric [14].

The creation of the open-source software Radiance [15] and

^{*} Corresponding author.

E-mail address: absepu@taltech.ee (A. Sepúlveda).

developments in multi-core CPUs, parallel computation, GPUs, and the Perez and CIE sky models improved the climate-based daylight simulations in terms of time costs and accuracy [4]. Practitioners were able to assess the dynamic daylight performance using Radiance-based tools such as DIVA for Rhino [16] or Fener not only in the early stages but also in retrofit solutions [17–19]. These tools can be used to assess additional functions of interest such as visual glare protection [20], thermal indoor comfort, energy performance (heating, cooling, and lighting), selection of complex fenestration systems (CFSs), and the design of shading controls [19]. A recent parametric study supported the use of external shutters to reduce heat loss through windows in winter and improve the indoor comfort in summer and explored the influence of the extra insulation around the perimeter of a roof window on its thermal transmittance [21]. The optimization of the indoor comfort in an office in Singapore showed potential energy savings of 34.3%, 7.15%, and 5.5% for lighting, lighting-cooling, and total energy, respectively [22]. Other studies showed that the layout of the windows and shading for heating and cooling led to the energy savings of 25%, 28%, and 45% in a test office room located in Tallinn, Milan, and Cairo, respectively [23], using an innovative method to generate the optimal shape of shading devices [24]. Daylight has a significant positive influence on the energy efficiency of buildings [25–28]. Daylight and solar heat gains in winter can reduce the energy consumption when a suitable shading control is considered [29]. Previous investigations emphasize the need to design synergistically glazed areas and shading to provide adequate daylight in building interiors and reduce energy consumption for lighting [30,31] and for heating and cooling [32,33]. External shading is an efficient solution to reduce glare risk for building occupants [34], and has the advantage of not relying on occupant operation; occupants often leave the operable internal shade closed and also use it when is not needed, causing an avoidable electric light energy consumption [35].

Another aspect that affects the indoor thermal comfort is the overheating risk in buildings. In 2013, a study on thermal comfort in 1134 English dwellings demonstrated that the renovation plans should include practical measures against overheating risk in residential buildings [36]. The severity of the seasonal overheating risk in dwellings is influenced by the urban surroundings, local architecture, occupant behavior, and climate. A previous study suggested nighttime ventilation and mechanical ventilation in combination with heat recovery from the exhaust air in winter to decrease the overheating risk [37]. Moreover, the use of window airing with nighttime ventilation at an educational building located in Cyprus allowed the fulfillment of overheating requirements [38]. However, using only night ventilation as a passive cooling solution in educational buildings in southern Europe was found to be insufficient against future overheating predictions (2050s–2090s) [38]. Another study showed that fuzzy-based AC controls could not avert the overheating problem of a sick building located in Italy; hence, a major renovation was suggested [39].

In cold climates, buildings with high thermal resistance are common to save heating energy in winter, and facades with high window-to-wall ratios (WWRs) are designed to increase the daylight provision [40]. However, these measures can generate thermal discomfort during the warm season. Estonia has specific overheating requirements that must be met if there is no mechanical space cooling system in a new or a renovated building. Overheating requirements in Estonia are based on the metric degree-hour (DH) (°C·h), which represents the accumulation of the hourly indoor temperature excess (related to a temperature set point) during a specific period of warm season (June 1–August 31). The maximum DH is 150 °C h and 100 °C h for residential and non-residential buildings, respectively. The temperature set point is 27 °C and 25 °C for residential and non-residential buildings, respectively [41,42]. Thus, the use of window airing, shading, and a suitable glazing system for windows have been studied as the main passive solutions for nZEB residential buildings in Estonia [43–45]. However, window airing is not permitted in overheating simulations of non-residential buildings. Installation of openable windows is not regulated by these requirements.

Window shading elements can reduce the overheating of residential premises depending on facade orientation and distance of neighboring buildings, especially at northern latitudes; thus, a careful envelope design is recommended [44]. Hamburg and Kalamees [46] determined that experimental analysis of three apartments per building was not sufficient to estimate the indoor comfort; hence, they supported the use of simulation-based methodology to assess thermal comfort in Estonian residential buildings. Another study developed in 2015 within nZEB Danish single-family homes shows the difficulties to achieve a good balance between daylight provision, energy consumption, and overheating risk: low g-values and high light transmittance values were recommended for south-oriented rooms and high g-values for north-facing windows to reduce the heating demand [47].

In Estonia, overheating is considered a limiting function of the daylight provision. According to the Estonian standard EVS 894:2008/A2:2015, the daylight requirements are expressed in terms of mean DF and depend on the building type. Parametric model-based methodology was applied to study the influence of different passive design solutions and ventilation systems on fulfillment in terms of daylight (mean DF \geq 1.5%) and overheating (DH < 150 °C h) in living rooms [48]. Other research focused on Estonian educational buildings; the fulfillment of the minimum mean DF requirement according to the Estonian standard EVS 894:2008/A2:2015 [49] and the minimum 55% sDA (at least 300 lux during 50% of occupied hours) were compared for a determined number of room variations. Hence, criterion based on sDA was more conservative than Estonian DF-based criterion for educational buildings [50]. In addition, the metric annual spatial exposure (ASE) [12] has been used to assess excessive possible discomfort for direct solar access; however, in this study we use overheating in Estonia as a limiting function of the daylight provision.

The European standard is based on the minimum DF and currently valid in Estonia in parallel with the Estonian standard but no studies have been conducted to evaluate its impact on the construction practice. Previous studies showed disagreements between dynamic and static daylight metrics in Estonia. Therefore, it is important to understand how the European standard affects the design of the building envelope and refurbishment plans. Moreover, it is necessary to quantify the disagreement between the current Estonian regulations based on DF and the sDA criterion without ignoring the overheating risk. The main aim of this study is to investigate the effect of different daylight assessment criteria on the combined fulfillment of daylighting and overheating requirements and its implications for the design of residential and office rooms in Estonia.

The objectives of this study can be summarized as follows:

1. To use the daylight assessment criteria based on sDA (IES LM-83-12) and minimum DF (European standard EN 17037:2018) to evaluate the actual Estonian standard EVS 894:2008/A2:2015 based on the mean DF and propose indications for further modifications of the Estonian regulation for residential and office buildings.
2. To investigate the overheating levels and the effect of window airing on residential buildings.
3. To determine the influence of the room parameters such as orientation, room width, room depth, window-to-wall ratio (WWR), and shading size on the fulfillment of daylight provision and the overheating levels in Estonian residential buildings.

2. Methodology

A simulation-based methodology with the single-zone approach was used for the assessment of daylighting and overheating. A parametric model of a generic residential/office room was created in Grasshopper environment that runs within the Rhinoceros 3D computer-aided design (CAD) application. The model generated two geometrical models (one for daylight and another for thermal indoor climate simulations) using

different room parameters (Fig. 1). The building typology used for this research is a common typology in Tallinn [51]. The building has five floors and a total height of 17 m, with the ground floor occupied by commercial facilities and four regular floors with 2.8 m floor-to-ceiling distance. The test room is located in the middle of the second and third floors to obtain an average obstruction by the surrounding buildings. The surrounding buildings are modeled as a continuous facade of the same height of the test building (17 m) and located at 45 m from the center of the test room toward four cardinal directions with a typical high-density city center setting and a sparse new development setting in Tallinn.

The room size parameters and number of orientations were selected to obtain a representative sample of typical residential living rooms and office rooms in Estonia. The small 3.5 m × 3.5 m rooms represent a single-employee office of approximately 12 m². Intermediate rooms represent living rooms and medium-size offices with an area of 20–40 m². The larger rooms with a size of 6.5 m × 7.5 m represent large offices of ~50 m².

The window sizes used in this study represent typical floor and regular sill (0.9 m from the floor) windows used in residential and office buildings in Estonia [51]. The window height can be 1.5 m or 2.4 m while the distance from the upper frame to the slab level is 0.37 m. The maximum width for a single glazed area is 1.5 m. WWRs values were calculated considering a frame width of 5 cm for each window (without dividers).

The different shading systems considered in the model are illustrated in Fig. 2. Thus, no shading system was considered for rooms facing north (N) because direct sunlight is not relevant for that orientation. However, for south (S), southeast (SE), and southwest (SW) orientations, fixed horizontal shading was used. Apart from horizontal shading, fixed vertical shadings were used in the east (E), northeast (NE), northwest (NW), and west (W) orientations. The reason for the different layout of shading devices for south, southeast, and southwest (horizontal) orientations and all the others (vertical and horizontal) is that horizontal shadings perform well for southerly orientations, and vertical shadings perform well for easterly and westerly orientations due to the low sun angle. In this study, the horizontal shadings for southerly orientations were extended on the side to increase protection from direct sunlight and also when the sun is not perpendicular to the façade; the vertical shadings for easterly and westerly orientations were added the horizontal overhang

to increase protection, creating a “crate” system that is also recommended in the literature [52,53]. The selected sizes for the shading device depths of 0.6 m and 0.9 m correspond to the recommended optimal sizes of shading in relation to window height (maximum 0.4 h, where h is the height of the window) [51]. The source of the fixed shading device is the façade plane.

2.1. Model for daylight simulations

One of the outputs of the parametric model is the building geometry for daylight simulations. Some examples of room variations are displayed in Fig. 2. This geometric information is required by DIVA for Rhino [54] to run the daylight calculations. The daylight analysis grid is located at 0.8 m height from the floor and the spacing between the grid points is 0.5 m [12]. DIVA is a Grasshopper plug-in for Rhinoceros that uses the validated software DAYSIM (Radiance-based software) for daylight calculations [55–57]. Specifically, DIVA components “daylight factor” and “annual daylight” were used to assess the daylight intensity according to the criteria of interest presented in Table 1.

For both residential and office test rooms, interior finishing materials had standard diffuse reflectance values, commonly used for daylight simulations when real building material data are not available [48,58, 59]. The reflectance of the opaque surfaces in the model is shown in Table 2. Moreover, triple glazed windows with 18 mm gap [60] were considered because of their reliability in terms of cost and energy performance within the Estonian context [40,61,62].

The minimum requirements for all the criteria (DF_{mean}, DF_{min}, and sDA) are shown in Table 1. The DF_{mean} criterion requires a minimum mean DF of 1.5% and 2.0% for residential and office rooms, respectively. IES LM-83-12 defines a minimum sDA of 55% (for a daylight autonomy (DA) threshold of 300 lux for all types of buildings). Thus, at least 55% of the area is lit with at least 300 lux in 50% of the occupied hours. For this study, a DA threshold of 500 lux was considered instead of 300 lux for office rooms as recommended by the European lighting standard EN12464-1. The European standard EN 17037:2018 specifies a target DF for 50% of the reference plane (half of the room closer to the window), and a minimum target DF should be met for 95% of the entire reference plane. According to Tables A3 and A4 in EN 17037:2018, the target DF (DT) and the minimum DF for Estonia are 2.2% and 0.7%, respectively.

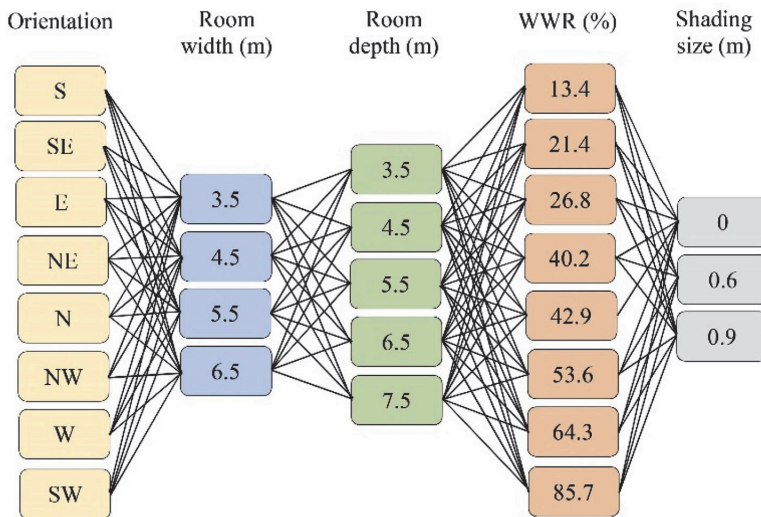


Fig. 1. Diagram of room parameter combinations. This is a single-column fitting Figure.

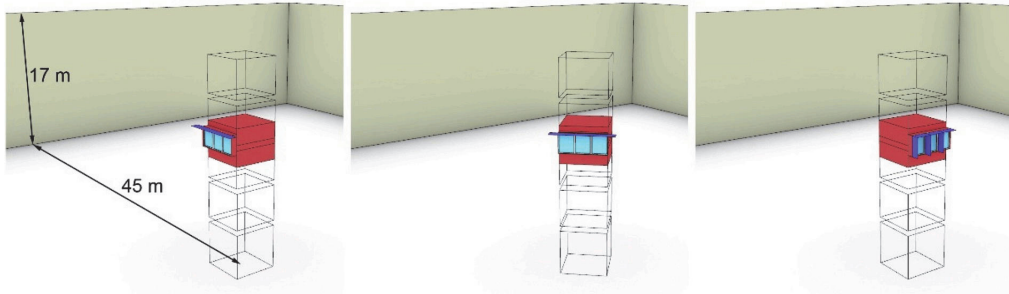


Fig. 2. Modeled 3.5 m × 3.5 m rooms S, SE, and E oriented for the daylight analysis (shading size of 0.6 m).

Table 1

Daylight requirements for each criteria [3,12,49].

Room type	Reference condition	Test condition
Residential	mean DF ≥ 1.5%	sDA ≥ 55%
	mean DF ≥ 1.5%	minimum DF ≥ 2.2%
Office	mean DF ≥ 2%	sDA ≥ 55%
	mean DF ≥ 2%	minimum DF ≥ 2.2%

Table 2

Reflectance of the opaque surfaces.

Surface	Reflectance
Ground	20%
Exterior facade	30%
Interior walls	70%
Floor	20%
Ceiling	70%
Shading	30%

The Radiance parameters used for the sDA and DF simulations were chosen following the recommendation made by Reinhart (Table 3) [12]. The minimum DA illuminance threshold was defined according to the requirements of the Estonian standard EVS 894:2008/A2:2015, which are 300 lux and 500 lux for residential and office rooms, respectively. The weather data for sDA simulations were obtained from the Tallinn-Harku meteorological station for the year 2014. The occupancy schedule used for climate-based daylight assessment in office rooms is from 08:00 to 18:00 during weekdays as required by the method LM-83-12 [12]. For residential rooms, an “always occupied” schedule was used because residential buildings are assumed to be occupied all day throughout the week. CIE overcast sky conditions were considered for DF calculations by DIVA (DAYSIM).

Table 3

Radiance parameters for sDA and DF simulations.

Ambient accuracy (-aa)	0.1
Ambient bounces (-ab)	5
Ambient divisions (-ad)	1500
Ambient resolution (-ar)	300
Ambient super-samples (-as)	20
Number of relays for secondary sources (-dr)	2
Direct sampling ratio (-ds)	0.2
Reflection limit (-lr)	12
Minimum weight of a traced ray (-lw)	0.004
Direct certainty (-dc)	0.75
Secondary source presampling density (-dp)	2048
Direct threshold (-dt)	0.05
Medium sample distance (-ms)	0.063
Specular sampling threshold (-st)	0.01

2.2. Model for overheating calculations in residential buildings

The Grasshopper plug-in ArchSIM [63] was used to define the thermal model for energy calculations at residential rooms. We used the .idf file generated by ArchSIM and set up all the desired parameters such as the number of warming days, frame width, or boundary conditions of each surface. We used the edited the .idf file as input to the validated software Energy Plus version 8.4 [64]. The variable of interest to assess the overheating at the parametric rooms was the hourly mean air temperature (T_h). The expression to calculate the overheating (DH) of a residential room during the warm season is the following:

$$DH = \sum_{h=1}^N (T_h - 27) (^\circ Ch) \quad (1)$$

where N is the number of occupied hours (from June 1 to August 31) for which the main air temperature exceeded 27 °C. According to the Estonian regulations [41], DH must not exceed 150 °Ch in residential buildings. High thermal mass materials were used for the walls, slab, and floor (Table 4). The material for the slab floor and interior walls is a 250 mm layer of concrete. The external wall has three layers of concrete and expanded polystyrene (total thickness of 480 mm) with a thermal transmittance of 0.128 W/(m²K). The g-value of the window is 0.37. The simplified model was used to define the window because it has been proved to be more conservative than the detailed model for overheating calculations [65].

The interior walls, slab, and floor were considered as adiabatic surfaces. This condition might be conservative for thermal calculations because, in reality, there is heat exchange between adjacent thermal zones. Owing to the high thermal mass of the materials, a large number of warming days is required to reach the stationary thermal conditions. Heat transfer through the exterior wall and solar exposure was also considered. The Estonian regulations define the usage profiles for internal gains (occupancy, lighting, and equipment) in residential buildings (Fig. 3). The maximum lighting usage rate is 0.2 with a power density of 8 W/m² (Table 5). The occupancy level is never null and is the highest from 23:00 to 6:00. The number of square meters per person for a multi-apartment building is 28.3 [42] and the mean level of activity is 1.2 MET.

The consideration of infiltration is mandatory according to the Estonian regulations. The infiltration air flow rate (q_i) is calculated using Eq. (2) (when the exhaust and supply air flow rate are the same):

$$q_i = \frac{q_{50}}{3.6x} A \quad (2)$$

where A is the area of the building envelope in m², q_{50} is the average air leakage rate of the building envelope that was set to 3 m³/(h·m²) according to the same regulation, and x is the building factor set to 20 because it is a four story building [42].

Mechanical ventilation was also considered, and two thresholds were

Table 4
Thermal and optical properties of the building envelope.

Element	Construction	Thermal transmittance (W/(m ² K))	g value (-)	Visual/Solar Transmittance (-)	Exterior/Interior emissivity (-)
External wall	Concrete 150 mm Expanded Polystyrene 280 mm	0.128	-	-	-
Floor slabs, Internal Walls	Concrete 50 mm Concrete 250 mm	3.59	-	-	-
Window [60]	Triple glazing	0.5	0.37	0.63/0.27	0.9/0.9

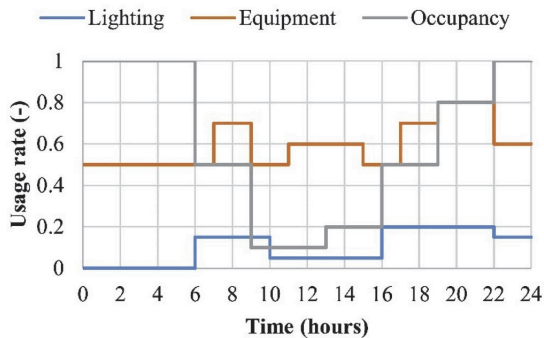


Fig. 3. Usage profiles of occupancy lighting and equipment according to residential buildings in Estonia [42]. This Figure is a single column fitting one.

Table 5
Internal gain parameters.

People density	0.0353 p/m ²
Metabolic Rate	1.2 MET
Equipment density	3 W/m ²
Lighting power density	8 W/m ²
Dimming Control	OFF
Target Illuminance	300 lux

defined: fresh air of 14.15 L/s per person and minimum fresh air of 0.5 L/s per area (m²). The airing position of the window was set to 10% as defined by Simson et al. [66]. With a set point of 25 °C and an openable area of 10% for the window, low heating energy is needed during the warm season due to the occasional low exterior temperatures in Tallinn. The heating system must be switched on with a set point of 21 °C for residential buildings (Table 6).

The first part of this methodology was to generate the room variations from the room parameters. The second step was to run the daylight simulations (DIVA for Rhino) using different assessment criteria, sDA, DF_{mean}, and DF_{min}, for residential and office rooms. Energy Plus was used for overheating simulations. Once the calculations were completed, different daylight criteria were compared. The effect of the window airing on overheating levels was analyzed, and the combined fulfillment of daylight and overheating was analyzed relative to the room parameters.

Table 6
HVAC settings for residential buildings in Estonia.

Heating system (SP)	ON (21 °C)
Cooling system (SP)	OFF (-)
Window airing (SP)	ON (25 °C)
Mechanical ventilation	ON
Minimum Fresh Air per Person	14.15 (L/s/p)
Minimum Fresh Air Area	0.5 (L/s/m ²)
Mechanical ventilation schedule	Always ON
Heat recovery temperature efficiency	80%

3. Results

In this section, we first compare different criteria for the assessment of daylight provision in residential and office spaces. Next, we show the effect of window airing as a cooling passive technique on overheating levels in residential rooms. Finally, we determine the influence of window airing and daylight criteria on the fulfillment of the daylight provision and overheating requirements in residential rooms.

3.1. Daylight provision

According to our results, all the tested room variations that fulfilled the minimum DF of 2.2% for the first half of the reference plane closer to the window also fulfilled the minimum DF of 0.7% for at least 95% of the reference plane. Hence, we take the minimum DF of 2.2% for the first half of the grid as the critical requirement that ensures the fulfillment of the European standard EN 17037:2018. The percentage of the simulated rooms (3520 combinations) associated with different daylight fulfillment cases is displayed in Fig. 4. There is no room that reaches sDA higher than 55% and a mean DF lower than 1.5 or 2.0 for residential or office use, respectively. In 29% and 32% of the residential and office cases, respectively, the Estonian DF requirement is met, but not the sDA. Nevertheless, there is a 70% agreement between sDA and DF_{mean} for both types of buildings. For residential rooms, the agreement between DF_{mean} and DF_{min} is 58%. There is no room that reaches a minimum DF higher than 2.2% and a mean DF lower than 1.5 or 2.0% for residential or office rooms, respectively. For office rooms, the agreement between DF_{mean} and DF_{min} is approximately 70%, likely due to the stricter DF_{mean} requirement for office use (2.0%) than for residential rooms (1.5%).

The minimum WWR (minWWR) to fulfill the daylight requirement for different criteria (DF_{mean}, DF_{min}, and sDA) and office room parameters are presented in Table 7. The IES LM-83-12 is one of the most conservative testing criteria. The NE, NW, and W-oriented office rooms with depths of at least 3.5 m do not fulfill sDA ≥ 55% when shading is used. However, the maximum recommended room depth is 5.5 m when no shading is used (minWWR of 0.86 for S orientation). For shading sizes of 0.6 m or 0.9 m installed in the S- and SE-oriented rooms, the maximum recommended room depth is 4.5 m (minWWR of 0.86). As expected, the shading size is related to the increase in minWWR required for any room combination.

As shown in Table 8, the fulfillment in terms of different daylight requirements in residential rooms is less restrictive than in office rooms: the maximum depth of the office rooms is equal to or less than that of the residential rooms for sDA/DF_{mean} criteria, when the room orientation or shading size is considered, because of the stricter daylight requirements for office rooms. Considering the IES LM-83-12 method for living rooms, the following results are obtained.

- Without shading, the maximum recommended room depth is 5.5 m with minimum WWRs varying from 0.40 to 0.86 depending on the orientation.

- With a shading size of 0.6 m, the maximum recommended room depth is 4.5 m for NE and NW orientations but 5.5 m for the other orientations (minWWR from 0.54 to 0.86).

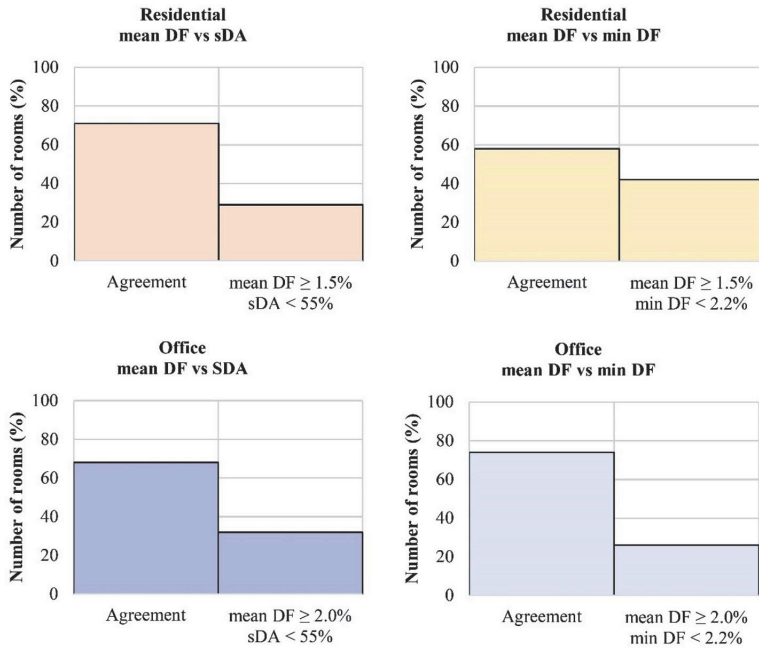


Fig. 4. Agreement analysis between different the daylight criteria used (Table 1).

Table 7

Minimum WWR to fulfill the daylight requirements (for DF_{mean}, DF_{min}, and sDA) defined in Table 1 for room parameters (office).

Office room depth (m)			3.5	4.5	5.5	6.5	7.5	
Shading size (m)	0 m	DF _{mean}	S,SE,E,NE,N,NW,W,SW	0.27	0.27	0.4	0.4	0.4
		DF _{min}	S,SE,E,NE,N,NW,W,SW	0.4	0.4	0.86	-	-
		sDA	S,SE,E,NE,N,NW,W,SW	0.4	0.4	0.86	-	-
	0.6 m	DF _{mean}	S,SE,SW	0.4	0.4	0.54	0.54	0.86
			E,NW,W	0.4	0.54	0.86	-	-
			NE	0.4	0.54	0.86	0.86	-
		DF _{min}	S	0.4	0.54	-	-	-
			SE,SW	0.4	0.86	-	-	-
			E,NE,NW,W	0.54	-	-	-	-
		sDA	S,SE	0.4	0.86	-	-	-
			E	0.86	-	-	-	-
			NE,NW,W	-	-	-	-	-
0.9 m	DF _{mean}	SW	0.54	0.86	-	-	-	
		S,SE,SW	0.4	0.54	0.86	0.86	-	
		E,NE,NW,W	0.54	0.86	-	-	-	
	DF _{min}	S,SE,SW	0.54	0.86	-	-	-	
		E,NE,NW,W	0.86	-	-	-	-	
		S,SE	0.54	0.86	-	-	-	
	sDA	E,NE,NW,W	-	-	-	-	-	
		SW	0.54	-	-	-	-	

Table 8

Minimum WWR to fulfill the daylight requirements (for criteria DF_{mean}, DF_{min} and sDA) defined in Table 1 for room parameters (residential).

Residential room depth (m)			3.5	4.5	5.5	6.5	7.5	
Shading size (m)	0 m	DF _{mean}	S,SE,E,NE,N,NW,W,SW	0.27	0.27	0.27	0.4	0.4
		DF _{min}	S,SE,E,NE,N,NW,W,SW	0.4	0.4	0.86	-	-
		sDA	S,W,E,SE,NW,SW	0.27	0.4	0.4	0.86	-
	0.6 m	DF _{mean}	NE	0.4	0.4	0.54	-	-
			N	0.4	0.4	0.86	-	-
			S,SE,SW	0.27	0.4	0.4	0.4	0.54
		DF _{min}	E,NE,NW,W	0.4	0.4	0.4	0.54	0.86
			S	0.4	0.54	-	-	-
			SE,SW	0.4	0.86	-	-	-
		sDA	E,NE,NW,W	0.54	-	-	-	-
			S	0.4	0.4	0.86	-	-
			SE	0.4	0.4	0.64	-	-
0.9 m	DF _{mean}	E,W	0.4	0.54	0.86	-	-	
		NE,NW	0.4	0.86	-	-	-	
		SW	0.4	0.4	0.54	-	-	
	DF _{min}	S,SE,SW	0.4	0.4	0.4	0.54	0.86	
		E	0.4	0.54	0.64	0.86	-	
		NE,NW,W	0.4	0.4	0.64	0.86	-	
	sDA	S,SE,SW	0.54	0.86	-	-	-	
		E,NE,NW,W	0.86	-	-	-	-	
		S,SE,SW	0.4	0.54	0.86	-	-	
	E	0.54	0.86	-	-	-		
	NE,NW	0.54	-	-	-	-		
	W	0.4	0.86	-	-	-		

- With a shading size of 0.9 m, the maximum recommended room depth depends also on the orientation: 3.5 m for NE, NW (minWWR = 0.54); 4.5 m for E and W (minWWR = 0.86), and 5.5 m for S, SE and SW (minWWR = 0.86).

When DF_{mean} criterion is considered, the maximum room depth is 7.5 m when no shading is used. However, the maximum depth is 5.5 m for rooms without shading when DF_{min} is considered. For DF_{min} criterion, the maximum recommended depths are 3.5 m (E, NE, NW, W), 4.5 m (S, SE, SW) when the shading size is 0.6 m (minWWR between 0.40 and 0.86), and 0.9 m (W, E, NE, NW orientations with minWWR = 0.64). Finally, the maximum room depth does not significantly change when DF_{mean} criterion is considered: 7.5 m for shading size ≤ 0.6 m (minWWR between 0.40 and 0.86) and 6.5 m for E,NE,NW,W-oriented living rooms with shading size of 0.9 m (minWWR = 0.86).

3.2. Overheating in residential rooms

The percentage of the residential rooms with and without window airing that fulfill the overheating requirement is shown in Fig. 5. The first ventilation case (MV) is based on infiltration and mechanical ventilation. The second ventilation case (NV) is based on infiltration, mechanical ventilation, and window airing. Logically, all the rooms that fulfill the DH requirement when mechanical ventilation is used are not overheated when window airing is added. On average, 40.7% of the S, E, W, SE, SW-oriented rooms are overheated using any ventilation type. However, less than 10% of the N, NE and NW-oriented rooms are unconditionally overheated. The average percentage of rooms that fulfill the DH requirement for any ventilation case depends strongly on the orientation: 46% for N, NE, NW; 20% for S, E, and 11% for W, SE, SW. Finally, 47% of the rooms achieve a DH lower than 150 °Ch when window airing is included.

The critical WWR*g-value (defined by Simson et al. [66] as a relevant design parameter when overheating is considered for mechanically ventilated rooms) is shown for different orientations and shading sizes in Fig. 6. For N, NE, and NW orientations, maximum WWR*g-value is between 0.05 (without shading) and 0.15 (NE). Since no shading was considered for N-oriented rooms, maximum WWR*g-value was set manually as a conservative estimate to the same limit as in the case without shading (0.08). Maximum WWR*g-value is 0.05 for the other orientations (for shading sizes of 0.6–0.9 m). The most restrictive orientations for mechanically ventilated rooms are W, SE, and SW. No W-oriented-room fulfills the DH requirements when only infiltration and mechanical ventilation are considered. Nevertheless, if a shading size of

0.9 m is used in SE and SW-oriented rooms, maximum WWR*g-value is 0.05.

The critical WWR*g-value for mechanically and naturally ventilated rooms is shown for different orientations and shading sizes in Fig. 7. For N, NE, and NW orientations, maximum WWR*g-value is from 0.10 (without shading) to 0.32; whereas it is between 0.05 and 0.21 for the other orientations. The most restrictive orientations for mechanically and naturally ventilated rooms are W, SE, and SW whose maximum WWR*g-values are between 0.05 and 0.16. Apart from E and S orientations, the use of shading has the highest impact on SW and SE orientations when natural ventilation is added: maximum WWR-g-value ranges from 0.05 without shading to 0.15 with a shading size of 0.9 m.

3.3. Daylighting and overheating in residential rooms

Following the individual analysis of the daylight provision and overheating, the combined fulfillment of both functions is analyzed depending on the ventilation system, room parameters, and daylight assessment criteria. As shown in Fig. 8, the average percentage (per orientation) of rooms that fulfill both requirements when window airing is added is 30% for DF_{mean} and 5% for DF_{min} . When sDA criterion is considered, the improvement in terms of percentage of rooms is one third (approximately 10% of all the rooms).

The window airing and sDA criterion allow the increment of 34% of the rooms that have insufficient daylight levels without overheating. If we consider DF_{mean} or DF_{min} , this increment is 16% or 41%, respectively. These differences can be explained by the strict requirements associated with sDA and DF_{min} . If sDA criterion is considered, the percentage of the rooms that have sufficient daylight without overheating increases by 10% in absolute value, whereas this increment is 27% and 5% for DF_{mean} and DF_{min} , respectively. The effect of window airing on the combined fulfillment for different room orientations is shown in Fig. 9. Thus, the relative impact of the orientations is similar for sDA and DF_{mean} criteria but the number of rooms that achieve the combined fulfillment is lower for any orientation when sDA is considered. The increment is higher for N, NE, NW (between 36% and 48%) than the other orientations when DF_{mean} is considered. The most restrictive orientations for the combined fulfillment are W, SE, and SW with a maximum increment of 14% for SE considering DF_{mean} . If sDA criterion is considered, the mean increment of the rooms that achieve the combined fulfillment is between 13% and 31% for NW, NE, N; however, this increment varies from 2% to 6% for the other orientations. Considering DF_{min} , the increment is 25%, 9%, and 5% for N, NE, NW orientations,

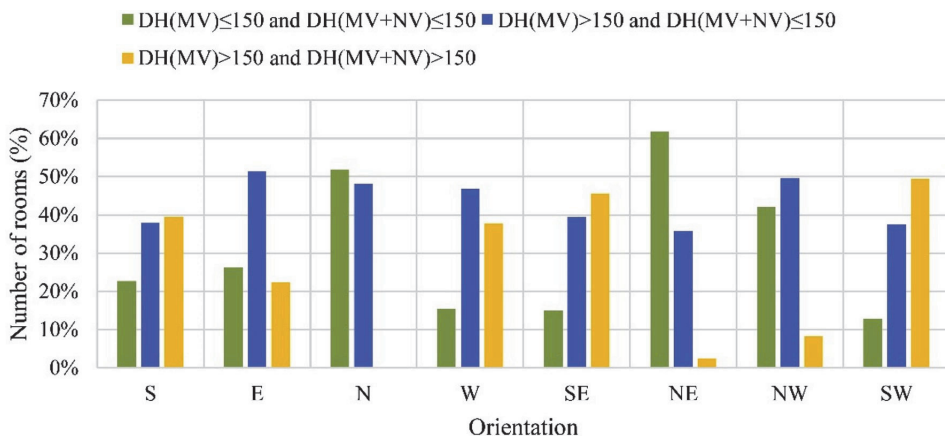


Fig. 5. Percentage of the residential rooms per orientation related to all the overheating fulfillment cases for different ventilation strategies: MV = Infiltration and mechanical ventilation, NV=Window airing technique.

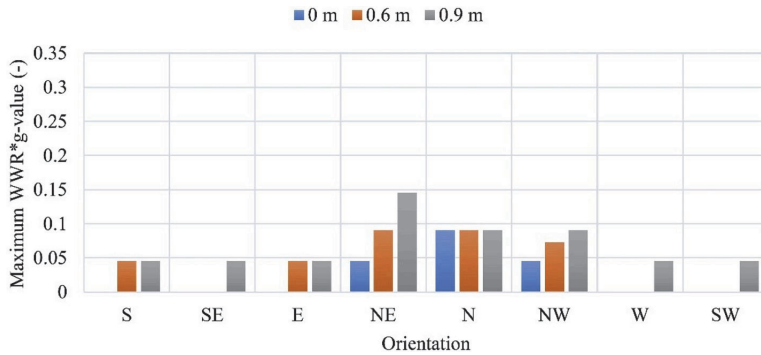


Fig. 6. Maximum WWR*g-value to avoid overheating according to the Estonian regulations for different orientations and shading sizes considering infiltration and mechanical ventilation.

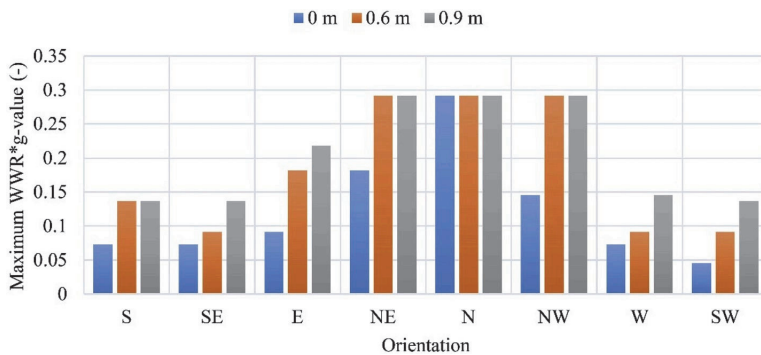


Fig. 7. Maximum WWR*g-value to avoid overheating according to the Estonian regulations for different orientations and shading sizes considering infiltration, mechanical ventilation, and window airing.

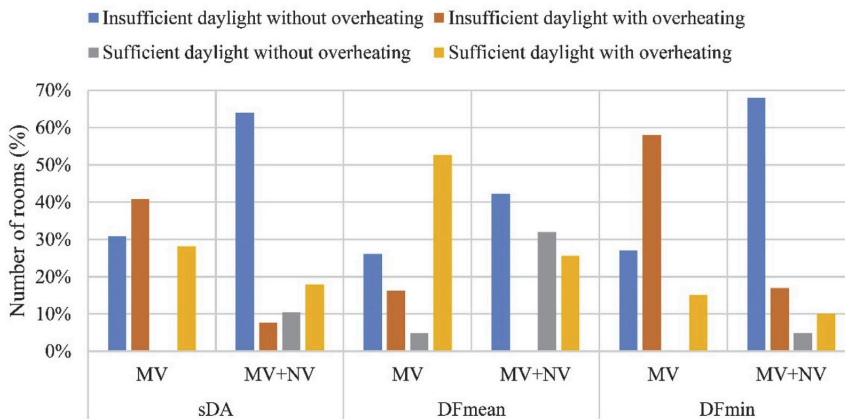


Fig. 8. Percentage of the residential rooms that fulfill both daylight and overheating requirements for different ventilation strategies: MV = Infiltration and mechanical ventilation, NV=Window airing technique.

respectively.

The level of combined fulfillment depending on the room dimension, orientation, and shading size is shown in Fig. 10. On the one hand, N orientations allow a higher flexibility for the design of residential rooms. On the other hand, most of the S, SE, W, and SW-oriented rooms cannot

meet both requirements when no shading is used. Most room combinations can fulfill the DF_{mean} criterion. Nevertheless, for high (6.5 m) or low (3.5–4.5) room depths and no shading, the combined fulfillment is compromised because of poor daylight or high overheating levels, respectively. The increment of the shading size allows the combined

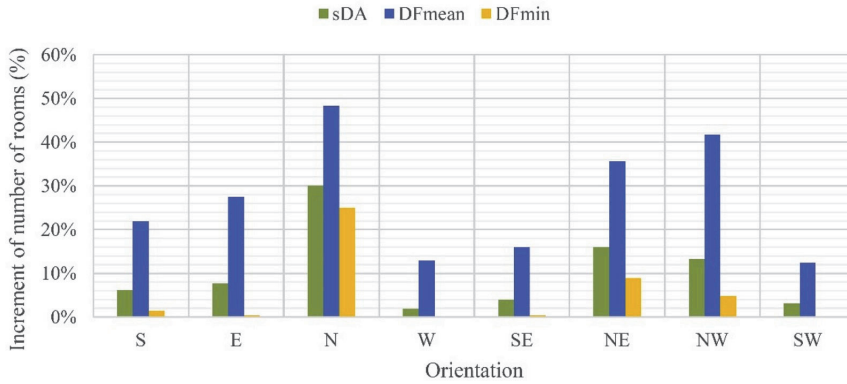


Fig. 9. Increment of the number of residential rooms with different orientations that fulfill daylight and overheating requirements when window airing is included.

w	d	Shading size (m)																							
		0								0.6								0.9							
		S	SE	E	NE	N	NW	W	SW	S	SE	E	NE	N	NW	W	SW	S	SE	E	NE	N	NW	W	SW
3.5	3.5	0	0	2	3	3	3	0	0	3	3	3	3	-	3	2	1	3	3	2	3	-	3	2	2
	4.5	1	1	1	3	3	3	1	0	3	2	2	2	-	2	2	2	2	2	2	1	-	1	1	2
	5.5	1	1	1	3	3	2	1	1	1	1	1	1	-	1	1	1	1	1	1	1	-	1	1	1
	6.5	0	0	1	1	1	1	0	0	1	1	1	1	-	1	1	1	1	1	1	1	-	1	1	1
	7.5	1	1	1	1	1	1	1	0	1	1	1	1	-	1	0	1	0	0	0	0	-	0	0	0
4.5	3.5	1	1	2	3	3	3	1	1	3	1	3	3	-	3	2	1	3	2	2	2	-	3	2	2
	4.5	1	0	1	3	3	3	0	0	2	2	2	2	-	3	1	1	2	2	2	1	-	2	1	2
	5.5	1	1	1	3	3	3	1	1	2	1	1	1	-	1	1	1	1	1	1	1	-	1	0	1
	6.5	1	1	1	2	1	1	1	1	1	1	1	1	-	1	1	1	1	1	1	1	-	1	0	1
	7.5	0	0	1	1	1	1	0	0	1	1	1	1	-	1	0	1	1	1	0	0	-	0	0	1
5.5	3.5	1	1	2	3	3	3	1	0	2	2	2	3	-	3	1	2	3	2	2	3	-	3	2	2
	4.5	0	0	1	3	3	3	0	0	2	1	2	3	-	3	1	1	2	2	2	2	-	2	2	2
	5.5	1	0	1	3	3	2	1	0	2	1	1	2	-	2	1	1	2	2	1	1	-	1	1	2
	6.5	1	1	1	3	3	2	1	1	1	1	1	1	-	1	1	1	1	1	1	1	-	1	0	1
	7.5	1	1	1	1	1	1	1	1	1	1	1	1	-	1	1	1	1	1	1	1	-	1	0	1
6.5	3.5	1	0	1	3	3	2	1	0	1	2	2	3	-	3	1	2	3	2	2	3	-	3	2	2
	4.5	0	0	1	3	3	2	0	0	2	1	2	3	-	3	1	1	2	2	2	2	-	2	1	2
	5.5	0	0	1	3	3	2	0	0	1	1	1	2	-	2	1	0	2	2	1	1	-	1	1	1
	6.5	1	1	1	1	2	2	1	0	1	1	1	1	-	1	0	1	1	1	1	1	-	1	0	1
	7.5	1	1	1	2	1	1	1	1	1	1	1	1	-	1	1	1	1	1	1	1	-	1	0	1

Fig. 10. Level of the combined fulfillment depending on the daylight criteria considered (3 = always, 0 = never, 1 = DF_{mean} is fulfilled, 2 = pair of criteria are fulfilled and white cells with “-” = not simulated) for different room (MV + NV) configurations where: w = room width (m) and d = room depth (m).

fulfillment of rooms with depths ≤5.5 m and different orientations such as S, SE, E, W, SW.

4. Discussion

Daylight assessment criterion based on the Estonian standard EVS 894:2008/A2:2015 (DF_{mean}) was compared with the European standard EN 17037:2018 (DF_{min}) and IES LM-83-12 (sDA) for 3520 residential/office rooms. Approximately 30% of the simulated residential and office rooms fulfill DF_{mean} but not the sDA criterion. The criterion based on sDA is more conservative than the Estonian DF-based criterion for educational buildings [50]. Moreover, the agreement between the fulfillment of DF_{min} and DF_{mean} criteria is 58% of the total room

combinations. For residential and office rooms, DF_{min} is more conservative than DF_{mean} due to the stricter requirements based on a target DF of 2.2% for the first half of the reference plane compared to the requirement defined by DF_{mean} (1.5% and 2.0% for residential and office rooms, respectively). DF_{min} and sDA can be considered equivalent criteria to assess the daylight provision for the most combinations while DF_{mean} criterion can be used for a less conservative room design. The results showed that a suitable combination of shading size and room depth depending on the room orientation considering climate-based daylight assessment criteria is key during the early stages of building design. The use of sDA instead of DF_{mean} can decrease the maximum room depth from 2 m (S) to 1 m (N, NW) when no fixed shading is used in office rooms. For residential rooms without shading, the decrease in

the maximum room depth is less than for office rooms: 2 m for NE, N-oriented rooms and 3 m for the other orientations. The increment of the shading size allows the design of rooms with higher WWR but lower depth, and vice versa, to ensure the fulfillment of the daylight requirements. In general, considering the same room dimension, orientation, and shading size, higher WWRs can be chosen for residential than for office rooms due to the stricter daylight requirements for any daylight criteria. These results are valid for glazing systems whose visual transmittance is approximately 63%. In addition, the presented rules of thumb are based on the room level, which can be used for each window-side room of multi-apartment buildings located in new urban areas in Estonia. Nevertheless, further daylight assessment should be conducted considering high-density urban areas.

The limiting function of the daylight provision in residential rooms is the overheating risk that depends strongly on the level of direct solar exposure through the windows during the warm season [66]. The results of this study showed that the effect of ventilation on the overheating fulfillment depends strongly on the room orientation. Thus, in at least 25% (and up to 51%) of S, E, W, SE, SW-oriented room combinations, fulfillment of the overheating requirement does not depend on the ventilation system. Thus, only a maximum of 10% of N, NE, NW-oriented room combinations are overheated even when window airing is added to the mechanical ventilation system. Nevertheless, at least 39% of the combination rooms become “not overheated” when window airing is added to the mechanical ventilation system. These results might be conservative for retrofit decisions because a simplified model [65] was used to characterize the optical and thermal performance of the windows, which are more suitable for early stages of the building design. In general, the use of fixed shading increases the glazed areas without increasing the risk of overheating in residential rooms. There are other actions on WWR and g-value [44] that can improve the protection against overheating depending on the orientation of the room and ventilation strategy used [48]. On the one hand, when only infiltration and mechanical ventilation are considered, maximum WWR*g-value is higher than 0.05 for NE, N, NW-oriented rooms when shading size is between 0.6 m and 0.9 m. S, SE, E, SW, and W are the most limited orientations with a maximum WWR*g-value of 0.05 (0 for W orientation). On the other hand, when window airing is added, the maximum WWR*g-value is between 0.10 and 0.32 for NE, N, and NW orientations for any shading size. For other orientations (S, SE, E, W, SW), maximum WWR*g-value is at least 0.05 without shading and up to 0.2 when shading size is 0.9 m. According to these results, we recommend the use of windows with lower g-values for the most problematic facade orientations; i.e., S, SE, E, W, and SW as a previous study on nZEB Danish single-family houses suggested [47]. The presented results can vary depending on the set point considered for the window airing strategy and openable area ratio. In this study, a set point of 25 °C (previous research used 27 °C [65]) was used for the window airing control with a 10% of openable area. A new methodology based on the multi-zone approach using different set points for window airing would help to understand how the overheating levels in residential rooms change.

When window airing is added, most of the NE, N, NW-oriented residential rooms with room depths lower than 5.5 m are considered good room designs because they fulfill both daylighting and overheating requirements for any daylight criteria considered. Nevertheless, as discovered in a previous research, in deep S-oriented rooms, either summer indoor comfort or daylight provision is compromised with the use of shading [47]. Moreover, the combined fulfillment in most of the SE, W, and SW-oriented rooms with depths ≥ 6.5 m and fixed shading depends on the daylight criteria (DF_{mean} , DF_{min} and sDA). The use of fixed shading allows the combined fulfillment in S-oriented rooms but decreases the maximum depth for N orientations. This result highlights the importance of a careful envelope design to achieve combined fulfillment for any daylight assessment criterion. The use of switchable shading devices combined with window airing strategies can improve

the flexibility of the building design in early stages. However, the investment amount may be higher than when traditional fixed shading is used.

5. Conclusions

This study evaluates the reliability of daylight assessment based on the Estonian standard EVS 891:2008/A2 2015 and the new European standard EN 17037:2018 through a more reliable dynamic daylight assessment method, IES LM-83-12, in residential and office buildings, and their relation with other building regulations such as the Estonian Minimum Requirements for Energy Performance n°68 of 2014. We investigated the relationship between the two daylight standards, which are both in use because Estonia is in the European Union, to predict the impact of the new standard on building regulations. The main outcomes of the research and potential applications of the results are as follows:

1. The Estonian daylight standard has limited reliability in properly predicting the daylight potentials of building interiors. In many cases, it overestimates daylight availability for different orientations. The present study will be presented to local authorities and regulatory bodies to increase their awareness about the need to promote a new and more efficient daylight regulation in Estonia. This will be done considering the new European standard also analyzed in this study. Hence, this research will contribute to the development of a compulsory building daylight regulation.

2. There is a strong disagreement between the two standards in assessing the daylight for residential and office buildings. This aspect will be considered in the development of the guidelines for the new daylight regulation.

3. Evidence strengthens the findings of the existing literature about the conflicting requirements of overheating in building regulations and the Estonian daylight standard. Considering the new European standard, the requirements will not change significantly. However, if the daylight regulation incorporates the results of the dynamic daylight analysis, the conflicts will increase because larger glazed areas will be necessary to fulfill the daylight requirement. Nevertheless, several cases that fulfill both requirements will increase when passive measures such as window airing are adopted. This suggests the a) synergistic formulation of daylighting and overheating requirements in new building regulations to make it easier for designers to fulfill both; b) promoting the use of building design features such as efficient materials and passive measures to reduce overheating while ensuring appropriate daylight levels.

This study focused only on a specific cost-optimal (within the Estonian context) triple glazed system ($T_{vis} = 0.63$, g-value = 0.37) and on fixed shading. In addition, the control algorithm for the window airing system was based on a basic set point (25 °C) between the heating set point (21 °C) and the overheating limit (27 °C) (defined in the Estonian regulation), with the window airing position of 10%. The rules of thumb used in this study might have lacked some special cases in terms of combined fulfillment that deserve further study from an architectural point of view. Furthermore, different assumptions in terms of window airing control and complex fenestration systems (glazing and shading system) have different impacts on daylight provision and risk of overheating. Therefore, future research should conduct sensitivity analyses for different window airing controls, glazing systems, and switchable shading devices. Another future path could be the development of prediction models to estimate the daylight provision and risk of overheating in Estonian buildings. Finally, this study can help architects, designers, and engineers understand the good practices not only in early stages of the design of the buildings but also in the retrofitting stage to achieve satisfactory levels of indoor comfort in buildings.

Declaration of competing interest

The authors declare that they have no known competing financial interests or personal relationships that could have appeared to influence the work reported in this paper.

Acknowledgements

This research was supported by the Estonian Centre of Excellence in Zero Energy and Resource Efficient Smart Buildings and Districts, ZEBE (grant No. 2014-2020.4.01.15-0016) and the programme Mobilitas Pluss (Grant No – 2014-2020.4.01.16-0024, MOBTP88) funded by the European Regional Development Fund (grant No. PSG409), and by the European Commission through the H2020 project Finest Twins (grant No. 856602).

Appendix A. Supplementary data

Supplementary data to this article can be found online at <https://doi.org/10.1016/j.buildenv.2020.107036>.

References

- [1] European Commission, Directive 2010/31/EU of the European Parliament and of the Council of 19 May 2010 on the Energy Performance of Buildings (Recast), 2010, https://doi.org/10.1007/978-1-137-54482-7_33.
- [2] K. Won Hee, G. Brager, S. Schiavon, S. Selkowitz, *Building Envelope Impact on Human Performance and Well-Being: Experimental Study on View Clarity*, Escholash. UC Open Access Publ., 2017.
- [3] European Commission, BS EN 17037:2018: Daylight in Buildings, 2018. <https://www.en-standard.eu/bs-en-17037-2018-daylight-in-buildings/>.
- [4] M. Ayoub, 100 Years of daylighting: a chronological review of daylight prediction and calculation methods, *Sol. Energy* (2019), <https://doi.org/10.1016/j.solener.2019.10.072>.
- [5] S.W. Lockley, Circadian rhythms: influence of light in humans. *Encycl. Neurosci.*, 2009, <https://doi.org/10.1016/B978-0-08045046-9.01619-3>.
- [6] J.F. Duffy, C.A. Czeisler, Effect of light on human circadian physiology, *Sleep Med. Clin.* (2009), <https://doi.org/10.1016/j.jsmc.2009.01.004>.
- [7] M. Knoop, O. Stefani, B. Bueno, B. Matusiak, R. Hobbday, A. Wirz-Justice, K. Martiny, T. Kantermann, M.P.J. Aarts, N. Zemmouri, S. Appelt, B. Norton, Daylight: what makes the difference? *Light. Res. Technol.* (2019) <https://doi.org/10.1177/1477153519869758>.
- [8] B.S. Bsi, *Lighting for Buildings*, 8206-2, Code of practice for daylighting, 2008.
- [9] C.F. Reinhart, J. Mardaljevic, Z. Rogers, Dynamic daylight performance metrics for sustainable building design, *LEUKOS - J. Illum. Eng. Soc. North Am.* (2006), <https://doi.org/10.1582/LEUKOS.2006.03.01.001>.
- [10] Y. Bian, Y. Ma, Analysis of Daylight Metrics of Side-Lit Room in Canton, South China: A Comparison between Daylight Autonomy and Daylight Factor, *Energy Build.* 2017, <https://doi.org/10.1016/j.buildenv.2016.12.059>.
- [11] A. Nabil, J. Mardaljevic, Useful Daylight Illuminances: A Replacement for Daylight Factors, *Energy Build.* 2006, <https://doi.org/10.1016/j.buildenv.2006.03.013>.
- [12] Illuminating Engineering Society, the Daylight Metric Committee, LM-83-12 Approved Metric: IES Spatial Daylight Autonomy (sDA) and Annual Sunlight Exposure (ASE), 2013.
- [13] I. Turan, A. Chegut, D. Fink, C. Reinhart, The value of daylight in office spaces, *Build. Environ.* (2020), <https://doi.org/10.1016/j.buildenv.2019.106503>.
- [14] N. Sokol, J. Martyniuk-Peczec, The review of the selected challenges for an incorporation of daylight assessment methods into urban planning in Poland, *Procedia Eng.*, 2016, <https://doi.org/10.1016/j.proeng.2016.08.814>.
- [15] G.J. Ward, The RADIANCE lighting simulation and rendering system, *Proc. 21st Annu. Conf. Comput. Graph. Interact. Tech. SIGGRAPH* (1994), <https://doi.org/10.1145/192161.192286>, 1994.
- [16] L.L.C. Solemma, DIVA, accessed, www.solemma.net, 2016. (Accessed 15 March 2019).
- [17] B. Bueno, J. Wienold, A. Katsifarakis, T.E. Kuhn, Fener: A Radiance-Based Modelling Approach to Assess the Thermal and Daylighting Performance of Complex Fenestration Systems in Office Spaces, *Energy Build.* 2015, <https://doi.org/10.1016/j.buildenv.2015.02.038>.
- [18] B. Bueno, J.M. Cejudo Lopez, A. Katsifarakis, H.R. Wilson, A systematic workflow for retrofitting office façades with large window-to-wall ratios based on automatic control and building simulations, *Build. Environ.* (2018), <https://doi.org/10.1016/j.buildenv.2018.01.031>.
- [19] B. Bueno, F. Ozceylan, A workflow for retrofitting faade systems for daylight, comfortable and energy efficient buildings, *IOP Conf. Ser. Earth Environ. Sci.* (2019), <https://doi.org/10.1088/1755-1315/225/1/012034>.
- [20] J. Wienold, J. Christoffersen, Evaluation Methods and Development of a New Glare Prediction Model for Daylight Environments with the Use of CCD Cameras, *Energy Build.* 2006, <https://doi.org/10.1016/j.buildenv.2006.03.017>.
- [21] M. Liu, P.K. Heiselberg, Y.I. Antonov, F.S. Mikkelsen, Parametric Analysis on the Heat Transfer, Daylight and Thermal Comfort for a Sustainable Roof Window with Triple Glazing and External Shutter, *Energy Build.* 2019, <https://doi.org/10.1016/j.buildenv.2018.11.001>.
- [22] K.H. Cheong, Y.H. Teo, J.M. Koh, U.R. Acharya, S.C. Man Yu, A simulation-aided approach in improving thermal-visual comfort and power efficiency in buildings, *J. Build. Eng.* (2020), <https://doi.org/10.1016/j.jobe.2019.100936>.
- [23] F. De Luca, H. Voll, M. Thalfeldt, Horizontal or vertical? Windows' layout selection for shading devices optimization, *Manag. Environ. Qual. Int. J.* (2016), <https://doi.org/10.1108/MEQ-05-2015-0102>.
- [24] J.A. Sargent, J. Niemasz, C.F. Reinhart, SHADERADE: combining rhinoceros and energyplus for the design of static exterior shading devices, in: *Proc. Build. Simul. 2011 12th Conf. Int. Build. Perform. Simul. Assoc.*, 2011.
- [25] D.A. Chi, D. Moreno, J. Navarro, Design optimisation of perforated solar façades in order to balance daylighting with thermal performance, *Build. Environ.* (2017), <https://doi.org/10.1016/j.buildenv.2017.09.007>.
- [26] M. Alva, A. Vlachokostas, N. Madamopoulos, Experimental demonstration and performance evaluation of a complex fenestration system for daylighting and thermal harvesting, *Sol. Energy* (2020), <https://doi.org/10.1016/j.solener.2020.01.012>.
- [27] T.E. Kuhn, C. Bühler, W.J. Platzer, Evaluation of overheating protection with sun-shading systems, *Sol. Energy* (2001), [https://doi.org/10.1016/S0038-092X\(01\)00017-2](https://doi.org/10.1016/S0038-092X(01)00017-2).
- [28] V. Ponnmalar, B. Ramesh, Energy efficient building design and estimation of energy savings from daylighting in Chennai, *Energy Eng. J. Assoc. Energy Eng.* (2014), <https://doi.org/10.1080/01998595.2014.10846858>.
- [29] S. Grynning, B. Time, B. Matusiak, Solar shading control strategies in cold climates - heating, cooling demand and daylight availability in office spaces, *Sol. Energy* (2014), <https://doi.org/10.1016/j.solener.2014.06.007>.
- [30] E.J. Gago, T. Muneer, M. Knez, H. Köster, Natural light controls and guides in buildings. Energy saving for electrical lighting, reduction of cooling load, *Renew. Sustain. Energy Rev.* (2015), <https://doi.org/10.1016/j.rser.2014.08.002>.
- [31] M. Haase, S. Grynning, Optimized facade design - energy efficiency, comfort and daylight in early design phase. *Energy Procedia*, 2017, <https://doi.org/10.1016/j.egypro.2017.09.666>.
- [32] S.H. Kim, K.J. Shin, H.J. Kim, Y.H. Cho, A study on the effectiveness of the horizontal shading device installation for passive control of buildings in South Korea, *Int. J. Polym. Sci.* (2017), <https://doi.org/10.1155/2017/3025092>.
- [33] X. Yu, Y. Su, Daylight availability assessment and its potential energy saving estimation - A literature review, *Renew. Sustain. Energy Rev.* (2015), <https://doi.org/10.1016/j.rser.2015.07.142>.
- [34] K.M. Al-Obaidi, M.A. Ismail, M.A.C. Munaaim, A.M. Abdul Rahman, Designing an integrated daylighting system for deep-plan spaces in Malaysian low-rise buildings, *Sol. Energy* (2017), <https://doi.org/10.1016/j.solener.2017.04.001>.
- [35] W. O'Brien, K. Kapsis, A.K. Athienitis, Manually-operated window shade patterns in office buildings: a critical review, *Build. Environ.* (2013), <https://doi.org/10.1016/j.buildenv.2012.10.003>.
- [36] A. Beizaee, K.J. Lomas, S.K. Firth, National survey of summertime temperatures and overheating risk in English homes, *Build. Environ.* (2013), <https://doi.org/10.1016/j.buildenv.2013.03.011>.
- [37] K.J. Lomas, S.M. Porritt, Overheating in buildings: lessons from research, *Build. Res. Inf.* (2017), <https://doi.org/10.1080/09613218.2017.1256136>.
- [38] C. Heracleous, A. Michael, Assessment of Overheating Risk and the Impact of Natural Ventilation in Educational Buildings of Southern Europe under Current and Future Climatic Conditions, *Energy* (2018), <https://doi.org/10.1016/j.energy.2018.10.051>.
- [39] G. Ulpiani, M. Benedettelli, C. di Perna, B. Naticchia, Overheating phenomena induced by fully-glazed facades: investigation of a sick building in Italy and assessment of the benefits achieved via model predictive control of the AC system, *Sol. Energy* (2017), <https://doi.org/10.1016/j.solener.2017.09.009>.
- [40] M. Thalfeldt, E. Pikas, J. Kurnitski, H. Voll, Facade Design Principles for Nearly Zero Energy Buildings in a Cold Climate, *Energy Build.*, 2013, <https://doi.org/10.1016/j.buildenv.2013.08.027>.
- [41] Estonian Government, Minimum requirements for energy performance, Annex 68 (2014). RT I, 24.01.3, (2012), <https://www.riigiteataja.ee/en/eli/520102014001>.
- [42] Estonian Government, N. 58 Ordinance, Methodology for calculating the energy performance of buildings, RT (2015) 21, 09.06.2015.
- [43] M. Maivel, J. Kurnitski, T. Kalmese, Field survey of overheating problems in Estonian apartment buildings, *Architect. Sci. Rev.* (2015), <https://doi.org/10.1080/00038628.2014.970610>.
- [44] H. Voll, M. Thalfeldt, F. De Luca, J. Kurnitski, T. Olesk, Urban planning principles of nearly zero-energy residential buildings in Estonia, *Manag. Environ. Qual. Int. J.* (2016), <https://doi.org/10.1108/MEQ-05-2015-0101>.
- [45] R. Simson, Overheating Prevention and Daylight in Buildings without Mechanical Cooling, Tallinn University of Technology, 2019, <https://doi.org/10.23658/taitech.54/2019>.
- [46] A. Hamburg, T. Kalmese, How well are energy performance objectives being achieved in renovated apartment buildings in Estonia? *Energy Build.* 2019 <https://doi.org/10.1016/j.buildenv.2019.07.006>.
- [47] L. Vanhoutteghem, G.C.J. Skarning, C.A. Hviid, S. Svendsen, Impact of Façade Window Design on Energy, Daylighting and Thermal Comfort in Nearly Zero-Energy Houses, *Energy Build.* 2015, <https://doi.org/10.1016/j.buildenv.2015.05.018>.
- [48] F. De Luca, T. Dogan, J. Kurnitski, Methodology for determining fenestration ranges for daylight and energy efficiency in Estonia, *Simul. Ser.*, 2018, <https://doi.org/10.22360/simaud.2018.simaud.007>.

- [49] Estonian Centre for Standardization, EVS 894:2008+A2:2015: Daylight in Dwellings and Offices, 2015. <https://www.evs.ee/en/evs-894-2008+a2-2015>.
- [50] F. De Luca, M. Kiil, R. Simson, J. Kurnitski, R. Murula, Evaluating daylight factor standard through climate based daylight simulations and overheating regulations in Estonia. *Proc. Build. Simul. 2019 16th Conf. Int. Build. Perform. Simul. Assoc.*, 2019.
- [51] TUT nZEB Research Group, LIGINULLENERGIA ELUHOONED RIDA- JA KORTERELAMUD, Tallinn, Estonia, 2017. https://kredex.ee/sites/default/files/2019-03/Liginullenergia_eluhooned_Rida_ja_korterelamu_juhend.pdf.
- [52] M. Dekay, G.Z. Brown, Sun, WIND & LIGHT: Architectural Design Strategies, 2001.
- [53] K. Haglund, Window selection methodologies and optimization in high performance commercial buildings, BEST2 Conf. Portl. (2010).
- [54] K. Lagios, J. Niemasz, C. Reinhart F, Animated building performance simulation (abps) – linking rhinoceros/grasshopper with radiance/daysim, *Conf. Proc. SimBuild 2010* (2010).
- [55] J.A. Jakubiec, C.F. Reinhart, Diva 2.0: integrating daylight and thermal simulations using rhinoceros 3D, DAYSIM and EnergyPlus. *Proc. Build. Simul. 2011 12th Conf. Int. Build. Perform. Simul. Assoc.*, 2011.
- [56] C.F. Reinhart, S. Herkel, The Simulation of Annual Daylight Illuminance Distributions-A State-Of-The-Art Comparison of Six RADIANCE-Based Methods, *Energy Build.*, 2000, [https://doi.org/10.1016/S0378-7788\(00\)00042-6](https://doi.org/10.1016/S0378-7788(00)00042-6).
- [57] C. Reinhart, B. Pierre-Felix, Experimental Validation of Autodesk® 3ds Max® Design 2009 and Daysim 3.0, LEUKOS - J. Illum. Eng. Soc. North Am., 2009, <https://doi.org/10.1582/LEUKOS.2009.06.01001>.
- [58] T. Dogan, Y.C. Park, A critical review of daylighting metrics for residential architecture and a new metric for cold and temperate climates, *Light. Res. Technol.* (2019), <https://doi.org/10.1177/1477153518755561>.
- [59] C.F. Reinhart, *Daylighting handbook II. Daylight simulations*. Dynamic Facades, Building Technology Press, Cambridge, MA, 2018.
- [60] CalumenLive, SGG CLIMATOP 6 (18 ARGON 90) 4 (18 ARGON 90) 4 COOL-LITE SKN 174 F2 PLANITHERM XN F5 (n.d.), (accessed June 14, 2019), <https://calumenlive.com/find-glazing>.
- [61] E. Pikas, M. Thalfeldt, J. Kurnitski, R. Liias, Extra Cost Analyses of Two Apartment Buildings for Achieving Nearly Zero and Low Energy Buildings, *Energy* (2015), <https://doi.org/10.1016/j.energy.2015.03.026>.
- [62] M. Thalfeldt, E. Pikas, J. Kurnitski, H. Voll, Window model and 5 year price data sensitivity to cost-effective façade solutions for office buildings in Estonia, *Energy* (2017), <https://doi.org/10.1016/j.energy.2017.06.160>.
- [63] T. Dogan, *Archsim Energy Modelling Software*, 2014.
- [64] U.S. Department of Energy, EnergyPlus Testing with HVAC Equipment Performance Tests CE100 to CE200 from ANSI/ASHRAE Standard 140-2011, Washington, D.C., 2015. https://energyplus.net/sites/all/modules/custom/nrel_custom/eplus_files/current_testing_reports/ASHRAE140-HVAC-CE100200-8.3.0-b45b06b780.pdf.
- [65] M. Thalfeldt, J. Kurnitski, H. Voll, Detailed and Simplified Window Model and Opening Effects on Optimal Window Size and Heating Need, *Energy Build.*, 2016, <https://doi.org/10.1016/j.enbuild.2016.06.002>.
- [66] R. Simson, J. Kurnitski, K. Kuusk, Experimental validation of simulation and measurement-based overheating assessment approaches for residential buildings, *Architect. Sci. Rev.* (2017), <https://doi.org/10.1080/00038628.2017.1300130>.

Paper III

Sepúlveda, A., De Luca, F., & Kurnitski, J. (2022). Daylight and overheating prediction formulas for building design in a cold climate. *Journal of Building Engineering*, 45, 103532.



Contents lists available at ScienceDirect

Journal of Building Engineering

journal homepage: www.elsevier.com/locate/job

Daylight and overheating prediction formulas for building design in a cold climate

Abel Sepúlveda^{a,*}, Francesco De Luca^a, Jarek Kurnitski^{a,b}^a Department of Civil Engineering and Architecture, Tallinn University of Technology, Estonia^b Smart City Center of Excellence, Tallinn University of Technology, Estonia

ARTICLE INFO

Keywords:

Daylight
Overheating
EN 17037
Thermal comfort
Visual comfort
Degree-hour

ABSTRACT

Indoor comfort in buildings has a critical impact on occupants' health and cognitive performance. The fulfillment of daylight provision and overheating risk requirements can be challenging. This paper proposes a coupled method based on prediction formulas that can be used to assess daylight provision and overheating risk in buildings. In addition, this method can be used for the design of interior floor plan and window sizing in order to rooms fulfill simultaneously both performances. The considered daylight provision requirements are based on the minimum Daylight Factor (minDF) defined by the European standard EN 17037, and the overheating risk requirements are based on the degree-hour (DH) metric adopted by the Estonian regulation. The minimum window-to-wall ratio (minWWR) to fulfill minDF-based requirements and maximum *g*-value to fulfill at the same time DH-based requirements for any room design can be calculated or represented graphically. The prediction accuracy in terms of relative RMSE is up to 0.20 for minDF and DH values. By using this approach, designers can minimize the number of design iterations during early stages, as well as the required computational time required by daylight and energy simulations. Furthermore, the proposed coupled method based on minDF and DH prediction formulas has big potential to help architects and designers to achieve the combined fulfillment between daylight provision and overheating protection during early stages of the design process within the Estonian context. Finally, the authors recommend the proposed coupled method to regulation makers for future building standards and regulations.

Abel Sepúlveda: Conceptualization, Software, Writing – Original Draft, Writing - Review & editing, Visualization, Formal, Methodology, Analysis Francesco De Luca: Supervision, Writing - Review & editing, Project administration Jarek Kurnitski: Funding acquisition, Project administration.

1. Introduction

The 80% of the world population will live in urban areas by 2030 [1]. Even nowadays, the achievement of energy-efficient buildings and human comfort is a challenge for architects and urban planners. Indoor and outdoor comfort are the main components of human comfort. At the same time, indoor comfort in buildings consists of two main components: visual and thermal comfort. On one hand, visual comfort has a critical impact on building users' performance and well-being [2–4]. According to the European standard EN 17037 "Daylight in Buildings", the level of visual comfort depends on the level of direct sun exposure,

view out of building occupants, glare protection, and daylight provision in indoor spaces [5]. In fact, daylight is the most preferred source of light by building users [6], having even an added value within the real estate market [7]. On the other hand, thermal discomfort caused by the overheating phenomenon, produced by the excess of indoor temperature, can have negative effects on building users' satisfaction and health on the long-term [8–10].

1.1. Conflict between daylight and overheating performances in buildings

Future climate conditions affected by the global warming effect will aggravate overheating risk in buildings. According to previous studies, efficient strategies to reduce future overheating risk levels are based on proper thermally insulated constructions, natural ventilation, and active cooling strategies [11–13]. Moreover, the urban heat island effect combined with the global warming effect will aggravate overheating risk in buildings [14]. Specifically, residential buildings are prone to

* Corresponding author. Tallinn University of Technology, Ehitajate tee 5, Tallinn, 19086, Estonia.
E-mail address: absepu@taltech.ee (A. Sepúlveda).

<https://doi.org/10.1016/j.job.2021.103532>

Received 27 August 2021; Received in revised form 20 October 2021; Accepted 26 October 2021

Available online 30 October 2021

2352-7102/© 2021 Elsevier Ltd. All rights reserved.

have overheating risk problems due to the lack of cooling or efficient natural/mechanical ventilation strategies [15–18]. The assessment of overheating risk in residential buildings has been widely investigated in temperate climates [19–23]. A recent investigation showed that the fulfillment of CIBSE TM59 [24] overheating requirements is extremely difficult to satisfy in an energy-efficient flat located in London [25].

In practice, the building envelope design has a critical impact not only on energy performance but also on the achievement of suitable level of visual comfort [26–28]. A suitable use of complex fenestration systems (glazing combined with shading systems) could balance visual comfort and energy efficiency in different climates [29–31]. Moreover, excessive direct sun exposure can lead to high levels of daylight provision and solar gains, increasing the indoor temperature and consequently overheating risk. Previous studies propose rules of thumb to help architects and designers to choose optimal design strategies and renovation plans during the early design stages that achieve a combined fulfillment of daylight and overheating requirements [18,32–34].

1.2. Background

Architects and designers can assess building performances such as daylight provision, energy performance, and overheating risk by using several methods to evaluate different design/retrofit decisions such as room dimensions, window-to-wall ratio (WWR), building orientation, type of shading device, shading size, window construction, or ventilation strategy among others. Simulation-aided methodologies based on daylight and energy simulations are necessary to assess multiple building performances [35–38]. Thus, a vast number of investigations focused on the optimization of different building performances, used optimization Grasshopper plug-ins within the software Rhinoceros 3D [39–42]. Additionally, recent investigations included machine learning technique to speedup multi-objective optimization of architectural spaces [42–45].

Several methods to predict building performances such as prediction formulas, graphical tools, and rules-of-thumb have been proposed since two decades ago. Regarding daylight provision, Reinhart and Lo Verso proposed several formulas to estimate the average daylight factor (DF) in a generic side-lit room depending on design parameters such as obstruction angle, mean reflectance of the opaque surfaces, visual transmittance of the glazing, total area of interior surfaces, and net glazing area [46]. Lee et al. used complex regression models for the estimation of climate-based daylight metrics such as spatial daylight autonomy (sDA), useful daylight autonomy (UDI) among others illuminance-based metrics [47]. Moreover, Loch et al. proposed rules of thumb to achieve suitable visual comfort based on the climate-based metrics sDA and annual sunlight exposure (ASE) in side-lit office rooms with balconies located in São Paulo, Brazil [48]. Sepúlveda et al. used a parametric approach to create rules of thumb for the combined fulfillment of daylight provision according to different regulations and standards and overheating requirements defined by Estonian regulations [49].

Other researchers focused on the definition of formulas to estimate the annual use of artificial lighting in commercial and office side-lit rooms [50–52]. Moret et al. developed formulas to predict energy savings of lighting, cooling, and heating [53]. In addition, Lo Verso et al. defined a set of mathematical models, which can be calibrated with 48 annual daylight/energy simulations, for the estimation of daylight provision and energy demand for lighting [54]. Cammarano et al. proposed a graphical tool to be calibrated with 48 cases for each considered climate (each case consists in one annual daylight/energy simulation) for the assessment of daylight and energy demanding in office rooms with different architectural features [55,56]. Finally, two previous investigations developed rule of thumbs for the size of fixed shading to fulfill daylight and overheating performances in Estonia [49,57].

1.3. Originality and aims of this research

The application of simulation-based workflows requires high-level expertise of different software and/or Grasshopper plug-ins in Rhinoceros 3D. Secondly, the evaluation of different building performances is normally a high computational-expensive process, even for coupled daylight and energy simulations. On one hand, there is a lack of prediction methods, which are easy to use by not simulation or optimization experts, for the combined assessment of daylight provision and overheating risk. On the other hand, the European standard EN 17037 allows the flexibility to fulfill daylight provision requirements in terms of the static DF daylight metric, which does not depend on climate conditions, being faster to calculate than other dynamic daylight metrics such as daylight autonomy (DA), UDI, and sDA [58–60]. Finally, Brembilla et al. highlighted the importance of coupling daylighting and overheating assessments to evaluate different building design strategies that meet both indoor visual and thermal comfort requirements in dwellings defined by energy policies such as nearly zero energy buildings (NZEB) regulations [61]. To this date, there is no coupled design method based on easy-to-use prediction formulas that considers overheating and daylight performances.

This paper aims to propose easy-to-use prediction formulas that can be used by architects and designers during early stages of the design process to achieve good balance between daylight and overheating protection efficiently. The daylight requirements are based on the DF metric according to static method defined by the European standard EN 17037 [5] and overheating risk requirements are based on the degree-hour metric (DH) adopted by the Estonian regulation [62]. Thus, the objectives of this paper can be summarized as follows:

- To develop a formula for the prediction of daylight assessment based on the DF metric proposed by the European standard EN 17037;
- To develop a formula for the prediction of overheating risk assessment based on the DH metric used by the Estonian regulation;
- To apply a coupled method based on DF and DH prediction formulas to conduct a window sizing (optical/thermal properties included) that allow the combined fulfillment of minimum daylight and overheating requirements in a residential building located in Tallinn, Estonia (59.47°N, 24.75°E).

2. Methodology

The workflow followed in this research consisted of the following steps, presented also as flowchart in Fig. 1:

- Step 1: the creation of the parametric model for the generation of all room combinations in the software Grasshopper for Rhinoceros 3D (section 2.1);
- Step 2: the definition of the daylight model in the Grasshopper plug-in HoneyBee and the energy model in EnergyPlus;
- Step 3: the comparison between the target and minimum DF-based requirements defined by the European standard EN 17037 for all European countries;
- Step 4: the analysis of the correlation between minDF and DH and design parameters such as window's thermal/optical properties, room orientation, room dimensions, WWR, and obstruction angle;
- Step 5: the definition of minDF and DH prediction formulas using polynomial fitting technique;
- Step 6: the proposal and application of a coupled method based on prediction formulas that can be used for the design of interior building floor plan and window sizing to achieve the combined fulfillment of minimum daylight provision requirements defined by the EN 17037 and overheating protection requirements based on the DH-metric.

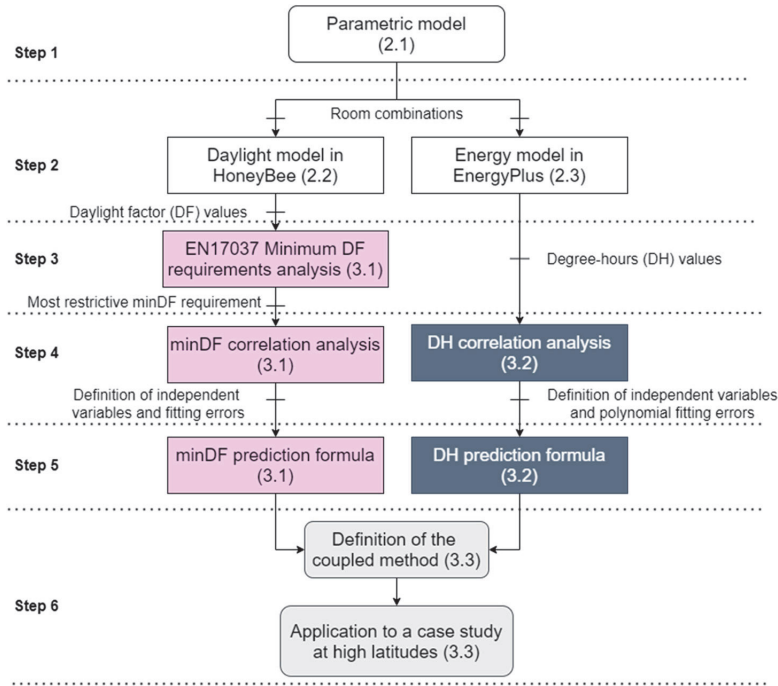


Fig. 1. Workflow followed in the research. The number in brackets refers to the section in which the step is presented and discussed.

2.1. Parametric model

A simulation-based methodology with a single-zone approach was used for the assessment of daylighting and overheating risk. A parametric model of a generic residential room was created in Grasshopper

plug-in for Rhinoceros software. The parametric model generated two geometrical models (one for daylight and another for thermal indoor climate simulations) using the same room parameters with different 3D model geometrical constructions as required by the daylight and thermal simulations (Fig. 2).

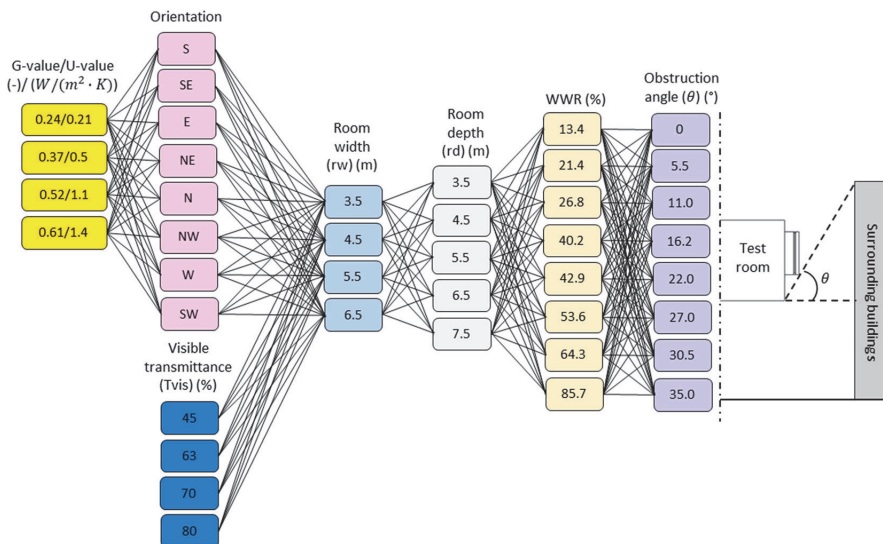


Fig. 2. Diagram of room parameter combinations and representation of the obstruction angle θ for a generic room. Window-to-wall ratio = WWR. An obstruction angle is considered null ($\theta = 0^\circ$) when the roof of the surrounding building/external obstruction is at the same level or below the floor level of the test room. The total number of room combinations is 5120 and 40960 for daylight and thermal simulations, respectively.

Table 1

Reflectance values for opaque surfaces recommended by the European standard EN 17037 for daylight simulations [5].

Surface	Reflectance (-)
Interior walls	0.5
Floor	0.2
Ceiling	0.7
External floor	0.2
External facade	0.30

Since our case study (section 3.3) is located in Tallinn, Estonia, the building typology used for this research was also used in previous investigation within the Estonian context [49]. We modeled the surrounding buildings at a distance of 17 m from the floor level of the test room, using a continuous facade and varied height to simulate the mean obstruction angle (θ) from 0° to 35.0° (Fig. 2). The room size parameters and number of orientations were selected to obtain a representative sample of typical residential bedrooms and living rooms in Estonia. Single bedrooms of approximately 12 m^2 are represented by the small $3.5 \text{ m} \times 3.5 \text{ m}$ rooms. Intermediate rooms represent kitchen-living rooms and medium-size bedrooms with an area of $20\text{--}40 \text{ m}^2$. Large kitchen-living rooms of $\sim 50 \text{ m}^2$ were represented by $6.5 \text{ m} \times 7.5 \text{ m}$ rooms.

We set the maximum width for a single glazed area as 1.5 m. The window height can be 1.5 m or 2.4 m while the room height was set to 2.8 m. Thus, considering all the room widths, window-to-wall-ratio (WWR) varied from 13.4% to 85.7% with a regular sill height of 0.9 m (when window height is 1.5 m) [49]. For the calculation of the WWR values, we considered a frame width of 5 cm for each individual window. The visible transmittance of the glazing system was varied from 45% to 80% and the g-values, which are associated to different glazing systems commonly considered within the Estonian context [63,64], were varied from 0.24 to 0.61 (with U-values from 0.21 to 1.4) (Fig. 2). Finally, we did not consider shading system in our parametric model because we aim to propose a coupled method to be used during early stage design to maximize daylight provision and quantify the potential overheating risk while minimizing design costs related to unnecessary shading system.

2.2. Daylight model

All daylight simulations were conducted through the Grasshopper plug-in Honeybee from Ladybug Tools based on the validated Radiance daylight simulation software [65,66]. The daylight analysis grid was located at 0.8 m height from the floor and the spacing between the grid points and distance from the walls was set to 0.5 m [5,60]. Diffuse reflectance values of opaque surfaces (Table 1) were set according to the

recommended values by the European standard EN 17037 [5].

The fulfillment of minimum daylight provision according to the static method defined by the EN 17037 consists in the simultaneous fulfillment of two conditions. The first condition (Cd1) is fulfilled if the minimum DF value for the first half of the reference plane closer to the window (minDF1) is higher than a target value (minDF1t), which depends on each EU country (1.5 %–2.8%) (e.g. minDF1>2.2% for Estonia, minDF1>1.8% for Spain, etc.). The second condition (Cd2) is fulfilled when the minimum DF value for at least the 95% of the entire the reference plane (minDF2t) should be higher than a target value, which depends on each EU country (0.5 %–0.9%) (e.g. minDF2>0.7% for Estonia, minDF2>0.6% for Spain, etc.) (Fig. 3).

The Radiance parameters used for the DF simulations were chosen following the recommendation made by Reinhart (Table 2) [60]. CIE overcast sky conditions were considered for DF calculations since DF metric does not depend on the room orientation [67].

2.3. Thermal model

The validated software Energy Plus was used for thermal indoor energy simulations [69] through the validated EnergyPlus software [69]. The hourly mean air temperature (T_h) was the variable of interest to assess the overheating risk in the rooms' parametric variations. The DH metric and its variations has been commonly used to quantify the overheating risk in buildings located at different climates [70–75]. Specifically, the overheating risk of residential buildings in Estonia is quantified in terms of the DH metric (Eq. (1)). Thus, the expression to calculate the DH metric of a residential room during the warm season is the following:

$$DH = \sum_{h=1}^N (T_h - 27) (^\circ\text{C} \cdot h) \quad (1)$$

where N is the number of occupied hours (from June 1 to August 31). According to the Estonian regulations, DH threshold must not exceed $150 \text{ }^\circ\text{C} \cdot \text{h}$ ($\text{maxDH}_{\text{EST}}$) in residential buildings [76]. Construction materials for the walls, slab, and floor are shown in Table 3. Slab floor and interior walls consist of 250 mm layer of concrete. The external wall is composed of three layers of concrete and expanded polystyrene, with a thermal transmittance of $0.128 \text{ W}/(\text{m}^2 \cdot \text{K})$. Moreover, we considered different type of window construction studied within the Estonian context (Table 3) [64]. Windows were modeled using a simplified model, which has been proved to be more conservative than the detailed model for overheating risk calculations [77]. Window simplified model is based on constant properties: solar/visible transmittance, U-value, and internal/external emissivity values. These optical and thermal properties were included as independent variables in our parametric model (Fig. 2) because they have big influence on daylight provision and overheating risk in buildings.

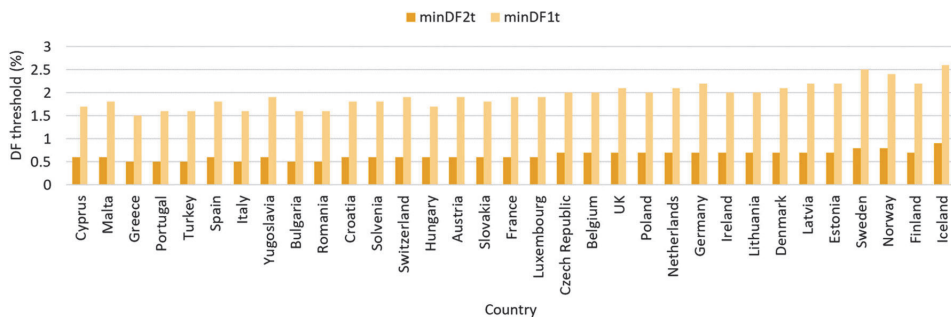


Fig. 3. Minimum thresholds for different European countries defined by the European standard EN 17037 for target DF for the first half of the reference plane closer to the window (minDF1) and minimum target DF for at least the 95% of the reference plane (minDF2).

Table 2
Radiance parameters used in Daylight Factor (DF) simulations [68].

Name	Description	Value
Ambient bounces (-ab)	The maximum number of diffuse bounces computed by the indirect calculation. A value of zero implies no indirect calculation.	5
Ambient divisions (-ad)	The error in the Monte Carlo calculation of indirect illuminance will be inversely proportional to the square root of this number. A value of zero implies no indirect calculation.	1500
Ambient resolution (-ar)	This value will approximately equal the error from indirect illuminance interpolation. A value of zero implies no interpolation.	300

Table 3
Thermal and optical properties of the building envelope.

Element	Construction	Thermal transmittance (W/(m ² ·K))	g values (-)	Visible Transmittance (%)	Exterior/Interior emissivity (-)
External wall	Concrete 150 mm Expanded Polystyrene 280 mm Concrete 50 mm	0.128	-	-	0.9/0.9
Floor slabs, Internal Walls	Concrete 250 mm	3.59	-	-	0.9/0.9
Window frame	Aluminium 50 mm	0.5	-	-	0.9/0.9
Window constructions	Variable	[0.21, 0.5, 1.1, 1.4]	[0.24, 0.37, 0.52, 0.61]	[56,56,63,78]	0.9/0.9

Slab floor and interior walls were considered as adiabatic surfaces [49]. However, we considered heat transfer through the exterior wall and solar exposure. Required usage profiles for internal gains in residential buildings by Estonian regulations can be seen in Fig. 4. For a multi-apartment building, the number of square meters per person is 28.3 [81] and the mean level of activity is 1.2 MET (Table 4).

The consideration of infiltration is mandatory by Estonian regulations. The infiltration air flow rate (q_i) is calculated using Eq. (2):

$$q_i = \frac{q_{50} \cdot A}{3.6x} \quad (2)$$

where A is the area of the building envelope in m², q_{50} is the average air leakage rate of the building envelope determined by means of an air leakage test at a pressure difference of 50 Pa, which characterizes the air tightness of the building envelope, was set to 3 m³/(h·m²) according to the same regulation, and x is the building factor set to 20 since the typical building in Tallinn has four stories [81].

HVAC settings used in our thermal model are displayed in Table 5. Mechanical ventilation was also considered: minimum fresh air of 14.15 L/s per person and minimum fresh air of 0.5 L/s per area (m²). We set airing position of the window to 10% as defined by Simson et al. [82] and T_h set point of 25 °C for opening the window as considered by Sepúlveda et al. [49]. Window airing in this context means that mechanical ventilation is operating and windows are opened to a fixed airing position to enhance air change in the room for ventilative cooling.

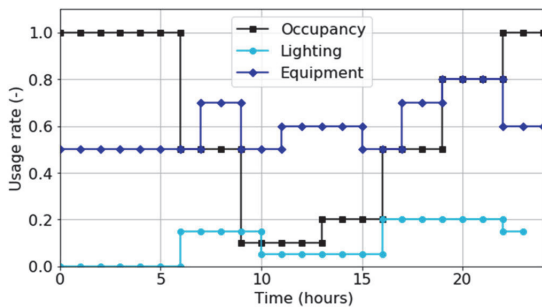


Fig. 4. Usage profiles of occupancy, lighting, and equipment for residential buildings in Estonia [81].

3. Results and discussion

3.1. Prediction of daylight provision

The aim of this section is to propose a formula for the estimation of the daylight provision of side-lit rooms. This prediction formula could help designers and practitioners not only to fulfill the minDF-based daylight requirements but also to understand the impact of the design parameters such as visible transmittance of the glazing system (T_{vis}), room depth (rd), room width (rw), and WWR on daylight provision.

The percentage of all the room combinations of our parametric model for different fulfillment conditions between Cd1 and Cd2 can be seen in Fig. 5. According to our results, there is no room combination that fulfills Cd2 and not Cd1 for any T_{vis} considered between 45% and 80%. Thus, for our parametric model based on side-lit rooms, Cd1 represent a more restrictive requirement than Cd2. From this point of the paper, the prediction of daylight provision is focused on the estimation of minDF1 (for Cd1) instead of minDF2 (for Cd2). The calculation of minDF1 speed up twice daylight simulations because only the half of the grid points is needed. From this point of the manuscript, we refer to minDF1 as minDF.

In general, minDF related to any room combination could depend on

Table 4
Internal gain parameters for Estonian residential buildings.

People density	0.0353 p/m ²
Metabolic Rate	1.2 MET
Equipment power density	3 W/m ²
Lighting power density	8 W/m ²
Dimming Control	OFF
Target Illuminance	300 lux

Table 5
HVAC settings for residential buildings in Estonia.

Heating system (SP)	ON (21 °C)
Cooling system (SP)	OFF (-)
Window airing (SP)	ON (25 °C)
Mechanical ventilation	Always ON
Minimum Fresh Air per Person	14.15 (L/s/p)
Minimum Fresh Air Area	0.5 (L/s/m ²)
Heat recovery temperature efficiency	80%

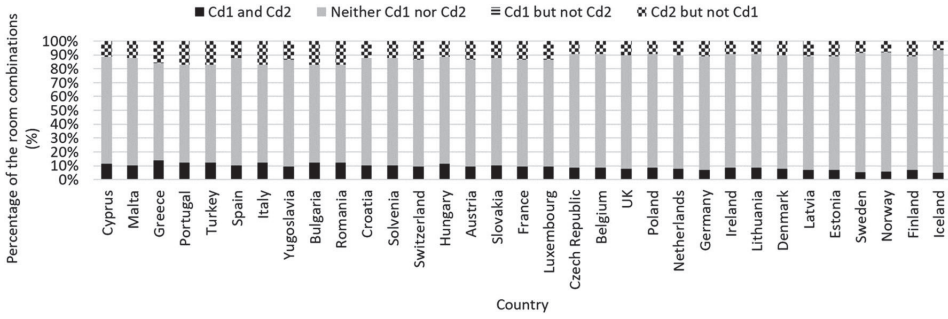


Fig. 5. Percentage of the rooms combinations of the parametric model that fulfills different combinations of conditions defined by the European standard EN 17037 (Cd1 and Cd2) for $T_{vis} = 80\%$. The first condition (Cd1) is fulfilled if $\min DF_1$ is higher than a target value (Fig. 3). The second condition (Cd2) is fulfilled when $\min DF_2$ is higher than a target value (Fig. 3).

the design parameters such as T_{vis} , θ , WWR, r_w , and r_d . Thus, the general prediction formula can be written as follows:

$$\begin{aligned} \min DF(T_{vis}, \theta, WWR, r_w, r_d) \\ = f(T_{vis}, \theta, WWR, r_w, r_d) \end{aligned} \quad (3)$$

Eq. (3) might be expressed as the product of one polynomial function ($p1(T_{vis})$) and the $\min DF$ related to $T_{vis} = 45\%$ for each room combination:

$$\min DF = p1(T_{vis})\min DF(45, \theta, WWR, r_w, r_d) \quad (4)$$

The linear correlation between $\min DF$ and $\min DF_{45}$ for each T_{vis} value is higher than 0.996 in terms of R^2 (Fig. 6a). Moreover, the dependency of the slopes from linear fitting functions (dotted lines from Fig. 6a) with T_{vis} values is strongly linear ($R^2 = 1$) (Fig. 6b). Therefore, Eq. (4) can be rewritten as follows:

$$\min DF = (aT_{vis} + b)\min DF(45, \theta, WWR, r_w, r_d) \quad (5)$$

$$\begin{aligned} \min DF &= (0.0264T_{vis} - 0.1913) \\ \min DF(45, \theta, WWR, r_w, r_d) \end{aligned} \quad (6)$$

where a and b are the fitting coefficients related to the dotted line shown in Fig. 6b. According to Fig. 6c, the agreement between simulated and predicted $\min DF$ values is 0.997 and 0.060 in terms of R^2 and RMSE, respectively.

Eq. (5) might be expressed as the product of two polynomial functions ($(aT_{vis} - b)$ and $p2(\theta)$) and the $\min DF$ related to $T_{vis} = 45\%$ and $\theta = 0^\circ$ for each room combination:

$$\min DF = (aT_{vis} + b)p2(\theta)\min DF(45, 0, WWR, r_w, r_d) \quad (7)$$

The linear correlation between $\min DF$ and $\min DF$ for $T_{vis} = 45\%$ and $\theta = 0^\circ$ for each θ value is higher than 0.960 in terms of R^2 (Fig. 7a). Moreover, the dependency of the slopes from linear fitting functions (dotted lines from Fig. 7a) with T_{vis} values is strongly linear ($R^2 = 0.968$) (Fig. 7b). Therefore, Eq. (7) can be rewritten as follows:

$$\begin{aligned} \min DF &= (aT_{vis} + b)(c\theta + d) \\ \min DF(45, 0, WWR, r_w, r_d) \end{aligned} \quad (8)$$

$$\begin{aligned} \min DF &= (aT_{vis} + b)(-0.0208\theta + 1.0773) \\ \min DF(45, 0, WWR, r_w, r_d) \end{aligned} \quad (9)$$

where c and d are the fitting coefficients related to the dotted lines shown in Fig. 7b. According to Fig. 7c, the agreement between simulated and predicted $\min DF$ values is 0.914 and 0.379 in terms of R^2 and RMSE, respectively.

In addition, the combination of design parameters WWR, r_w , and r_d can be expressed as the window-to-floor ratio (WFR):

$$WFR = \frac{\text{Window area}}{\text{Floor area}} = \frac{rhWWR}{rd} \quad (10)$$

where rh is the room height. Thus, Eq. (8) can be written as follows:

$$\min DF = (aT_{vis} + b)(c\theta + d)\min DF(45, 0, WFR) \quad (11)$$

The linear correlation between $\min DF$ and WFR for $T_{vis} = 45\%$ and

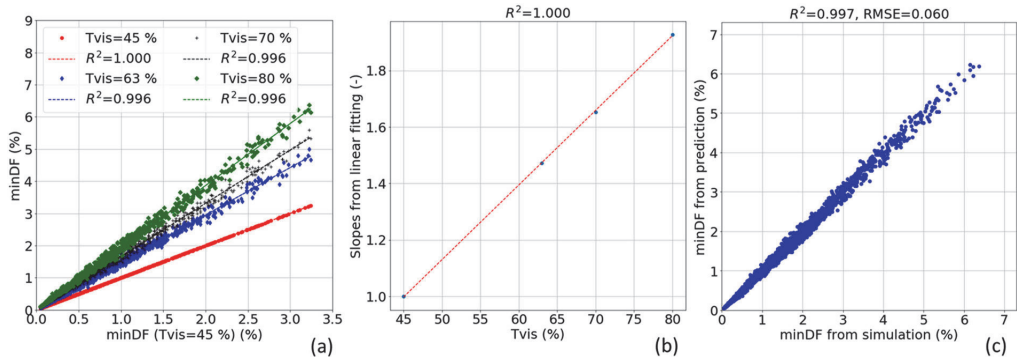


Fig. 6. Linear dependency between minimum daylight factor of the half of the reference plane closest to the window ($\min DF$) for different T_{vis} values and $\min DF$ for $T_{vis} = 45\%$ (a). Linear dependency between the slopes from linear fitting functions (a) and different T_{vis} values and $\min DF$ for $T_{vis} = 45\%$ (b). Agreement between $\min DF$ from simulations and prediction formula (Eq. (6)) (c).

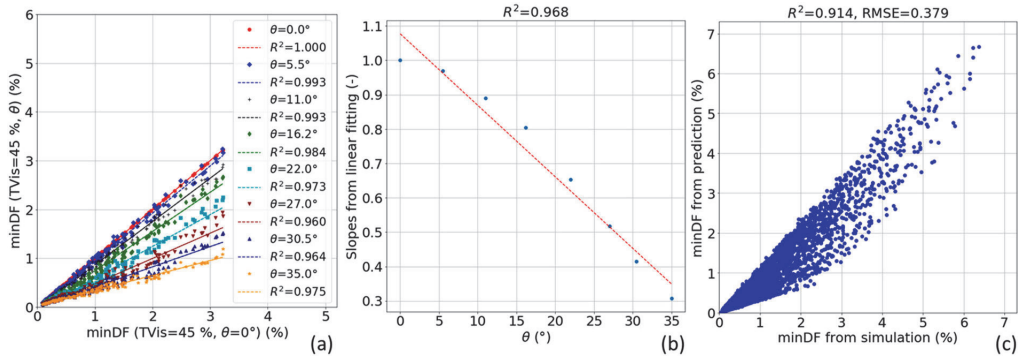


Fig. 7. Linear dependency between minimum daylight factor of the half of the reference plane closest to the window (minDF) for different θ values and minDF for $Tvis = 45\%$ and $\theta = 0^\circ$ (a). Linear dependency between the slopes from linear fitting functions (a) and different $Tvis$ values and minDF for $Tvis = 45\%$ (b). Agreement between simulated and predicted minDF values (Eq. (9)) (c).

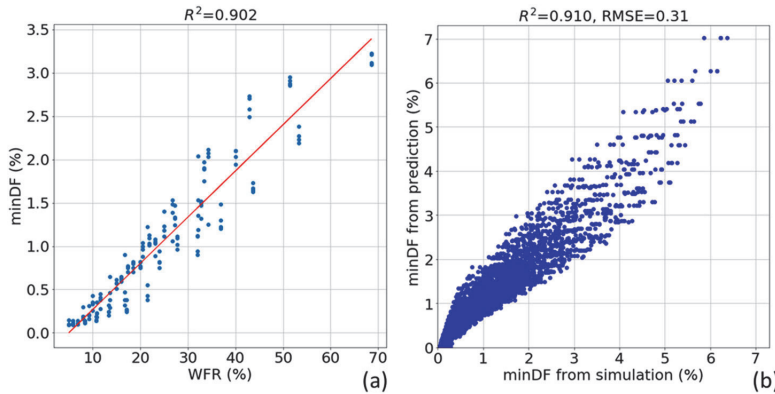


Fig. 8. Linear dependency between minimum daylight factor of the half of the reference plane closest to the window (minDF) for and window-to-floor ratio (WFR) (for $Tvis = 45\%$ and $\theta = 0^\circ$) (a). Agreement between simulated and predicted minDF values (Eq. (13)) (b).

$\theta = 0^\circ$ is 0.902 in terms of R^2 (Fig. 8a). Therefore, Eq. (7) can be rewritten as follows:

$$minDF = (aTvis + b)(c\theta + d)(eWFR + f) \tag{12}$$

$$minDF = (aTvis + b)(c\theta + d)(0.0533WFR - 0.2637) \tag{13}$$

where e and f are the fitting coefficients related to the dotted lines displayed in Fig. 8a. According to Fig. 8b, the agreement between simulated and predicted minDF values is 0.910 and 0.310 in terms of R^2 and RMSE, respectively.

The minDF relative deviation in terms of (Root mean square error (RMSE)/minDF1t or target minDF) for different European countries can be seen in Fig. 9. Although the RMSE/minDF1t tends to be higher in

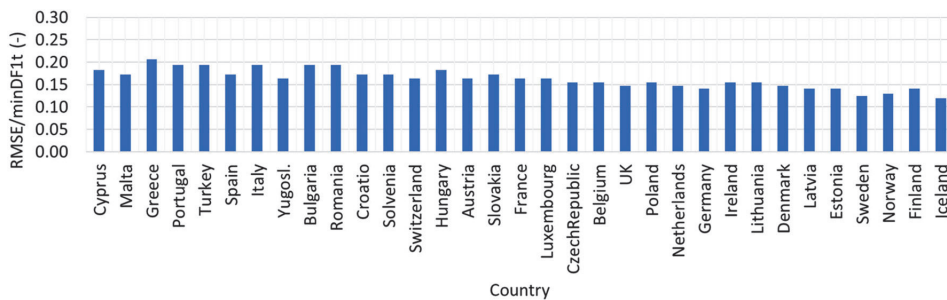


Fig. 9. Relative deviation (Root mean square error/minDF1t) of the prediction of minDF with respect to simulated minDF values (5120 room combinations) for linear polynomial fitting strategy. RMSE is 0.31 (Fig. 8b) and the target minDF value (minDF1t) depends on each EU country according to the European standard EN 17037 (1.5 %–2.8%).

countries with lower target minDFs (e.g. Cyprus:1.7%, Malta:1.8%, Greece:1.5%, Portugal:1.6%, etc.) than countries with higher daylight requirements such as Denmark (2.1%), Estonia (2.2%), Norway (2.4%), Sweden (2.5%), or Iceland (2.8%). The relative RMSE for any European country is up to 0.21.

As explained, a , b , c , d , e , and f are the fitting coefficients, whose values depend on the reflectance values of the interior/exterior scene and room typology. Meaning that each combination of reflectance values and room typology, a calibration of the minDF formula is needed. Each new calibration would require at least 6 minDF simulations. The calibration would have three steps, as we have shown in this section 3.1. Despite the substantial computational time savings (6 instead of 5120 minDF simulations), the accuracy of the prediction formula could be compromised. A minDF relative deviation of 0.21 could be acceptable when the number of minDF simulations is very large and the computational speed is a primary aspect within the design process. The proposed minDF prediction formula Eq. (13) can be used for parametric analyses that consider the following design parameter ranges: $T_{vis} = 45\text{--}80\%$, $\theta = 0\text{--}35^\circ$, $rw = 3.5\text{--}6.5$ m, $rd = 3.5\text{--}7.5$ m, and $WWR = 13.4\text{--}85.7\%$. Outside these ranges because the accuracy of the prediction formula might vary. By using the minDF prediction formula (Eq. (13)), the designer can assess calculate the minimum WWR for each room i ($minWWR_i$) that ensures a minDF1t: considering Eq. (10), Eq. (12) can be rewritten as follows:

$$minWWR_i = \left(\frac{rd_i}{erh_i} \right) \left(\frac{minDF_C}{(aT_{vis} + b)(c\theta_i + d)} - f \right) \quad (14)$$

where the $minDF_C$ is the target minDF for European country C (e.g. $minDF_C = 2.2\%$ for Estonia) according to the European standard EN 17037. For instance, if we consider $T_{vis} = 63\%$, $\theta_i = 15.8^\circ$ and $minDF_C = 2.2\%$ (Estonian context), the minWWR values calculated with Eq. (14) for different room depths (3.5, 4.5, 5.5, 6.5, and 7.5 m) are the following: 53.0%, 68.1%, 83.3%, 98.4%, and 113.6%. Since WWR values above 90% are not technically viable in practice, the maximum room depth is 5.5 m (with minWWR = 83.3%) to ensure minDF = 2.2% according to our approximation, which agrees with the rule of thumb proposed in previous investigation within the Estonian context: maximum room depth of 5.5 m with a minWWR of 86% [35]. An example of use of the minWWR formula (Eq. (14)) to a case study is presented in section 3.3.

3.2. Prediction of overheating risk

The aim of this section is to propose a formula for the estimation of the overheating risk of side-lit rooms in terms of the DH metric. The DH prediction formula could be used by architects and designers to facilitate and speed up assessment of the potential overheating risk of a

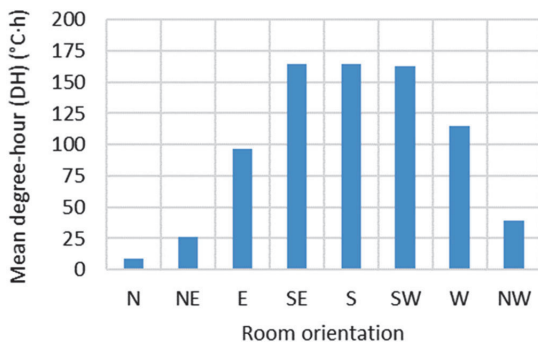


Fig. 10. Mean DH value (among 5120 room combinations) for different room orientations.

determined room design or for room/window sizing during early stages, without the need of complex and time-consuming simulations. Among 5120 simulated room combinations for each orientation, the critical orientations are the south orientations as can be seen in Fig. 10. In the first part of this analysis, we consider S orientation since its mean DH value is the highest, leading to high relative deviations in terms of RMSE/maxDH_{EST} (with maxDH_{EST} = 150 °C h).

In general, DH related to any room combination with a certain orientation (Ori) (e.g. Ori = S) could depend on the design parameters such as g (g -value), θ , and WFR. Thus, the general prediction formula can be written as follows:

$$DH_{Ori} = f(g, \theta, WFR) \quad (15)$$

According to Fig. 11, $DH_{Ori}(g, \theta, WFR)$ can be expressed linearly with $DH_{Ori}(g_0, \theta, WFR)$ with $g_0 = 0.24$ (-) for each room combination:

$$DH_{Ori}(g, \theta, WFR) = A(g)DH_{Ori}(g_0, \theta, WFR) + B(g) \quad (16)$$

The linear correlation between $DH_{Ori}(g, \theta, WFR)$ and $DH_{Ori}(g_0, \theta, WFR)$ for each g -value is higher than 0.844 in terms of R^2 (Fig. 11a). Moreover, the dependency of the slopes from linear fitting functions (dotted lines from Fig. 11a) with g -values is strongly linear ($R^2 = 0.969\text{--}0.977$) (Fig. 11c and d). Therefore, Eq. (16) can be rewritten as follows:

$$DH_{Ori}(g, \theta, WFR) = A(g)DH_{Ori}(g_0, \theta, WFR) + B(g) \quad (17)$$

$$\begin{aligned} DH_{Ori}(g, \theta, WFR) &= (a_1g + a_2) \\ DH_{Ori}(g_0, \theta, WFR) &+ (b_1g + b_2) \end{aligned} \quad (18)$$

$$DH_{Ori}(g, \theta, WFR) = (1.422g + 0.682)DH_{Ori}(g_0, \theta, WFR) + (341.146g - 86.024) \quad (19)$$

where $A(g)$ and $B(g)$ are the fitting coefficients related to the dotted lines displayed in Fig. 11a. According to Fig. 11d (Eq. (19)), the agreement between simulated and predicted DH_S values is 0.924 and 0.215 in terms of R^2 and RMSE/DHmax, respectively.

At the same time, $DH_{Ori}(g_0, \theta, WFR)$ can be correlated linearly with $DH_{Ori}(g_0, \theta_0, WFR)$ with $\theta_0 = 0^\circ$ for each room combination:

$$\begin{aligned} DH_{Ori}(g_0, \theta, WFR) &= C(\theta) \\ DH_{Ori}(g_0, \theta_0, WFR) &+ D(\theta) \end{aligned} \quad (20)$$

The linear correlation between $DH_{Ori}(g_0, \theta, WFR)$ and $DH_{Ori}(g_0, \theta_0, WFR)$ for each θ value is higher than 0.972 in terms of R^2 (Fig. 12a). Moreover, the dependency of the slopes from linear fitting functions (dotted lines from Fig. 12a) with θ is strongly linear ($R^2 = 0.922\text{--}0.961$) (Fig. 12b). Therefore, Eq. (20) can be rewritten as follows:

$$\begin{aligned} DH_{Ori}(g_0, \theta, WFR) &= C(\theta) \\ DH_{Ori}(g_0, \theta_0, WFR) &+ D(\theta) \end{aligned} \quad (21)$$

$$\begin{aligned} DH_{Ori}(g_0, \theta, WFR) &= (c_1\theta + c_2) \\ DH_{Ori}(g_0, \theta_0, WFR) &+ (d_1\theta + d_2) \end{aligned} \quad (22)$$

$$\begin{aligned} DH_{Ori}(g_0, \theta, WFR) &= (-0.006\theta + 1.005) \\ DH_{Ori}(g_0, \theta_0, WFR) &+ (-0.384\theta - 0.4108) \end{aligned} \quad (23)$$

where $C(\theta)$ and $D(\theta)$ are the fitting coefficients associated to the dotted lines shown in Fig. 12a. Thus, Eq. (17) can be expressed as follows:

$$\begin{aligned} DH_{Ori}(g, \theta, WFR) &= A(g)(C(\theta) \\ DH_{Ori}(g_0, \theta_0, WFR) &+ D(\theta)) + B(g) \end{aligned} \quad (24)$$

According to Fig. 12d (predicted values calculated with Eq. (23)), the agreement between simulated and predicted DH_S values is 0.945 and 0.183 in terms of R^2 and RMSE/DHmax, respectively.

Finally, $DH_{Ori}(g_0, \theta_0, WFR)$ can be expressed as a parabolic function with WFR as independent variable for each room combination according to Fig. 13a (Eq. (25) and Eq. (26)). The dependency is strongly parabolic

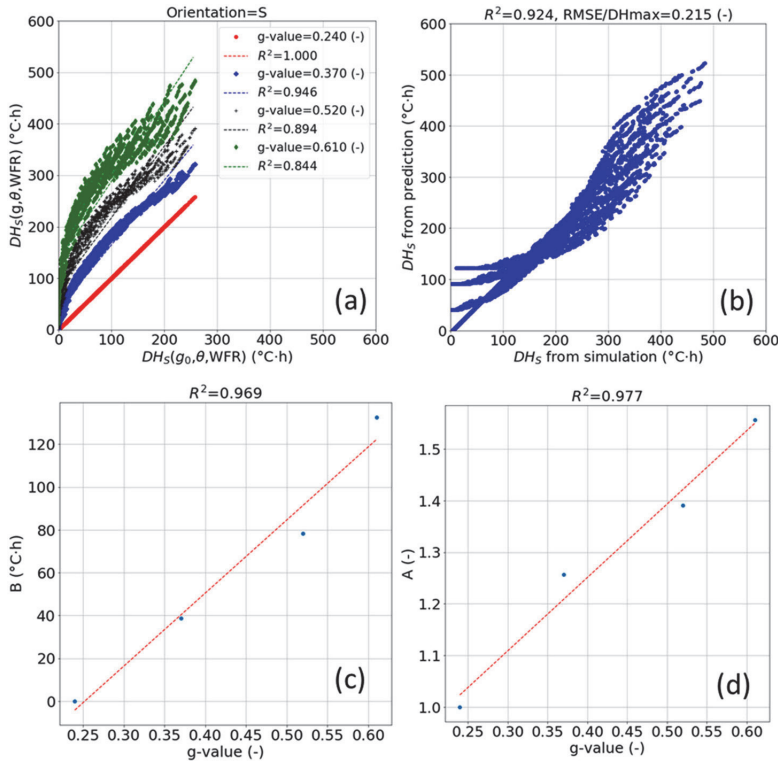


Fig. 11. Linear dependency between degree-hours (DH) for south oriented rooms for different g-values (g) ($DH_S(g, \theta, WFR)$) and DH_S for $g_0 = 0.24$ (-) ($DH_S(g_0, \theta, WFR)$) (a). Linear dependency between A(c) and B(d) coefficients and different g-values. Agreement between $DH_S(g, \theta, WFR)$ from simulations and prediction formula (b) (Eq. (19)).

($R^2 = 0.984$) (Fig. 13a):

$$DH_{On}(g_0, \theta_0, WFR) = e_1 WFR^2 + e_2 WFR + e_3 \quad (25)$$

$$DH_{On}(g_0, \theta_0, WFR) = -0.058 WFR^2 + 8.771 WFR - 6.817 \quad (26)$$

Moreover, Eq. (24) can be rewritten as follows:

$$DH_{On}(g, \theta, WFR) = A(g) [C(\theta) (e_1 WFR^2 + e_2 WFR + e_3) + D(\theta)] + B(g) \quad (27)$$

where e_1 , e_2 , and e_3 are the fitting coefficients associated to lines displayed in Fig. 13a. According to Fig. 13b (predicted values calculated with Eq. (27)), the agreement between simulated and predicted DH_S values is 0.952 and 0.172 in terms of R^2 and RMSE/DHmax, respectively. For the rest of room orientations, the RMSE/DHmax is below 0.20 (Table 6).

As explained in this section 3.2, the 11 fitting coefficients (a_1 , a_2 , b_1 , b_3 , c_1 , c_2 , d_1 , d_2 , e_1 , e_2 , and e_3) for the DH prediction formula (Eq. (27)) depend mainly on the room orientation (Table 6), room typology, natural ventilation control, HVAC settings, and opaque constructions materials. Meaning that each combination of natural ventilation control, room typology, HVAC settings, and opaque constructions materials, a calibration of the DH formula is needed. Each new calibration would require at least 11 minDF simulations. The calibration would have three steps, as we have shown in this section 3.2. Despite the substantial computational time savings (11 instead of 5120 DH simulations for each orientation), the accuracy of the prediction formula could be compromised. A DH relative deviation of 0.20 could be acceptable when the

number of DH simulations is very large and the computational speed is the main design criterion. The proposed minDF prediction formula Eq. (13) can be used for parametric analyses that consider the following design parameter ranges: g-value = 0.27–0.61 (-), $\theta = 0$ –35°, rw = 3.5–6.5 m, rd = 3.5–7.5 m, and WWR = 13.4–85.7%. An example of use of the DH formula (Eq. (27)) for window sizing is presented in section 3.3.

Moreover, the consideration of a maxDH lower than 150 °C h by local regulations would lower the accuracy of the DH prediction formula and higher polynomial fitting order might be needed to maintain an acceptable relative deviation. For a different climate, not only maxDH (defined by local regulations) would be different, but also the warm season considered typical HVAC settings, ventilation strategies, and envelope optical/thermal properties. Theoretically, all these aspects could influence on the accuracy of the prediction of the DH metric.

According to minDF (Eq. (13)) and DH (Eq. (27)) prediction formulas, for g-value = 0.37, $T_{vis} = 63\%$, and $\theta_i = 15.8^\circ$, the maximum room depth to fulfill both requirements is 5.5 m (Table 7). This is only possible for N, NE, and NW room orientations according to our predictions. This fact is supported also by rules of thumb for side-lit rooms without shading recommended in a previous investigation within the Estonian context [49].

3.3. Coupled method for window sizing in residential rooms in a cold climate

The aim of this section is to define a coupled method based on the developed prediction formulas (Eq. (14) and Eq. (27)). We combined

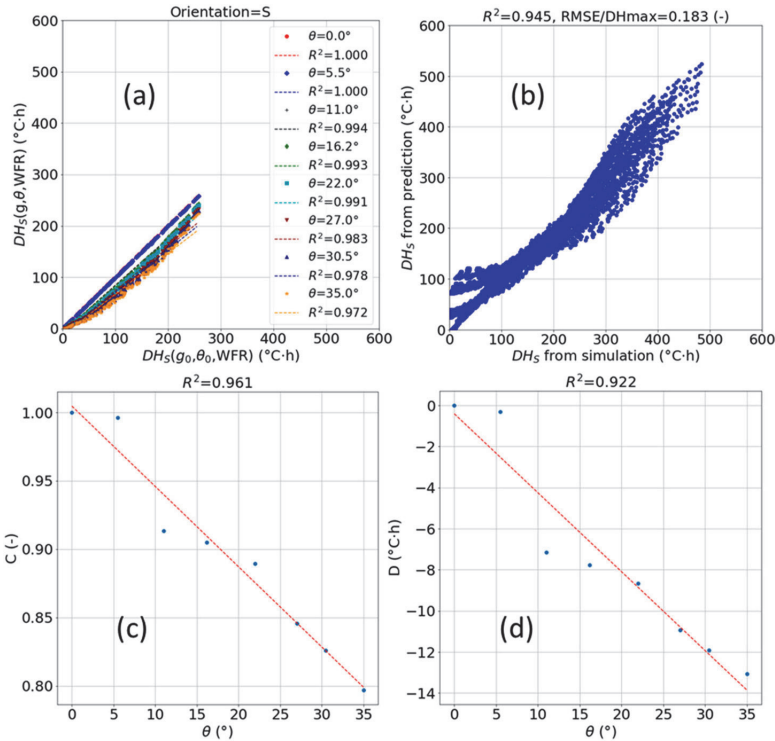


Fig. 12. Linear dependency between degree-hours (DH) for south oriented rooms for different g-values (g) ($DH_S(g, \theta, WFR)$) and ($DH_S(g_0, \theta_0, WFR)$) (a). $g_0 = 0.24$ (-) and $\theta_0 = 0^\circ$. Linear dependency between C (c) and D (d) coefficients and different θ values. Agreement between $DH_S(g, \theta, WFR)$ from simulations and prediction formula (b) (Eq. (24)).

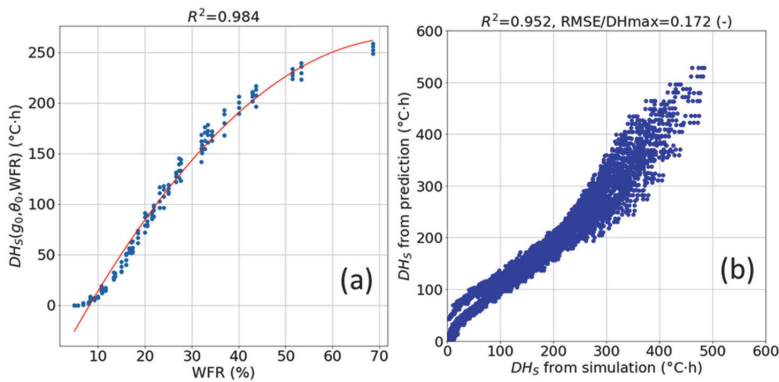


Fig. 13. Linear dependency between degree-hours (DH) for south oriented rooms ($DH_S(g_0, \theta_0, WFR)$) and window-to-floor ratio (WFR) (a). $g_0 = 0.24$ (-) and $\theta_0 = 0^\circ$. Agreement between $DH_S(g_0, \theta, WFR)$ from simulations and prediction formula (b) (Eq. (27)).

them in order to choose design decisions that help to achieve a good balance between daylight provision and overheating risk protection in a new residential building in Estonia. These design decisions consist of the selection of window's size and thermal properties for each designed bedroom and kitchen-living rooms. On one hand, a good level of daylight provision is achieved when the minimum requirement according to the minDF-based method defined by the European standard EN 17037 is fulfilled. On the other hand, the maximum overheating risk

level is based on the DH-metric, which has the potential to be adopted by EU countries as overheating metric in the future. We considered the design of a multi-store building located in a middle-density urban area of Tallinn, Estonia (Lat. 59.39°, Lon. 24.67°) (Fig. 14). The building has a length of 82 m and a width of 17 m. The number of floors is 10 floors where the first floor is habitated for commercial, building access, and parking uses. There are 12 apartments of 94.5 m² (13.5 m width x 7 m depth) per floor and the floor height is 3 m where 2.8 m is the room

Table 6

Fitting coefficients and relative deviation in terms of DH RMSE/maxDH (-) for different room orientations and fitting strategy explained in this section 3.2 (Eq. (27)). RMSE = Root Mean Square Error and maxDH = 150 °C h according to the Estonian regulation.

	N	NE	E	SE	S	SW	W	NW
a1	9.632	5.943	2.928	2.003	1.422	1.771	2.666	4.409
a2	-1.255	-0.308	0.361	0.548	0.682	0.598	0.394	0.000
b1	35.214	90.872	239.231	347.875	341.146	309.132	208.895	86.555
b2	-9.763	-24.273	-61.272	-87.680	-86.024	-77.670	-53.236	-22.904
c1	-0.027	-0.031	-0.025	-0.012	-0.006	-0.014	-0.027	-0.031
c2	0.811	0.978	1.083	1.046	1.005	1.060	1.067	0.928
d1	0.003	0.007	-0.207	-0.525	-0.384	-0.624	-0.236	0.051
d2	-0.222	-0.821	-1.967	0.215	-0.411	-0.441	-5.783	-2.907
e1	0.021	0.032	-0.018	-0.060	-0.058	-0.074	-0.062	0.004
e2	-0.684	-0.381	5.115	8.792	8.771	10.086	8.930	2.792
e3	4.659	-1.021	-46.563	-65.734	-68.171	-70.123	-61.321	-27.913
RMSE/maxDH (-)	0.088	0.159	0.195	0.183	0.172	0.179	0.190	0.156

Table 7

Predicted degree-hours (DH) (Eq. (27)) and minDF (Eq. (13)) values for room combinations that fulfil minDF ≥ 2.2% and DH ≤ 150 °C h. The visible transmittance of the glazing (Tvis) is 63% and the g-value 0.37. The mean obstruction angle (θ) is 15.8°.

Room orientation	rd (m)	WWR (%)	DH (°C·h)	minDF (%)
NE	3.5	53.6	44.9	2.228
		64.3	65.1	2.731
	4.5	85.7	118.1	3.737
		85.7	70.1	2.842
		85.7	46.5	2.272
N	3.5	53.6	14.5	2.228
		64.3	24	2.731
	4.5	85.7	50.9	3.737
		85.7	26.5	2.842
		85.7	15.3	2.272
NW	3.5	53.6	76.5	2.228
		64.3	95.8	2.731
	4.5	85.7	135.4	3.737
		85.7	100	2.842
		85.7	78.2	2.272

height. Each apartment has one 4 × 6 m bedroom and one 6 × 6 m open kitchen-living room. The mean obstruction angles are between 0° (higher floors) and 20° (lower floors).

For a certain room *i*, when minWFR = maxWFR (equivalent to minWWR = maxWWR) there is a unique combination of *g*-value and *Tvis* values that ensure the combined fulfillment between daylight provision and overheating protection. For a certain *Tvis* value and room *i*, there is a maximum *g*-value ($g_{max,i}$) (Eq. (28)) from the combination of Eq. (14) and Eq. (27).

$$g_{max,i} = \frac{maxDH - a_2 [(c_1\theta_i + c_2)(e_1WFR^2 + e_2WFR + e_3) + (d_1\theta_i + d_2)] - b_2}{a_1 [(c_1\theta_i + c_2)(e_1WFR^2 + e_2WFR + e_3) + (d_1\theta_i + d_2)] + b_1} \quad (28)$$

If the window have a *g*-value lower or equal to $g_{max,i}$, the room *i* will

not be overheated (DH ≤ maxDH). On the contrary, if the *g*-value is higher than $g_{max,i}$ there room *i* will be overheated. If we consider a *Tvis* range from 50% to 80%, the g_{max} values for each room *i* can be seen in Fig. 15. For SE oriented rooms, the g_{max} value is much lower than for NW oriented rooms, this is because SE oriented rooms are more prone to overheating and therefore windows with low *g*-value are needed [82]. In addition, for rooms with NW orientation, depending on the *Tvis* considered the g_{max} values goes from 0.4 to 0.7 for *Tvis* values from 50% to 80%, respectively. In fact, for a certain room *i* when *Tvis* increases, minWWR decreases because there is no need for larger window sizes if the glazing system is more transparent. Thus, this leads to a decrease of maxWWR (if we consider during the design minWWR = maxWWR), which allows a selection of a higher *g*-value. In summary, Fig. 15 shows that highly transparent glazing systems with low *g*-values are preferred design solutions to achieve a good-balance between daylight provision and overheating protection.

Specifically, the selection of windows constructions with *Tvis* of 80% and *g*-value of 0.27 could achieve both performances in SE oriented rooms. For NW oriented room, a *Tvis* of 60% and *g*-value of 0.5 could achieve both performances. The minWWR for each room is shown in Fig. 16. The minWWR values are between 40-60% and 52-72% for SE and NW-oriented rooms, respectively. Thus, these minWWR differences for each room orientation are due to slight variations of room depth (rd_i) and obstruction level (θ_i). In summary, from these two analyses (Figs. 15 and 16), we could select the window construction depending on the room orientation (*Tvis* and *g*-values) and window size. Apart from the selection of the window's *g*-value and *Tvis*, it is also possible to consider as design solution such different room depths [83] or orientation/typology of the building floor plan [84]. However, the presented prediction formulas cannot be used in parametric analyses regarding the set point for the window airing operation [18] or nighttime ventilation [85] since we did not consider these design parameters as independent variables.

According to our case study, the prediction accuracy in terms of relative RMSE is 0.130 and 0.199 for minDF and DH values, respectively

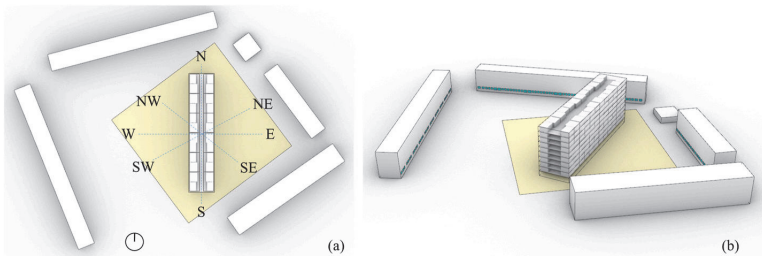


Fig. 14. Top view (a) and perspective view (b) of the building (E-W) and surrounding environment used in the case study in Tallinn, Estonia.

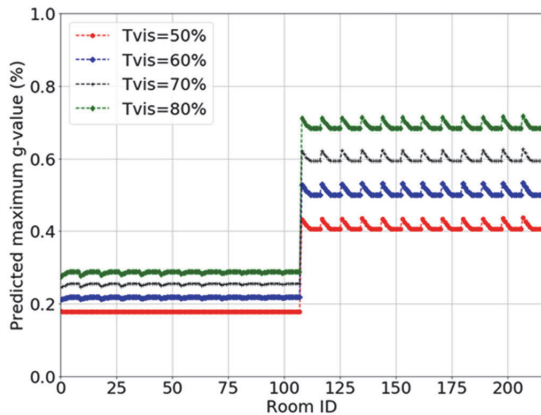


Fig. 15. Maximum g-value (g_{max}) for each room residential building located in Tallinn, Estonia ($T_{vis} = 50\text{--}80\%$) to achieve a good balance between daylight provision and overheating protection ($\min WFR = \max WFR$) (Eq. (28)). Room ID range 1–108 and 109–215 refers to SE and NW oriented rooms, respectively.

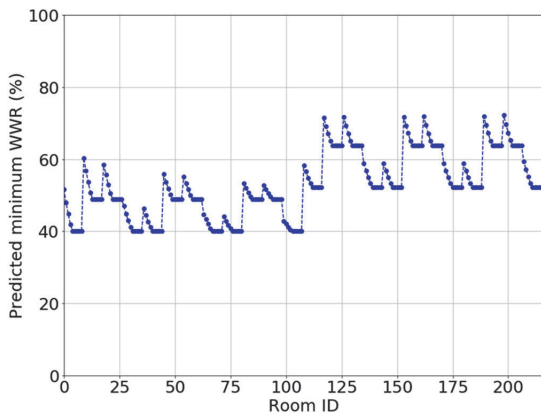


Fig. 16. Minimum window-to-wall ratio ($\min WWR$) for each room of the residential building located in Tallinn, Estonia ($T_{vis} = 80\%$ for SE rooms and $T_{vis} = 60\%$ for NW rooms) to reach sufficient daylight provision according to EN 17037 (Eq. (14)). Room ID range 1–108 and 109–215 refers to SE and NW oriented rooms, respectively.

(Fig. 17). For SE rooms, the deviations are lower than for NW rooms because of the lower g-value selected (0.27 against 0.50). In fact, the fitting accuracy decreases with the g-value, as can be seen in Fig. 11a. Moreover, DH deviations are higher than initially calculated (0.156 from Table 6) because the case study only contains SE/NW oriented rooms (216 combinations), while for the calculation of 0.156 a wide range of room configurations was used (5120 combinations).

A relative RMSE of 0.20 might not be acceptable for pure assessment purposes in existing buildings. Thus, the use of our coupled method might be justified during early stages, when the number of simulations is very large and the accuracy is not the main priority. However, our coupled method is opposite to a “black box” approach, which is typical of machine learning-based multi-optimization approaches. Although the prediction of daylight and thermal performances can be very accurate ($R^2 \sim 0.99$) but the training of the prediction models require much large datasets for each variable (~ 100) [86]. Our coupled method be represented graphically, which can be attractive for architects and designers, since these type of user-friendly 2D methods are key to process and

communicate to the designer [87].

Firstly, the main advantage of using the prediction formulas is the minimization of the time-consuming design iterations to achieve the combined fulfillment of daylight and overheating performances in new buildings. Secondly, by using our graphical coupled method, designers and architects can understand the impact of their design decisions on the combined fulfillment of daylight and overheating requirements without conducting simulations. Therefore, our proposed method based on Eq. (14) and Eq. (28), can help architects and designers to make fast performance-driven decisions regarding window sizing process during early stages.

4. Conclusions

This paper proposes a coupled method based on prediction formulas that can be used to consider efficiently daylight provision and overheating protection in buildings during early stages of the design process within the Estonian context. This method could be used by architects and designers to understand better the influence of design solutions on daylight provision and overheating risk, and to speedup design decisions during early stages. The main outcomes of this research and potential applications of the results are the following:

- (1) Within the context of the European standard EN 17037, the fulfillment of a target minimum DF of the half of the reference plane closer to the window side ($\min DF$) in side-lit rectangular rooms implies the fulfillment of a target minimum DF in at least 95% of the reference plane. The definition of a prediction formula based on polynomial fitting for the estimation of $\min DF$ based on visible transmittance of the glazing, room depth, window-to-wall ratio (WWR), and obstruction angle parameters is viable in terms of computation time with a relative accuracy of 0.21 for any European country. Moreover, the definition of an overheating risk prediction formula based on polynomial fitting for the estimation of the Degree-hour (DH) metric, which is used by the Estonian regulation, based on g-value, window-to-floor ratio (WFR), and obstruction angle parameters is viable in terms of computation time with a relative accuracy of 0.21 for the design of residential buildings within the Estonian context.
- (2) The proposed coupled method based on $\min DF$ and DH prediction formulas has big potential to help designers to consider a performance-driven criterion based on daylight provision and overheating risk requirements during early stages design. Thus, they could create interior floor and window sizing plans efficiently. Combining the prediction formulas, the window's size and properties (g-value and visible transmittance) that ensure the combined fulfillment of $\min DF$ -based and DH-based requirements can be calculated and represented graphically. By using this design approach, designers can save considerable computation time required by daylight and energy simulations because there is no need to conduct time-consuming iterative design processes based on simulations to design well daylit and not overheated buildings.
- (3) The authors recommend to regulation makers the consideration of the coupled method based on prediction formulas proposed in this paper. European countries might adopt DH-based overheating protection requirements with climate-dependent thresholds as benchmark to assess overheating risk in buildings. Furthermore, the achievement of the combined fulfillment between DF-based daylight provision requirements according to the European standard EN 17037 and DH-based overheating protection requirements in buildings would be much simpler and affordable during the early stages of the design process.

Our coupled method was applied to a single case study located in a cold climate. Moreover, an accuracy of 0.20 for $\min DF$ and DH

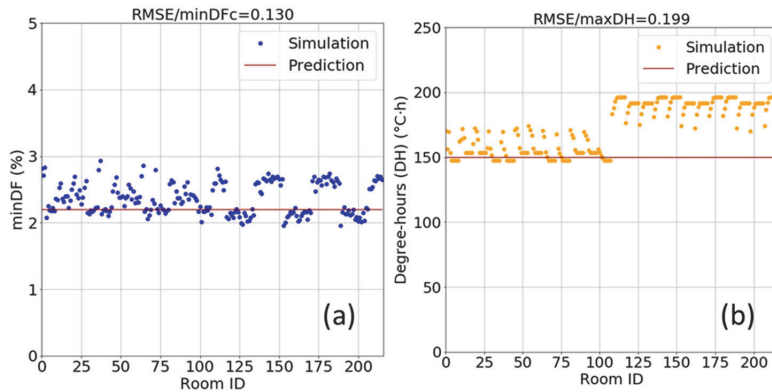


Fig. 17. Comparison between simulated and predicted minDF (left figure) and DH (right figure) values for each room. Room ID range 1–108 and 109–215 refers to SE (Tvis = 80% and g-value = 0.27) and NW (Tvis = 60% and g-value = 0.5) oriented rooms, respectively. The minDF and DH values were calculated for rooms with minWWR obtained with Eq. (14) and Eq. (27), respectively. RMSE = Root mean square error, minDFc = 2.2%, and maxDH = 150 °C·h.

predictions might not be acceptable for some design criteria. We studied side-lit room typology specific to Estonia. Thus, the viability of the proposed coupled method based on prediction formulas should be further quantified for different climates, construction materials, and room typologies (e.g. rooms with multiple orientations). The accuracy of DH predictions was quantified for a specific combination of HVAC settings recommended for the Estonian context by local regulations and previous investigations. Settings such as the natural ventilation strategy (e.g. openable area and temperature set point), infiltration rates, construction materials, or occupancy profiles are influenced in practice by specific local regulations of each European country. Therefore, further investigations should study the validity of approaches based on DH prediction formula in different climate and regulation contexts. Finally, this coupled method will be implemented as an interactive tool such as a Grasshopper plug-in for Rhinoceros 3D that could be used not only by architects and designers as a design tool but also for educational purposes. This interactive tool could be included in a general framework to optimize the design of residential buildings within the Estonian context.

Declaration of competing interest

The authors declare that they have no known competing financial interests or personal relationships that could have appeared to influence the work reported in this paper.

Acknowledgements

This research was partially supported by the Estonian Centre of Excellence in Zero Energy and Resource Efficient Smart Buildings and Districts, ZEBE (grant No. 2014-2020.4.01.15-0016), the programme Mobilitas Plus (Grant No – 2014-2020.4.01.16-0024), and Dora Plus PhD student mobility (T1.2) funded by the European Regional Development Fund, by the Estonian Research Council (grant No. PSG409) and by the European Commission through the H2020 project Finest Twins (grant No. 856602).

References

- [1] H. Sanaieian, M. Tenpierik, K. Van Den Linden, F. Mehdizadeh Seraj, S.M. Mofidi Shemrani, Review of the impact of urban block form on thermal performance, solar access and ventilation, *Renew. Sustain. Energy Rev.* (2014), <https://doi.org/10.1016/j.rser.2014.06.007>.
- [2] R. Samuels, Solar efficient architecture and quality of life: the role of daylight and sunlight in ecological and psychological well-being, *Energy Environ. Into* 1990s, Proc. 1st World Renew. Energy Congr. Environ. Into (1990), 1990s. Proc. 1st World Renew. Energy Congr.
- [3] S.W. Lockley, Circadian rhythms: influence of light in humans, in: *Encycl. Neurosci.*, 2009, <https://doi.org/10.1016/B978-008045046-9.01619-3>.
- [4] K. Won Hee, G. Brager, S. Schiavon, S. Selkowitz, *Building Envelope Impact on Human Performance and Well-Being: Experimental Study on View Clarity*, Escholarsh. UC Open Access Publ., 2017.
- [5] European Commission, BS EN 17037:2018: Daylight in Buildings, 2018. <https://www.en-standard.eu/bs-en-17037-2018-daylight-in-buildings/>.
- [6] M. Knoop, O. Stefani, B. Bueno, B. Matusiak, R. Hobday, A. Wirz-Justice, K. Martiny, T. Kantermann, M.P.J. Aarts, N. Zemmouri, S. Appelt, B. Norton, Daylight: what makes the difference? *Light. Res. Technol.* (2019) <https://doi.org/10.1177/1477153519869758>.
- [7] I. Turan, A. Chegut, D. Fink, C. Reinhart, The value of daylight in office spaces, *Build. Environ.* (2020), <https://doi.org/10.1016/j.buildenv.2019.106503>.
- [8] A. Beizaee, K.J. Lomas, S.K. Firth, National survey of summertime temperatures and overheating risk in English homes, *Build. Environ.* (2013), <https://doi.org/10.1016/j.buildenv.2013.03.011>.
- [9] C. Liu, T. Kershaw, D. Fosas, A.P. Ramallo Gonzalez, S. Natarajan, D.A. Coley, High resolution mapping of overheating and mortality risk, *Build. Environ.* (2017), <https://doi.org/10.1016/j.buildenv.2017.05.028>.
- [10] M. Santamouris, D. Kolokotsa, On the impact of urban overheating and extreme climatic conditions on housing, energy, comfort and environmental quality of vulnerable population in Europe, *Energy Build.* 98 (2015), <https://doi.org/10.1016/j.enbuild.2014.08.050>.
- [11] M. Hamdy, S. Carlucci, P.J. Hoes, J.L.M. Hensen, The impact of climate change on the overheating risk in dwellings—a Dutch case study, *Build. Environ.* 122 (2017), <https://doi.org/10.1016/j.buildenv.2017.06.031>.
- [12] C. Heracleous, A. Michael, Assessment of overheating risk and the impact of natural ventilation in educational buildings of Southern Europe under current and future climatic conditions, *Energy* (2018), <https://doi.org/10.1016/j.energy.2018.10.051>.
- [13] E. Rodrigues, M.S. Fernandes, Overheating risk in Mediterranean residential buildings: comparison of current and future climate scenarios, *Appl. Energy* 259 (2020), <https://doi.org/10.1016/j.apenergy.2019.114110>.
- [14] S. Yannas, J. Rodríguez-Álvarez, Domestic overheating in a temperate climate: feedback from London residential schemes, *Sustain. Cities Soc.* 59 (2020), <https://doi.org/10.1016/j.scs.2020.102189>.
- [15] M. Hamdy, L.M. Jan Hensen, Ranking of dwelling types in terms of overheating risk and sensitivity to climate change, *Int. Conf. IBPSA - Build. Simul.* (2015), BS 2015, Conf. Proc., 2015.
- [16] D. Fosas, D.A. Coley, S. Natarajan, M. Herrera, M. Fosas de Pando, A. Ramallo-Gonzalez, Mitigation versus adaptation: does insulating dwellings increase overheating risk? *Build. Environ.* 143 (2018) <https://doi.org/10.1016/j.buildenv.2018.07.033>.
- [17] K.J. Lomas, S.M. Porritt, Overheating in buildings: lessons from research, *Build. Res. Inf.* (2017), <https://doi.org/10.1080/09613218.2017.1256136>.
- [18] R. Simson, Overheating Prevention and Daylight in Buildings without Mechanical Cooling, Tallinn University of Technology, 2019, <https://doi.org/10.23658/taltech.54/2019>.
- [19] J. Morey, A. Beizaee, A. Wright, An investigation into overheating in social housing dwellings in central England, *Build. Environ.* 176 (2020), <https://doi.org/10.1016/j.buildenv.2020.106814>.
- [20] K. Mourkos, C.J. Hopfe, R.S. McLeod, C. Goodier, M. Swainson, The impact of accurately modelling corridor thermodynamics in the overheating risk assessment of multi-residential dwellings, *Energy Build.* 224 (2020), <https://doi.org/10.1016/j.enbuild.2020.110302>.
- [21] R. Gupta, M. Gregg, Assessing energy use and overheating risk in net zero energy dwellings in UK, *Energy Build.* 158 (2018), <https://doi.org/10.1016/j.enbuild.2017.10.061>.

- [22] M. Maivel, J. Kurnitski, T. Kalamees, Field survey of overheating problems in Estonian apartment buildings, *Architect. Sci. Rev.* (2015), <https://doi.org/10.1080/00038628.2014.970610>.
- [23] H. Voll, F. De Luca, V. Pavlovas, Analysis of the insolation criteria for nearly-zero energy buildings in Estonia, *Sci. Technol. Built Environ.* (2016), <https://doi.org/10.1080/23744731.2016.1195657>.
- [24] CIBSE, Design Methodology for the Assessment of Overheating Risk in Homes, 2017. <https://www.cibse.org/knowledge/knowledge-items/detail?id=a0q0O00000DVrTqQAL>.
- [25] K. Mourkos, R.S. McLeod, C.J. Hopfe, C. Goodier, M. Swainson, Assessing the application and limitations of a standardised overheating risk-assessment methodology in a real-world context, *Built. Environ.* 181 (2020), <https://doi.org/10.1016/j.buildenv.2020.107070>.
- [26] F. De Luca, A. Sepúlveda, T. Varjas, Static shading optimization for glare control and daylight, in: *ECAADE2021, Towar. A New, Config. Archit.*, Faculty of Technical Sciences, University of Novi Sad, 2021.
- [27] A. Sepúlveda, F. De Luca, J. Kurnitski, Optimization workflow for the design of efficient shading control strategies, in: *17th IBPSA Int. Conf. Exhib.*, 2021. Bruges, Belgium.
- [28] B. Bueno, A. Sepúlveda, Easy-to-implement simulation strategies for dynamic glare risk assessment based on the European Daylighting Standard, in: *7th IBPSA Int. Conf. Exhib.*, 2021. Bruges, Belgium.
- [29] S. Hoffmann, E.S. Lee, A. McNeil, L. Fernandes, D. Vidanovic, A. Thanachareonkit, Balancing Daylight, Glare, and Energy-Efficiency Goals: an Evaluation of Exterior Coplanar Shading Systems Using Complex Penetration Modeling Tools, *Energy Build.* 2016, <https://doi.org/10.1016/j.enbuild.2015.12.009>.
- [30] D. Uribe, S. Vera, W. Bustamante, A. McNeil, G. Flamant, Impact of different control strategies of perforated curved louvers on the visual comfort and energy consumption of office buildings in different climates, *Sol. Energy* (2019), <https://doi.org/10.1016/j.solener.2019.07.027>.
- [31] B. Bueno, A. Sepúlveda, A specific building simulation tool for the design and evaluation of innovative fenestration systems and their control, *Int. Build. Perform. Simul. Assoc. -IBPSA- Build. Simul.* 2019. 16th Conf. IBPSA. Proc. Rome (2019), Italy, 2-4 Sept. 2019, <http://publica.fraunhofer.de/dokumente/N-565205.html>.
- [32] A. Sepúlveda, F. De Luca, M. Thalfeldt, J. Kurnitski, Analyzing the fulfillment of daylight and overheating requirements in residential and office buildings in Estonia, *Built. Environ.* 180 (2020), <https://doi.org/10.1016/j.buildenv.2020.107036>.
- [33] F. De Luca, M. Kiil, R. Simson, J. Kurnitski, R. Murula, Evaluating daylight factor standard through climate based daylight simulations and overheating regulations in Estonia, in: *Proc. Build. Simul.* 2019 16th Conf, *Int. Build. Perform. Simul. Assoc.*, 2019.
- [34] L. Vanhoutteghem, G.C.J. Skarning, C.A. Hviid, S. Svendsen, Impact of Façade Window Design on Energy, Daylighting and Thermal Comfort in Nearly Zero-Energy Houses, *Energy Build.* 2015, <https://doi.org/10.1016/j.enbuild.2015.05.018>.
- [35] F. De Luca, T. Dogan, J. Kurnitski, Methodology for Determining Fenestration Ranges for Daylight and Energy Efficiency in Estonia, *Simul. Ser.*, 2018, <https://doi.org/10.22360/simaud.2018.simaud.007>.
- [36] K.H. Cheong, Y.H. Teo, J.M. Koh, U.R. Acharya, S.C. Man Yu, A simulation-aided approach in improving thermal-visual comfort and power efficiency in buildings, *J. Build. Eng.* (2020), <https://doi.org/10.1016/j.jobe.2019.100936>.
- [37] T. Srisamranrungruang, K. Hiyama, Balancing of natural ventilation, daylight, thermal effect for a building with double-skin perforated facade (DSPF), *Energy Build.* 210 (2020), <https://doi.org/10.1016/j.enbuild.2020.109765>.
- [38] R.M. Reffat, R.M. Ahmad, Determination of optimal energy-efficient integrated daylighting systems into building windows, *Sol. Energy* 209 (2020), <https://doi.org/10.1016/j.solener.2020.08.086>.
- [39] M. Rabani, H. Bayera Madessa, N. Nord, Achieving zero-energy building performance with thermal and visual comfort enhancement through optimization of fenestration, envelope, shading device, and energy supply system, *Sustain. Energy Technol. Assess.* 44 (2021), <https://doi.org/10.1016/j.seta.2021.101020>.
- [40] A. Toutou, M. Fikry, W. Mohamed, The parametric based optimization framework daylighting and energy performance in residential buildings in hot arid zone, *Alexandria Eng. J.* 57 (2018), <https://doi.org/10.1016/j.aej.2018.04.006>.
- [41] R.A. Mangkuto, M. Rohmah, A.D. Asri, Design optimisation for window size, orientation, and wall reflectance with regard to various daylight metrics and lighting energy demand: a case study of buildings in the tropics, *Appl. Energy* (2016), <https://doi.org/10.1016/j.apenergy.2015.11.046>.
- [42] L. Zhu, B. Wang, Y. Sun, Multi-objective optimization for energy consumption, daylighting and thermal comfort performance of rural tourism buildings in north China, *Built. Environ.* 176 (2020), <https://doi.org/10.1016/j.buildenv.2020.106841>.
- [43] P. Geyer, S. Singaravel, Component-based machine learning for performance prediction in building design, *Appl. Energy* 228 (2018), <https://doi.org/10.1016/j.apenergy.2018.07.011>.
- [44] B. Chegari, M. Tabaa, E. Simeu, F. Moutaouakkil, H. Medromi, Multi-objective optimization of building energy performance and indoor thermal comfort by combining artificial neural networks and metaheuristic algorithms, *Energy Build.* 239 (2021), <https://doi.org/10.1016/j.enbuild.2021.110839>.
- [45] B. Ekici, Z.T. Kazanasmaz, M. Turrin, M.F. Tasgetiren, I.S. Sariyildiz, Multi-zone optimisation of high-rise buildings using artificial intelligence for sustainable metropolises. Part 1: background, methodology, setup, and machine learning results, *Sol. Energy* 224 (2021), <https://doi.org/10.1016/j.solener.2021.05.083>.
- [46] C.F. Reinhart, V.R.M. Lo Verso, A rules of thumb-based design sequence for diffuse daylight, *Light. Res. Technol.* 42 (2010), <https://doi.org/10.1177/1477153509104765>.
- [47] J. Lee, M. Boubekri, F. Liang, Impact of building design parameters on daylighting metrics using an analysis, prediction, and optimization approach based on statistical learning technique, *Sustain. Times* 11 (2019), <https://doi.org/10.3390/su11051474>.
- [48] I. Loche, C. Bleil de Souza, A.B. Spaeth, L.O. Neves, Decision-making pathways to daylight efficiency for office buildings with balconies in the tropics, *J. Build. Eng.* 43 (2021), <https://doi.org/10.1016/j.jobe.2021.102596>.
- [49] A. Sepúlveda, F. De Luca, M. Thalfeldt, J. Kurnitski, Analyzing the fulfillment of daylight and overheating requirements in residential and office buildings in Estonia, *Built. Environ.* 180 (2020), <https://doi.org/10.1016/j.buildenv.2020.107036>.
- [50] M. Krarti, P.M. Erickson, T.C. Hillman, A simplified method to estimate energy savings of artificial lighting use from daylighting, *Built. Environ.* 40 (2005), <https://doi.org/10.1016/j.buildenv.2004.08.007>.
- [51] P. Ihm, A. Nemri, M. Krarti, Estimation of lighting energy savings from daylighting, *Built. Environ.* 44 (2009), <https://doi.org/10.1016/j.buildenv.2008.04.016>.
- [52] S.L. Wong, K.K.W. Wan, T.N.T. Lam, Artificial neural networks for energy analysis of office buildings with daylighting, *Appl. Energy* 87 (2010), <https://doi.org/10.1016/j.apenergy.2009.06.028>.
- [53] S. Moret, M. Noro, K. Papamichael, Daylight harvesting: a multivariate regression linear model for predicting the impact on lighting, cooling and heating, *Build. Simul. Appl.* (2013).
- [54] V.R.M. Lo Verso, G. Mihaylov, A. Pellegrino, F. Pellerey, Estimation of the daylight amount and the energy demand for lighting for the early design stages: definition of a set of mathematical models, *Energy Build.* 155 (2017), <https://doi.org/10.1016/j.enbuild.2017.09.014>.
- [55] S. Cammarano, A. Pellegrino, V.R.M. Lo Verso, C. Aghemo, Assessment of daylight in rooms with different architectural features, *Built. Res. Inf.* 43 (2015), <https://doi.org/10.1080/09613218.2014.922359>.
- [56] A. Pellegrino, S. Cammarano, V.R.M. Lo Verso, V. Corrado, Impact of daylighting on total energy use in offices of varying architectural features in Italy: results from a parametric study, *Built. Environ.* 113 (2017), <https://doi.org/10.1016/j.buildenv.2016.09.012>.
- [57] TUT nZEB Research Group, LIGNULENERGIA ELUHOONED RIDA- JA KORTERELAMUD, Tallinn, Estonia, 2017. https://kredex.ee/sites/default/files/2019-03/Lignullenergia_eluhooned_Rida_ja_korterelamu_juhend.pdf.
- [58] N.S. Shafavi, M. Tahsildoost, Z.S. Zomorodian, Investigation of illuminance-based metrics in predicting occupants' visual comfort (case study: architecture design studios), *Sol. Energy* (2020), <https://doi.org/10.1016/j.solener.2019.12.051>.
- [59] A. Nabil, J. Mardaljevic, Useful Daylight Illuminances: A Replacement for Daylight Factors, *Energy Build.* 2006, <https://doi.org/10.1016/j.enbuild.2006.03.013>.
- [60] Illuminating Engineering Society, the Daylight Metric Committee, LM-83-12 Approved Metric: IES Spatial Daylight Autonomy (sDA) and Annual Sunlight Exposure (ASE), 2013.
- [61] E. Brembilla, C.J. Hopfe, J. Mardaljevic, A. Mylona, E. Mantesi, Balancing daylight and overheating in low-energy design using CIBSE improved weather files, *Built. Serv. Eng. Technol.* 41 (2020), <https://doi.org/10.1177/0143624419889057>.
- [62] Estonian Government, Estonian Government Ordinance No 63, Ordinance No 63. (11.12.2018) Hoone energiatõhususe miinimumnõuded. (Minimum requirements for energy performance of buildings), Riigi Teataja 14 (2018), I, 13.12.2018, <https://www.riigiteataja.ee/akt/113122018014?leiaKehiv>.
- [63] R. Simson, J. Kurnitski, M. Maivel, Summer thermal comfort: compliance assessment and overheating prevention in new apartment buildings in Estonia, *J. Build. Perform. Simulat.* (2017), <https://doi.org/10.1080/19401493.2016.1248488>.
- [64] M. Thalfeldt, E. Pikas, J. Kurnitski, H. Voll, Façade Design Principles for Nearly Zero Energy Buildings in a Cold Climate, *Energy Build.*, 2013, <https://doi.org/10.1016/j.enbuild.2013.08.027>.
- [65] F. Kharvari, An empirical validation of daylighting tools: assessing radiance parameters and simulation settings in Ladybug and Honeybee against field measurements, *Sol. Energy* 207 (2020), <https://doi.org/10.1016/j.solener.2020.07.054>.
- [66] Honey Bee. <https://www.ladybug.tools/ladybug.html>, 2020.
- [67] B.S. BSI, Lighting for Buildings, Code of practice for daylighting, 2008, 8206-2.
- [68] G.J. Ward, RTRACE, (n.d.). https://floyd.lbl.gov/radiance/man_html/rtrace-1.html.
- [69] U.S. Department of Energy, EnergyPlus Testing with HVAC Equipment Performance Tests CE100 to CE200 from ANSI/ASHRAE Standard 140-2011, 2015. Washington, D.C. https://energyplus.net/sites/all/modules/custom/nrel_cust_om/epluss_files/current_testing_reports/ASHRAE140-HVAC-CE100200-8.3.0-b45b06b780.pdf.
- [70] M. Etxebarría-Mallea, X. Oreği, O. Grijalba, R. Hernández-Minguillón, The impact of energy refurbishment interventions on annual energy demand, indoor thermal behaviour and temperature-related health risk, *Energy Pol.* 153 (2021), <https://doi.org/10.1016/j.enpol.2021.112276>.
- [71] Y. Ji, R. Fitton, W. Swan, P. Webster, Assessing overheating of the UK existing dwellings - a case study of replica Victorian end terrace house, *Built. Environ.* 77 (2014), <https://doi.org/10.1016/j.buildenv.2014.03.012>.
- [72] I.G. Dino, C. Meral Akgül, Impact of climate change on the existing residential building stock in Turkey: an analysis on energy use, greenhouse gas emissions and occupant comfort, *Renew. Energy* 141 (2019), <https://doi.org/10.1016/j.renene.2019.03.150>.

- [73] T. Van Hooff, B. Blocken, J.L.M. Hensen, H.J.P. Timmermans, Reprint of: on the predicted effectiveness of climate adaptation measures for residential buildings, *Build. Environ.* 83 (2015), <https://doi.org/10.1016/j.buildenv.2014.10.006>.
- [74] A. O' Donovan, M.D. Murphy, P.D. O'Sullivan, Passive control strategies for cooling a non-residential nearly zero energy office: simulated comfort resilience now and in the future, *Energy Build.* 231 (2021), <https://doi.org/10.1016/j.enbuild.2020.110607>.
- [75] V. Pérez-Andreu, C. Aparicio-Fernández, A. Martínez-Ibernón, J.L. Vivancos, Impact of climate change on heating and cooling energy demand in a residential building in a Mediterranean climate, *Energy* 165 (2018), <https://doi.org/10.1016/j.energy.2018.09.015>.
- [76] Estonian Government, Minimum requirements for energy performance, Annex 68 (2012). RT I, 24.01.2014, 3, <https://www.riigiteataja.ee/en/eli/520102014001>.
- [77] M. Thalfeldt, J. Kurnitski, H. Voll, Detailed and Simplified Window Model and Opening Effects on Optimal Window Size and Heating Need, *Energy Build.* 2016, <https://doi.org/10.1016/j.enbuild.2016.06.002>.
- [78] T. Simko, T. Moore, Optimal window designs for Australian houses, *Energy Build.* 250 (2021), <https://doi.org/10.1016/j.enbuild.2021.111300>.
- [81] Estonian Government, N. 58 Ordinance, Methodology for calculating the energy performance of buildings, RTI 2015 (2015) 21, 09.06.
- [82] R. Simson, J. Kurnitski, K. Kuusk, Experimental validation of simulation and measurement-based overheating assessment approaches for residential buildings, *Architect. Sci. Rev.* (2017), <https://doi.org/10.1080/00038628.2017.1300130>.
- [83] S. Sayın, G. Çelebi, A practical approach to performance-based building design in architectural project, *Build. Res. Inf.* 48 (2020), <https://doi.org/10.1080/09613218.2019.1669008>.
- [84] A. Sepúlveda, F. De Luca, A multi-objective optimization workflow based on solar access and solar radiation for the design of building envelopes in cold climates, in: *Symp. Simul. Archit. Urban Des.*, TU Wien, Vienna, 2020. https://www.researchgate.net/publication/341775963_A_Multi-Objective_Optimization_Workflow_based_on_Solar_Access_and_Solar_Radiation_for_the_Design_of_Building_Envelopes_in_Cold_Climates.
- [85] H. Voll, M. Thalfeldt, F. De Luca, J. Kurnitski, T. Olesk, Urban planning principles of nearly zero-energy residential buildings in Estonia, *Manag. Environ. Qual. Int. J.* (2016), <https://doi.org/10.1108/MEQ-05-2015-0101>.
- [86] S. Wang, Y.K. Yi, N. Liu, Multi-objective optimization (MOO) for high-rise residential buildings' layout centered on daylight, visual, and outdoor thermal metrics in China, *Build. Environ.* 205 (2021), <https://doi.org/10.1016/j.buildenv.2021.108263>.
- [87] S. Kleindienst, M. Andersen, Comprehensive annual daylight design through a goal-based approach, *Build. Res. Inf.* 40 (2012), <https://doi.org/10.1080/09613218.2012.641301>.

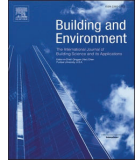
Paper IV

Sepúlveda, A., Bueno, B., Wang, T., & Wilson, H. R. (2021). Benchmark of methods for annual glare risk assessment. *Building and Environment*, 201, 108006.



Contents lists available at ScienceDirect

Building and Environment

journal homepage: www.elsevier.com/locate/buildenv

Benchmark of methods for annual glare risk assessment

Abel Sepúlveda^{c,*}, Bruno Bueno^a, Taoning Wang^b, Helen Rose Wilson^a^a Fraunhofer Institute for Solar Energy Systems ISE, Germany^b Building Technology and Urban Systems, Lawrence Berkeley National Laboratory, USA^c Tallinn University of Technology, Department of Civil Engineering and Architecture, Estonia

ARTICLE INFO

Keywords:

Glare
Radiance
BSDF
Complex fenestration systems
Fabric shading
Visual comfort

ABSTRACT

Visual comfort in buildings has a critical impact on occupants' health and mental performance. Among the visual comfort functions, daylighting glare is the most complex phenomenon to assess by architects and practitioners. This paper aims to benchmark state-of-the-art methods for annual glare analysis and develop strategies to reduce the computational time (CPU time) without compromising the accuracy of glare calculations. The Radiance-based tool *rtrace* and the Radiance-based five-phase method (5pm) are applied to a single room. Analytical isotropic fabric systems are parametrized in terms of specular/diffuse scattering components and cut-off angle. Peak extraction considered by Radiance's aBSDF material primitive is key to having an accurate representation of the luminance maps and vertical illuminance at eye level and glare calculations. A minimum number of ambient bounces (ab parameter) of 4 when using Radiance's *rtrace* program achieves the best trade-off between accuracy in vertical illuminance and daylight glare probability (DGP), and CPU time. Based on semi-annual and five days per week simulations for visible sun positions, sampling strategies can decrease the CPU time for annual glare simulations up to 86% when considering clear sky conditions. The most suitable method for DGP simulations depends strongly on the Radiance parameters and the chosen sampling strategy.

1. Introduction

Visual comfort in buildings has a critical impact on occupants' health [1,2] and mental performance [3]. At the same time, daylight is the most preferred light source by building users [4]. Many contemporary buildings are designed with highly glazed facades, which might be beneficial for daylighting indoor spaces and visual contact with the outside. Nevertheless, excess light can be disturbing for the human eye. Most of the international building standards include recommendations to ensure visual comfort and energy performance [5,6]. According to the European Standard EN 17037:2018 [7], the achievement of suitable visual comfort depends on the level of daylight provision, view out, sunlight exposure, and glare protection in indoor spaces. The requirements of view out and sunlight exposure are based on metrics that can be calculated geometrically. Daylight provision can be quantified in terms of metrics for which consolidated calculation methods exist [8–11]. By contrast, glare protection is difficult to assess since it depends on many factors [12], some of them related to the psychology and physiology of human beings [13]. Survey techniques in combination with simulation-based methods have been widely used to predict glare

in indoor spaces [14–17].

1.1. The daylight glare probability metric

A recent comparative study that involved 22 different glare metrics showed that the DGP is the most robust glare metric for office-like test rooms [18]. There are two main effects to quantify visual glare in practice. The saturation effect is related to the brightness of the field of view. The contrast effect is influenced by the luminance distribution of the scene. The DGP formula was proposed by Wienold and Christoffersen [17]. The first term is proportional to the vertical illuminance at eye level (E_v) and represents the saturation effect. The second term quantifies the contrast effect of the scene, which is related to the luminance of the glare sources L_s (cd/m^2), the solid angle subtended by the sources ω_s (sr), Guth's position index (P), and E_v (Eq. (1)). For DGP values lower than 0.2, additional experiments are recommended to confirm the validity of the equation in that region [17].

$$DGP = 5.87 \cdot 10^{-5} E_v + 9.18 \cdot 10^{-2} \log \left(1 + \sum_i \frac{L_{s,i}^2 \cdot \omega_{s,i}}{E_v^{1.87} P_i^2} \right) + 0.16 \quad (1)$$

Glare protection classes defined in the EN 17037:2018 [7] are based

* Corresponding author.

E-mail address: absepu@taltech.ee (A. Sepúlveda).

Nomenclature		
CFS	Complex Fenestration System	resolution –t 3 7
BSDF	Bidirectional Scattering Distribution Function	t37a Radiance aBSDF material with tensor tree angular resolution –t 3 7
BSDF material	Radiance material defined with BSDF data set without considering peak extraction	t38 Radiance BSDF material with tensor tree angular resolution –t 3 8
aBSDF material	Radiance BSDF material with peak extraction	t38a Radiance aBSDF material with tensor tree angular resolution –t 3 8
CIE	Commission Internationale de l'Éclairage	t39 Radiance BSDF material with tensor tree angular resolution –t 3 9
E_v	Vertical illuminance at eye level	t39a Radiance aBSDF material with tensor tree angular resolution –t 3 9
CPU time	Computational time	t45 Radiance BSDF material with tensor tree angular resolution –t 4 5
DGP	Daylight Glare Probability	t45a Radiance aBSDF material with tensor tree angular resolution –t 4 5
DGPs	Simplified Daylight Glare Probability	Klemsa Radiance aBSDF material with Klems basis angular resolution (145×145)
eDGPs	Enhanced Simplified Daylight Glare Probability	τ_{nn} Normal-normal visible transmittance or openness factor
fDGp	Percentage of glare discomfort hours during a year with a threshold (DGpT)	τ_{nh} Normal-hemispherical visible transmittance
DC	Two-phase method	τ_{ndif} Normal-diffuse visible transmittance
3pm	Three-phase method	$\tau_{dir,dir}$ Direct-direct visible transmittance
3 pmD	Three-phase method considering direct component of the solar radiation	$\tau_{dir,h}$ Direct-hemispherical visible transmittance
cds	Direct sun coefficient simulation	$\tau_{dir,dif}$ Direct-diffuse visible transmittance
5pm	Five-phase Method	ρ_{ndif} Normal-diffuse visible reflectance
ab	Number of ambient bounces	
ad	Number of ambient divisions	
MF	Number of Reinhart sky-patch subdivisions	
t37	Radiance BSDF material with tensor tree angular	

on previous studies with fabrics and the DGP developed by Wienold [19]. For DGP values lower or equal to 0.35, daylight glare is considered imperceptible. DGP values higher than 0.35 and lower than 0.40 are associated with perceptible but mostly not disturbing visual glare. When DGP values are higher than 0.40 and lower than 0.45, glare is perceptible and often disturbing. Finally, DGP values higher than 0.45 are associated with disturbing daylighting glare. According to EN 17037, the annual percentage of discomfort glare hours (fDGpT) should be lower than 5% for a shading device to protect against glare.

1.2. Annual glare risk assessment

The development of the open-source software Radiance based on the ray-tracing technique allowed reliable climate-based daylight modelling in buildings (CBDDM) [20]. The Radiance program evalglare can calculate several glare metrics [21,22]. DGP calculations use evalglare to process a rendering of a scene (.hdr file) as seen from an observer for which glare is to be evaluated. A suitable daylight model (daylight method, sky model, optical properties of the opaque surfaces, and complex fenestration systems (CFSs) in a room) is crucial to calculate reliable illuminance values and luminance distributions of the field of view. Several sky models can be modelled in Radiance: from continuous sky models based on CIE [23] or Perez skies [24] to discretized skies using Tregenza or Reinhart subdivision schemes [25]. While continuous sky models are commonly used when using the classic Radiance *rtrace* method, discrete skies are applied to matrix-based daylight methods [26,27]. The Radiance *rtrace* method has been used mainly for static glare analysis because of its reliability and high computational requirements (CPU time) [28]. Speedup strategies such as the use of *rtrace* with null ambient bounces (ab 0) to generate the luminance maps in combination with vertical illuminance calculations were used to approximate the DGP. Wienold et al. called this approximation of the DGP method “enhanced simplified DGP” (eDGPs) [19].

Matrix-based methods can recycle information from the whole scene: view, daylight, and sky matrix. The most widely used matrix-based methods are the 2-phase (DC), 3-phase (3pm), and 5-phase method (5pm). The transmission matrix contains the optical properties of the

CFS for the input and output angular hemispheres. These optical properties are calculated from bidirectional scattering distribution function (BSDF) datasets, which represent the angular distribution of light scattered by the CFS. BSDF datasets can be obtained via measurement using a photogoniometer [29–31] or via simulation using ray-tracing or analytical techniques [32,33]. As an example of ray-tracing techniques, the Radiance *genBSDF* program was used to generate BSDF datasets of CFS such as venetian blinds [34] and complex three-dimensional textiles [35,36].

The DC and 3pm are reliable for annual daylighting calculations with static and switchable CFSs, respectively [27]. The 5pm applies the indirect contribution from the sky from the 3pm and the direct component of the sun from an accurate DC simulation using a large number of Reinhart sky subdivisions (MF parameter) [37]. Indeed, the 5pm and *rtrace* methods were proven to be more reliable than the 3-phase method for DGP calculations [26,38]. Abravesh et al. proposed another method for annual glare assessments based on the eDGPs where E_v is calculated using the 3pm [39].

CFSs with angle-dependent specular transmittance such as glazing systems or simple fabrics (with assumable isotropic light scattering and a view-through specular component without light-redirecting effects) can be modelled using the BRDFfunc material primitive in Radiance [19] (based on the Roos model function [40]). For more complex shading devices, optical characterization using anisotropic and/or high-resolution BSDF datasets is recommended in the literature.

Many factors can influence the choice of the best method for annual glare assessment: the type of CFS and its model material, parameters for renderings, parameters for illuminance calculations, number of time steps, number of scenes (different viewpoints, viewing directions, surface materials, etc.), and number of CFSs. In practice, there is a lack of consideration of trade-off criteria for annual glare assessment. Suitable knowledge of these factors could help software developers to implement optimized models for glare risk assessment. This paper’s findings could also guide experienced architects and practitioners to set up annual glare simulations according to the detailed method proposed in the EN 17037 standard. The practical implications of this research can contribute to the efficient design of building facades based on glare

Table 1

Radiance parameters used for glare simulations by *rtrace* and 5 pm cd refer to the direct coefficient sun simulation. 3 pmD refers to 3pm simulation of the 5pm considering only the direct component of the solar radiation.

Radiance parameters		
5pm	3pm	Sky generation: +s (CIE clear sky) -m 1 (MF = 1) Daylight matrix: n 25 -c 1500 -ab 4 -ad 1024 -lw 9.76e-4 View matrix: n 25 -c 10 -ab 10 -ad 65536 -lw 1.53e-5 -pj 0.7 -x 900 -y 900
	3pmD	Sky generation: +s (CIE clear sky) -m 1 (MF = 1) -d (direct component of the sun) Daylight matrix: n 25 -c 1500 -ab 0 -ad 1024 -lw 9.76e-4 View matrix: n 25 -c 10 -ab 1 -ad 65536 -lw 1.53e-5 -pj 0.7 -x 900 -y 900
	cds	Sky generation: MF = 3 (1297 sky subdivisions) [27] Daylight coefficient matrix: n 25 -ab 1 -ad 1024 -pj 0.7 -dc 1 -dt 0 -dj 0 -x 900 -y 900 MF = 3
rtrace		-n 25 -lw 1/ad -aa 0.1 -as 1000 -x 900 -y 900 (The selection of -ad and -ab parameters is justified in section 3)

protection and daylight provision.

1.3. Aims of the investigation

The aims of this paper can be summarized as follows:

- To benchmark state-of-the-art methods for annual glare analysis in terms of accuracy and computational time (CPU time),
- To analyse the influence of Radiance parameters and Radiance materials on the accuracy of daylight glare calculations,
- To propose time step sampling strategies to speed up the CPU time of annual glare calculations.

2. Methodology

We used a simulation-based methodology, based on static and annual glare analyses of synthetic fabrics, to study how modelling factors can influence daylight glare calculations in terms of accuracy and CPU time. We evaluated glare simulations' accuracy in terms of vertical illuminance at eye level, DGP, and luminance maps. The analysed factors are the following: optical behaviour of CFS, the method to generate BSDF datasets, Radiance material to model CFS, daylight calculation method, Radiance parameters, and sampling strategy (selection of time steps representative of one year for annual glare calculations).

2.1. Daylight methods and radiance parameters

We used the Radiance software v5.4.a for illuminance calculations and renderings [41]. Specifically, the chosen daylight methods were the classic ray-tracing-based daylight method *rtrace* [42] and matrix-based methods 3pm and 5pm [26]. A BSDF Klems data set in.xml format (transmission matrix) is required in 3pm and 3 pmD simulations while CFS in cds phase and *rtrace* method can be modelled with different Radiance materials explained in sections 2.2 and 2.3. One of the difficulties in applying these methods is the selection of Radiance parameters for the simulation. We studied the sensitivity of ambient bounces (ab parameter) and ambient divisions (ad parameter) when using the daylight methods *rtrace* and 3pm [42]. In addition, we analysed the sensitivity to the ad parameter and the number of Reinhart sky-patch subdivisions (MF parameter) in 5pm calculations [43]. The parameters ab and ad determine the accuracy of the calculation for indirect light from the sky. The MF parameter is related to the accuracy of the sun positions and sky modelling in the direct sun coefficient calculation (cds) within the 5pm simulation. Additional Radiance parameters used for the calculations in this investigation can be seen in Table 1. These Radiance parameters are recommended in several Radiance tutorials [37,44] and previous investigations [45,46]. We used 25 cores of a Linux

Table 2

Optical properties for BRTDfunc model for 4 synthetic fabrics (modelled by Roos parameters $p = 4.0$, $q = 2.9$ [40]). τ_{nn} is the normal-normal transmittance, τ_{ndif} is the normal-diffuse transmittance, and ρ_{ndif} is the normal-diffuse reflectance.

Name	τ_{nn} (-)	τ_{ndif} (-)	ρ_{ndif} (-)	Cut-off angle (°)
T100	1.0	0	0	90
T5	0.05	0.15	0.60	70
T3	0.03	0.15	0.60	70
T1	0.01	0.15	0.60	70

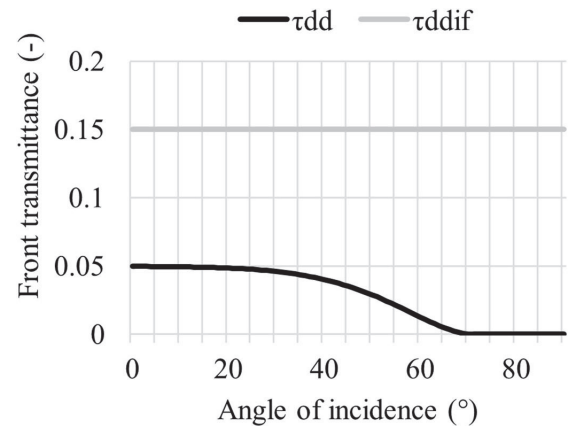


Fig. 1. Analytical fabric model based on the BRTDfunc model.

machine cluster of 56 CPUs to run all the simulations (Processor Intel(R) Xeon(R) CPU E5-2697 v3 @ 2.60 GHz).

2.2. Selection of fenestration systems

In this study, we consider synthetic fabrics with different optical properties. This allows us to parametrize important characteristic of shading devices such as the specular/diffuse split and the cut-off angle (minimum incident angle for which a CFS completely blocks specular transmission), which are used in the EN 17037 for classification. Fabrics are in general anisotropic depending on the weaving direction. However, for the purposes of this analysis, fabrics are modelled with the Radiance primitive BRTDfunc as being isotropic (due to random or uniform microgeometry [47]) with a main view-through component. The BRTDfunc material considers separate specular and diffuse components and a cut-off angle. This approach is a modified version of the analytical Roos model for fabrics defined by Wienold et al. [19]. BSDF of these synthetic fabrics are then generated for the analysis. The accuracy of the simulations with different BSDF representations is assessed as compared with the simulation results using the original material definition (i.e., the BRTDfunc model is considered the "gold standard" in this particular study).

One set of fabrics are considered, Table 2 shows the main optical properties for three synthetic fabrics (normal-normal transmittances: 5%, 3%, and 1%) and a representation of a window hollow (no glazing nor shading) named T100 (100% transmission). The cut-off angle of fabrics T5, T3, and T1 was set to 70°. The diffuse reflectance was set to 60% related to a light grey coloured fabric.

2.3. Generation of BSDF datasets

In this paper, BSDF data sets were generated using direct functional sampling [47,48], as an alternative to the virtual goniophotometer approach as described by McNeil et al. [32,33] and implemented in the

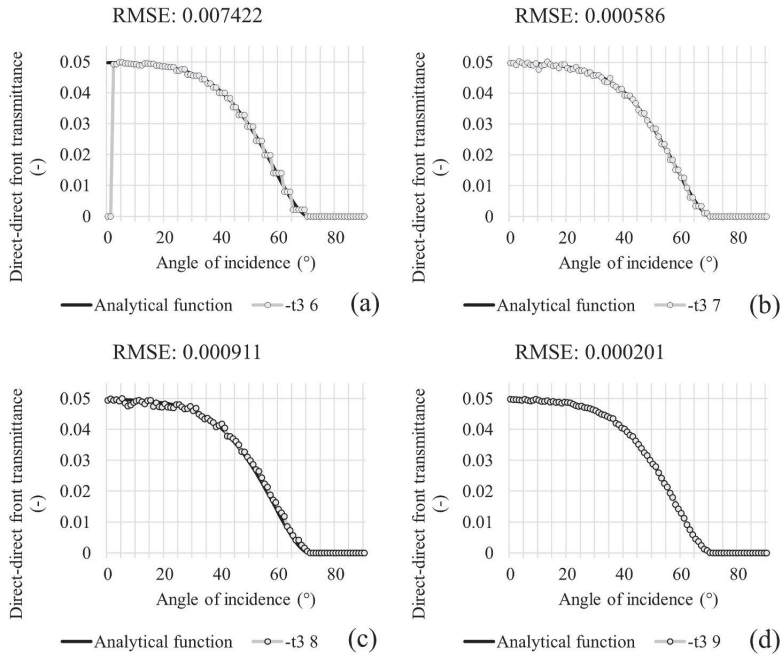


Fig. 2. Direct-direct transmittance depending on the angle of incidence for four different isotropic tensor-tree BxDF generated with the Radiance program bsdf2tree. The angular resolution (α) of the isotropic tensor-tree (-t3 α) BxDFs are 6 (a), 7 (b), 8 (c), and 9 (d).

Radiance *genBSDF* program. Direct functional sampling consists of applying the mathematical function that represents the optical behaviour of the material (e.g., the BRTDfunc), sampling rays for each incident and outgoing projected solid angle as required by the BxDF format (e.g. tensor tree generation 7 or Klems). By default, complete sampling consists of 1024 rays per solid angle. However, an adaptive sampling mechanism is in place to reduce the sampling time. Adequate sampling

resolution to obtain a robust approximation of the direct-direct transmission can be evaluated using the Nyquist sampling frequency law [49], where, for example, a 0.5° subtended angle of direct-direct transmission would require a sampling resolution of generation 9 tensor tree, roughly a 0.35° subtended angle.

An analytical fabric model based on the BRTDfunc material is analysed. The direct-direct and direct-diffuse transmittance functions and

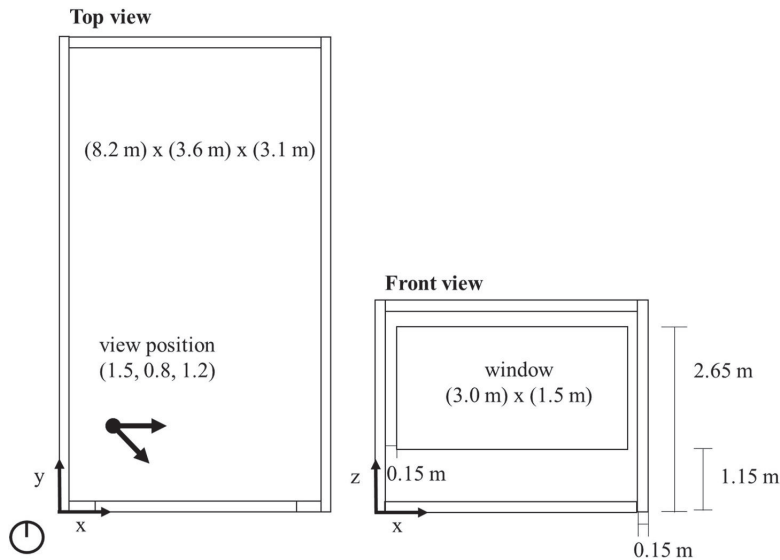


Fig. 3. Geometrical information for the south-oriented room, occupant's position and viewing directions.

Table 3a
Reflectance values for opaque surfaces recommended by the standard EN17037 [7].

Surface	Reflectance
Interior walls	50%
Floor	20%
Ceiling	70%
External floor	20%

the cut-off angle of the T5 fabric (Table 1) are illustrated in Fig. 1, where the direct-direct transmittance falls to zero at the cut-off angle of 70° and the direct-diffuse transmittance is constant.

Tensor-tree BSDFs were generated using the bsdf2tree program, where the incident and scattered ray pairs are sampled over each solid angle depending on the tensor-tree resolution. A subtended apex angle of 0.533° (the solid angle of the solar disk) is assumed for direct-direct transmission. Rays scattered beyond this solid angle are allocated to the direct-diffuse transmission. Fig. 2 shows that, with an adaptive sampling algorithm, increasing the resolution of the tensor tree decreases the RMSE of direct-hemispherical transmissivity between the

Table 3b

Summary of all the analyses conducted in this investigation. Sec. = section, DCM = daylight calculation method, rΔ = relative deviation, Glaz = solar-control double glazing unit, and aΔ = absolute deviation. The time steps are for February 5, Freiburg, Germany. Viewing angle refers to the angle between viewing direction and window plane.

Sec.	Time steps	Viewing angle	CFSs	Radiance material	DCM	Metrics	Output
3.1.1	11:00	–	T100 T5 T3 T1	BRTDfunc	3pm 5pm rtrace	rΔE _v (%)	Optimal Radiance parameters
3.1.2	11:00	45°	T5	BRTDfunc, t45a t45 t39a t39 t38a t38	3pm 5pm	DGP (–) E _v (lux)	Suitable material representations
	16:00		T3 T1	t37at37 Klemsa	rtrace		
3.2	Annual	0°	T1/T3/T5	BRTDfunc	5pm rtrace	CPU time	Fastest daylight calculation method
3.3.1	11:00	0°	T1 T3 T5	BRTDfunc	rtrace	aΔCPU time (s) aΔDGP (–) aΔE _v (lux)	Optimal ab parameter
3.3.2	Annual	45°	Glaz + T1 Glaz + T3 Glaz + T5	Klemsa	5pm rtrace	CPU time (h) aΔfDGPt (%)	Optimal time step sampling strategy

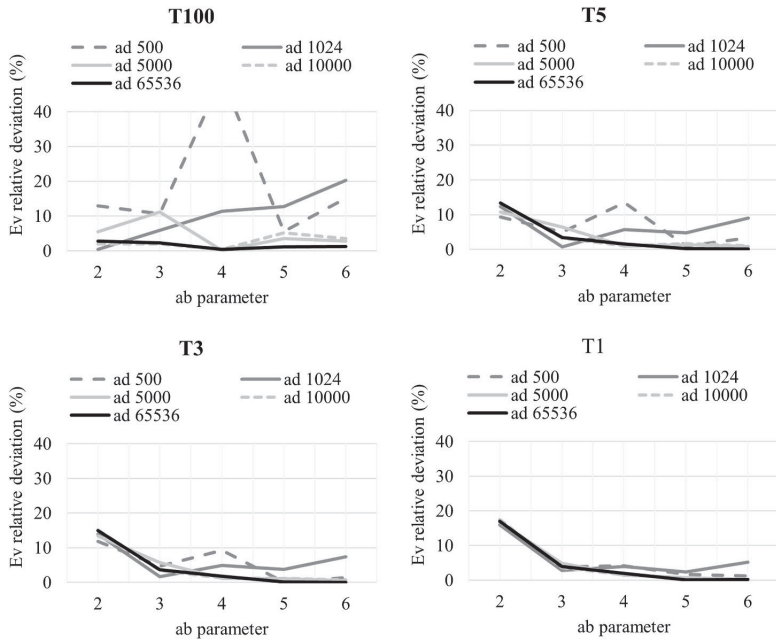


Fig. 4. Relative deviation (with respect to the previous ab value: 2 relative to 1, 3 relative to 2, etc.) of vertical illuminance at eye level (Ev) calculated with the 3-phase method (11:00 February 5) for different ad, ab parameters, and fabrics T100 (upper left), T5 (upper right), T3 (bottom left), and T1 (bottom right).

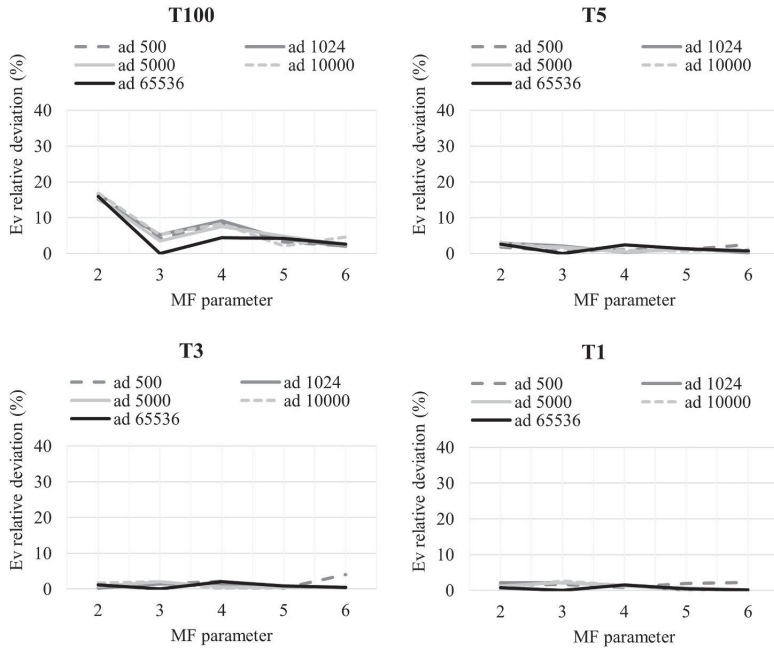


Fig. 5. Relative deviation (with respect to the previous ab value: 2 relative to 1, 3 relative to 2, etc.) of vertical illuminance at eye level (Ev) calculated with the 5-phase method (11:00 February 5) for different ad, ab parameters, and fabrics T100 (upper left), T5 (upper right), T3 (bottom left), and T1 (bottom right).

BSDF and the analytical function.

We analysed the following angular resolutions: Klems basis, t37, t38, and t39. Although only isotropic materials are considered in this study,

an anisotropic tensor-tree t45 was included in the comparison. For a generic tensor tree $-t3/-t4$ k, k refers to generation of 2^{2k} directions per hemisphere [26]. BSDF datasets were modelled with BSDF and aBSDF

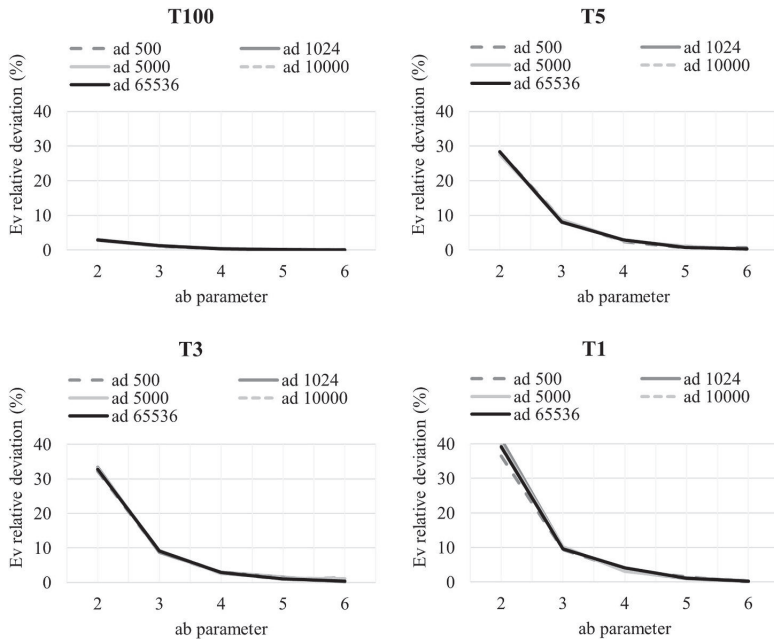


Fig. 6. Relative deviation (with respect to the previous ab value: 2 relative to 1, 3 relative to 2, etc.) of vertical illuminance at eye level (Ev) calculated with the *rtrace* method (11:00 February 5) for different ad, ab parameters, and fabrics T100 (upper left), T5 (upper right), T3 (bottom left), and T1 (bottom right).

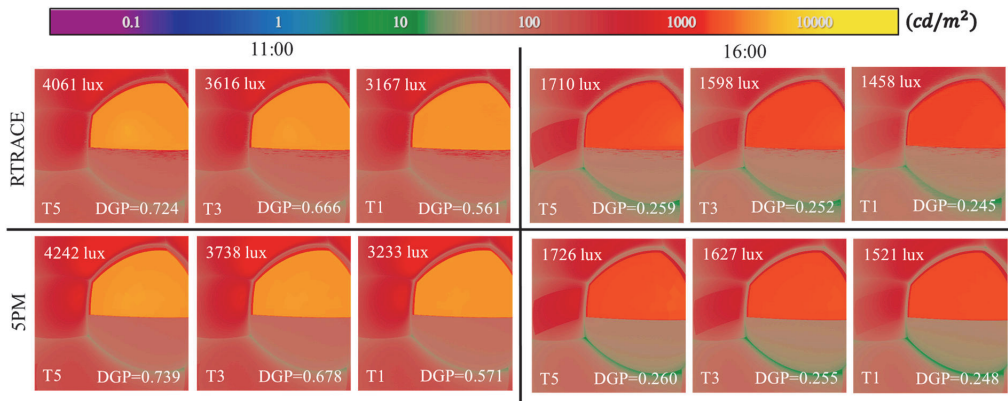


Fig. 7. Luminance maps, vertical illuminances and DGP at 11:00 (first three columns) and at 16:00 (last three columns) on February 5, in Freiburg, Germany, generated by the 5pm (upper row) and *rtrace* (bottom row) methods when using isotropic fabrics with different openness factor (5%, 3%, and 1%) defined with an analytical BRDFfunc model.

materials in Radiance. The aBSDF material definition includes a peak extraction algorithm, which separates the transmission peaks, associated with the view-through component of the transmission, from the rest of the BSDF dataset [47]. We did not use proxy geometry of fabrics because the storage of their tiny geometry leads to very large computational consuming simulations. Therefore, we assigned these material definitions directly to a polygon surface that represents the window.

2.4. Definition of the case study

This study considers a south-oriented test room with two different viewing directions, parallel to the window plane and 45° towards the window (Fig. 3). All the opaque surfaces were modelled with the Plastic material primitive in Radiance with reflectance values recommended by the European standard EN17037 [7] (Table 3a). The room is located in Freiburg, Germany (latitude: 48°N). The day of study for the static analyses is February 5 because of the low solar altitude, which is critical for daylight glare. No exterior obstacle is considered in this case study. We assumed clear sky conditions for all the simulations (CIE clear sky with the presence of the sun) as is recommended by the EN 17037 for the verification of the glare protection capabilities of shadings for a critical situation [7]. In fact, typical weather files might hide a glare risk if, for a particular situation with a critical sun position, the weather file indicates a cloudy sky. Therefore, we believe that for annual glare analyses, clear skies should be considered in the simulation. This represents a worst-case scenario which is suitable for choosing (sizing) a glare protection device.

3. Results

This section 3 is divided into three parts. The first two aim to benchmark simulation methods in terms of accuracy and computational speed, respectively, while the third part proposes strategies for computationally efficient annual glare simulations. For each part, we have selected a fit-to-purpose simulation setup, which is summarized in Table 3b.

3.1. Benchmark of methods in terms of accuracy

3.1.1. Sensitivity analysis of radiance parameters

This static analysis aims to investigate the influence of Radiance parameters and the openness factor (fabrics T100, T5, T3, and T1) on vertical illuminance at eye level calculated by different methods (3pm,

5pm, and *rtrace*). The analysed time instant for this sensitivity analysis is 11:00 on February 5. At this time, the solar disk is in the field of view. We assumed an acceptable relative deviation in terms of vertical illuminance of 15%. In Fig. 4, the vertical illuminance at eye level calculated with the 3-phase method for different ad and ab parameters is shown. The minimum values of the ad and ab parameters to have an acceptable vertical illuminance are 5000 and 3, respectively.

The vertical illuminance at eye level calculated with the 5pm for different Radiance parameters can be seen in Fig. 5. The Radiance parameters chosen for this sensitivity analysis are ad and MF in the direct sun coefficient simulation (cds). The ab and ad parameters for the 3-phase method were set to 10 and 65536, respectively [37] to minimize the uncertainty from 3pm and 3 pmD calculations. The minimum values of ad and MF parameters for the cds phase in order to have acceptable vertical illuminance calculated by the 5pm are 500 and 3, respectively.

Fig. 6 shows the vertical illuminance at eye level calculated with the *rtrace* method for different ad and ab parameters. The minimum values of ad and ab parameters to have acceptable vertical illuminance are ad 500 and ab 4, respectively. Previous investigation regarding complex 3D textiles used an ab parameter of 5 for the time-point DGP calculations [36]. In summary, the ad parameter does not have significant influence on illuminance calculations when an analytical BRDFfunc model is applied to characterize the optical behaviour of fabrics. However, the ab and MF parameters have relevant influence on the results, with 3 and 4 being the minimum recommended ab parameters when using the 3pm and *rtrace* method, respectively. The minimum MF parameter for 5pm simulations is 3. In section 3.3.1, we review this conclusion when we analyse the sensitivity of DGP to the ab parameter for generic glare protection fabrics.

3.1.2. Comparison of methods and material models

The aim of this static analysis is to study the influence of different Radiance materials, angular resolutions to represent the BSDF data, and daylight calculation methods on vertical illuminance, DGP, and luminance maps. Two time steps were considered: February 5 at 11:00, when the solar disk is in the field of view, and 16:00, when the solar disk is not in the field of view (but a bright patch from direct solar transmission onto the east-oriented wall is present). In this study, one viewing direction is selected: 45° towards the window. In this analysis, we focused on three isotropic fabrics: T5, T3, and T1 (see section 2.2), which were modelled using different Radiance materials (BRDFfunc, BSDF, and aBSDF) and angular resolutions (Klems basis and tensor tree). We

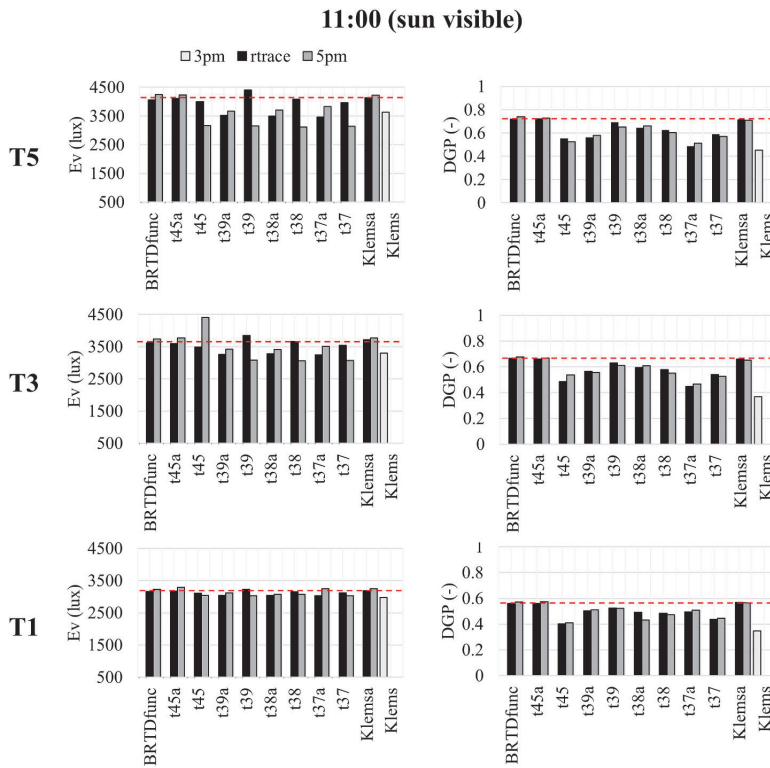


Fig. 8. Vertical illuminance at eye level (left column) and DGP values (right column) at 11:00 (February 5) for different daylight methods, Radiance materials, and fabrics (T5 (first row), T3 (second row), and T1 (third row)). The suffix a refers to the Radiance material aBSDF. The number of ambient divisions (ad parameter) is 1024, 500, and 1e6 for 5pm, *rtrace* (BRTDfunc and aBSDF material), and *rtrace* (BSDF material). Discontinuous line refers to the reference value (BRTDfunc material).

generated four BSDF datasets considering tensor tree formalisms (resolutions -t3 7, -t3 8, -t3 9, and -t4 5 by using the BSDF2tree method (see section 2.3)). Two Radiance materials were used: aBSDF (with peak extraction algorithm) and BSDF (without peak extraction algorithm) materials. An additional BSDF dataset using the Klems angular description (145×145 patches) was generated and modelled with aBSDF material (with peak extraction). Radiance parameters for the simulations are indicated in Table 1. Here, the ambient bounces and ambient divisions were set to $ab = 4$ and $ad = 500$, respectively, according to section 3.1.1. However, this ad value leads to an underestimation of the illuminance when tensor-tree BSDF formats without peak extraction are used with *rtrace*. In order to get acceptable results in this case, the ad parameter has to be increased to $ad = 1e6$ [47]. This leads to 51 times more CPU time when using tensor-tree BSDF formats without peak extraction in the DGP calculation. On the other hand, it was demonstrated that the results of the 5pm do not improve in a conclusive fashion when either the ad or the MF parameters are increased. The luminance maps for fabrics T5, T3, and T1 are displayed in Fig. 7. In general, the *rtrace* and 5pm methods show good agreement in terms of vertical illuminance, DGP values, and luminance distributions.

The results of the comparison are shown in Fig. 8 and Fig. 9. The comparison is very different, depending on whether the solar disk is in the field of view or not. If the solar disk is not within the field of view, all analysed cases predict a similar DGP, which ranges between 0.24 and 0.26. The difference in vertical illuminance calculated by the different methods ranges between 200 lux and 400 lux. The lowest value of vertical illuminance is obtained with the 3pm, which scatters the light into large solid angles (Klems patches), sometimes leading to

discrepancies for point-in-space calculations. It is, however, known that the 3pm calculates the average illuminance over a plane reliably and is therefore suitable for daylighting calculations.

For the time step in which the solar disk is in the field of view, the discrepancies among the different methods are significant. The reference values for the comparison are those calculated by directly applying the BRTDfunc material in the ray-tracing calculation, because this material is the one used to generate the BSDF. The material definitions and BSDF resolutions that get closer to the reference value are t45a and Klemsa, both applying the peak extraction algorithm. A tensor-tree format without peak extraction must have a resolution of exponent 9 (2^9) to reach a DGP value within ± 0.05 of the one calculated for the reference case (by using $ad = 1e6$). The peak extraction algorithm combined with the tensor-tree format does not improve the comparison.

It can be concluded that the choice of the optical representation of the fenestration has a critical impact on the DGP calculation. As reported in the literature [26,38], the 3pm is not suitable for DGP calculations when the solar disk is in the field of view. However, due to its simplicity and low computational requirements, the Klems BSDF with peak extraction (aBSDF Radiance material) might offer an efficient representation of anisotropic fabrics with a main view-through component for glare calculations.

3.2. Benchmark of methods in terms of computational speed

In this section 3.2, a detailed time analysis for annual glare assessments is presented. For annual simulations, the number of time steps, scenes and CFSs affect the CPU time, which can be decisive in

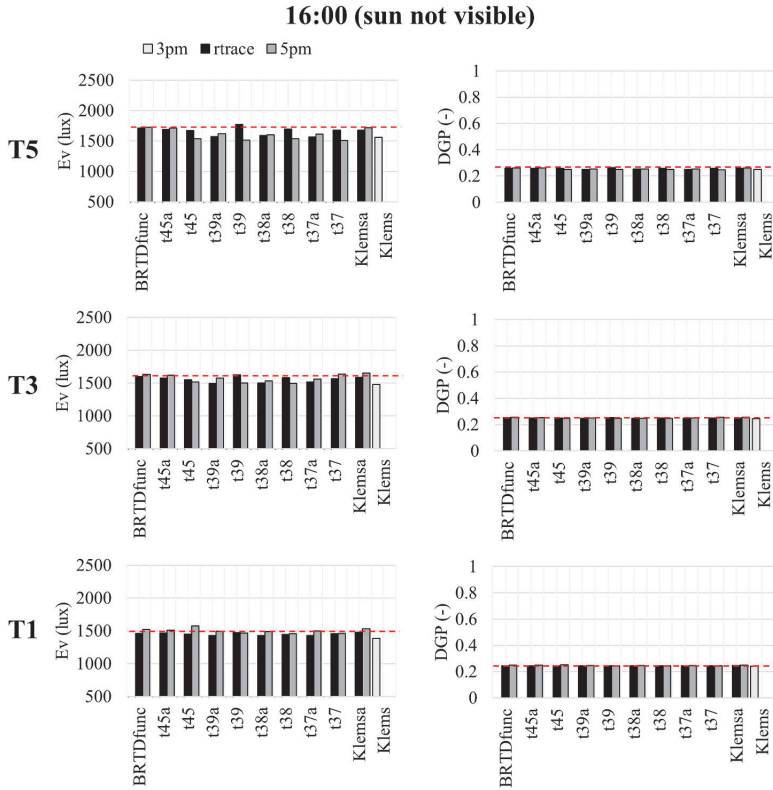


Fig. 9. Vertical illuminance at eye level (left column) and DGP values (right column) at 16:00 (February 5) for different daylight methods, Radiance materials, and fabrics (T5 (first row), T3 (second row), and T1 (third row)). The suffix refers to the Radiance material aBSDF. The number of ambient divisions (ad parameter) is 1024, 500, and 1e6 for 5pm, *rtrace* (BRTDfunc and aBSDF material), and *rtrace* (BSDF material). Discontinuous line refers to the reference value (BRTDfunc material).

determining the most suitable daylight calculation method. Typically, the number of time steps in annual glare simulations is referred to daytime hours (4380). The number of different scenes depends on the number of view positions and directions to assess glare risk as well as the different geometrical models (geometrical variations of the 3D model that represent the interior/exterior scenes). As mentioned in section 1, the 5pm reuses information referring to the scene. Nevertheless, a direct simulation based on the DC (phase cds) must be conducted for every window state, which may compromise the use of the 5pm when the number of different facade states or scenes is large. Moreover, the *rtrace* method does not reuse information for the scene or the sky, being slower than the 5pm for annual DGP calculations without a sampling strategy. Annual glare analyses with different Radiance parameters and sampling strategies could justify the use of one or the other method.

The first objective of this section 3.2 is to define the CPU time required by any annual glare assessment when using the *rtrace* and 5pm methods. This time analysis is based on formulas that represent the coding structure of the required Radiance commands to run the *rtrace* method and 5pm simulations [27]. The second objective is to propose a criterion based on CPU time for the selection of the daylight method depending on the annual glare analysis of interest. The independent variables that define any annual glare analysis are the number of scenes (n), number of time steps (h), and the number of CFSs considered (c). Thus, the CPU time required by the 3pm can be expressed as follows:

$$\tau_{3pm} = I_s h + n(I_M + I_{dc} h c) \quad (2)$$

Where:

- t_s = CPU time required to create a sky vector (S) (the same for illuminance calculations and rendering generation),
- t_M = CPU time required to create the view (V) and daylight (D) matrices (for illuminance calculations and rendering generation),
- t_{dc} = CPU time required for the multiplication of the matrices V, T, D, and S (for illuminance calculations and rendering generation).

The CPU time required by the 5pm for the direct 3pm (3 pmD) is the following:

$$\tau_{3pmD} = I_{sD} h + n(I_{MD} + I_{dcD} h c) \quad (3)$$

Where:

- t_{sD} = CPU time required to create a sky vector (S_D) with the exclusive contribution of the sun (the same for illuminance calculations and rendering generation),
- t_{MD} = CPU time required to create the octree (black plastic material), view with $ab = 1$ (V_D), and daylight with $ab = 0$ (D_D) matrices (for illuminance calculations and rendering generation),
- t_{dcD} = CPU time required for the multiplication of the matrices V_D , T, D_D , and S_D (for illuminance calculations and rendering generation),

The CPU time required by the cds phase of the 5pm is the following:

$$\tau_{cds} = I_{sF} h + n(I_{MF} + I_{cds} c + I_{dcF} h c) \quad (4)$$

Where:

t_{sF} = CPU time required to create a sky vector (S_{cds}) with only the contribution of the sun and selected Reinhart sky subdivisions (MF) (the same for illuminance calculations and rendering generation),
 t_{MF} = CPU time required to create the suns (the same for illuminance calculations and rendering generation) and material map generation (for rendering),
 t_{cds} = CPU time required to create the octree (black plastic material) and sun coefficient matrix C_{cds} (for illuminance calculations and rendering generation),
 t_{dcS} = CPU time required for the multiplication of the matrixes C_{cds} and S_{cds} (for illuminance calculations and rendering generation).

The computational time required by arithmetic operations of all results from the previous phases (3pm, 3 pmD, and cds) can be expressed as:

$$\tau_m = t_0nhc \quad (5)$$

Where:

t_0 = CPU time required by the arithmetic combination of the results from the phases 3pm, 3 pmD, and cds (for illuminance calculations and rendering generation).

Finally, the CPU time required by the 5pm is the sum of all the previously defined CPU times:

$$\tau_{5pm} = \tau_{3pm} + \tau_{3pmD} + \tau_{cds} + \tau_m \quad (6)$$

In addition, the CPU time required by the *rtrace* method is the following:

$$\tau_{rtrace} = t_c nhc \quad (7)$$

Where:

t_c = CPU time required by the sky and octree generation (common for illuminance calculations and rendering) and the commands *rtrace* (for illuminance calculations and rendering generation) and command *evalglare* (for DGP calculations).

Combining equations (6) and (7), we can express mathematically whether the *rtrace* method is faster than the 5pm for the same generic daylight glare analysis:

$$\tau_{rtrace} \leq \tau_{5pm} \quad (8)$$

$$t_c nhc \leq \tau_{3pm} + \tau_{3pmD} + \tau_{cds} + \tau_m \quad (9)$$

$$t_c nhc \leq T_s h + T_M n + T_{dc} nhc + t_{cds} nc \quad (10)$$

In order to speed up the glare calculations, we propose to analyse fewer time steps when using *rtrace* than when using the 5pm. Furthermore, equation (10) can be rewritten as follows:

$$t_c nhc \leq T_s H + T_M n + T_{dc} nHc + t_{cds} nc \quad (11)$$

where h and H are the time steps for *rtrace* and for the 5pm, respectively. The maximum number of time steps when using *rtrace* (Eq. (12)) (h_{max}) depends on time parameters ($t_c, T_s, T_M, T_{dc}, t_{cds}$), the number of scenes (n), the number of CFS (c) and the number of time steps considered when using the 5pm (H).

$$h_{max} = \frac{(T_M + t_{cds}c)n + (T_s + T_{dc}nc)H}{t_c nc} \quad (12)$$

For an initial annual glare evaluation (considering clear sky conditions), only one window state is considered ($c = 1$) and the most problematic viewpoint/direction is analysed ($n = 1$). This initial annual glare assessment is key to identify time steps with a risk of daylight glare. In practice, these time steps could be analysed when comparing different shading devices that could provide a desired degree of glare protection. Thus, h_{max} can be expressed as follows:

Table 4
 Values of all time parameters for *rtrace* and 5pm calculations when using -n 25 (Eq. (13)).

		Parameter	Value (seconds)
5pm	3pm	t_s	0.1
		t_M	8453.2
	3pmD	t_{dc}	6.0
		t_{sD}	0.05
		t_{MD}	520.2
	cds	t_{dcD}	5.5
		t_{sF}	0.1
		t_{MF}	1.0
		t_{cds}	22125
		t_{dcF}	3.0
Arith. comb		t_0	6.1
rtrace ab = [-5]		t_c	[7.0, 32.4, 60, 72.6,77.6]

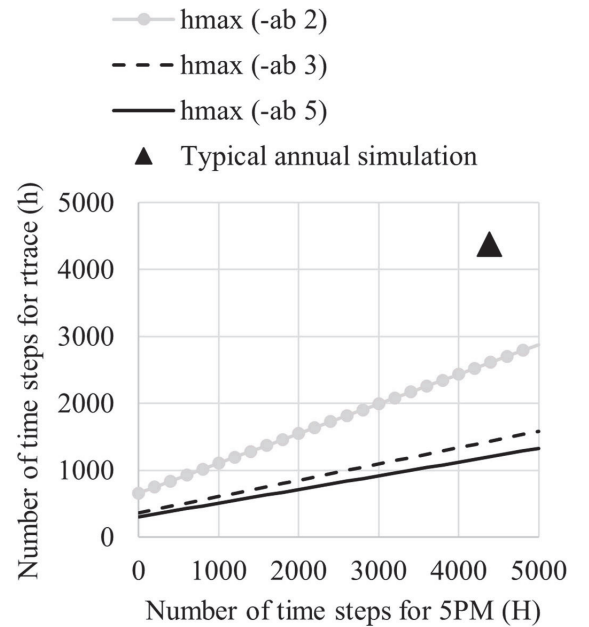


Fig. 10. Maximum number of time steps to run with *rtrace* method depending on the number of time steps chosen to run the 5pm (for one scene and one window state).

$$h_{max} = \frac{(T_M + t_{cds})}{t_c} + \frac{(T_s + T_{dc})}{t_c} H \quad (13)$$

The value of the time parameters depends on the Radiance parameters and the machine used to run the glare simulations. We used 25 cores of a Linux machine cluster of 56 CPUs to run all the simulations (Processor Intel(R) Xeon(R) CPU E5-2697 v3 @ 2.60 GHz). The Radiance parameters used for each phase of the 5pm are shown in Table 1. In practice, at least an initial static calculation using *rtrace* and 5pm is necessary in order to calculate all the time parameters that can be seen in Table 4.

The graphical representation of Eq. (13) can be seen in Fig. 10. The fastest method to assess glare risk in terms of DGP, depending on the combination of h and H, can be determined from Fig. 10. Thus, the 5pm is faster than the *rtrace* method for all the points above the line which

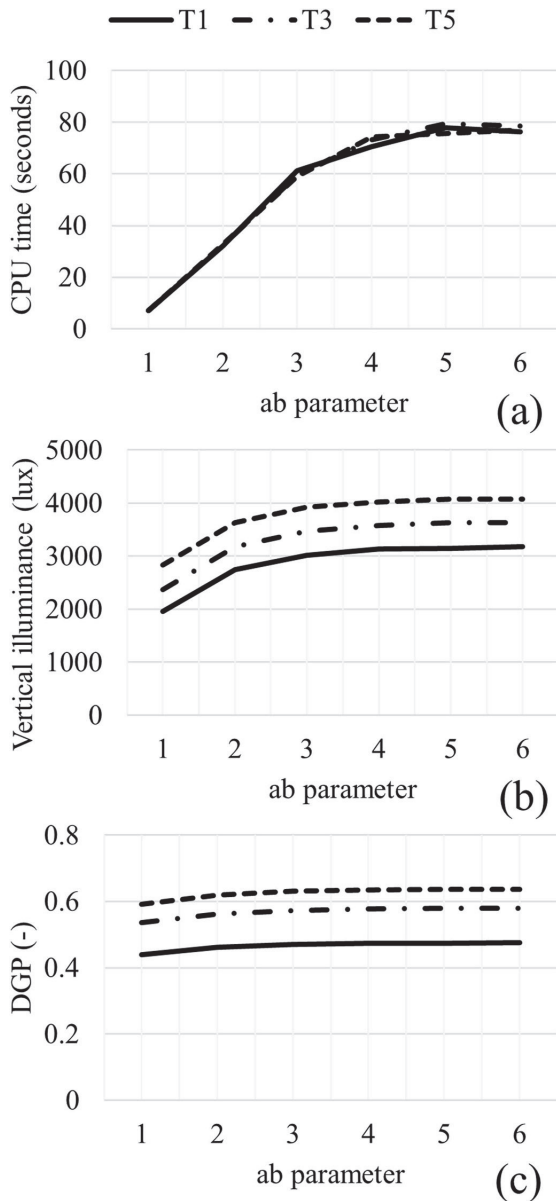


Fig. 11. Required CPU time (a), vertical illuminance (b), and DGP (c) calculated with the *rtrace* method for different ab parameters and isotropic fabrics (T5, T3, and T1). The number of cores to run the Radiance simulations was 25 (-n 25).

represents h_{max} . By contrast, for all the combinations of h and H below the line, the *rtrace* method is faster than the 5pm for the annual glare analysis of interest.

A typical annual simulation of 4380 time steps with 5pm delivers results 7 times faster than the *rtrace* method with ab 5 (from Eqs. (6) and (7)). On the other hand, a single-hour 5pm simulation (without pre-calculated matrices) requires the same CPU time as 174 h simulated with the *rtrace* method. For ab 2, the feasible range of h_{max} is between 522 and

2097 h when a single scene and CFS are considered. Nevertheless, the range of h_{max} is between 174 and 699 h for ab 5. Thus, there is high potential to speed up annual glare simulations by selecting adequate sampling strategies. We defined a simple criterion based on CPU time for the selection of the fastest method to be used in annual glare assessments. In addition, the proposed expressions Eq. (2), Eq. (6), and Eq. (7) can be used as prediction formulas to approximate CPU time required by daylight calculation methods such as 3pm, 5pm, and *rtrace*, respectively.

3.3. Strategies for computationally efficient annual glare calculations

In previous sections, we have analysed how Radiance parameters, daylight calculation methods, and CFS models affect glare calculations in terms of accuracy and CPU time. The objective here is to optimize annual glare simulations in terms of accuracy and CPU time. The factors analysed are the ab parameter for glare protection fabrics (isotropic fabrics), and sampling strategies. For all of the analyses of this section 3.3, the fabrics were modelled with the analytical BRDFfunc model presented in section 2.3.

3.3.1. Optimization of radiance parameters

Section 3.1.1 analysed the sensitivity of the vertical illuminance on the number of ambient divisions (parameter ad) and the number of ambient bounces (parameter ab). It was concluded that values ad = 500 and ab = 4 provided stable illuminance results with *rtrace*. We refine the analysis by investigating the sensitivity of DGP to the ab parameter for generic glare protection fabrics, looking for a satisfactory trade-off between accuracy and CPU time. For this purpose, we apply a single time step analysis (static glare calculation). The CPU time required for an annual glare calculation could be calculated from Eq. (7). The analysed time step for this sensitivity analysis is February 5 at 11:00, when the solar disk is in the field of view. In addition, the viewing direction was set parallel to the window plane. Synthetic, isotropic fabrics T5, T3, and T1 are used in the analysis. The ad parameter was set to 500, as proven to be reliable in section 3.1.1, while the ab parameter ranged from 1 to 6. As can be seen from Fig. 11 c, the sensitivity of the DGP to the number of ambient bounces is weaker than that of the illuminance for all the fabrics considered. CPU times vary from 12 s for ab 1, to approximately and 109 s for ab 6.

On the one hand, if we consider a convergence criterion based on illuminance, for ab = 4, the CPU time is approximately 110 s and the absolute deviations in terms of vertical illuminance and DGP would be lower than 150 lux and 0.005, respectively. On the other hand, if we consider a DGP-based convergence criterion based on a maximum absolute deviation of 0.005, the minimum ab parameter would be 3 for all the tested fabrics. Thus, for ab = 3, the CPU time is approximately 60 s, and the absolute deviations in terms of vertical illuminance and DGP are 286 lux and 0.0023, respectively.

According to this analysis, we recommend two different minimum number of ambient bounces depending of the desired trade-off between accuracy and CPU time. On one hand, ab = 4 to have a good trade-off between DGP, vertical illuminance, and CPU time. On the other hand, ab = 3 to speed up glare simulations by 17% but decreasing accuracy of illuminance calculations. In practice, this decision depends on the trade-off between illuminance/DGP accuracy and CPU time. A lower ab parameter can be very valuable in early stages of the building design process when glare risk in multiple indoor spaces with several fabrics must be assessed. It must be nevertheless noted that, for specific case studies with complex scenes and fenestration materials, optimal ab parameters might vary from those recommended here. A convergence study such as the one presented here is to be conducted in those cases.

3.3.2. Sampling strategies for annual glare calculations

The aim of this analysis is to propose efficient sampling strategies for annual glare assessment under clear sky conditions. We quantified annual glare protection with the annual glare metric fDGpT defined by

Table 5
Sampling strategies and their associated number of time steps. SDn/SVn represents the sum of daily daytime/visible sun time steps each n days during the first semimanual period.

(Sampling strategy) Number of time steps		December 21- June 21	
		Daytime	Visible sun
Day steps	1	(SD1) 2190	(SV1) 820
	3	(SD3) 703	(SV3) 276
	5	(SD5) 420	(SV5) 168
	7	(SD7) 298	(SV7) 119
	9	(SD9) 227	(SV9) 94
	11	(SD11) 180	(SV11) 77

the European standard EN 17037 (maximum fDGpt = 5%). In this case, we defined our CFS as a combination of a solar-control double glazing unit (DGUSC) “ipasal neutral 50/27” ($\tau_{nh} = 49\%$) [50] and an isotropic fabric T1 as the interior shading system. We selected fabric T1, T3, and T5 to cover a range of fabrics with openness factor between 1% and 5% for accuracy comparisons. However, we analysed only T1 in terms of CPU time since time parameters are similar in both cases (Table 4). The chosen viewing direction of the room occupant is 45° towards the window plane (critical scenario). As demonstrated in section 3.2, we need to define the number of time steps of the simulation in order to establish the most computationally efficient method to run an annual glare assessment. The analysed sampling strategies are shown in Table 5. Since only sunny skies should be considered in the glare evaluation, the simulation of only half of the year (from winter to summer solstice) already provides all sun positions in the sky and reduces the computational time by half. Another sampling strategy consists of simulating only the time steps where the solar disk is in the field of view (“visible” sun hours). Thus, the number of hours of “visible” sun hours depends strongly on the scene elements such as viewing position/direction, window size, room orientation, etc. This strategy assumes that no diffuse and/or specular reflection of the sun on any surface of the scene or the shading device will cause glare when this is not in the field of view, which is a reasonable assumption in many cases.

The maximum number of time steps is associated with the sampling strategy SD1 (2190) daylighting hours for a half-year simulation), which is the sampling strategy proposed by the EN 17037 standard for clear skies. The required CPU time is 21.3 h (Eq. (5)) and 66.9 h (Eq. (6)) when using the 5pm and the *rtrace* method (*ab* = 4), respectively. Therefore, we chose the 5pm to run the annual glare analyses using the different sampling strategies defined in Table 5. The Radiance parameters used in the simulations can be seen in Table 1. In addition, an aBSDF Radiance material with Klems angular resolution and peak extraction was used to model the CFS for the direct sun coefficient calculation (phase cds).

The time steps considered by each sampling strategy can be seen in Fig. 12. In this analysis, we vary the frequency of DGP calculation (day steps) from 1 (daily) to 11 (once every 11 days).

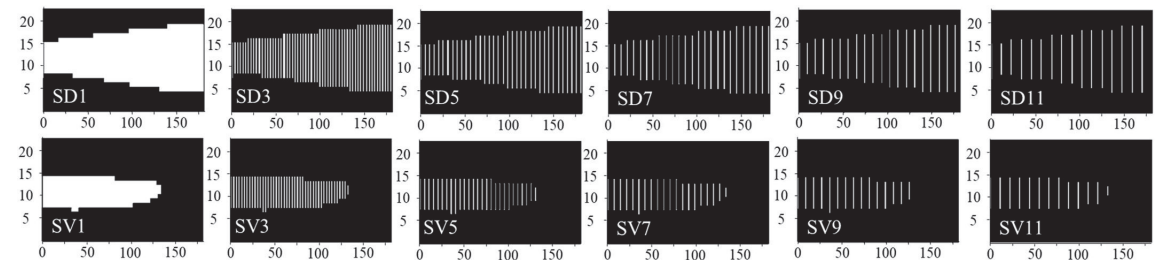


Fig. 12. Time steps considered by each sampling strategy. The horizontal axis represents the days of the first half of the year and the vertical axis represents the hours per day. SDn (upper row)/SVn (bottom row) represents the sum of daily daytime/visible sun time steps each n days during the first semimanual period.

The first step is to compare the required computational time for each sampling strategy (Fig. 13). The CPU time can vary from 21 h to approximately 9 h depending on the sampling strategy used. For a day step of 1, the consideration of visible sun (SV1) instead of daytime hours decreases the CPU time by 35% compared to strategy SD1.

Once we have analysed the sampling strategies in terms of CPU time, we need to compare these sampling strategies in terms of accuracy. We set SD1 as our reference sampling strategy because it has the maximum number of time steps within the sampling strategies presented. Fig. 14 shows the absolute deviation of the fDGpt value for each sampling strategy from that for strategy SD1 when using T1, T3, and T5. Sampling strategies based on daytime hours (SD1, SD3, SD5, SD7, SD9, and SD11) can produce a maximum absolute fDGpt deviation up to 1.2%, 2.4%, and 2.5%, when using T1, T3, and T5, respectively. Consideration of only the “sun visible” hours (SV1, SV3, SV5, SV7, SV9, and SV11) leads to a maximum absolute fDGpt deviation up to 1.7%, 3%, and 3.5%, when using T1, T3, and T5, respectively.

A good trade-off between accuracy and CPU time depends on the shading device and the number of hours of visible sun for a certain view position and direction. From the cases analysed, a sampling strategy SD7 can be safely applied assuming an absolute f0.45 (fDGpt with DGpt = 0.45) deviation of less than 1% (CPU reduction of 57% by using with the *rtrace* method (*ab* = 4) with respect SD1 with the 5pm). If a f0.45 deviation of 2% was acceptable, e.g. for comparing design alternatives, a sampling strategy SV5 would be appropriate (CPU reduction 76%). There are also other approaches to reduce the simulation time of annual glare simulations based on GPU technology, which should be further investigated [51].

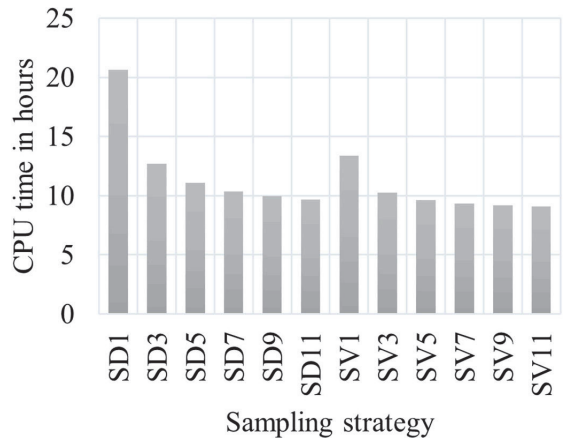


Fig. 13. Required CPU time for the 5pm depending on the sampling strategy.

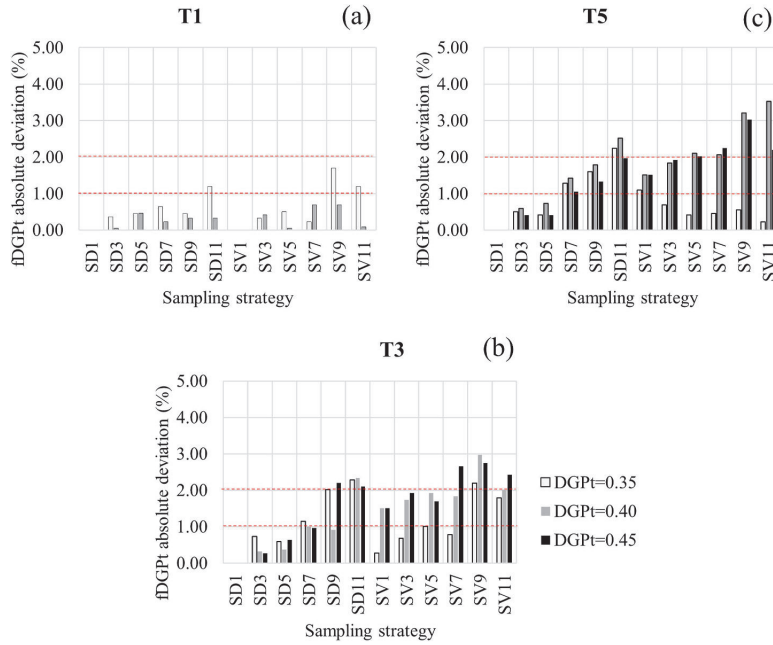


Fig. 14. Absolute deviations in terms of the annual glare metric defined by EN17037 (fDGpT) for different sampling strategies and isotropic fabrics: T1 (a), T3 (b), and T5 (c). The sampling strategy SD1 (daytime hours each day during the semi-annual period) was set as the benchmark for the deviation calculation.

Table 6

CPU times for different daylight methods, fabric T1, viewing direction 45° towards to the window, and sampling strategy SV5 (168 h/year).

	5pm	rtrace (-ab 4)
Predicted CPU time (h)	9.6	3.4
Real CPU time (h)	9.8	3.6

3.3.3. Prediction of the computational time

In cases in which many annual simulations are required, it might be advisable to calculate in advance the computational cost of alternative sampling strategies. The formulation presented in section 3.2, in particular Eqs. (6) and (7), can be used for this purpose.

The computational cost of the SV5 sampling strategy (DGP calculated for the daily visible sun hours once every 5 days) is calculated by the 5pm and rtrace methods for the T1 fabric and a viewing direction 45° towards the window (Table 6). The required CPU time by the 5pm to solve for 168 h/year is 9.8 h against 3.6 h when using rtrace (-ab 4). The predicted CPU time shows good agreement with actual CPU times. For the calculation of 168 DGP values, one window state, and one scene, the rtrace method with ab 4 is faster than the 5pm according to Fig. 15. The graph also shows that rtrace method is faster than the 5pm for a SD7 sampling strategy (298 DGP values). On the other hand, the 5pm is faster than rtrace for a SD1 sampling strategy (2190 DGP values).

4. Conclusions

This paper benchmarks state-of-the-art methods for annual glare analysis in terms of accuracy and computational time. We investigated the influence of Radiance parameters and CFS models on glare assessment. The choice of suitable Radiance parameters, depending on the daylight calculation method, is crucial to ensure suitable accuracy and low CPU time for annual glare calculations. A criterion based on computational time was proposed for the selection of the fastest daylight

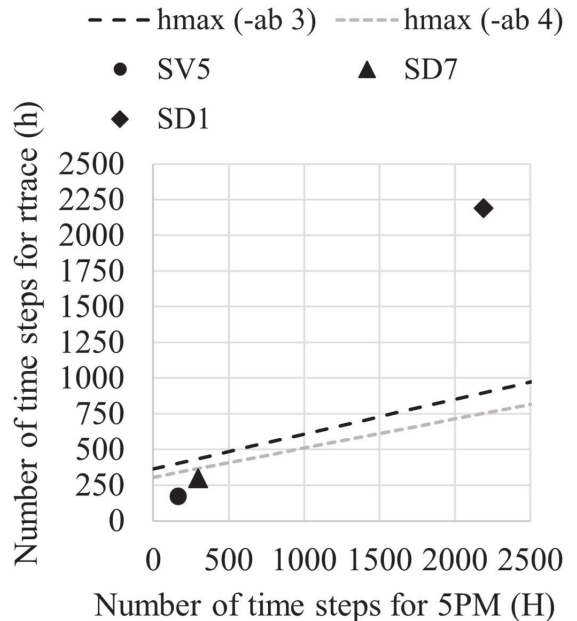


Fig. 15. Maximum number of time steps to run with the rtrace method depending on the number of time steps chosen to run using the 5pm for different sampling strategies (for one scene and one window state). SDK and SVK are sampling strategies based on selected daytime and “sun visible” hours each K days of the semi-annual period, respectively.

calculation method for annual glare analysis. Different sampling strategies based on semi-annual periods and sun visibility were evaluated in terms of annual glare protection performance and computational time. The findings of this paper can help architects and practitioners to set up parameters and calculation methods for efficient annual glare calculations.

The main outcomes of the research and potential applications of the results are the following:

1. For the particular case of fabrics with a view-through specular component without light-redirecting effects, the combination of a low-resolution BSDF, such as the Klems format, and a peak extraction algorithm, such as the one offered by Radiance's aBSDF material, provide a suitable representation for glare analysis using the 5pm or rtrace methods. Furthermore, for fabrics in which rotational invariance can be assumed, a representation based on the Radiance BRDF material can be useful, because it only requires the normal-normal transmittance, the normal-diffuse transmittance and the cut-off angle of the fabric.
2. A suitable sampling strategy for annual glare risk assessments can make a time step-based ray-tracing method (the *rtrace* method in this paper) more computationally efficient than the alternative five-phase method. For cases in which no diffuse and/or specular reflections of the sun from any surface of the scene or the shading device will cause glare when this is not in the field of view, a sampling strategy that takes into account only the hours when the solar disk is in the field of view can reduce the computational time considerably. This strategy can be combined with semi-annual evaluations (for clear skies) and a suitable sampling strategy (e.g. one day per week) to further reduce the computational time. The sensitivity analysis of Radiance parameters for the *rtrace* method presented in the study can help to optimize the computational cost of simulations. Thus, by using this methodology, designers could efficiently compare several CFSs in terms of annual glare protection performance during early stages of the building design process. Recent developments in GPU acceleration might further improve the computational cost of time step-based ray-tracing in the future.

Declaration of competing interest

The authors declare that they have no known competing financial interests or personal relationships that could have appeared to influence the work reported in this paper.

Acknowledgements

This research was partially supported by the Estonian Centre of Excellence in Zero Energy and Resource Efficient Smart Buildings and Districts, ZEBE (grant No. 2014-2020.4.01.15-0016), the programme Mobilitas Pluss (Grant No – 2014-2020.4.01.16-0024, MOBTP88), and Dora Plus PhD student mobility (T1.2) funded by the European Regional Development Fund, by the Estonian Research Council (grant No. PSG409) and by the European Commission through the H2020 project Finest Twins (grant No. 856602). This research was partially supported by a Fraunhofer ICON Grant.

References

- [1] S.W. Lockley, Circadian rhythms: influence of light in humans, in: *Encycl. Neurosci.*, 2009, <https://doi.org/10.1016/B978-008045046-9.01619-3>.
- [2] J.F. Duffy, C.A. Czeisler, Effect of light on human circadian physiology, *Sleep Med. Clin.* (2009), <https://doi.org/10.1016/j.jsmc.2009.01.004>.
- [3] K. Won Hee, G. Brager, S. Schiavon, S. Selkowitz, *Building Envelope Impact on Human Performance and Well-Being: Experimental Study on View Clarity*, *Escholarsh. UC Open Access Publ.*, 2017.
- [4] M. Knoop, O. Stefani, B. Bueno, B. Matusiak, R. Hobday, A. Wirz-Justice, K. Martiny, T. Kantermann, M.P.J. Aarts, N. Zemouri, S. Appelt, B. Norton, Daylight: what makes the difference? *Light. Res. Technol.* (2019) <https://doi.org/10.1177/1477153519869758>.
- [5] S.T. Taylor, LEED® and Standard 62.1, ASHRAE J., 2005.
- [6] Bre, Building Research Establishment Environmental Assessment Methodology (BREEAM), *Www.breem.org.*, 2013.
- [7] European Commission, BS EN 17037:2018: Daylight in Buildings, 2018. <https://www.en-standard.eu/bs-en-17037-2018-daylight-in-buildings/>.
- [8] B.S. Bsi, 8206-2: Lighting for Buildings, Code of practice for daylighting, 2008.
- [9] C.F. Reinhart, J. Mardaljevic, Z. Rogers, Dynamic daylight performance metrics for sustainable building design, LEUKOS - J. Illum. Eng. Soc. North Am. (2006), <https://doi.org/10.1582/LEUKOS.2006.03.01.001>.
- [10] A. Nabil, J. Mardaljevic, Useful Daylight Illuminance: A Replacement for Daylight Factors, *Energy Build.*, 2006, <https://doi.org/10.1016/j.enbuild.2006.03.013>.
- [11] Illuminating Engineering Society, the Daylight Metric Committee, LM-83-12 Approved Metric: IES Spatial Daylight Autonomy (sDA) and Annual Sunlight Exposure (ASE), 2013.
- [12] W.K.E. Osterhaus, Discomfort glare assessment and prevention for daylight applications in office environments, in: *Sol. Energy*, 2005, <https://doi.org/10.1016/j.solener.2004.11.011>.
- [13] C. Pierson, J. Wienold, M. Bodart, Discomfort glare perception in daylighting: influencing factors, in: *Energy Procedia*, 2017, <https://doi.org/10.1016/j.egypro.2017.07.332>.
- [14] R.A. Mangkuto, K.A. Kurnia, D.N. Azizah, R.T. Atmodipoeiro, F.X.N. Soelami, Determination of discomfort glare criteria for daylight space in Indonesia, *Sol. Energy* (2017), <https://doi.org/10.1016/j.solener.2017.04.010>.
- [15] J.A. Yamin Garretón, E.M. Colombo, A.E. Pattini, A global evaluation of discomfort glare metrics in real office spaces with presence of direct sunlight, *Energy Build.* (2018), <https://doi.org/10.1016/j.enbuild.2018.01.024>.
- [16] N.S. Shafavi, M. Tahsildoost, Z.S. Zomorodian, Investigation of illuminance-based metrics in predicting occupants' visual comfort (case study: architecture design studios), *Sol. Energy* (2020), <https://doi.org/10.1016/j.solener.2019.12.051>.
- [17] J. Wienold, J. Christoffersen, Evaluation methods and development of a new glare prediction model for daylight environments with the use of CCD cameras, *Energy Build.* (2006), <https://doi.org/10.1016/j.enbuild.2006.03.017>.
- [18] J. Wienold, T. Iwata, M. Sarey Khanie, E. Erell, E. Kaftan, R.G. Rodriguez, J. A. Yamin Garretón, T. Tzempelikos, I. Konstantzos, J. Christoffersen, T.E. Kuhn, C. Pierson, M. Andersen, Cross-validation and robustness of daylight glare metrics, *Light. Res. Technol.* (2019), <https://doi.org/10.1177/1477153519826003>.
- [19] J. Wienold, K. Tilmann E, J. Christoffersen, M. Andersen, Annual glare evaluation for fabrics, PLEA 2017 edinburgh des. To thrive. https://www.researchgate.net/publication/329538959/Annuaire_evaluation_for_fabrics, 2017.
- [20] G.J. Ward, The RADIANCE lighting simulation and rendering system, in: *Proc. 21st Annu. Conf. Comput. Graph. Interact. Tech. SIGGRAPH*, 1994, <https://doi.org/10.1145/192161.192286>, 1994.
- [21] C. Pierson, J. Wienold, M. Bodart, Daylight discomfort glare evaluation with evalglare: influence of parameters and methods on the accuracy of discomfort glare prediction, *Buildings* (2018), <https://doi.org/10.3390/buildings8080094>.
- [22] Corrigendum to: investigation of Evalglare software, daylight glare probability and high dynamic range imaging for daylight glare analysis (*Lighting Research and Technology*, (2013), *Light. Res. Technol.* 45 (4) (2018) 450–463, <https://doi.org/10.1177/1477153518758844>, 10.1177/1477153518758844).
- [23] S. Darula, R. Kuttler, CIE General sky standard defining luminance distributions, *ESim 2002 Can. Conf. Build. Energy Simul.* (2002).
- [24] J. Mardaljevic, Sky models for lighting simulation, in: *Daylight Simul. Validation, Sky Model, Daylight Coefficients*, 1999.
- [25] S. Subramaniam, R. Mistrick, A more accurate approach for calculating illuminance with daylight coefficients, *Illum. Eng. Soc. Annu. Conf.* 2017 (2018).
- [26] E.S. Lee, D. Geisler-Moroder, G. Ward, Modeling the direct sun component in buildings using matrix algebraic approaches: methods and validation, *Sol. Energy* (2018), <https://doi.org/10.1016/j.solener.2017.12.029>.
- [27] S. Subramaniam, Daylighting simulations with radiance using matrix-based methods, https://www.researchgate.net/publication/325248488_Daylighting_simulations_with_Radiance_using_matrix_based_methods, 2017.
- [28] N.L. Jones, C.F. Reinhart, Speedup potential of climate-based daylight modelling on GPUs, in: *Conf. Build. Simul. 2017 15th Int. Conf. Int. Build. Perform. Simul. Assoc.*, 2017, pp. 975–984. San Francisco, <https://pdfs.semanticscholar.org/a42a/ec2b555c308449583a27e2315cd666f1ceb.pdf>.
- [29] P. Apian-Bennewitz, New scanning goniophotometer for extended BRDF measurements, in: *Reflection, Scatt. Diff. From Surfaces II*, 2010, <https://doi.org/10.1117/12.860889>.
- [30] J.C. Stover, *Optical Scattering: Measurement and Analysis*, third ed., 2012, <https://doi.org/10.1117/3.975276>.
- [31] G. Ward, Reducing anisotropic BSDF measurement to common practice, in: *Eurographics Work. Mater. Appear. Model.*, 2014.
- [32] A. McNeil, genBSDF Tutorial, 2015. https://radiance-online.org/learning/tutorials/Tutorial-genBSDF_v1.0.1.pdf.
- [33] A. McNeil, C.J. Jonsson, D. Appelfeld, G. Ward, E.S. Lee, A validation of a ray-tracing tool used to generate bi-directional scattering distribution functions for complex fenestration systems, *Sol. Energy* (2013), <https://doi.org/10.1016/j.solener.2013.09.032>.
- [34] D. Uribe, S. Vera, W. Bustamante, A. McNeil, G. Flamant, Impact of different control strategies of perforated curved louvers on the visual comfort and energy consumption of office buildings in different climates, *Sol. Energy* (2019), <https://doi.org/10.1016/j.solener.2019.07.027>.

- [35] A. Sepúlveda, Validation of a geometrical model in RADIANCE for the design of textile shading devices. <https://www.radiance-online.org/community/workshops/2018-loughborough/presentations/22-TextileShadingModel.pdf>, 2018.
- [36] A.G. Mainini, A. Zani, G. De Michele, A. Speroni, T. Poli, M. Zinzi, A. Gasparella, Daylighting Performance of Three-Dimensional Textiles, *Energy Build*, 2019, <https://doi.org/10.1016/j.enbuild.2019.02.036>.
- [37] A. McNeil, The 5-phase method. <https://www.radiance-online.org/community/workshops/2013-golden-co/McNeil-5phase.pdf>, 2013.
- [38] E.S. Lee, D. Geisler-Moroder, G. Ward, Validation of the five-phase method for simulating complex fenestration systems with radiance against field measurements. <https://escholarship.org/uc/item/24h966pp>, 2018.
- [39] M. Abravesh, B. Bueno, S. Heidari, T.E. Kuhn, A method to evaluate glare risk from operable fenestration systems throughout a year, *Build. Environ.* (2019), <https://doi.org/10.1016/j.buildenv.2019.106213>.
- [40] J. Karlsson, A. Roos, Modelling the angular behaviour of the total solar energy transmittance of windows, *Sol. Energy* 69 (2000), [https://doi.org/10.1016/S0038-092X\(00\)00083-9](https://doi.org/10.1016/S0038-092X(00)00083-9).
- [41] Radiance 5.4a (2020-09-06), (n.d.). <https://github.com/LBNL-ETA/Radiance/releases/tag/e147df6a>.
- [42] G.J. Ward, RTRACE, (n.d.). https://floyd.lbl.gov/radiance/man_html/rtrace.1.html.
- [43] M. Inanici, A. Hashemloo, An investigation of the daylighting simulation techniques and sky modeling practices for occupant centric evaluations, *Build. Environ.* (2017), <https://doi.org/10.1016/j.buildenv.2016.09.022>.
- [44] A. McNeil, BSDFs, Matrices and Phases, 2014, p. 158. https://www.radiance-online.org/community/workshops/2014-london/presentations/day1/McNeil_BSDFsandPhases.pdf.
- [45] C.F. Reinhart, S. Herkel, The Simulation of Annual Daylight Illuminance Distributions-A State-Of-The-Art Comparison of Six RADIANCE-Based Methods, *Energy Build*, 2000, [https://doi.org/10.1016/S0378-7788\(00\)00042-6](https://doi.org/10.1016/S0378-7788(00)00042-6).
- [46] E. Brembilla, D.A. Chi, C.J. Hopfe, J. Mardaljevic, Evaluation of Climate-Based Daylighting Techniques for Complex Fenestration and Shading Systems, *Energy Build*, 2019, <https://doi.org/10.1016/j.enbuild.2019.109454>.
- [47] G.J. Ward, T. Wang, D. Geisler-Moroder, E.S. Lee, L.O. Grobe, J. Wienold, J. C. Jonsson, Modeling specular transmission of complex fenestration systems with data-driven BSDFs, *Build. Environ.* (2021), <https://doi.org/10.1016/j.buildenv.2021.107774>.
- [48] G. Ward, bsd2tree, 2013, p. 2. https://www.radiance-online.org/learning/documentation/manual-pages/pdfs/bsd2tree.pdf/at_download/file.
- [49] T. Berger, Rate-distortion theory, in: *Wiley Encycl. Telecommun.*, 2003, <https://doi.org/10.1002/0471219282.eot142>.
- [50] INTERPANE Glasgesellschaft mbH, PERFORMANCE DATA FOR LOW E AND SOLAR CONTROL GLASS. https://www.interpane.com/fileadmin/user_upload/pdf-files/daten-und-richtlinien/en/INT_Pocket_USA_200x525_230418.pdf, 2018.
- [51] N. Jones, Better, faster, stronger super-fast glare analysis and real-time visualization, 61, https://www.radiance-online.org/community/workshops/2019-new-york-ny/presentations/day2/11_Jones.pdf, 2019.

Curriculum vitae

Abel Sepúlveda Luque

E-mail absepu@taltech.ee

Institutions and positions

04.02.2019–30.08.2022 The Fraunhofer-Gesellschaft, Visiting Researcher (0,10)
31.08.2018–21.06.2022 Tallinn University of Technology , Junior Researcher (1,00)

Education

2015–2017 Master in Industrial Engineering
2010–2015 Bachelor’s Degree in industrial Technologies Engineering

R&D related managerial and administrative work

2018 Researcher at Fraunhofer ISE
2018 Research assistant at Fraunhofer

Creative work

2022 Finalist of the Healthy Homes Design Competition 2022 – International conference CLIMA 2022

2019 (Rigi Kaltbad, Switzerland, Daylight Academy (DLA)) <https://www.ethz.ch/en/the-eth-zurich/sustainability/education/summer-and-winter-schools/ETHSustainabilitySummerSchool.html>.

2018 (Loughborough University, UK) <https://www.radiance-online.org/community/workshops/2018-loughborough>.

Academic degrees

Abel Sepúlveda Luque, Phd student, (sup) Francesco De Luca; Kimmo Sakari Lylykangas, Performance-driven and Integrated Design Methods for Architecture and Urban Design, Tallinn University of Technology School of Engineering, Department of Civil Engineering and Architecture.

Honours & awards

- 2021 Dora Plus Action 1 – Short-Term Study Mobility, BS2021 conference, Bruges, Belgium
- 2021 Dora Plus Action 1 – Short-Term Study Mobility, Radiance Workshop, Bilbao, Spain
- 2020 Dora Plus Action 1 – Long-Term Study Mobility, Fraunhofer ISE, Freiburg
- 2017 Distinction in master thesis: “Chiller control at part load: characteristic curves and optimal control strategies”

Fields of research

ETIS CLASSIFICATION: 4. Natural Sciences and Engineering; 4.17. Energetic Research;
CERCS CLASSIFICATION: T140 Energy research

Projects in progress

- PSG409 “New generation dynamic sizing methods for heating and cooling systems in intermittently operated buildings (1.01.2020–31.12.2023)”, Martin Thalfeldt, Tallinn University of Technology , School of Engineering, Department of Civil Engineering and Architecture.

Publications

2022

De Luca, F., Sepúlveda, A., & Varjas, T. (2022). Multi-performance optimization of static shading devices for glare, daylight, view and energy consideration. *Building and Environment*, 109110

Vikberg H, Sepúlveda A, De Luca F. Delightful Daylighting: A Framework for Describing the Experience of Daylighting in Nordic Homes and Coupling It with Quantitative Assessments. *Energies*. 2022; 15(5):1815. <https://doi.org/10.3390/en15051815>

Nasim Eslamirad, Abel Sepúlveda, Francesco De Luca, Kimmo Sakari Lylykangas. Evaluating Outdoor Thermal Comfort Using a Mixed-Method to Improve the Environmental Quality of a University Campus. *Energies*. 2022; 15 (4):1577

Sepúlveda, A.; De Luca, F.; Kurnitski, J. (2022). Daylight and overheating prediction formulas for building design in a cold climate. *Journal of Building Engineering*. DOI: 10.1016/j.jobbe.2021.103532

2021

Sepúlveda, A.; Bueno, B.; Wang, T.; Rose Wilson, H. (2021). Benchmark of methods for annual glare risk assessment. *Building and Environment*, 201, #108006. DOI: 10.1016/j.buildenv.2021.108006

Sepúlveda, A.; De Luca, F.; Varjas, T. (2021). Influence of daylight modeling decisions on daylight provision and glare protection. *Proceedings of the Symposium on Simulation for Architecture and Urban Design (SimAUD): 2021 Symposium on Simulation for Architecture and Urban Design*, A. Chronis, G. Wurzer, W.E. Lorenz, C.M. Herr, U. Pont, D. Cupkova, G. Wainer, Online, 15-17 April 2021. ACM Digital Library

Sepúlveda, A.; De Luca, F.; Kurnitski, J. (2021). Optimization workflow for the design of efficient shading control strategies. *Proceedings of Building Simulation 2021: 17th Conference of IBPSA: Proceedings of Building Simulation 2021: 17th Conference of IBPSA*. ACM Digital Library

De Luca, F.; Sepúlveda, A. (2021). Analyzing daylight and solar access performance in urban environments in Estonia. *Proceedings of Building Simulation 2021: 17th Conference of IBPSA: 17th IBPSA International Conference and Exhibition (BS2021), Bruges, Belgium, 1-2-3 September 2021*. IBPSA

Bueno, B.; Sepúlveda, A. (2021). Easy-to-implement simulation strategies for dynamic glare risk assessment based on the European Daylighting Standard. *Proceedings of Building Simulation 2021: 17th Conference of IBPSA: Proceedings of Building Simulation 2021: 17th Conference of IBPSA*. IBPSA

2020

Sepúlveda, A.; De Luca, F.; Thalfeldt, M.; Kurnitski, J. (2020). Analyzing the fulfillment of daylight and overheating requirements in residential and office buildings in Estonia. *Building and Environment*. DOI: 10.1016/j.buildenv.2020.107036

Bueno, B.; Wilson, H. R.; Sepúlveda, A.; Sunkara, S.; Kuhn, T. E. (2020). Simulation-based design of an angle-selective and switchable textile shading system. *Building and Environment*, #107227. DOI: 10.1016/j.buildenv.2020.107227

De Luca, F.; Naboni, E.; Lobaccaro, G.; Sepúlveda, A. (2020). Building Cluster Optimization to Integrate Energy Performance and Outdoor Thermal Comfort. *Proceedings of the Symposium on Simulation for Architecture and Urban Design (SimAUD): 2020 Symposium on Simulation for Architecture and Urban Design, A. Chronis, G. Wurzer, W.E. Lorenz, C.M. Herr, U. Pont, D. Cupkova, G. Wainer, TU Wien, Vienna (online), 25-27 May 2020*. San Diego, USA: The Society for Modeling and Simulation International (SCS), Association for Computing Machinery (ACM), 345–348

Sepúlveda Luque, A.; De Luca, F. (2020). A Multi-Objective Optimization Workflow based on Solar Access and Solar Radiation for the Design of Building Envelopes in Cold Climates. *Proceedings of the Symposium on Simulation for Architecture and Urban Design (SimAUD): 2020 Symposium on Simulation for Architecture and Urban Design, A. Chronis, G. Wurzer, W.E. Lorenz, C.M. Herr, U. Pont, D. Cupkova, G. Wainer, TU Wien, Vienna (online), 25-27 May 2020*. San Diego, USA: The Society for Modeling and Simulation International (SCS), Association for Computing Machinery (ACM), 131–138

2019

Bueno Unzeta, B.; Sepúlveda Luque, A. (2019). A Specific Building Simulation Tool for the Design and Evaluation of Innovative Fenestration Systems and their Control. *Proceedings of 16th IBPSA International Conference and Exhibition (BS2019), 16: 16th IBPSA International Conference and Exhibition (BS2019), Angelicum Congress Centre, Rome, Italy, 02-04 September 2019*. Ed. V. Corrado, E. Fabrizio, A. Gasparella, and F. Patuzzi. International Building Performance Association (IBPSA), 1288–1295. DOI: 10.26868/25222708.2019.210222

Elulookirjeldus

Abel Sepúlveda Luque

E-post absepu@taltech.ee

Töökohad ja ametid

04.02.2019–30.08.2022 The Fraunhofer-Gesellschaft, Visiting Researcher (0,10)
31.08.2018–21.06.2022 Tallinn University of Technology , Junior Researcher (1,00)

Haridustee

2015–2017 Master in Industrial Engineering
2010–2015 Bakalaureusekraad tööstustehnoloogias

Teadusorganisatsiooniline ja -administratiivne tegevus

2018 Researcher at Fraunhofer ISE
2018 Research assistant at Fraunhofer

Loometöö

2022 Finalist of the Healthy Homes Design Competition 2022 – International conference CLIMA 2022

2019 ETH Sustainability Winter School 2019: Perspectives on Daylight (Rigi Kaltbad, Switzerland, Daylight Academy (DLA)) <https://www.ethz.ch/en/the-eth-zurich/sustainability/education/summer-and-winter-schools/ETHSustainabilitySummerSchool.html>.

2018 2018 Radiance International Workshop (Loughborough University, UK) <https://www.radiance-online.org/community/workshops/2018-loughborough>.

Teaduskraadid

Abel Sepúlveda Luque, doktorant, (juh) Francesco De Luca; Kimmo Sakari Lylykangas, Performance-driven and Integrated Design Methods for Architecture and Urban Design (Arhitektuuri ja linnaplaneerimise jõudluse ja integreeritud projekteerimismeetodid), Tallinna Tehnikaülikool, Inseneriteaduskond, Ehituse ja arhitektuuri instituut.

Teaduspreemiad ja tunnustused

2021 Dora Plus Action 1 – lühiajaline õpiränne, BS2021 konverents, Brügge, Belgia

2021 Dora Plus Action 1 – lühiajaline õpiränne, kiirguse töötuba, Bilbao, Hispaania

2020 Dora Plus Action 1 – pikaajaline õpiränne, Fraunhofer ISE, Freiburg

2017 Erinevus magistritöös: “Jahuti juhtimine osalisel koormusel: tunnuskõverad ja optimaalsed juhtimisstrateegiad”

Teadustöö põhisuunad

ETIS KLASSIFIKAATOR: 4. Loodusteadused ja tehnika; 4.17. Energeetikaalased uuringud;

CERCS KLASSIFIKAATOR: T140 Energeetika

Jooksvad projektid

- PSG409 “Uue generatsiooni dünaamilised meetodid kütte- ja jahutussüsteemide dimensioneerimiseks vahelduva kasutusega hoonetes (1.01.2020–31.12.2023)”, Martin Thalfeldt, Tallinna Tehnikaülikool, Inseneriteaduskond, Ehituse ja arhitektuuri instituut.

Publikatsioonid

2022

De Luca, F., Sepúlveda, A., & Varjas, T. (2022). Multi-performance optimization of static shading devices for glare, daylight, view and energy consideration. *Building and Environment*, 109110

Vikberg H, Sepúlveda A, De Luca F. Delightful Daylighting: A Framework for Describing the Experience of Daylighting in Nordic Homes and Coupling It with Quantitative Assessments. *Energies*. 2022; 15(5):1815. <https://doi.org/10.3390/en15051815>

Nasim Eslamirad, Abel Sepúlveda, Francesco De Luca, Kimmo Sakari Lylykangas. Evaluating Outdoor Thermal Comfort Using a Mixed-Method to Improve the Environmental Quality of a University Campus. *Energies*. 2022; 15 (4):1577

Sepúlveda, A.; De Luca, F.; Kurnitski, J. (2022). Daylight and overheating prediction formulas for building design in a cold climate. *Journal of Building Engineering*. DOI: 10.1016/j.jobee.2021.103532

2021

Sepúlveda, A.; Bueno, B.; Wang, T.; Rose Wilson, H. (2021). Benchmark of methods for annual glare risk assessment. *Building and Environment*, 201, #108006. DOI: 10.1016/j.buildenv.2021.108006

Sepúlveda, A.; De Luca, F.; Varjas, T. (2021). Influence of daylight modeling decisions on daylight provision and glare protection. *Proceedings of the Symposium on Simulation for Architecture and Urban Design (SimAUD): 2021 Symposium on Simulation for Architecture and Urban Design, A. Chronis, G. Wurzer, W.E. Lorenz, C.M. Herr, U. Pont, D. Cupkova, G. Wainer, Online, 15-17 April 2021*. ACM Digital Library

Sepúlveda, A.; De Luca, F.; Kurnitski, J. (2021). Optimization workflow for the design of efficient shading control strategies. *Proceedings of Building Simulation 2021: 17th Conference of IBPSA: Proceedings of Building Simulation 2021: 17th Conference of IBPSA*. ACM Digital Library

De Luca, F.; Sepúlveda, A. (2021). Analyzing daylight and solar access performance in urban environments in Estonia. *Proceedings of Building Simulation 2021: 17th Conference of IBPSA: 17th IBPSA International Conference and Exhibition (BS2021), Bruges, Belgium, 1-2-3 September 2021*. IBPSA

Bueno, B.; Sepúlveda, A. (2021). Easy-to-implement simulation strategies for dynamic glare risk assessment based on the European Daylighting Standard. *Proceedings of Building Simulation 2021: 17th Conference of IBPSA: Proceedings of Building Simulation 2021: 17th Conference of IBPSA*. IBPSA

2020

Sepúlveda, A.; De Luca, F.; Thalfeldt, M.; Kurnitski, J. (2020). Analyzing the fulfillment of daylight and overheating requirements in residential and office buildings in Estonia. *Building and Environment*. DOI: 10.1016/j.buildenv.2020.107036

Bueno, B.; Wilson, H. R.; Sepúlveda, A.; Sunkara, S.; Kuhn, T. E. (2020). Simulation-based design of an angle-selective and switchable textile shading system. *Building and Environment*, #107227. DOI: 10.1016/j.buildenv.2020.107227

De Luca, F.; Naboni, E.; Lobaccaro, G.; Sepúlveda, A. (2020). Building Cluster Optimization to Integrate Energy Performance and Outdoor Thermal Comfort. *Proceedings of the Symposium on Simulation for Architecture and Urban Design (SimAUD): 2020 Symposium on Simulation for Architecture and Urban Design, A. Chronis, G. Wurzer, W.E. Lorenz, C.M. Herr, U. Pont, D. Cupkova, G. Wainer, TU Wien, Vienna (online), 25-27 May 2020*. San Diego, USA: The Society for Modeling and Simulation International (SCS), Association for Computing Machinery (ACM), 345–348

Sepúlveda Luque, A.; De Luca, F. (2020). A Multi-Objective Optimization Workflow based on Solar Access and Solar Radiation for the Design of Building Envelopes in Cold Climates. *Proceedings of the Symposium on Simulation for Architecture and Urban Design (SimAUD): 2020 Symposium on Simulation for Architecture and Urban Design, A. Chronis, G. Wurzer, W.E. Lorenz, C.M. Herr, U. Pont, D. Cupkova, G. Wainer, TU Wien, Vienna (online), 25-27 May 2020*. San Diego, USA: The Society for Modeling and Simulation International (SCS), Association for Computing Machinery (ACM), 131–138

2019

Bueno Unzeta, B.; Sepúlveda Luque, A. (2019). A Specific Building Simulation Tool for the Design and Evaluation of Innovative Fenestration Systems and their Control. *Proceedings of 16th IBPSA International Conference and Exhibition (BS2019), 16: 16th IBPSA International Conference and Exhibition (BS2019), Angelicum Congress Centre, Rome, Italy, 02-04 September 2019*. Ed. V. Corrado, E. Fabrizio, A. Gasparella, and F. Patuzzi. International Building Performance Association (IBPSA), 1288–1295. DOI: 10.26868/25222708.2019.210222

ISSN 2585-6901 (PDF)
ISBN 978-9949-83-856-1 (PDF)